Biochemical evidence that the Dlk1 and Grb10 signalling proteins interact through a common growth regulatory pathway

Hu, Xiao

Award date:
2018

Awarding institution:
University of Bath

Biochemical evidence that the Dlk1 and Grb10 signalling proteins interact through a common growth regulatory pathway

Xiao Hu

A thesis submitted for the degree of Doctor of Philosophy

University of Bath

Department of Biology and Biochemistry

FEBRUARY 2018

Acknowledgments

I would like to thank my supervisor Professor Andrew Ward for his support throughout my PhD. Thanks for always being so patient with me. His wisdom and braveness will always inspire me. I feel so lucky to be his student and have learnt so much about research as well as life from Andrew.

I want to express my special thanks to my supervisor Dr. Jim Caunt for his advice and discussion in the first two and half years of my PhD. I still can't believe that I have lost him forever. But I will never forget his big smile.

Thanks Dr. Francoise Koumanov and Professor David Tosh for their help in the last year of my PhD.

Thank you so much Dr. Kim Moorwood! I would never have completed my PhD without your help when Andrew was ill and away.

I would like to thank University of Bath and Chinese Studentship Council for funding.

Finally, I would like to thank my parents for their endless love.

Abstract

Paternally-expressed *Dlk1* promotes fetal growth, while maternally-expressed *Grb10* inhibits fetal growth. The respective growth-regulatory roles are consistent with the predominant theory for the evolution of imprinted gene expression, the parent-offspring conflict hypothesis. This predicts that in mammals imprinting has evolved because of differing parental interests in the distribution of maternal resources to her offspring, at least in species where females tend to reproduce with more than one mate during their reproductive lifespan. Genetic evidence indicates that *Dlk1* and *Grb10* control embryo size and adult body composition, potentially through a common pathway. However, the biochemical links between them are still lacking.

Here, I combined biochemical methods, including two sets of TMT quantitative proteomics using pMEFs and liver derived from E14.5 WT, $Dlk1^{+/p}$, $Grb10^{m/+}$ and $Grb10^{m/+}/Dlk1^{+/p}$ mouse embryos. I found that Dlk1 and Grb10 proteins oppositely affected the expression of each other *in vitro* and *in vivo*. Proteomics analyses uncovered that $Dlk1^{+/p}$ embryos were divergent from $Grb10^{m/+}$ and $Grb10^{m/+}/Dlk1^{+/p}$ which were similar at a proteomics level, supporting the genetic findings from previous studies. Furthermore, GO-term enrichment analysis revealed that RTK related biological processes were significantly enriched in $Dlk1^{+/p}$, $Grb10^{m/+}$ and $Grb10^{m/+}/Dlk1^{+/p}$ embryos. Several RTKs and their signal partners displayed reduced expression in the knockout pMEF and liver proteomes. In particular, cell signalling studies in E14.5 pMEFs of the four genotypes suggested that PDGFR signalling may play essential roles in fetal growth regulation through a Dlk1/Grb10 growth-regulatory axis.

Abbreviations

Akt	Protein kinase B
APS	Ammonium persulfate
ATP	Adenosine-5'-triphosphate
BAT	Brown adipose tissue
BCA	Bicinchoninic acid
BSA	Bovine serum albumin
CDK1	*Cyclin dependent kinase 1*
CDKN1C	*Cyclin dependent kinase inhibitor 1C*
C/EBPα	CCAAT/Enhancer binding protein alpha
CHO	Chinese hamster ovary
CHX	Cycloheximide
CNS	Central nervous system
CREB	cAMP response element binding protein
DAPI	4', 6'-diamino-2-phenylindole
Dlk1	*Delta-like 1*
Dlk1	Delta-like non-canonical notch ligand 1
DMEM	Dulbecco's modified Eagle's medium
DMSO	Dimethyl sulphoxide
DNA	Deoxyribonucleic acid
DPX	Dibutyl phthalate and xylene
DTT	Diothiothreitol
E9.5	Embryonic day 9.5
E14.5	Embryonic day 14.5
E16.5	Embryonic day 16.5
ECL	Enhanced chemiluminescence substrate
EDTA	Ethylenediaminetetraacetic acid
EGF	Epidermal growth factor
EGFR	Epidermal growth factor receptor

EGTA	Ethylene glycol-bis (β-aminoethyl ether)-N,N,N',N'-tetraacetic acid
ELISA	Enzyme-linked immunosorbent assay
EphR B6	Ephrin receptor B6
Erbb2	Erb-B2 receptor tyrosine kinase 2
Erk1/2	Extracellular signal-regulated kinase 1/2
FBS	Fetal bovine serum
FDS	False discovery rate
FGF1	Fibroblast growth factor 1
FGFR1	Fibroblast growth factor receptor 1
FTMS	Fourier transform mass spectrometry
g	Gram
g	Gravity
GAP	GTPase-activating protein
GDP	Guanosine diphosphate
GFP	Green fluorescent protein
GO	Gene ontology
Grb2	Growth factor receptor bound protein 2
Grb10	*Growth factor receptor bound protein 10*
Grb10	Growth factor receptor bound protein 10
GTP	Guanosine-5'- triphosphate
HCL	Hierarchical clustering
H&E staining	Haemotoxylin and Eosin staining
HEK293	Human embryonic kidney 293
HGFR	Hepatocyte growth factor receptor
HPLC	High-performance liquid chromatography
h/hr	Hour
HRP	Horseradish peroxidase
IF	Immunofluorescence
IGF1	*Insulin-like growth factor 1*

IGF1R	*Insulin-like growth factor 1 receptor*
IGF2	*Insulin-like growth factor 2*
IGF2R	*Insulin-like growth factor 2 receptor*
IGF1	Insulin-like growth factor 1
IGF1R	Insulin-like growth factor 1 receptor
IGF2	Insulin-like growth factor 2
IGF2R	Insulin-like growth factor 2 receptor
IHC	Immunohistochemistry
Insr	*Insulin receptor*
IR	Insulin receptor
IP	Immunoprecipitation
IRS1/2	Insulin receptor substrate 1/2
ITMS	Ion trap mass spectrometry
kb	Kilobase
kDa	Kilodaltons
KO	Knockout
KRAS	Kirsten rat sarcoma GTPase
kV	Kilovolts
LB	Lysogeny broth
LC	Liquid chromatography
MAPK	Mitogen-activated protein kinase
MEF	Mouse embryonic fibroblast
MEK	MAPK/ERK kinase
mRNA	Messenger ribonucleic acid
MS	Mass spectrometry
MS/MS	Tandem mass spectrometry
ms	Millisecond
mTOR	Mammalian target of rapamycin
mTORC1	Mammalian target of rapamycin complex 1
m/z	Mass to charge ratio

MuSK	Muscle-specific Kinase
Nedd4	Neural precursor cell expressed developmentally down-regulated protein 4
NGS	Normal goat serum
PBS	Phosphate-buffered saline
PCR	Polymerase chain reaction
PCA	Principle component analysis
PDGF	Platelet derived growth factor
PDGFR	Platelet derived growth factor receptor
PDGFRa	Platelet Derived Growth Factor Receptor alpha
PDGFRb	Platelet Derived Growth Factor Receptor beta
PFA	Paraformaldehyde
PI3K	Phosphoinositide 3-kinase
PKA	Protein kinase A
PKC	Protein kinase C
pMEF	Primary mouse embryonic fibroblast
ppm	Parts per million
PTPRF	Protein tyrosine phosphatase, receptor type F
PVDF	Polyvinylidene fluoride
Ras	Rat sarcoma GTPase
RNA	Ribonucleic acid
RNAi	RNA interference
rpm	Revolutions per minute
RTK	Receptor tyrosine kinase
RT-qPCR	Reverse transcription quantitative polymerase chain reaction
S	Serine
SDS	Sodium dodecylsulphate
SDS-PAGE	Sodium dodecylsulphate polyacrylamide gel electrophoresis
SEM	Standard error of the mean
Ser	Serine

SH2	Src homology 2 domain
SH3	Src homology 3 domain
siRNA	Short interfering RNA
Src	Sarcoma GTPase
STAT3	Signal transducer and activator of transcription 3
T	Threonine
T25	25 cm^2 cell culture flask
T75	75 cm^2 cell culture flask
TACE	TNF-a converting enzyme
TBS	Tris-buffered saline
TBST	Tris-buffered saline with Tween-20
TEMED	N,N,N',N-tetramethylethylenediamine
TGFB	Transforming growth factor beta
Thr	Threonine
TMB	3,3′,5,5′-Tetramethylbenzidine
TMT	Tandem mass tag
TNFα	Tumour necrosis factor alpha
Tween-20	Polyoxyethylene sorbitan monolaureate
Tyr	Tyrosine
UTR	Untranslated region
VEGFR2	Vascular Endothelial Growth Factor Receptor 2
VEGFR3	Vascular Endothelial Growth Factor Receptor 3
WAT	White adipose tissue
WB	Western blotting
WT	Wild-type
Y	Tyrosine

Table of contents

List of Figures

List of Tables

Chapter 1

Introduction

1.1 Genomic Imprinting

Mammals inherit two gene copies from their parents, and the two parental genomes are expressed equally in the offspring based on Mendelian inheritance. However, Mendel's law is not applied to all the mammalian genes. A small group of genes called imprinted genes follow a parent-of-origin-specific expression pattern (Figure 1.1). In the case of imprinted genes, one gene copy from the paternal or maternal allele is suppressed by epigenetic modifications, such as DNA methylation and histone modification (Inbar-Feigenberg *et al*., 2013). So far, only about 150 imprinted genes have been identified in mouse among which less than half have been proved to exist in human (Bartolomei and Ferguson-Smith, 2011; Peters, 2014). Imprinted genes are usually found in clusters within the genome and controlled by a common imprinting control region (ICR). DNA methylation in the ICR plays an essential role in regulating the expression or suppression of genes within an imprinted gene locus (Barlow and Bartolomei, 2014). Imprinted genes attracted attention because many of them are widely expressed in the embryo and placenta (Fowden *et al*., 2011). Many of them are involved in prenatal and postnatal development, energy homeostasis, and some are involved in social behaviours (Garfield *et al*., 2011; Dent and Isles, 2014; Peters, 2014; Charalambous *et al*., 2012; Charalambous *et al*., 2014). Research predicted that more than 1000 gene loci are imprinted in mouse brain, but this prediction is currently lacking confirmation by biological experiments (Kelsey and Bartolomei, 2012). However, we could expect more imprinted genes than currently known might exist in mammalian genomes.

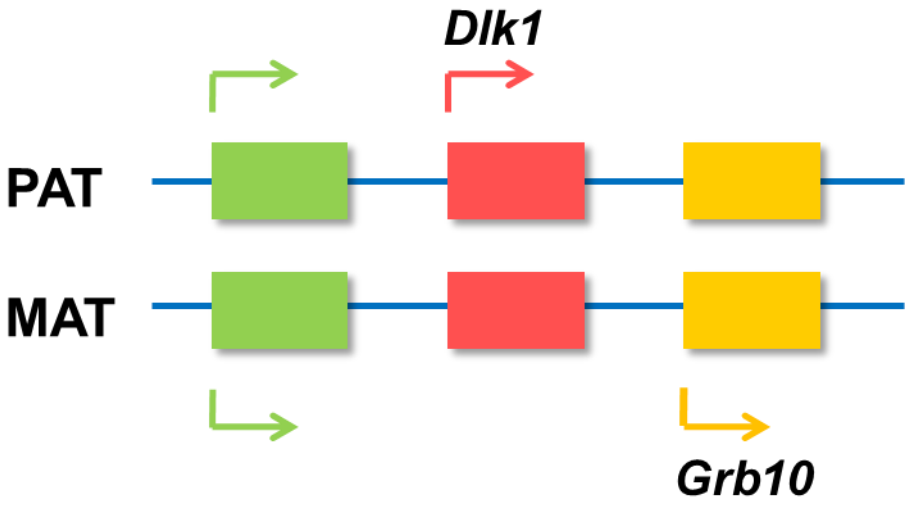

Figure 1.1 Parent-of-origin-specific expression of the imprinted gene. Coloured boxes represent genes and arrows indicated expressed allele. The green boxes and arrows represent the majority of mammalian genes, expressed from both parental alleles. *Delta-like 1* (*Dlk1*) and *growth factor receptor–bound protein 10* (*Grb10*) exemplify genes expressed from the paternally-inherited (PAT) and maternally-inherited (MAT) alleles, respectively.

The evolutionary benefits of imprinted gene expression are still under debated. For instance, genes with biallelic (non-imprinted) expression could better protect the genome from recessive mutations and deletions compared to imprinted genes (Holman and Kokko, 2014). So what can an imprinted gene benefit from their monoallelic expression? The widely accepted theory for genomic imprinting is the parent-offspring conflict hypothesis (Haig, 2014). This predicts that parental interests in the distribution of maternal resources to their offspring are different, at least in species where females may reproduce with more than one mate during their reproductive lifespan (Patten *et al*., 2014). Therefore, paternally-expressed genes tend to promote the allocation of maternal resources to the offspring, leading to the enhancement of fetal and placental growth, while maternally-expressed genes restrict it (Fowden *et al*., 2011). Arguably, the most compelling examples are the first two identified imprinted genes, *Insulin growth factor 2* (*Igf2*), encoding a paternally-expressed growth promoting ligand insulin growth factor 2 (IGF2)

and *Insulin growth factor 2 receptor* (*Igf2r*), which codes for a maternally-expressed cell surface receptor Insulin growth factor 2 receptor (IGF2R) that inhibits growth by targeting Igf2 for lysosomal degradation (Barlow *et al*., 1991; DeChiara *et al*., 1991; Nordin *et al*., 2014). No other antagonistic pair of imprinted genes has since been identified. A pair of oppositely imprinted genes, *Dlk1* and *Grb10*, may fit the bill since both genes code for cell signalling proteins, as paternally expressed *Dlk1* promotes while the maternally expressed *Grb10* restricts embryo growth (Madon-Simon *et al*., 2014). It may not be possible to explain the genomic imprinting evolution with one single theory, and some non-conflict hypotheses, such as co-adaptive gene evolution, were also used to demonstrate the genomic imprinting (Spencer and Clark, 2014; Wilkins, 2014). Further functional study of the identified imprinted genes will help us to understand the evolutionary basis and advantages of mammalian genomic imprinting.

1.2 *Dlk1* in mouse development

1.2.1 *Dlk1* expression in mouse and protein structure

The paternally-expressed imprinted gene *Dlk1* encodes delta-like 1 protein (Dlk1), also known as preadipocyte factor 1 (Pref-1) or fetal antigen 1 (FA1), which belongs to the epidermal growth factor-like (EGF-like) protein family that consists of Notch signalling receptors and ligands (Moon *et al*., 2002). *Dlk1* is widely expressed in most embryonic tissues, while its expression is limited to a few adult tissues, with the highest expression levels in pituitary and adrenal gland (Wang *et al*., 2006; Falix *et al*., 2012; Charalambous *et al*., 2014). This indicates a critical role of *Dlk1* in mouse early embryonic development. In particular, *Dlk1* is not expressed in adult adipose and muscle tissues, yet *Dlk1* does influence the adult adipose and muscle mass (Moon *et al*., 2002; Charalambous *et al*., 2014). Therefore, it can be predicted that *Dlk1* controls the postnatal body proportions (fat and lean mass ratio) through its actions in early embryonic development stage.

EGF-like proteins interact with each other through their EGF-like repeats and regulate cells to make fate decisions (Baladrón *et al*., 2005; Sánchez-Solana *et al*., 2011). However, Dlk1 is recognized as a non-canonical Notch ligand, lacking a Delta-Serrate-LAG-2 (DSL) domain which can directly interact with Notch receptors. Therefore, Dlk1 may not be the ligand of Notch receptors although it regulates Notch1 signalling through a negative feedback mechanism (Falix *et al*., 2012). Hence, identification of Dlk1 receptors and interacting proteins is essential to understand Dlk1 functions and mechanisms of action. Specifically, Dlk1 is a single transmembrane protein, containing a region of six N-terminal EGF-like repeats, a juxtamembrane domain, a transmembrane part and a cytoplasmic tail at the C-terminal (Figure 1.2) (Smas and Sul, 1993; Wang and Sul, 2006; Hudak and Sul, 2013). Dlk1 can be cleaved by TNF-a converting enzyme (TACE) at the juxtamembrane region, and the full length extracellular domain of Dlk1 (soluble Dlk1) containing the

juxtamembrane region (approximate 50 kDa) alone can account for the regulation of several differentiation processes (Smas *et al*., 1997; Wang and Sul, 2006; Andersen *et al*., 2013). The membrane bounded part of Dlk1 also possesses different cellular functions from the soluble Dlk1 (Mortensen *et al*., 2012; Traustadóttir *et al*., 2013; Shin *et al*., 2014).

Figure 1.2 Modular structure of Dlk1 protein. N, N-terminal; S, signal sequence; Green boxes (1-6) indicate the six EGF-like repeats. Jm, juxtamembrane domain; Tm, transmembrane domain (phospholipid cell membrane illustrated); Cy, cytoplasmic domain; C, C-terminal.

1.2.2 Biological functions of Dlk1

Dlk1 protein functions have been uncovered using several genetic mouse models. The first *Dlk1* knockout mice displayed significant embryo growth retardation (Moon *et al*., 2002). And the adult *Dlk1* knockout mice developed enlarged livers with higher lipid contents and increased adipose tissue mass, including white adipose tissue (WAT) and brown adipose tissue (BAT), compared to their wild type (WT) littermates (Moon *et al*., 2002). However, the obese phenotype was observed only in mice fed with a high fat diet (Moon *et al*., 2002). In addition, the higher adipose tissue mass was due to enlarged adipocyte cell size and not cell number (Moon *et al*., 2002). A second *Dlk1* knockout mouse model revealed that *Dlk1* was related to B cell development (Raghunandan *et al*., 2008). Moreover, our group has shown that the same *Dlk1* knockout mouse was born about 20% smaller and grew up with a greater fat mass content than WT littermates fed with a normal chow diet (Madon-Simon *et al*., 2014). Thirdly, conditional deletions of *Dlk1* in pancreas, pituitary and placenta did not compensate the phenotype from global knockout of *Dlk1*, suggesting that *Dlk1* controlled embryo growth through actions in multiple tissues (Appelbe *et al*., 2012).

In contrast, transgenic mice with overexpression of the ectodomain of Dlk1 (soluble Dlk1) in adipose tissue or liver both exhibited reduced adipose tissue mass and lower body weight in adults (Lee *et al*., 2003). Consistent with the results from *Dlk1* knockout mice, the decreased fat pad mass was related to smaller adipocyte cell size and not cell number (Moon *et al*., 2002; Lee *et al*., 2003). In addition, overexpression of soluble Dlk1 reduced the expression levels of some transcription factors, such as CCAAT/Enhancer Binding Protein Alpha (C/EBPα), associated with the inhibition of adipocyte differentiation (Lee *et al*., 2003). Furthermore, an endogenous *Dlk1* overexpression mouse model, overexpressing the whole Dlk1 protein, displayed reduced fat mass due to the smaller adipocyte cell size (Charalambous *et al*., 2014). However, endogenous *Dlk1* overexpression mice presented unchanged adipogenesis as no expression changes of adipose differentiation markers or mature adipocyte markers were found between the transgenic and WT mice (Charalambous *et al*., 2014). This *Dlk1* transgenic mouse model has enhanced insulin sensitivity and switches the energy source of muscle mass from glucose to fatty acids, potentially explaining the reduced fat mass (Charalambous *et al*., 2014). Hence, the membrane bound regions of Dlk1 may also be essential to the balance of adipocyte differentiation. It was reported that the membrane bound Dlk1 inhibited preadipocyte proliferation by altering the cell cycle, resulting in the inhibition of adipocyte differentiation (Mortensen *et al*., 2012; Traustadóttir *et al*., 2013). Despite the controversial influences of Dlk1 in adipogenesis. It can be concluded that Dlk1 plays critical roles in adipose tissue development through embryogenesis.

It is also clear that Dlk1 promotes skeletal muscle development. In *Dlk1* knockout mice, myogenic programming was inhibited along with altered expression levels of myogenic transcription factors. As a result, *Dlk1* null mice exhibited reduced muscle mass at 12 weeks old (Andersen *et al*., 2013). By

contrast, *Dlk1* ablation enhanced adult muscle regeneration by regulating the expression of myogenic markers (Andersen *et al*., 2013). Collectively, Dlk1 is a key factor in muscle development through embryogenesis and adult muscle regeneration (Andersen *et al*., 2013). So far, most of the Dlk1 studies in adipogenesis and myogenesis focus on the investigations at the transcriptional level. The upstream cell signalling events involving Dlk1 that control these transcriptional changes are not well understood.

A few Dlk1 studies in human have indicated similar functions to those defined from mouse models. Dlk1 expression level was reported to be increased in serum samples from obese patients, suggesting that Dlk1 might be used as a marker of human obesity (Chacón *et al*., 2008). Dlk1 levels in maternal serum collected during pregnancy was correlated with small-for-gestational-age (SGA) infants, and Dlk1 levels can be an indicator of healthy or pathological SGA infants (Cleaton *et al*., 2016). Dlk1 is also involved in negative feedback inhibition of human skeletal stem cell differentiation (Abdallah *et al*., 2004).

1.2.3 Potential Dlk1 signalling

As a member of EGF-like protein family, Dlk1 was considered to be involved in Notch signalling especially Notch1 receptor (Traustadóttir *et al*., 2016). Notch signalling pathway was found to be downregulated by Dlk1 in E16.5 embryos through comparison of WT and *Dlk1* null embryonic tissues by mRNA array. This study also provided evidence that Dlk1 can interact with Notch1 receptor through EGF repeat 5 and 6 domains of Dlk1, using a mammalian two-hybrid system (Traustadóttir *et al*., 2016). However, more *in vitro* and *in vivo* evidence is needed to confirm conclusively the direct interaction of Dlk1 and Notch1. Hence, Dlk1 may regulate downstream signals through Notch1 receptor dependent or independent pathways. Besides, Dlk1 may interact with itself, again as uncovered by experiments using a mammalian two-hybrid system, although cellular function of Dlk1 self-interaction has not yet been explored

(Traustadóttir *et al*., 2017). Furthermore, it has been found that Dlk1 inhibited preadipocyte differentiation via insulin/IGF signalling (Zhang *et al*., 2003; Tseng *et al*., 2005). Whereas Nueda and co-workers (2007) reported that Dlk1 promoted adipogenesis in the multi-potential mesenchymal cell line C3H10T1/2 through negatively regulating Notch 1 receptor. In mouse embryonic fibroblast (MEF) cell lines, Dlk1 was found to activate components of the Mitogen-activated protein kinase (MAPK) pathway and sox9 expression, leading to the inhibition of adipogenesis (Wang *et al*., 2010). These results suggested that the roles of Dlk1 in adipogenesis were cell type specific. In addition, Dlk1 has been shown to prevent chondrogenesis and adipogenesis in cell culture by inhibiting the Phosphoinositide 3-kinase/Protein kinase B (PI3K/Akt) pathway (Chen *et al*., 2011). It is not yet possible to identify the definitive Dlk1 pathways, in several biological processes, due to the lack in knowledges of Dlk1 interacting receptors and other signalling proteins.

Dlk1 is expressed from the paternal *Dlk1-Gtl2* locus while the corresponding maternal *Dlk1* allele is imprinted, and the *cis* locus expresses several non-coding miRNA (Qian *et al*., 2016; Serrano-Lopez and Cancelas, 2016; Schneider *et al*., 2016). Strikingly, Qian and colleagues recently reported that miRNAs expressed from the maternal *Dlk1-Gtl2* locus could block multiple components of Akt mediated mammalian target of rapamycin (mTOR) pathway, maintaining the quiescence of fetal liver hematopoietic stem cells (HSCs) and long-term HSCs derived from adult mouse liver (Qian *et al*., 2016). However, the direct interactions between Dlk1 and mTOR signalling on biochemical level are still unknown.

1.3 *Grb10* in mouse development

1.3.1 *Grb10* expression in mouse and protein structure

Unlike all other imprinted genes, *Grb10* has an unusual tissue specific expression pattern in mouse. Specifically, *Grb10* is paternally-expressed in embryonic CNS and adult brain, while maternal *Grb10* is broadly expressed in the embryo except in CNS tissues (Garfield *et al*., 2011). In adults, the maternal Grb10 expression is restricted to muscle, fat, pancreas, oviduct, uterine horn, testis *et al*, with the highest expression in pancreas and very low level in liver (Smith *et al*., 2007; Wang *et al*., 2007; Garfield *et al*., 2011; Cowley *et al*., 2014; Kabir and Kazi, 2014). So far, *Grb10* is the first identified imprinted gene which has varied imprinted patterns for the paternal and maternal alleles, having separate functions in different tissues (Garfield *et al*., 2011; Plasschaert and Bartolomei, 2015).

Grb10 encodes the growth factor receptor–bound protein 10 (Grb10) which belongs to an adaptor protein family also including Grb7 and Grb14 (Holt and Siddle, 2005). Proteins of this family have similar structures containing an N-terminal proline-rich (P) region, a RAS-association-like binding (RA) domain, a pleckstrin homology (PH) domain, a between PH and SH2 (BPS) domain, and a Src homology 2 region (SH2) domain at the C-terminal end (Figure 1.3) (Ceccarelli and Sicheri, 2009). Grb10 had the ability to bind to a variety of receptor tyrosine kinases (RTKs) through the SH2 domain, including insulin-like growth factor 1 receptor (IGF1R), platelet derived growth factor receptor (PDGFR), epidermal growth factor receptor (EGFR) and vascular endothelial growth factor receptor 2 (VEGFR2) (Wang *et al*., 1999; Murdaca *et al*., 2004; Plasschaert and Bartolomei, 2015). Particularly, Grb10 interacted with insulin receptor (IR) through the SH2 and BPS domains (Holt and Siddle, 2005). Based on *in vitro* studies, Grb10 can form protein complexes with Akt or neural precursor cell expressed developmentally down-regulated protein 4 (Nedd4) through the SH2 domain, and complex formation was associated with

phosphorylation, and also ubiquitination and degradation of IR and IGF1R (Jahn *et al*., 2002; Vecchione *et al*., 2003). Grb10 structural studies revealed that the RA-PH regions of Grb10 can physically bind to the Ras proteins, and this was supported by the *in vitro* study using mouse fibroblasts (Deng *et al*., 2008; Depetris *et al*., 2009).

Figure 1.3 Grb10 modular protein structure. P, proline-rich domain; RA, RAS-association-like binding domain; PH, pleckstrin homology domain; BPS, between PH and SH2 domain; SH2, Src homology 2 domain. Graph is modified from Holt and Siddle, 2005.

1.3.2 Biological functions of Grb10

Biological functions of *Grb10* have been discovered by using several *Grb10* knockout and overexpression mouse models developed by different groups. Maternal *Grb10* obeyed the parent-offspring conflict theory for imprinting evolution (Haig, 2014). Maternally expressed *Grb10* limited embryo and placental growth, since maternal *Grb10* knockout mice had a 25-30% larger body size than WT mice after birth (Charalambous *et al*., 2003; Charalambous *et al*., 2010; Madon-Simon *et al*., 2014). As adults, *Grb10* knockout mice had increased lean mass and reduced adipose mass, and this was associated with improved glucose handling and insulin sensitivity. These findings were reported by three groups using different *Grb10* knockout mouse lines (Smith *et al*., 2007; Wang *et al*., 2007; Madon-Simon *et al*., 2014). Conversely, *Grb10* transgenic mice were heavier than WT with enlarged fat tissues at 5 months old, including WAT and BAT (Liu *et al*., 2014). The combined evidence suggests that *Grb10* promotes adipose tissue growth and restricts muscle development. In addition, *Grb10* overexpression mice displayed retarded growth during postnatal development and insulin resistance, supporting the growth suppressor role of *Grb10* (Shiura *et al*., 2005). A fat tissue specific *Grb10* knockout mouse model provided further evidence for a role of *Grb10* in

adipogenesis, except that white adipose depots were significantly enlarged, as they were in *Grb10* knockout models, perhaps suggesting both direct and indirect effects on adipose development or homeostasis. *Grb10* deletion in fat tissue reduced the expression levels of lipolytic enzymes and fatty acid oxidation in BAT, leading to enhanced accumulation of lipid droplets in WAT and BAT (Liu *et al*., 2014). A possible reason for the converse phenotypes of global and conditional *Grb10* knockout mice might be that *Grb10* controls postnatal fat tissue formation through multiple tissues. Furthermore, conditional deletion or knockdown of *Grb10* in mouse pancreas revealed that *Grb10* inhibited pancreas and pancreatic b-cell development (Doiron *et al*, 2012; Zhang *et al*, 2012). Also, the pancreas-specific *Grb10* deletion enhanced the insulin sensitivity and glucose handling (Zhang *et al*., 2012; Ward, 2012). Two studies reported that the enlarged muscle tissue in neonatal and postnatal *Grb10* knockout mice displayed a higher proliferation rate of muscle stem cell and myofiber. *Grb10* was involved in proliferation and not the differentiation process, supporting an inhibitory role of *Grb10* in muscle development (Holt *et al*., 2012; Mokbel *et al*., 2014).

Grb10 alleles in mother and offspring acted in a coordinated manner to maximise offspring growth and physiology (Cowley *et al*., 2014). This was achieved by the maternal *Grb10* allele regulating nutrient supply to offspring through the placenta and mammary gland, while *Grb10* in offspring regulates demand for nutrients, at least during the postnatal suckling period in mouse (Cowley *et al*., 2014). The dual role for Grb10 in mother and offspring has been suggested to be the best example yet identified of co-adaptive gene evolution as the driving force for imprinted gene expression (Wolf, 2013; Cowley *et al*., 2014; Wilkins, 2014).

All of the above functions are associated with the maternal *Grb10* allele. It has been shown that *Grb10* is expressed in the developing and adult brain, but

exclusively from the paternal allele. Paternal knockout of *Grb10* has been associated with specific deficits in social dominance behaviour (Garfield *et al*., 2011).

1.3.3 Grb10 adaptor signalling

Grb10, as an adaptor, has the ability to recruit various signalling molecules through its multiple function domains (Figure 1.3). In particular, insulin receptor substrate 1/2 (IRS1/2) and Akt phosphorylation levels were reduced by *Grb10* overexpression in Chinese hamster ovary (CHO/IR) cells under insulin stimulation, suggesting a negative role of *Grb10* in insulin signalling (Wick *et al*., 2003). In mouse embryonic fibroblasts, Grb10 can bind to Nedd4 and then form a Grb10/Nedd4 protein complex, and the complex was involved in the IGF1R degradation and internalization through receptor multi-ubiquitination (Vecchione *et al*., 2003; Monami *et al*., 2008). These other studies supported the evidence that Grb10 negatively regulates IR and IGF1R signalling *in vitro* (Wick *et al*., 2003; Vecchione *et al*., 2003; Monami *et al*., 2008). Besides, a siRNA knockdown of endogenous *Grb10* in NIH 3T3 cells resulted in decreased IRS, Akt and extracellular signal regulated kinase 1/2 (Erk1/2) phosphorylation levels induced by insulin growth factor 1 (IGF1), further supporting the inhibitory role of Grb10 towards IGF signalling (Dufresne and Smith, 2005). By contrast, another study reported that Grb10 promoted VEGFR2 phosphorylation by binding to Nedd4 which caused ubiquitination and degradation of VEGFR2 in human embryonic kidney cells 293 (HEK293) cell line, uncovering a positive feedback to the RTK from Grb10 (Murdaca *et al*., 2004). Moreover, it was reported that prolonged insulin stimulation caused the IR degradation, and endogenous Grb10 was related to IR proteasome degradation following insulin treatment of Hela cells (Ramos *et al*., 2006). In addition, *in vivo* experiments provided evidence that Grb10 acted as a negative regulator of insulin sensitivity in muscle, fat and at the whole body level (Wang *et al*., 2007; Smith *et al*., 2007; Madon-Simon *et al*., 2014).

Specifically, *Grb10* knockout increased the IRS1, Akt and MAPK phosphorylation levels in muscle and fat tissues stimulated by insulin (Wang *et al*., 2007; Smith *et al*., 2007). Additionally, IGF injection activates a lower IRS1 and Akt phosphorylation level in adult muscle compared to insulin injection (Smith *et al*., 2007). Recently, Grb10 has been identified as the direct substrate of mammalian target of rapamycin complex 1 (mTORC1), and Grb10 phosphorylation by mTORC1 at the S501/503 sites leads to a negative feedback on mTORC1 and IR/IGF1R *in vitro* and *in vivo* (Hsu *et al*., 2011; Yu *et al*., 2011; Liu *et al*., 2014). These studies filled the gap between insulin and mTOR signalling in which Grb10 acted as a key negative regulator (Yea and Fruman, 2011; Liu and Liu 2014). Furthermore, global loss of *Grb10* in mouse enhanced the hematopoietic stem cell proliferation through activation of Akt/mTORC1 pathway (Yan *et al*., 2016). Collectively, Grb10 might be an essential signal regulator of mTOR pathway.

It was well established that Grb10 negatively regulate Insulin/IGF signalling *in vitro* and *in vivo* (Desbuquois *et al*., 2013). Yet it is unlikely that Grb10 is involved in the growth through Insulin/IGF signalling. Insulin signalling was known to have little effects on growth (Desbuquois *et al*., 2013; Plasschaert and Bartolomei, 2015). By contrast, IGF signalling was the major fetal growth regulatory pathway in mouse (Peters, 2014). Especially, the paternally expressed *Igf2* and maternally expressed *Igfr2r* established the first growth-regulatory axis involved in imprinting in mammals (Baker *et al*., 1993; Lau *et al*., 1994; Wang *et al*., 1994). However, *Grb10* and *Igf2* double knockout mice exhibited distinguishable phenotypes from either *Grb10* or *Igf2* single knockout mice, suggesting that *Grb10* regulated embryo growth independently from *Igf2* (Charalambous *et al*., 2003). Moreover, the epistasis tests of *Grb10* against *Igf1r* and *Insr* knockout mice revealed that *Grb10* acts primarily on growth independently of *Igf1r* and *Insr* (Charalambous *et al*., 2003), although *Grb10* had high affinity for *Igf1r* and even higher for *Insr* (unpublished data). All

Grb10 epistasis tests suggest that Grb10 is a growth regulator independent of Insulin/IGF signalling. Consequently, little is known about the upstream or downstream effectors of Grb10 involved in the regulation of growth.

1.4 Antagonistic roles of Dlk1 and Grb10 in mouse development

Many of Dlk1 and Grb10 functions are well illustrated in mouse by *Dlk1* and *Grb10* knockout models. The main phenotypes of *Dlk1* and *Grb10* knockout mice are listed and compared below (Figure 1.4). Dlk1 and Grb10 each form a link between disrupted growth in early life and physiological changes in later life, particularly altered body composition (lean/adipose tissue proportions) and glucose-regulated metabolism, suggesting both may be key genetic factors in the developmental programming of life-long health (Moon *et al*., 2002; Charalambous *et al*., 2003; Smith *et al*., 2007; Wang *et al*., 2007; Charalambous *et al*., 2014; Madon-Simon *et al*., 2014). Although this programming phenomenon is well established there is essentially no understanding of the underlying mechanism. The $Dlk1^{+/p}$ and $Grb10^{m/+}$ mice are proposed to be the first genetic models for developmental programming. This project will test that Dlk1 and Grb10 act antagonistically through a common pathway on the biochemical level using *Dlk1* and *Grb10* single and double knockout mouse models.

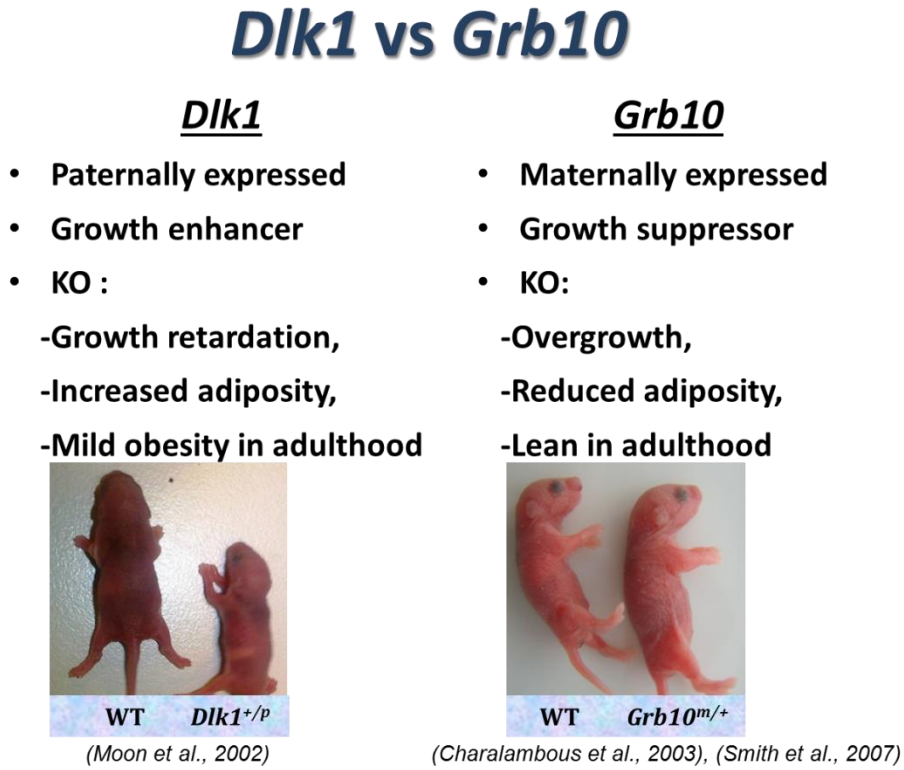

Figure 1.4 Antagonistic functions of *Dlk1* and *Grb10* in embryonic growth and adult body composition. Knockout phenotypic features summarised from (Moon *et al*., 2002; Charalambous *et al*., 2003; Smith *et al*., 2007; Madon-Simon *et al*., 2014).

Crosses of *Dlk1*$^{+/p}$ and *Grb10*$^{m/+}$ mice indicated that double knockout mice had a phenotype very similar to that of *Grb10* single knockouts prenatally and postnatally. This indicated that *Dlk1* and *Grb10* play antagonistic roles in mouse development in a common genetic pathway (Figure 1.5). Furthermore, Dlk1 acted upstream, as an inhibitor of Grb10, which in turn is an inhibitor of growth (Madon-Simon *et al*., 2014). Currently, the biochemical interactions between Dlk1 and Grb10 proteins remain undefined. Studies of mTOR provided a potential link between the two factors. Two groups using phopho-proteomics approaches found that Grb10 was a direct substrate of mTORC1 negatively regulating mTOR and IGF/IR signalling *in vitro* (Hsu *et al*., 2011; Yu *et al*., 2011). Another group uncovered that Grb10 controlled adipogenesis and thermogenesis through a negative feedback to mTORC1 signalling *in vivo* (Liu *et al*., 2014). By contrast, miRNAs expressed from the

paternal *Dlk1-Gtl2* locus negatively regulated the mTOR pathway in HSCs (Qian *et al*., 2016). Paternal *Dlk1* expression also can be affected by the miRNAs expressed from the maternal *Dlk1-Gtl2* locus (Charalambous *et al*., 2012). Therefore, Dlk1 may be involved in mTOR signalling activity directly or indirectly. Collectively, these studies suggested that Dlk1 and Grb10 possibly control growth, metabolism or some other biological processes by regulating the mTOR pathway. Do Dlk1 and Grb10 interact via mTOR signalling or any other signal pathways during developmental programming? Can further signalling changes be detected in *Dlk1* and *Grb10* knockout mice using an unbiased approach? The large-scale quantitative proteomics could be used for in-depth study of Dlk1 and Grb10 signalling. The investigation will contribute to our understanding of Dlk1 and Grb10 functions, mammalian development as well as imprinted gene evolution.

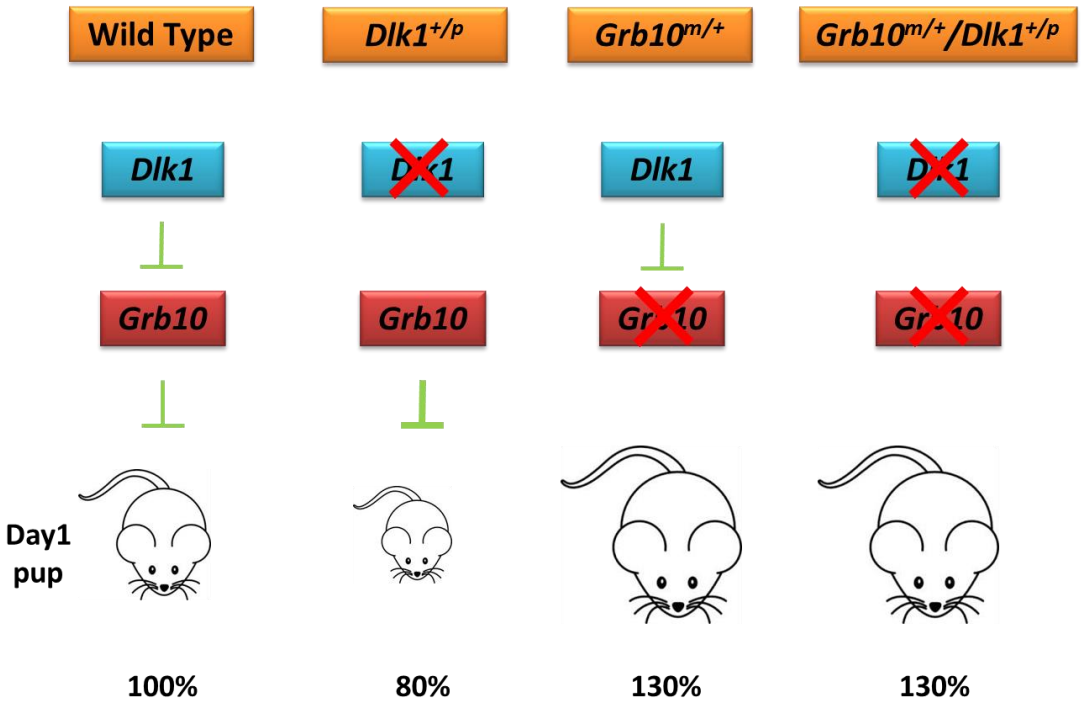

Figure 1.5 Evidence that *Dlk1* and *Grb10* regulate mouse embryonic growth in a common genetic pathway. Figure is modified from Madon-Simon *et al*., 2014.

1.5 TMT quantitative proteomics

Evidence from our laboratory indicates that the oppositely imprinted *Dlk1* and *Grb10* genes control the mouse fetal growth antagonistically through a common genetic pathway (Madon-Simon *et al*., 2014). Dlk1 and Grb10 protein expression levels were reciprocally affected by disruption of each other in pMEFs and livers derived from E14.5 (Chapter 3). However, the signalling pathways involving Dlk1 and Grb10 in regulation of mouse development are still unknown. An in-depth study of the functions and cross talk between Dlk1 and Grb10 on the embryonic level is needed to understand their roles in mouse growth and development, including mechanisms of adipogenesis and myogenesis. The new isobaric tandem mass tag (TMT) reagents and improvements in quantitative proteomics currently allow the labelling of up to ten samples in a single analysis. This allowed comparison of two biological replicates each of E14.5 pMEF and liver samples of the four genotypes, WT, $Dlk1^{+/p}$, $Grb10^{m/+}$ and $Grb10^{m/+}/Dlk1^{+/p}$. The proteomes and phosphoproteomes from WT, $Dlk1^{+/p}$, $Grb10^{m/+}$ and $Grb10^{m/+}/Dlk1^{+/p}$ E14.5 pMEFs and livers were analysed and compared. The candidate signal pathways and proteins associated with Dlk1 and Grb10 may be revealed by bioinformatics analyses, including principle component analysis (PCA), Gene ontology (GO)-term enrichment and clustering.

1.6 Aims

In this work, WT, *Dlk1*$^{+/p}$, *Grb10*$^{m/+}$ and *Grb10*$^{m/+}$/*Dlk1*$^{+/p}$ knockout mice (Raghunandan *et al*., 2008; Garfield *et al*., 2011) were used to provide whole liver tissue and to derive embryonic day 14.5 (E14.5) primary mouse embryonic fibroblasts (pMEFs) as *in vivo* and *in vitro* models, respectively.

The aim was to address the following questions:

1. What are the phenotypic differences of WT, *Dlk1*$^{+/p}$, *Grb10*$^{m/+}$ and *Grb10*$^{m/+}$/*Dlk1*$^{+/p}$ mice at E14.5 and 6-month of age?
2. Do Dlk1 and Grb10 proteins affect the expression of each other in E14.5 embryonic cells and tissues?
3. How is Dlk1 and Grb10 downstream signal activity, including Akt, Erk1/2 and mTOR, altered in *Dlk1*$^{+/p}$, *Grb10*$^{m/+}$ and *Grb10*$^{m/+}$/*Dlk1*$^{+/p}$ mice?
4. Can further Dlk1 and Grb10 signalling components be discovered by comparing the proteomes and phosphoproteomes of E14.5 WT, *Dlk1*$^{+/p}$, *Grb10*$^{m/+}$ and *Grb10*$^{m/+}$/*Dlk1*$^{+/p}$ pMEFs and livers?
5. Can candidate genes or pathways identified using proteomics analyses be validated, for example, by western blotting?

Chapter 2

Materials and Methods

2.1 Materials

All chemicals used in this study were purchased from Sigma-Aldrich (Gillingham, UK) or Fisher Scientific (Loughborough, UK) unless stated otherwise.

2.1.1 Mice

In *Dlk1* knockout mice, the promoter and first three exons of paternal *Dlk1* allele were deleted and replaced with a neomycin resistance cassette (*neo*^{r}) (Raghunandan *et al*., 2008). To generate *Grb10* knockout mice, a *LacZ:neomycin*^{r} gene-trap cassette was inserted and replaced an 11bp fragment of *Grb10* exon 8 (Garfield *et al*., 2011). Those mouse stains were maintained on a C57BL/6xCBA mixed inbred genetic background. Only *Grb10*$^{+/p}$ females were used to cross with *Dlk1*$^{+/p}$ or WT males to produce *Grb10*$^{m/+}$ and *Grb10*$^{m/+}$/*Dlk1*$^{+/p}$ mice. *Dlk1*$^{+/p}$ mice used in this study were generated by crossing *Dlk1*$^{+/p}$ males with WT or *Grb10*$^{+/p}$ females. Note that, due to the opposite imprints of the two genes, this heterozygote cross produces WT, *Dlk1*$^{+/p}$, *Grb10*$^{m/+}$ and *Grb10*$^{m/+}$/ *Dlk1*$^{+/p}$ offspring in a 1:1:1:1 ratio (Figure 2.1). Offspring with the *Dlk1*$^{+/p}$ and *Grb10*$^{m/+}$ heterozygous mutations are functionally null for those respective genes.

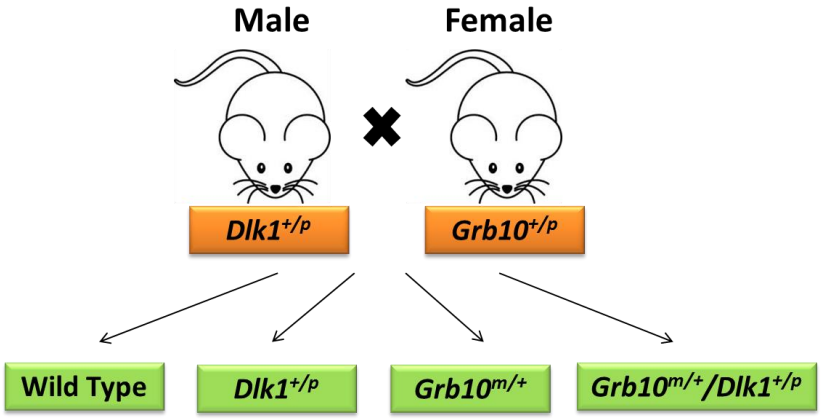

Figure 2.1 Breeding schema for generation of *Dlk1* and *Grb10* single and double knockout mice. *Dlk1*$^{+/p}$ males and *Grb10*$^{+/p}$ females were crossed to produce offsprings.

Mice were kept with a 13 h of light and 11 h of dark cycle. Temperature and humidity were set as 21°C ± 2°C and 55 ± 10%, respectively. Mice were maintained with food (CRM formula, Special Diets Services, UK) and water available *ad libidum*. Ventilated cages were used to house the mice. Two to six mice were kept in each cage. Mice were weaned and ear clipped at 21 days or a few days later. Adult mice were culled by cervical dislocation. E14.5 embryos were immersed in ice cold PBS for at least 5 min for the confirmation of death. All the procedures were in accordance with Schedule 1 of the UK Home Office regulations.

2.1.2 Buffers

PBS pH7.2

154 mM NaCl, 12.5 mM $Na_2HPO_4.12H_2O$.

1X TAE buffer

2 M Tris.Cl, 50 mM Ethylenediaminetetraacetic acid (EDTA), 5.7% (v/v) acetic acid

TBS pH7.5

10 mM Tris.Cl, 154 mM NaCl.

TBST pH7.5

10 mM Tris.Cl, 154 mM NaCl, 0.1% (v/v) Tween-20.

Lysis buffer

10 mM Tris.Cl, pH7.6, 5 mM EDTA, 1 mM Ethylene glycol-bis (β-aminoethyl ether)-N,N,N',N'-tetraacetic acid (EGTA), 50 mM NaCl, 30 mM sodium pyrophosphate, 50 mM NaF, 100 µM sodium orthovanadate, 1% (v/v) Triton X-100, 1 mM Diothiothreitol (DTT), and a protease inhibitor tablet (Roche, West Sussex, UK).

3X Sample buffer

30 mM Tris.Cl pH6.8, 1% SDS, 5% Glycerol, 100 mM DTT, 0.05% Bromophenol blue.

Sodium dodecylsulphate polyacrylamide gel electrophoresis (SDS-PAGE) running buffer

25 mM Tris.Cl, 0.2 M glycine, 0.1% (w/v) Sodium dodecylsulphate (SDS).

SDS-PAGE wet transfer buffer

25 mM Tris.Cl, 0.2 M glycine, 20% (v/v) methanol.

SDS-PAGE blocking buffer

5% (w/v) dried skimmed milk powder or 5% (w/v) bovine serum albumin (BSA) in TBS-Tween.

Antigen retrieval solution pH6.0

0.173 g citric acid, 4.1 ml 1 M sodium citrate, 495.9 ml Milli-Q (MQ) water.

2.1.3 Antibodies

Details of the primary and secondary antibodies used for Western blotting (WB) and Immunoprecipitation (IP) in this study, including working dilutions, are listed in Table 2.1. Antibodies were diluted in SDS-PAGE blocking buffer.

A

Antibody	Epitope	Species	Supplier	Code	Dilution
Akt	Total	Mouse mAb	CST	2920	1:2000
Akt	p-Ser473	Rabbit mAb	CST	4060	1:2000
Dlk1	Total	Goat pAb	R&D	AF8277	1:1000
Erbb2	Total	Mouse mAb	Thermo	MA5-13105	1:200
Erk1/2	Total	Rabbit mAb	CST	9102	1:1000
Erk1/2	p-Thr202 & p-Tyr204	Mouse mAb	Sigma	M9692	1:4000
FGFR1	Total	Rabbit mAb	CST	9740	1:500
GAPDH	Total	Mouse mAb	Proteintech	60004-1	1:5000
GAPDH	Total	Rabbit mAb	CST	2118	1:10000
Grb2	Total	Rabbit mAb	CST	3972	1:500
Grb10	Total	Rat pAb	Monash	N/A	1:250
IRb	Total	Mouse mAb	CST	3020	1:500
p70 S6K	Total	Rabbit mAb	CST	2708	1:1000
p70 S6K	p-Thr389	Rabbit mAb	CST	9234	1:1000
PI3K p85	Total	Rabbit pAb	UBI	06-195	1:500
PDGFRa	Total	Rabbit mAb	CST	3174	1:500
PDGFRb	Total	Mouse mAb	CST	3175	1:500
Tyrosine	p-Tyr-100	Mouse mAb	CST	9419	1:20

B

Antibody	Supplier	Code	Dilution
HRP Goat anti-rabbit	Vector	PI-1000	1:5000
HRP Goat anti-mouse	Vector	PI-2000	1:5000
HRP Goat anti-rat	Vector	PI-9401	1:5000
IRDye 800CW Donkey anti-mouse	LI-COR	926-32212	1:10000
IRDye 800CW Goat anti-rat	LI-COR	926-32219	1:10000
DyLight 680 conjugated goat anti-rabbit	CST	5366	1:15000

Table 2.1 Primary and secondary antibodies used for WB and IP. Antibody clones, supplier, product information and working dilution are listed in columns from left to right. mAb, monoclonal antibody; pAb, polyclonal antibody; HRP, Horseradish peroxidase; BL, Bethyl Laboratories, Montgomery, US; CST, Cell Signaling Technology, Hitchin, UK; LI-COR, LI-COR Biosciences, Cambridge, UK; Monash, Monash University, Melbourne, Australia; R&D, R&D Systems, Abingdon, UK; Sigma, Sigma-Aldrich, Gillingham, UK; Thermo, Thermo Fisher Scientific, Gillingham, UK; UBI, Upstate Biotech Incorporated, New York, US; Vector, Vector Laboratories, Peterborough, UK. **A)** Table of primary antibodies. **B)** Table of secondary antibodies.

2.1.4 Growth factors and inhibitors

All the growth factors and inhibitors used in cell culture are listed in Table 2.2. Regulators were diluted in pre-warmed Dulbecco's Modified Eagle's medium (DMEM) to the listed concentrations.

A

Recombinant cell signal proteins	Supplier	Code	Concentration
Recombinant Murine PDGF-AA	Peprotech	315-17	30 ng/ml
Recombinant Murine PDGF-BB	Peprotech	315-18	30 ng/ml
Recombinant Murine EGF	Peprotech	315-09	100 ng/ml
Recombinant Murine FGF1	Peprotech	450-33A	10 ng/ml
Recombinant Mouse IGF1	Sigma	I8779	50 ng/ml
Insulin from bovine pancreas	Sigma	I6634	20 nM

B

Inhibitors	Supplier	Code	Concentration
Rapamycin	Selleckchem	S1039	100 nM
Torin1	Selleckchem	S2827	250 nM
CHX	Sigma	C1988	10 ug/ml

Table 2.2 Regulators and inhibitors used in this study. Regulators, product supplier, product information and working concentration are listed in columns from left to right. Peprotech, London, UK; Sigma, Sigma-Aldrich, Gillingham, UK; Selleckchem, Houston, US. **A)** Regulators used in cell culture experiments. **B)** Inhibitors used in cell culture experiments.

2.2 Methods

2.2.1 Genotyping

Ear clips of adult mice and tails of E14.5 embryos were used for genotyping. Crude DNA were extracted from each ear clip or tail by adding 600 μl fresh 100 mM NaOH in an 1.5 ml microfuge tube with a pierced lid. NaOH solution was heated by immersing the lower part of tubes in boiling water for 10 min. Then 100 μl 1 M Tris-HCl (pH8) was added to each tube after cool down. The solution was stored at -20°C, and 1 μl was used as the DNA template for polymerase chain reaction (PCR). *Dlk1* and *Grb10* genotyping was carried out separately with either *Dlk1* primers (Dlk1 5'-CCA AAT TGT CTA TAG TCT CCC TC-3', Neo 5'-CAT CTG CAC GAG ACT AGT G-3', Screen 5'-CTG TAT GAA GAG GAC CAA GG-3') or *Grb10* primers (Grb10F 5'-CCA AGT GGA GAG TAC CAT GCC-3', Grb10R 5'-TCA CCT GAC AGG CAC CTC CCC-3' and βgeoR2 5′-CTT CCG CTT AGT GAC AAC G-3′) (Raghunandan *et al*., 2008; Garfield *et al*., 2011). *Dlk1* primers generated a 414 bp band for WT and a 495 bp band for mutant alleles (Raghunandan *et al*., 2008). *Grb10* primers yielded a 393 bp band for WT and a 177 bp band for mutant alleles. All PCR reactions were done with 7.5 μl 2X GoTaq Green Maser Mix (Promega, Southampton, UK), 0.75 μl *Dlk1* or *Grb10* primers (6 pmol/μl), 5.75 μl MQ water, and 1 μl DNA

template using a BioRad T100 PCR machine (BioRad, Hemel Hempstead, UK).

Dlk1 genotyping PCR reaction was performed with denaturation at 95°C for 2 min, 40 annealing cycles (94°C for 30 sec, 57°C for 30 sec, and 72°C for 45 sec), and elongation at 72°C for 3 min. *Grb10* genotyping PCR reaction was carried out with denaturation at 95°C for 2 min, 30 annealing cycles (95°C for 30 sec, 60°C for 30 sec, and 72°C for 45 sec), and elongation at 72°C for 3 min. 2.5% (w/v) electrophoresis gels were used for *Dlk1* and *Grb10* genotyping. Agarose (Invitrogen, Gillingham, UK) was dissolved in 1X TAE buffer heated by a microwave oven for 2 min. 2 μl ethidium bromide (Sigma, Gillingham, UK) was added to each 100 ml melted gel solution cooled to approximately 60°C. The gel was cast with wells at one end such that 15 μl PCR product could run alongside 6 μl of a 1kb DNA ladder (Promega, Southampton, UK) using 1X TAE buffer in an Wide Mini-sub Cell GT electrophoresis tank (BioRad, Hemel Hempstead, UK). Bands were separated by electrophoresis using a power source (BioRad PowerPac 300, Hemel Hempstead, UK) running at 80 V for 35 min (*Dlk1*) and 80 V for 45 min (*Grb10*). Gels were visualized using UV light transilluminator and pictures were taken with a ChemiDoc-It^2 Imager (UVP, Cambridge, UK).

2.2.2 Body composition assay

Body mass and compositions of mice at 6 months old were measured and recorded. Body mass was measured by an electronic scale. Body composition assay including fat and lean mass were performed using a Mini-spec body composition analyser (Bruker, Coventry, UK) according to the manufacturer's instructions. Briefly, the mouse was restrained in a glass tube that was inserted into the body composition analyser for a whole body scan, lasting about 1 min. Once the scan was finished, the mouse was returned to the cage immediately.

2.2.3 Preparation of E14.5 pMEFs and livers

The whole uterus of a 14.5-day pregnant mouse was dissected out and immersed in cold 0.1% PBS for at least 5 min. Then individual embryos were separated from their placentae and the yolk sac was peeled from each embryo. After being dried and weighted, a portion of the tail from each embryo was dissected and stored at -20°C for genotyping, and then each E14.5 embryo was kept in 1 ml pre-warmed DMEM medium. Each embryo was decapitated and eviscerated, and the liver was collected and stored at -80°C. The rest of the embryo was minced using a pair of scissors. 3 ml 0.25**%** (w/v) Trypsin-EDTA solution (Sigma, Gillingham, UK) was added to the mince in a 15 ml Falcon tube and incubated at 37°C for 20 min. Then another 3 ml 0.25**%** Trypsin-EDTA solution was added to each tube and incubated at 37°C for another 20 min. To stop the trypsinization, 6 ml complete medium (DMEM medium, 10% (v/v) fetal bovine serum (FBS) (Gibco, Gillingham, UK), 1% (v/v) streptomycin (1000 U)/penicillin (10 mg/ml) (Sigma, Gillingham, UK), and 1 mM L-glutamine (Sigma, Gillingham, UK)) was added to each tube. Tissue and medium mixture was mixed well by hand then span down in a ALC PK110 centrifuge (Thermo Scientific, Gillingham, UK) at 180 *g* for 5 min. Cell pellets were mixed with 12 ml pre-warmed complete medium and cultured in a T75 tissue culture flask (Fisher Scientific, Loughborough, UK) as passage 0 (P0). Flasks were incubated for 24-48 h at 37°C with 5% CO_2. This method was modified from Takahashi and Yamanaka (2006).

2.2.4 Maintenance of E14.5 pMEFs

E14.5 pMEFs were cultured with 7 ml or 12 ml complete medium in T25 or T75 tissue culture flasks, respectively. Cells were washed twice with 0.1% PBS (1 ml/25 cm^2), pre-warmed to 37°C, and replenished with pre-warmed complete medium every 48-72 h. Cell splitting was carried out when cells reached about 80% confluence, as judged by eye. Medium was removed through a glass

pipette (Fisher Scientific, Loughborough, UK) by an aspirator (Welch Vacuum, Ilmenau, Germany), and then washed with 0.1% PBS (1 ml/25 cm^2) twice. 1 ml/25 cm^2 0.25**%** Trypsin-EDTA solution was added to the flasks and incubated at 37°C for 5 min. Flasks were given a slap on the side to dislodge the cells from the bottom. Then, twice volume of complete medium was added to the flask to stop the trypsin reaction. Cell suspension was separated evenly to three flasks.

To freeze the pMEFs, cell suspension was transferred to a 15 ml Falcon tube and centrifuged at 120 *g* for 4 min. Cell pellets were re-suspended in 900 µl FBS and transferred to a Cryo-Tube vial (Fisher Scientific, Loughborough, UK). Then 100 µl Dimethyl sulphoxide (DMSO) was added to each vial. Vials were placed in a tissue-padded polystyrene box, filled with isopropanol, and placed at -80°C overnight. The next day vials were moved to liquid nitrogen for long term storage. Frozen cells were thawed rapidly by placing Cryo-Tube vials in a water bath at 37°C. Once melted, cell suspension was added to 5 ml pre-warmed DMEM and then centrifuged at 180 *g* for 4 min. Cell pellets were re-suspended in 12 ml complete medium and transferred to a T75 flask. Flasks were placed in the 37°C incubator and cells allowed to attach for 4-6 h prior to a change of medium.

2.2.5 Stimulation and inhibition of E14.5 pMEFs

E14.5 pMEFs were cultured in 6-well cell culture plates, T25 flasks, T75 flasks or 10cm cell culture dishes (Fisher Scientific, Loughborough, UK) until the cell confluence was higher than 80% for stimulation or inhibition experiments. Cells were washed twice with pre-warmed 0.1% PBS and then this was replaced with pre-warmed DMEM medium which contained 1% (v/v) streptomycin (1000 U)/penicillin (10 mg/ml) and 0.1% (w/v) BSA for overnight serum starvation. On the following day, cells were treated with 10% pre-warmed FBS or different regulators following the concentrations listed in Table 2.2 as described before.

Cells were incubated with the regulators for sampling at different time points, varying from 5 min to 48 h.

2.2.6 Total protein extractions from E14.5 pMEFs and livers

To extract total proteins from E14.5 pMEFs, 60 µl or 100 µl lysis buffer was added to each well in a 6-well plate or T25 flask. All reactions were stopped simultaneously by washing with cold 0.1% PBS twice, and then lysis buffer was added. The plate or flask was rotated briefly to ensure all cells had been exposed to the buffer. Then a cell scraper (Fisher Scientific, Loughborough, UK) was used to remove the cells from the base into the lysis buffer. The scraper was washed in PBS between wells or flasks. Cell lysates were transferred to ice cold 1.5 ml microfuge tubes and incubated on ice for 20 min with vortex mixing every 5 min. Tubes were centrifuged at 14769 *g* for 10 min in a Biofuge Primo R centrifuge pre-chilled to 4°C (Thermo Scientific, Gillingham, UK). The supernatants were transferred to a fresh tube and stored at -80°C. E14.5 livers were weighted and recorded, and then 5x volumes of lysis buffer were added to each liver sample. The mixtures were transferred to a Precellys lysing tube (Bertin, Montigny-le-Bretonneux, France) and homogenized 3 times for 15 sec using a Minilys personal homogenizer (Bertin, Montigny-le-Bretonneux, France). Then cell suspensions were moved to a 1.5 ml microfuge tube and centrifuged at 14769 *g* for 10 min in a Biofuge Primo R centrifuge pre-chilled to 4°C (Thermo Scientific, Gillingham, UK). Supernatants were collected and stored at -80°C.

2.2.7 Protein concentration bicinchoninic acid (BCA) assay

BSA solutions with known concentrations ranged from 0 to 2 mg/ml were used to plot the standard curve. Protein concentrations were measured by mixing 10 µl lysate or BSA solution with 200 µl BCA protein assay working reagent (Fisher Scientific, Loughborough, UK) in a clear bottom 96-well microplate (Fisher Scientific, Loughborough, UK) according to the manufacturer's

instructions. Plates were incubated at 37°C for 30 min and then cooled to room temperature. Absorbance at 560nm was read using a Modulus^{TM} microplate multimode reader (Turner Biosystems, Sunnyvale, US). A standard curve based on BSA solution with known concentration was plotted in Excel. Unknown sample concentration was determined by fitting to the standard curve.

2.2.8 Sodium dodecylsulphate polyacrylamide gel electrophoresis (SDS-PAGE)

To denature proteins, lysate from E14.5 pMEF or liver sample was mixed with 3X sample buffer or commercial 5X sample buffer (National Diagnostics, Nottingham, UK) in a pierced 1.5 ml microfuge tube. Then sample tubes were held in boiling water for 10 min. Samples were stored at -80°C and re-boiled for 2 min before use each time. 10% SDS-PAGE mini gels were used to run the SDS-PAGE WB. Each two resolving gels were made from 2.5 ml 1.5 M Tris.Cl (pH8.9), 3.3 ml 30% 37:1 acry:bis (National Diagnostics, Nottingham, UK), 4 ml MQ H_20, 200 µl 10% SDS, 67 µl Ammonium persulfate (APS), and 4 µl N,N,N',N-tetramethylethylenediamine (TEMED). Each two stacking gels consisted of 1.26 ml 0.5 M Tris.Cl (pH6.8), 0.8 ml 30% 37:1 acry:bis, 2.9 ml MQ H_20, 100 µl 10% SDS, 50 µl APS, and 5 µl TEMED. Commercial mini-PROTEAN TGX precast 10% gels were purchased from BioRad (BioRad, Hemel Hempstead, UK). 10-20 µg/well protein extracts were loaded onto gels alongside with 2 µl pre-stained DNA markers (NEB, Hitchin, UK). Gel eletrophoresis was carried out in SDS-PAGE running buffer using the Mini PROTEIN tetra system (BioRad, Hemel Hempstead, UK) at 200 V for 30-50 min until blue Bromophenol dye had run just off the end of the gel. Proteins were transferred from gels to polyvinylidene fluoride (PVDF) membranes (Millipore, Watford, UK) in SDS-PAGE transfer buffer using a Criterion Blotter wet transfer tank (BioRad, Hemel Hempstead, UK) at 100 V for 90 min. After transfer, membranes were washed with MQ water once and then blocked in

SDS-PAGE blocking buffer for 1 h with gentle shaking. Primary antibody incubation was performed at 4°C overnight. Membranes were incubated with secondary antibodies labelled with horseradish peroxidase (HRP) or fluorescent dyes for 1 h or 45 min at 4°C, respectively. Membranes were washed with 0.1% TBS/tween-20 for 3x 5 min before and after secondary antibody incubation. For enhanced chemiluminescence substrate (ECL) detection, 1 ml ECL detection reagent (Amersham, Buckinghamshire, UK) was poured on each 6x9 cm membrane and incubated at room temperature for 1 min. Chemiluminescence was detected using a Fusion SL Chemiluminescence System (Vilber, Marne-la-Vallée, France). For infrared fluorescence detection, membranes were scanned using an Odyssey CLx infrared imaging system (LI-COR Biosciences, Cambridge, UK) according to the manufacturer's protocol. Membrane stripping was carried out by serially incubating the membrane in MQ water, 200 mM NaOH, and MQ water for 5 min on a rocking platform at room temperature. Re-probing of the stripped membrane started from the blocking step. Quantitative analysis of protein bands on the blots was performed using software ImageJ 1.48v or Li-COR Image Studio ver 5.0.

2.2.9 Dlk1 sandwich enzyme-linked immunosorbent assay (ELISA)

WT, *Dlk1*$^{+/p}$, and *Grb10*$^{m/+}$ pMEFs were cultured in a 6-well plate until reaching about 80% confluence, and then cells were replaced with fresh complete medium once. Cell medium from each well was collected 24 h or 48 h later and kept in individual 2 ml microfuge tubes. A 6-well plate containing the same amount of medium and no cells was prepared as a blank control plate. Medium from *Dlk1*$^{+/p}$ pMEFs was used as a negative control. Medium from three wells of each sample were collected for Dlk1 ELISA. Dlk1 ELISA was carried out using an antibody specific to human Dlk1 (capture) and an antibody specific to mouse Dlk1 (detection), following with a HRP-conjugated anti-mouse secondary antibody incubation and 3,3′,5,5′-Tetramethylbenzidine (TMB)

detection. A Dlk1 standard curve was plotted using recombinant mouse Dlk1 protein with known concentration. Sample concentrations were determined by fitting TMB readings to the Dlk1 standard curve (Cleaton *et al.*, 2016). Medium samples were prepared and sent to Dr. Claire L Dent in Queen Mary University of London who carried out the Dlk1 sandwich ELISA.

2.2.10 Mouse phospho-receptor tyrosine kinase (RTK) array analysis

Mouse phospho-RTK array kit (R&D systems, Abingdon, UK) was used to perform the analysis according to manufacturer's instructions. 500 µg cell lysates from each sample were incubated with an array at 4°C overnight. An HRP-conjugated anti-mouse secondary antibody from the kit was used to detect the primary antibody on each array. After all the incubation and wash steps, 1 ml ECL detection reagent was poured on each array and incubated at room temperature for 1 min. Luminescence from secondary antibodies was on the array was detected by a Fusion SL Chemiluminescence System (Vilber, Marne-la-Vallée, France). Dot pixel intensities from each dot on each array were analysed using ImageJ 1.48v software.

2.2.11 Immunoprecipitation (IP)

MEFs were cultured in T75 flasks or 10cm dishes. After overnight serum starvation (see section 2.2.5), cells were treated with PDGF-AA/BB for 5 min or 30 min. Then 450 µl complete lysis buffer was added to each flask or dish. Cell lysates were vortexed for 2 min and then centrifuged at 12000 x g for 10 min at 4°C. Supernatants were transferred to a new tube. Protein concentrations were measured (see section 2.2.7) and equal amounts of total protein from each sample were incubated with an anti-phospho-tyrosine antibody conjugated sepharose beads at 4°C with rotation for overnight. Beads were washed with 500 µl lysis buffer three times before being incubated with protein lysates. The next day, lysate and bead mixtures were centrifuged at 12000 x g for 30 sec. Supernatants were discarded. And beads were washed

with 500 µl lysis buffer twice and 500 µl PBS three times. 20 µl 2X sample buffer were added to each sample and then boiled for 5 min. Samples left in each tube were loaded on to 10% protein gels for a subsequent Western blotting analysis (see section 2.2.8).

2.2.12 Tissue wax sectioning

E14.5 whole embryos after dissection were fixed in 4% PFA at 4°C overnight. Subsequently, embryos were washed with PBS once and stored in 70% ethanol at 4°C. In the Leica TP 1020 tissue processor (Leica Biosystems, Milton Keynes, UK), tissues were washed twice for 2 h in the following series of solutions: 70% ethanol, 90% ethanol, 100% ethanol, Histoclear (National Diagnostics, Nottingham, UK) and wax. Then tissues were embedded in pre-warmed wax and poured into plastic moulds to form blocks. Paraffin-embedded tissue blocks were cut using a Leica RM 2155 microtome (Leica Biosystems, Milton Keynes, UK) at 8 µm for each section and placed on polysine slides (Fisher Scientific, Loughborough, UK). Slides were incubated at 40°C overnight and then stored at 4°C.

2.2.13 Immunohistochemistry (IHC) of wax sections

Tissue sections were dewaxed in Histoclear twice for 10 min, rehydrated sequentially in 100% ethanol, 70% ethanol and 50% ethanol for 7 min, and washed with PBS with shaking for 5 min. Slides were immersed into antigen retrieval solution and boiled in a microwave oven for 20 min. After cooling to room temperature, sections were washed twice with PBS for 5 min. Before serum blocking, sections were separated from each other by drawing wax circles around them. Blocking was performed with 95 µl diluted normal goat serum (55 µl serum in 3.3 ml PBS) (CST, Hitchin, UK) on each section for 20 min at room temperature. Each section was incubated in 95 µl primary antibody at 4°C for 16-18 h. Following this, sections were washed with 0.25%

Triton X-100 (250 μl Triton X-100 in 100 ml PBS) and PBS with shaking for 5 min. Then sections were treated with goat biotinylated secondary antibody diluted in normal goat serum blocking solution for 30 min at room temperature and washed with 0.5% Triton X-100 (500 μl Triton X-100 in 100 ml PBS) and PBS with shaking for 5 min. Next, each section was incubated with 3% hydrogen peroxide, streptavidin-horseradish peroxidase complex (ABC kit, Vector Laboratories, Peterborough, UK) and diaminobenzidine (DAB kit, Vector Laboratories, Peterborough, UK) for 5 min, 30 min and 5 min, respectively. Sections were counterstained with Harris Haemotoxylin for 30 sec and then cleared and dehydrated in 1% HCl in 70% ethanol for 30 sec, 1% NH_3 in 70% ethanol for 1 min, 70% ethanol for 30 sec and Histoclear twice for 2 min each. Lastly, sections were mounted with DPX mounting medium and imaged under a Nikon E800 microscope and a Nikon digital Sight DS-U1 camera (Nikon, Kingston Upon Thames Surrey, UK) which were controlled using NIS Elements D 2.30 software.

2.2.14 Statistical analysis

GraphPad Prism 6 software was used to perform all statistical analyses except that of proteomics data. Standard error of the mean (SEM) and P values were calculated by the software and data was further analysed using either One-way ANOVA with Tukey's *post hoc* tests or Two-way ANOVA with Bonferroni post-tests or Unpaired t-test with two-tailed tests as indicated in the results. $P<0.05$ was considered as significant.

2.2.15 Sample preparation and labelling for tandem mass tag (TMT) quantitative proteomic analysis

TMT tag labelling and TMT proteomics analysis was performed by Dr Kate Heesom at the University of Bristol Proteomic Facility who also provided the methods in the following sections (2.2.17-2.2.18).

Tissues (pMEFs and livers) were derived from WT, *Dlk1*$^{+/p}$, *Grb10*$^{m/+}$, and *Grb10*$^{m/+}$/*Dlk1*$^{+/p}$ E14.5 embryos (see section 2.2.3). P0 pMEFs were grown in T75 flasks with complete medium (see section 2.2.4) until reaching about 90% confluence. Total proteins were extracted from the P0 or P1 pMEFs and fresh livers (see section 2.2.6). Two biological replicates of each genotype were prepared for TMT quantitative proteomic analysis with the duplicates chosen from different litters. Protein concentrations were measured by BCA assay as described in section 2.2.7. Protein sample qualities were verified by Dlk1, Grb10 and GAPDH western blotting. 100 µg of each sample were sent for TMT analysis. Two independent TMT analyses were performed on E14.5 pMEF and liver samples separately. Aliquots of 100 µg of eight samples per TMT experiment were digested with 2.5 µg trypsin at 37°C overnight. Digested peptides from each sample were labelled by a unique TMT tag from TMT 10plex reagents according to the manufacturer's protocol (Thermo Fisher Scientific, Gillingham, UK). Then the labelled samples were pooled.

2.2.16 High pH reversed-phase chromatography

For the total proteome analysis, an aliquot of 50 µg of the pooled sample was evaporated to dryness and resuspended in buffer A (20 mM ammonium hydroxide, pH 10) prior to fractionation by high pH reversed-phase chromatography using an Ultimate 3000 liquid chromatography system (Thermo Fisher Scientific, Gillingham, UK). In brief, the sample was loaded onto an XBridge BEH C18 Column (130Å, 3.5 µm, 2.1 mm X 150 mm, Waters, UK) in buffer A and peptides eluted with an increasing gradient of buffer B (20 mM Ammonium Hydroxide in acetonitrile, pH 10) from 0-95% over 60 minutes. The resulting fractions were evaporated to dryness and resuspended in 1% formic acid prior to analysis by nano-Liquid chromatography (nano-LC) tandem mass spectrometry (MS/MS) using an Orbitrap Fusion Tribrid mass spectrometer (Thermo Fisher Scientific, Gillingham, UK).

For the phosphoproteome analysis, the remainder of the TMT-labelled pooled sample was evaporated to dryness and subjected to TiO2-based phosphopeptide enrichment according to the manufacturer's instructions (Pierce, Thermo Fisher Scientific, Gillingham, UK). The phospho-enriched sample was evaporated to dryness and then resuspended in 1% formic acid prior to analysis by nano-LC MS/MS using an Orbitrap Fusion Tribrid mass spectrometer (Thermo Fisher Scientific, Gillingham, UK).

2.2.17 Nano-LC Mass Spectrometry

High pH RP fractions were further fractionated using an Ultimate 3000 nano-High-performance liquid chromatography (nano-HPLC) system in line with an Orbitrap Fusion Tribrid mass spectrometer. In brief, peptides in 1% formic acid were injected onto an Acclaim PepMap C18 nano-trap column (Thermo Fisher Scientific, Gillingham, UK). After washing with 0.5% (v/v) acetonitrile 0.1% formic acid peptides were resolved on a 250 mm × 75 μm Acclaim PepMap C18 reverse phase analytical column (Thermo Fisher Scientific, Gillingham, UK) over a 150 min organic gradient, using 7 gradient segments (1-6% solvent B over 1 min., 6-15% B over 58 min., 15-32% B over 58 min., 32-40% B over 5 min., 40-90% B over 1 min., held at 90% B for 6 min and then reduced to 1% B over 1 min.) with a flow rate of 300 nl/min (Solvent A was 0.1% formic acid and Solvent B was aqueous 80% acetonitrile in 0.1% formic acid). Peptides were ionized by nano-electrospray ionization at 2.0 kV using a stainless steel emitter with an internal diameter of 30 μm (Thermo Fisher Scientific, Gillingham, UK) and a capillary temperature of 275°C.

All spectra were acquired using an Orbitrap Fusion Tribrid mass spectrometer combined with Xcalibur 2.0 software (Thermo Fisher Scientific, Gillingham, UK) and operated in data-dependent acquisition mode using an SPS-MS3 workflow. FTMS1 spectra were collected at a resolution of 120,000, with an automatic gain control (AGC) target of 200,000 and a max injection time of 50 ms. The

TopN most intense ions were selected for MS/MS. Precursors were filtered according to charge state (to include charge states 2-7) and with monoisotopic precursor selection. Previously interrogated precursors were excluded using a dynamic window (40 s +/-10 ppm). The MS2 precursors were isolated with a quadrupole mass filter set to a width of 1.2 m/z. ITMS2 spectra were collected with an AGC target of 5000, max injection time of 120 ms and CID collision energy of 35%.

For FTMS3 analysis, the Orbitrap was operated at 60, 000 resolution with an AGC target of 50 000 and a max injection time of 120ms. Precursors were fragmented by high energy collision dissociation (HCD) at a normalised collision energy of 55% to ensure maximal TMT reporter ion yield. Synchronous Precursor Selection (SPS) was enabled to include up to 5 MS2 fragment ions in the FTMS3 scan.

2.2.18 Proteomics data analysis

Raw MS data files were analysed by MaxQuant v1.5.3.8 software with an Andromeda search engine and searched against Uniprot Mouse database downloaded on 170415 (73324 entries). MaxQuant created a reverse of the Uniprot Mouse library to get an estimate of false discovery rate (FDR). Default MaxQuant FDR was set to >1%. The software also created a library of known common contaminants which were excluded from the following bioinformatics analyses. MaxQuant analysis was carried out in collaboration with Professor Ian Prior from the University of Liverpool. For each protein, ratios of MS intensities from *Dlk1*$^{+/p}$, *Grb10*$^{m/+}$ and *Grb10*$^{m/+}$/*Dlk1*$^{+/p}$ were calculated using WT as the denominator. Then the ratios were $\log_2$ transformed. Average $\log_2$ transformed values were calculated from the biological replicates for each TMT. The mean values were used for the following analyses. 4-fold and 1.5-fold change was used as the threshold for proteome and phospho-proteome data sets, respectively. Uniprot identifiers were converted to Entrez gene (Gene ID) by the Uniprot online tool "Retrieve/ID mapping" (http://www.uniprot.org/uploadlists/) if necessary.

Gene ontology (GO)-term enrichment analysis was performed using the online GO-term analysis tool "Gorilla" (http://cbl-gorilla.cs.technion.ac.il/) (Eden *et al*., 2007; Eden *et al*., 2009). This tool calculated p-values of enriched GO-terms from target gene list against background gene list with multiple testing using FDR (Eden *et al*., 2009). Genes out of the fold change threshold were set as the target gene list and the whole dataset as the background list. P-value threshold was set as 10^{-5} for E14.5 pMEF and liver proteome and 10^{-3} for E14.5 pMEF and liver phospho-proteome data sets. Biological process, molecular function and cellular component enriched terms were all searched. P-values of the enriched GO-terms were $\log_{10}$ transformed and expressed as a Heatmap using MeV v4.9.0 software (Saeed *et al*., 2006).

Principle component analysis (PCA) was performed on log_2 transformed ratios using JMP10 software. All the proteins with missing values from any TMT tags were deleted from the PCA analysis. Pearson correlation coefficient (***r***) was calculated using GraphPad Prism 6 software. Hierarchical clustering (HCL) analysis using Pearson correlation coefficient (***r***) was visualized with MeV v4.9.0 software. Scatter plots of the whole data sets were generated with GraphPad Prism 6 software.

Clustering analysis was carried out using GProX v1.1.16 software (Rigbolt *et al*., 2011). TMT ratios were log_2 transformed and unsupervised gene clusters were identified using a fuzzy c-means algorithm. The E14.5 pMEF proteome dataset was grouped into 4 clusters with settings of regulations threshold=$\pm$2, fuzzification=2, iterations=200. The E14.5 pMEF phospho-proteome dataset was grouped into 6 clusters with settings of regulations threshold=$\pm$0.58, fuzzification=2, iterations=200. The E14.5 liver proteome dataset was grouped into 6 clusters with settings of regulations threshold=$\pm$2, fuzzification=2, iterations=200. The E14.5 liver phospho-proteome dataset was grouped into 5 clusters with settings of regulations threshold=$\pm$0.58, fuzzification=2, iterations=200. Genes grouped into the same cluster from each individual dataset were retrieved from GProX v1.1.16 software. Then GO-term enrichment analysis was performed for each gene cluster using “GOrilla” online tool, as described before. The gene list from each cluster was set as the target list and the whole dataset as the background list. P-value threshold was set as 10^{-3}. Biological process, molecular function and cellular component enriched terms were all searched. P-values of the enriched GO-terms were log_{10} transformed and expressed as a Heatmap using MeV v4.9.0 software (Saeed *et al*., 2006).

Chapter 3

Biochemical studies of Dlk1 and Grb10 in E14.5 embryos

3.1 Background

Evidence derived from transgenic mouse models indicates that there is a genetic interaction between *Dlk1* and *Grb10* in the regulation of early embryonic development and postnatal physiology, with *Dlk1* acting as an upstream inhibitor of *Grb10* (Madon-Simon *et al*., 2014). However, no studies have attempted to establish the biochemical interactions between the protein products of these genes and how this governs altered embryo size and adult body composition. Dlk1 and Grb10 proteins are both important cell signalling factors during mouse development. Dlk1 has been shown to inhibit Notch1 signalling (Traustadóttir *et al*., 2016), however, it is a non-canonical ligand from the EGF-like protein family lacking a DSL domain which can directly interact with Notch receptors (Traustadóttir *et al*., 2016; Traustadóttir *et al*., 2017). Physiologically relevant receptors of Dlk1 are still unknown. Grb10 is a signalling adaptor protein that is identified as a direct substrate of mTORC1 and can bind to several RTKs, including the IR and IGFR (Yu *et al*., 2011; Hsu *et al*., 2011; Plasschaert and Bartolomei, 2015). In addition, Grb10 was reported to be phosphorylated and stabilized by mTORC1 and mediated a negative feedback upon IR/IGFR and mTORC1 signalling *in vitro* and *in vivo* (Yu *et al*., 2011; Hsu *et al*., 2011; Liu *et al*., 2014). This project will attempt to uncover the Dlk1 and Grb10 signalling network, possibly through RTK or mTOR signalling pathways, in the mouse fetus at E14.5, using undifferentiated pMEFs and livers derived from WT, $Dlk1^{+/p}$, $Grb10^{m/+}$ and $Grb10^{m/+}/Dlk1^{+/p}$ mice. Serum was used to activate RTK downstream signalling pathways in pMEFs from the four genotypes, and mTOR inhibitor rapamycin (Yu *et al*., 2011; Hsu *et al*., 2011) and mTORC1 specific inhibitor Torin1 (Thoreen *et al*., 2009; Hsu *et al*., 2011) were used to block the downstream signal activities of mTOR. This chapter will address the following questions:

1) Does *Dlk1* or *Grb10* deletion alter E14.5 embryo size and also adult (6 months old) body composition, as shown previously?

2) Does *Dlk1* or *Grb10* deletion affect expression level of the other signalling protein in knockout tissues and cells, and if so does Dlk1 act at the biochemical level as an upstream inhibitor of Grb10?
3) How do RTK downstream signalling pathways respond to *Dlk1* and *Grb10* single and double knockout?
4) Do signalling changes in knockout tissues or cells support the antagonistic functions of *Dlk1* and *Grb10* based on genetic evidence?
5) Does mTORC1 inhibition result in altered Grb10 expression level?

3.2 Results

3.2.1 E14.5 fetuses with *Grb10*$^{m/+}$ and *Grb10*$^{m/+}$/*Dlk1*$^{+/p}$ genotypes exhibited overgrowth in comparison with WT and *Dlk1*$^{+/p}$

To determine the impacts of *Dlk1* and *Grb10* on fetal growth, wet weights of E14.5 embryos from WT, *Dlk1* and *Grb10* single and double knockout were recorded and analysed (Figure 3.1). Compared to WT and *Dlk1*$^{+/p}$, *Grb10*$^{m/+}$ and *Grb10*$^{m/+}$/*Dlk1*$^{+/p}$ embryos were significantly heavier (Figure 3.1B). The mean wet weights of WT, *Dlk1*$^{+/p}$, *Grb10*$^{m/+}$ and *Grb10*$^{m/+}$/*Dlk1*$^{+/p}$ embryos were 0.1992$\pm$0.01 g, 0.2034$\pm$0.01 g, 0.2872$\pm$0.02 g and 0.2575$\pm$0.01 g, respectively. *Grb10*$^{m/+}$ and *Grb10*$^{m/+}$/*Dlk1*$^{+/p}$ embryos were about 44% and 29% heavier than WT (Figure 3.1A). No statistical significance was found between E14.5 *Grb10*$^{m/+}$ and *Grb10*$^{m/+}$/*Dlk1*$^{+/p}$ embryos, indicating an indistinguishable phenotype between these two genotypes (Figure 3.1B). *Dlk1*$^{+/p}$ pups were born 20% smaller than WT as reported (Moon *et al*., 2003; Madon-Simon *et al*., 2014). However, at E14.5 WT and *Dlk1*$^{+/p}$ embryos had a similar body weight with no statistical difference, revealing that *Dlk1* may affect fetal growth later in gestation stage (Figure 3.1).

A

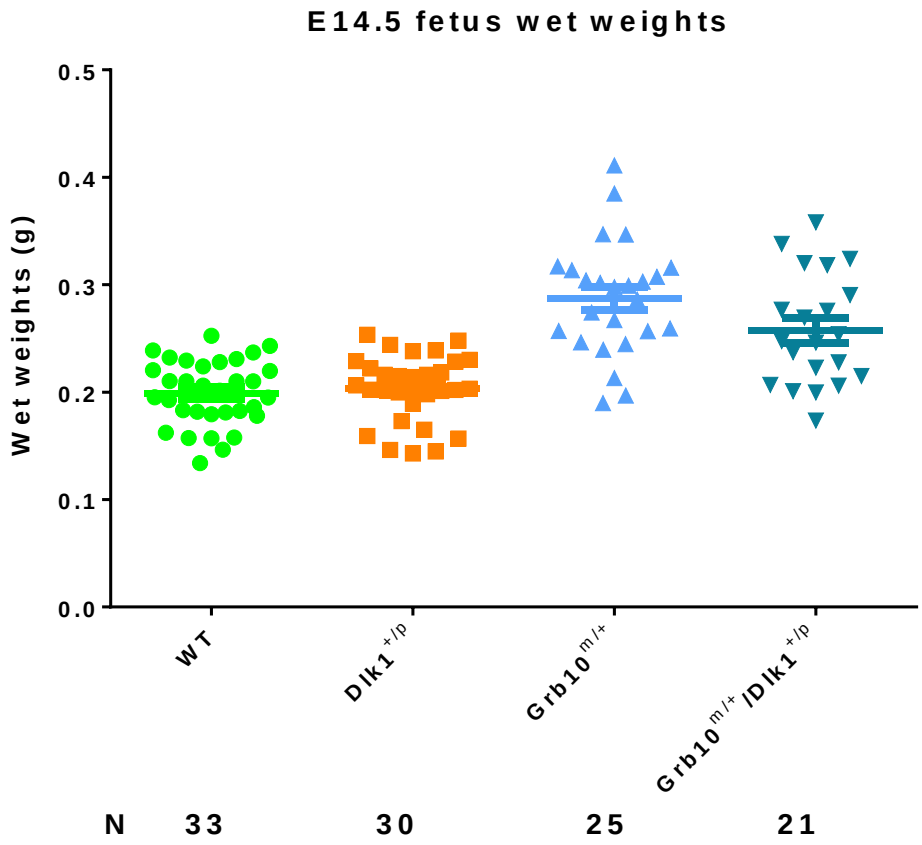

B

WT vs. *Dlk1*$^{+/p}$	**ns**
WT vs. *Grb10*$^{m/+}$	********
WT vs. *Grb10*$^{m/+}$/*Dlk1*$^{+/p}$	********
***Dlk1*$^{+/p}$ vs. *Grb10*$^{m/+}$**	********
***Dlk1*$^{+/p}$ vs. *Grb10*$^{m/+}$/*Dlk1*$^{+/p}$**	********
***Grb10*$^{m/+}$ vs. *Grb10*$^{m/+}$/*Dlk1*$^{+/p}$**	**ns**

Figure 3.1 Comparisons of fetal weights at E14.5 among the four genotypes. A) *Grb10*$^{m/+}$ and *Grb10*$^{m/+}$/*Dlk1*$^{+/p}$ fetuses were significantly heavier than WT and *Dlk1*$^{+/p}$. WT, green scatters; *Dlk1*$^{+/p}$, orange scatters; *Grb10*$^{m/+}$, light blue scatters; *Grb10*$^{m/+}$/*Dlk1*$^{+/p}$, dark blue scatters. **B)** Summary of statistical analysis among the four genotypes. All values represent means plus SEM and have been subject to One-way ANOVA with Tukey's *post hoc* analysis. WT n=33, *Dlk1*$^{+/p}$ n=30, *Grb10*$^{m/+}$ n=25, *Grb10*$^{m/+}$/*Dlk1*$^{+/p}$ n=21. **** P<0.0001.

3.2.2 Level of adiposity were increased in *Dlk1*$^{+/p}$ adult mice, whereas *Grb10*$^{m/+}$ and *Grb10*$^{m/+}$/*Dlk1*$^{+/p}$ adult mice were leaner compared to WT

For the investigation of *Dlk1* and *Grb10* influences on postnatal development, total body mass and body composition of knockout mice and their WT littermates were analysed at 6 months old. Female and male mice were compared separately to exclude any sex bias. Although *Grb10*$^{m/+}$ and *Grb10*$^{m/+}$/*Dlk1*$^{+/p}$ mice were slightly heavier than WT and *Dlk1*$^{+/p}$ mice (Figure 3.2A, B), both females and males showed no significant difference in body mass according to genotype (Figure 3.2I, J).

Dlk1$^{+/p}$ females were phenotypically fatter as the ratios of fat mass/body weight and fat mass/lean mass were both significantly elevated compared to WT (Figure 3.2C, G, I). Meanwhile, the content of lean mass in *Dlk1*$^{+/p}$ females was significantly decreased when expressed as the ratio of body weight in comparison with WT (Figure 3.2E, I). The ratio of fat mass/lean mass was significantly higher in *Dlk1*$^{+/p}$ males compared to WT (Figure 3.2H, J). The ratios of fat mass and lean mass of the body weight in *Dlk1*$^{+/p}$ males had similar trends as the *Dlk1*$^{+/p}$ females. However, no statistically significant differences were found between *Dlk1*$^{+/p}$ and WT males (Figure 3.2D, F, J).

Grb10$^{m/+}$ females and males had less fat mass and more lean mass contents compared to WT (Figure 3.2C-H). The ratio of fat mass and body weight was significantly reduced in female *Grb10*$^{m/+}$/*Dlk1*$^{+/p}$ mice compared to WT (Figure 3.2C, I). No significance was found between *Grb10*$^{m/+}$ and WT females and males in consideration of lean mass (Figure 3.2I, J).

Dlk1$^{+/p}$ and *Grb10*$^{m/+}$ mice displayed opposite phenotypes. *Dlk1*$^{+/p}$ mice tended to contain more fat mass, while *Grb10*$^{m/+}$ mice tended to contain more lean mass (Figure 3.2C-H). In comparisons of *Dlk1*$^{+/p}$ and *Grb10*$^{m/+}$ mice, fat mass

was significantly increased in *Dlk1*$^{+/p}$ mice, and lean mass was significantly higher in *Grb10*$^{m/+}$ mice in both males and females (Figure 3.2I, J).

Grb10$^{m/+}$ and *Grb10*$^{m/+}$*/Dlk1*$^{+/p}$ mice showed a similar body composition phenotype. Both tend to content more lean mass and less fat mass. Moreover, no significant differences were found between *Grb10*$^{m/+}$ and *Grb10*$^{m/+}$*/Dlk1*$^{+/p}$ mice in any comparisons. However, body composition measurements of *Grb10*$^{m/+}$*/Dlk1*$^{+/p}$ mice fell between those of *Grb10*$^{m/+}$ and WT mice (Figure 3.2A-J).

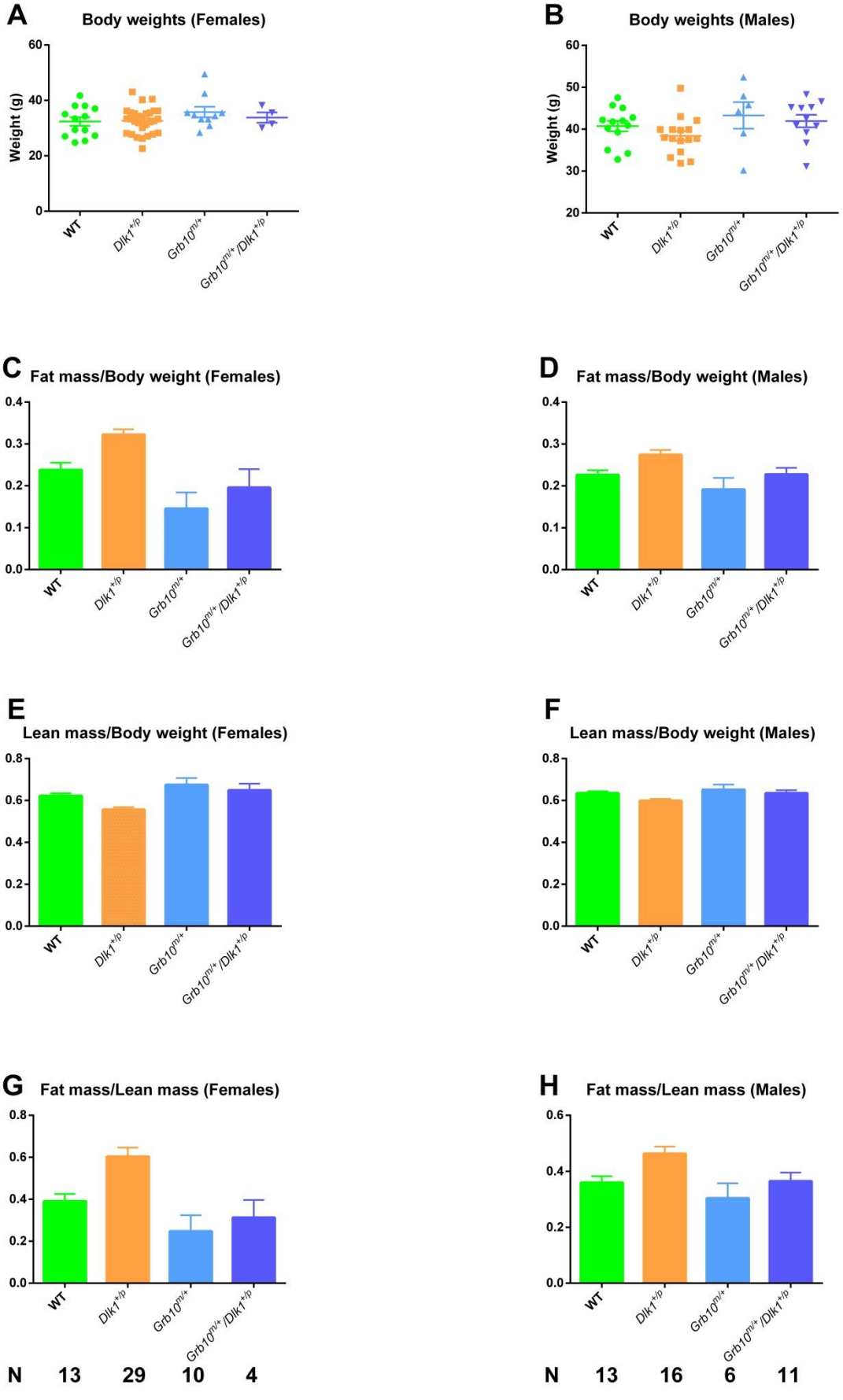
A
Body weights (Females)
Weight (g)
60
40
20
0
WT
Dlk1+/p
Grb10m/+
Grb10m/+/Dlk1+/p
B
Body weights (Males)
Weight (g)
60
50
40
30
20
WT
Dlk1+/p
Grb10m/+
Grb10m/+/Dlk1+/p
C
Fat mass/Body weight (Females)
0.4
0.3
0.2
0.1
0.0
WT
Dlk1+/p
Grb10m/+
Grb10m/+/Dlk1+/p
D
Fat mass/Body weight (Males)
0.4
0.3
0.2
0.1
0.0
WT
Dlk1+/p
Grb10m/+
Grb10m/+/Dlk1+/p
E
Lean mass/Body weight (Females)
0.8
0.6
0.4
0.2
0.0
WT
Dlk1+/p
Grb10m/+
Grb10m/+/Dlk1+/p
F
Lean mass/Body weight (Males)
0.8
0.6
0.4
0.2
0.0
WT
Dlk1+/p
Grb10m/+
Grb10m/+/Dlk1+/p
G
Fat mass/Lean mass (Females)
0.8
0.6
0.4
0.2
0.0
WT
Dlk1+/p
Grb10m/+
Grb10m/+/Dlk1+/p
N 13 29 10 4
H
Fat mass/Lean mass (Males)
0.6
0.4
0.2
0.0
WT
Dlk1+/p
Grb10m/+
Grb10m/+/Dlk1+/p
N 13 16 6 11

I

	Females			
	Body weight	**Fat mass/ Body weight**	**Lean mass/ Body weight**	**Fat mass/ Lean mass**
WT vs. *Dlk1*$^{+/p}$	ns	*	*	*
WT vs. *Grb10*$^{m/+}$	ns	*	ns	ns
WT vs. *Grb10*$^{m/+}$/*Dlk1*$^{+/p}$	ns	ns	ns	ns
***Dlk1*$^{+/p}$ vs. *Grb10*$^{m/+}$**	ns	****	****	***
***Dlk1*$^{+/p}$ vs. *Grb10*$^{m/+}$/*Dlk1*$^{+/p}$**	ns	*	ns	ns
***Grb10*$^{m/+}$ vs. *Grb10*$^{m/+}$/*Dlk1*$^{+/p}$**	ns	ns	ns	ns

J

	Males			
	Body weight	**Fat mass/ Body weight**	**Lean mass/ Body weight**	**Fat mass/ Lean mass**
WT vs. *Dlk1*$^{+/p}$	ns	ns	ns	*
WT vs. *Grb10*$^{m/+}$	ns	ns	ns	ns
WT vs. *Grb10*$^{m/+}$/*Dlk1*$^{+/p}$	ns	ns	ns	ns
***Dlk1*$^{+/p}$ vs. *Grb10*$^{m/+}$**	ns	**	*	**
***Dlk1*$^{+/p}$ vs. *Grb10*$^{m/+}$/*Dlk1*$^{+/p}$**	ns	ns	ns	ns
***Grb10*$^{m/+}$ vs. *Grb10*$^{m/+}$/*Dlk1*$^{+/p}$**	ns	ns	ns	ns

Figure 3.2 Analysis of body mass and fat/lean body composition in 6 months old adult mice. A-B) Total body weights of female and male mice from all four genotypes. WT, green scatters; *Dlk1*$^{+/p}$, orange scatters; *Grb10*$^{m/+}$, light blue scatters; *Grb10*$^{m/+}$/*Dlk1*$^{+/p}$, dark blue scatters. **C-D)** Ratios of fat mass/body weight in females and males among the four genotypes. **E-F)** Ratios of lean mass/body weight in female and male mice among the four genotypes. **G-H)** Ratios of fat mass/lean mass in females and males from all four genotypes. WT, green bar; *Dlk1*$^{+/p}$, orange bar; *Grb10*$^{m/+}$, light blue bar; *Grb10*$^{m/+}$/*Dlk1*$^{+/p}$, dark blue bar. **I-J)** Summary of statistical analysis about fat

and lean mass content in females and males among the four genotypes. All values represent means plus SEM and have been subject to One-way ANOVA with Tukey's *post hoc* analysis. WT n=26 (Female n=13, Male n=13), *Dlk1*$^{+/p}$ n=45 (Female n=29, Male n=16), *Grb10*$^{m/+}$ n=16 (Female n=10, Male n=6), *Grb10*$^{m/+}$*/Dlk1*$^{+/p}$ n=15 (Female n=4, Male n=11). * P<0.05, ** P<0.01, *** P<0.001, **** P<0.0001.

3.2.3 Grb10 expression level was elevated in E14.5 *Dlk1*$^{+/p}$ pMEFs

To investigate whether Grb10 expression levels were affected by paternal *Dlk1* deletion, total proteins were extracted from E14.5 WT and *Dlk1*$^{+/p}$ pMEFs. Cells were starved overnight, stimulated with 10% FBS and then harvested after different time intervals. Western blots were performed using an anti-Grb10 antibody. In the first two hours of FBS stimulation, Grb10 expression increased in both WT and *Dlk1*$^{+/p}$ pMEFs. Expression dropped to a relatively low level from 4-6 h and then increased to peak levels at 16 h before falling again until the end of the time-course at 24 h (Figure 3.3). For each blot, the lysates harvested from *Grb10*$^{m/+}$ pMEFs cultured in complete medium containing 10% FBS was used as the control. Grb10 proteins were detected in most samples as bands at approximately 60 and 75 kDa, as seen previously (Liu *et al*., 2014). No Grb10 expression was detected in *Grb10*$^{m/+}$ pMEFs as expected (Figure 3.3A), although a protein of around 190 kDa was detected specifically in *Grb10*$^{m/+}$ lysates which could represent a fusion protein comprised of Grb10 and β-geo because of the *β-geo* gene trap insertion in the maternal *Grb10* knockout allele (Garfield *et al*., 2011) (Figure 3.3A). Grb10 expression levels were consistently elevated in *Dlk1*$^{+/p}$ pMEFs compared with WT at all time points, however, no statistically significant differences were found comparing WT and *Dlk1*$^{+/p}$ pMEFs after normalising to GAPDH loading control (Figure 3.3B).

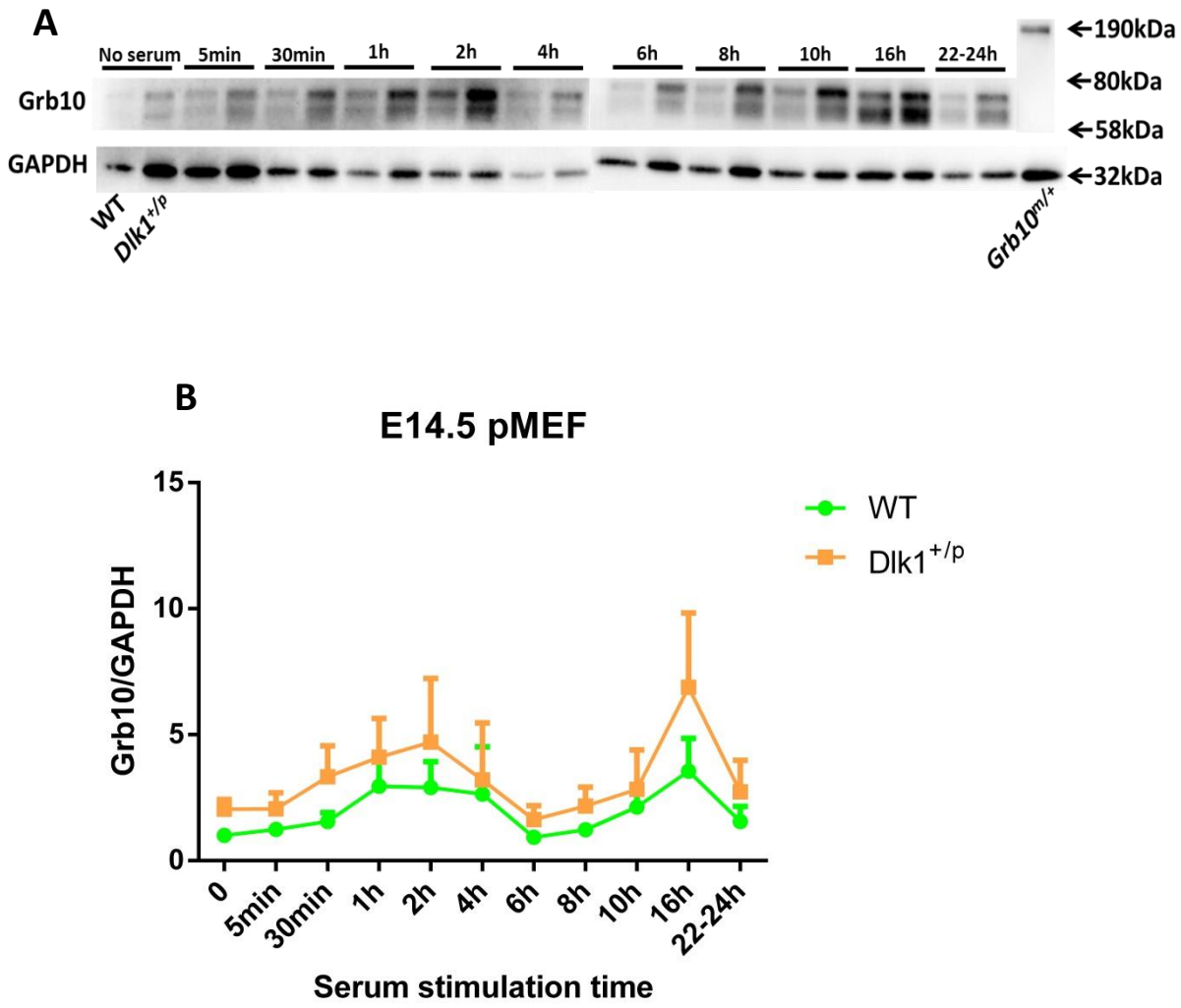

Figure 3.3 Grb10 expression levels at different serum stimulation time intervals. At all the time points before and after serum stimulation, Grb10 expression was elevated in *Dlk1*$^{+/p}$ pMEFs compared to WT. But no statistically significant differences were observed. **A)** A typical Western blot (one of five repeats of this experiment). No serum stimulated pMEFs of WT and *Dlk1*$^{+/p}$ were used as the blank controls. *Grb10*$^{m/+}$ pMEFs cultured in serum were used as the negative controls. GAPDH protein level was used as the loading control. **B)** Western blots from 5 repeats of the experiment were measured and quantified for this graph of Grb10 expression, normalised to the GAPDH housekeeping protein control. WT, green line; *Dlk1*$^{+/p}$, orange line. All values represent means plus SEM and have been subject to Two-way ANOVA with Bonferroni post-tests.

3.2.4 E14.5 *Dlk1*$^{+/p}$ pMEFs had a faster Grb10 turnover compared to WT

To determine the half-lives of Grb10 in WT and *Dlk1*$^{+/p}$ pMEFs, 10 ug/ml cycloheximide (CHX) was applied to block protein synthesis in growing pMEFs. Grb10 levels in WT and *Dlk1*$^{+/p}$ pMEFs were measured on Western blots using an anti-Grb10 antibody over a time-course of up to 32 h (Figure 3.4). After 32 h of CHX treatment, Grb10 expression was almost undetectable in WT and *Dlk1*$^{+/p}$ pMEFs (Figure 3.4A). Grb10 turnover was faster in *Dlk1*$^{+/p}$ pMEFs in response to CHX inhibition as the calculated Grb10 half-lives in WT and *Dlk1*$^{+/p}$ pMEFs were 2.757 h and 1.984 h, respectively (Figure 3.4B). Consistent with the Grb10 expression pattern under serum stimulation, Grb10 expression levels were higher in *Dlk1*$^{+/p}$ pMEFs at all time points (Figure 3.4). However, no statistical significance was found between WT and *Dlk1*$^{+/p}$ pMEFs at any time points by Two-way ANOVA analysis (Figure 3.4B).

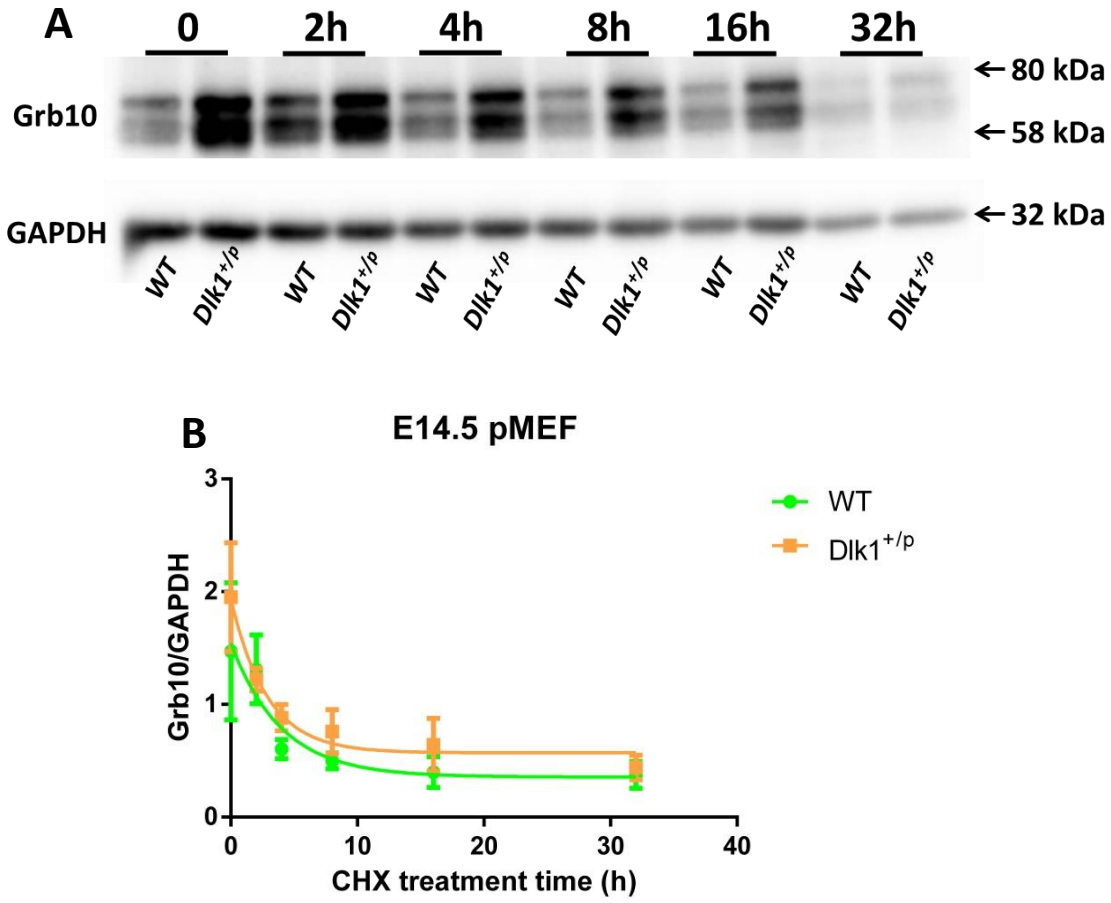

Figure 3.4 Analysis of Grb10 expression levels in WT and *Dlk1*$^{+/p}$ pMEFs with CHX treatment. Grb10 protein levels declined gradually after CHX addition to WT and *Dlk1*$^{+/p}$ pMEFs. Grb10 levels dropped more rapidly in *Dlk1*$^{+/p}$ pMEFs during the CHX treatment. **A)** Western blots representative of three independent experiments. WT and *Dlk1*$^{+/p}$ pMEFs with no CHX treatment were used as the negative controls. GAPDH protein level was used as the loading control. **B)** Grb10 expression was normalised to the loading control and expressed as a line graph. WT, green line; *Dlk1*$^{+/p}$, orange line. All values represent means plus SEM and have been subject to Two-way ANOVA with Bonferroni post-tests. Half-lives of Grb10 were calculated by one phase decay curve using GraphPad Prism 6.

3.2.5 Dlk1 expression was reduced in E14.5 *Grb10*$^{m/+}$ pMEFs compared to WT

To compare the Dlk1 expression levels in E14.5 WT and *Grb10*$^{m/+}$ pMEFs, Dlk1 sandwich ELISA was performed using pMEF medium. Dlk1 protein was undetectable by western blotting because the extracellular Dlk1 region (soluble Dlk1) was cleaved and released to the cell medium by TACE (Hudak and Sul, 2013). Dlk1 expression level was higher in medium harvested after 48 h than 24 h (Figure 3.5). Interestingly, lower Dlk1 expression level was detected in *Grb10*$^{m/+}$ pMEFs compared to WT at both 24 h and 48 h, suggesting Grb10 promoted Dlk1 expression in pMEFs (Figure 3.5). However, no statistical significance was found in Dlk1 levels between WT and *Grb10*$^{m/+}$. Low level of Dlk1 expression was detected in *Dlk1*$^{+/p}$ and control (no cell) medium due to the background. As described in section 3.3, Grb10 expression was higher in E14.5 *Dlk1*$^{+/p}$ pMEFs compared to WT (Figure 3.3). Collectively, Dlk1 and Grb10 expression was oppositely affected in *Grb10*$^{m/+}$ and *Dlk1*$^{+/p}$ pMEFs.

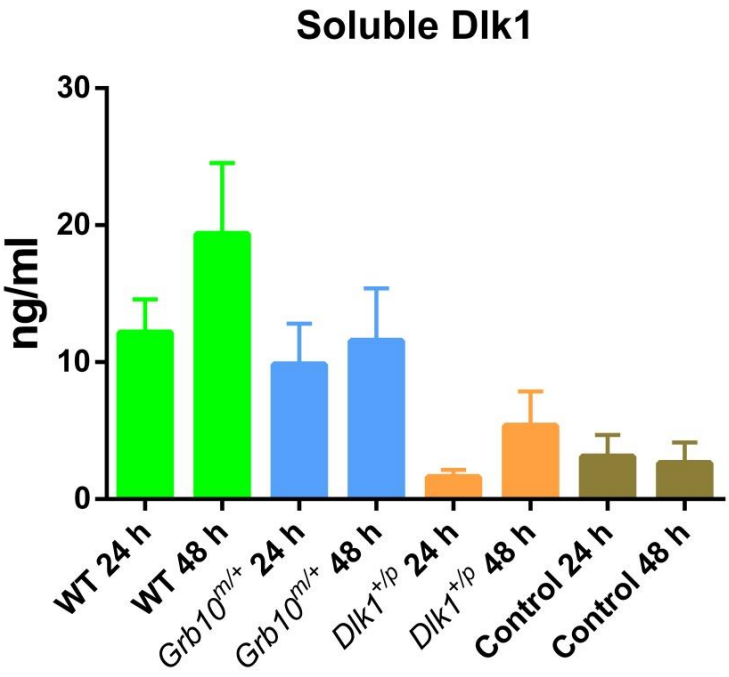

Figure 3.5 ELISA of soluble Dlk1 expression level in medium harvested from WT and *Grb10*$^{m/+}$ pMEFs. Dlk1 levels were measured and presented as a bar graph. Medium collected from plates with no cells were used as the blank controls (Control). *Dlk1*$^{+/p}$ pMEFs were used as the negative controls. WT, green bar; *Grb10*$^{m/+}$, blue bar; *Dlk1*$^{+/p}$, orange bar; Control, brown bar. All values represent means plus SEM of three experiments and have been subject to One-way ANOVA with Tukey's *post hoc* analysis.

3.2.6 Expression of Dlk1 or Grb10 in E14.5 liver was significantly altered in *Grb10*$^{m/+}$ and *Dlk1*$^{+/p}$ samples, respectively

To investigate the expression patterns of *Dlk1* and *Grb10* in embryonic livers, total proteins of E14.5 livers from WT, *Dlk1*$^{+/p}$, *Grb10*$^{m/+}$ and *Grb10*$^{m/+}$/*Dlk1*$^{+/p}$ were extracted. Dlk1 and Grb10 western blotting showed that *Dlk1* or *Grb10* deletions altered the expressions of each other in E14.5 livers. Specifically, Grb10 expression was significantly decreased in *Dlk1*$^{+/p}$ livers (Figure 3.6A, C), while Dlk1 expression was significantly increased in *Grb10*$^{m/+}$ livers (noting that Dlk1 was undetectable in E14.5 pMEFs) (Figure 3.6B, D). As shown previously, a 190 kDa band, potentially representing a Grb10: β-geo fusion protein was detected specifically in *Grb10*$^{m/+}$ and *Grb10*$^{m/+}$/*Dlk1*$^{+/p}$ E14.5 livers (Figure 3.6A). No Dlk1 expression was found in *Grb10*$^{m/+}$ and *Grb10*$^{m/+}$/*Dlk1*$^{+/p}$ E14.5 livers (Figure 3.6B). An opposite expression pattern was found in E14.5 pMEFs by Grb10 Western and Dlk1 ELISA (Figure 3.3, 3.5).

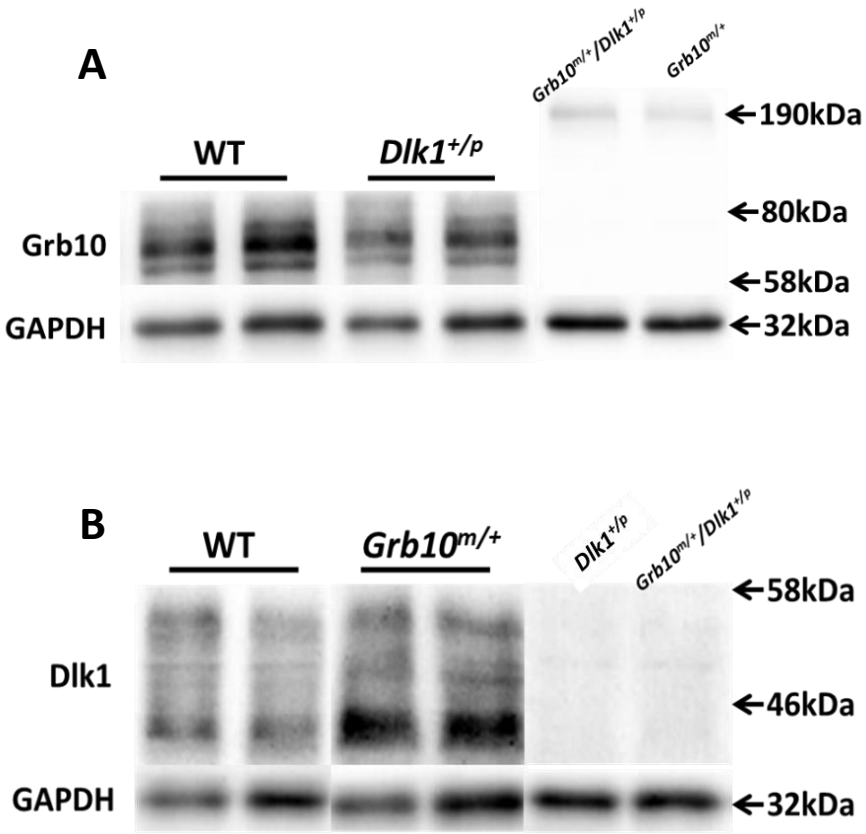

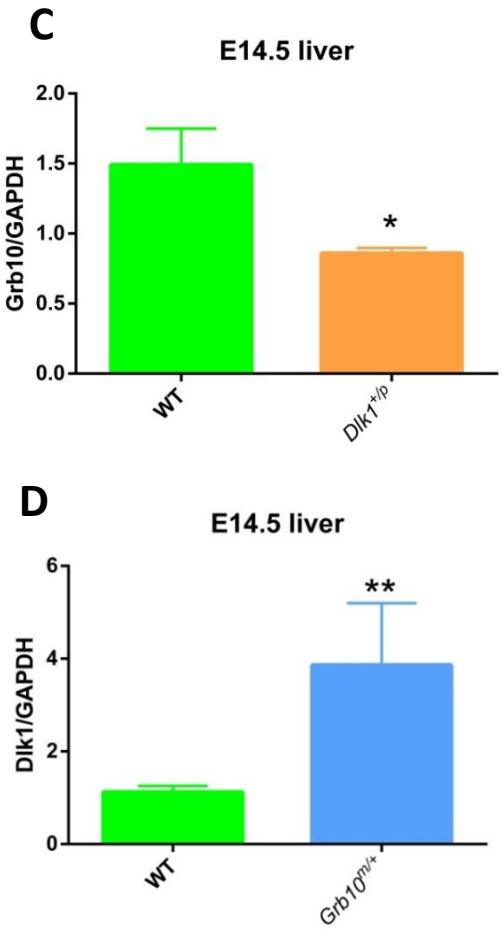

Figure 3.6 *Dlk1* and *Grb10* expression patterns in E14.5 WT, *Dlk1*$^{+/p}$, *Grb10*$^{m/+}$ and *Grb10*$^{m/+}$*/Dlk1*$^{+/p}$ livers. Western blots representative of three independent experiments for: **A)** Grb10 (*Grb10*$^{m/+}$ and *Grb10*$^{m/+}$*/Dlk1*$^{+/p}$ liver lysates were used as the negative controls) and **B)** Dlk1 (*Dlk1*$^{+/p}$ and *Grb10*$^{m/+}$*/Dlk1*$^{+/p}$ liver lysates were used as the negative controls). GAPDH levels were used as the loading controls. Grb10 or Dlk1 expression level was normalised to the loading control and expressed as a bar graph for: **C)** Grb10 and **D)** Dlk1. WT, green bar; *Grb10*$^{m/+}$, blue bar; *Dlk1*$^{+/p}$, orange bar. All values represent means plus SEM and have been subject to unpaired T-test with two-tailed analysis. WT n=9, *Dlk1*$^{+/p}$ n=8, *Grb10*$^{m/+}$ n=3, *Grb10*$^{m/+}$*/Dlk1*$^{+/p}$ n=3. * P<0.05, ** P<0.001.

3.2.7 Similar downstream PI3K-Akt and ERK-MAPK activities were found in WT and *Dlk1*$^{+/p}$, *Grb10*$^{m/+}$ and *Grb10*$^{m/+}$/*Dlk1*$^{+/p}$ pMEFs under serum stimulation

To evaluate the downstream signal responses to serum stimulation in WT and knockout pMEFs, Akt and Erk1/2 phosphorylation status was checked. Cells were cultured in DMEM medium without serum for overnight starvation. The next day, cells were stimulated by adding 10% FBS then harvested after different time intervals from 5 min to 2 h. No phosphorylated Akt and only a low level of Erk1/2 phosphorylation were detected in the absence of serum in pMEFs of all four genotypes (Figure 3.7A). In WT and *Dlk1*$^{+/p}$ pMEFs, Akt and Erk1/2 exhibited rapid responses to the serum stimulation with phosphorylation levels reaching to a maximum at 5 min. Subsequently, levels of phosphorylated Erk1/2 started to drop and were lowest at 2 h, whereas higher Akt phosphorylation levels were sustained up to 2 h after serum stimulation (Figure 3.7). *Grb10*$^{m/+}$ and *Grb10*$^{m/+}$/*Dlk1*$^{+/p}$ pMEFs showed similar Akt and Erk1/2 phosphorylation patterns with WT and *Dlk1*$^{+/p}$, except phosphorylated Akt levels were slightly higher and phosphorylated Erk1/2 levels were slightly lower. Notably, changes in Akt and Erk1/2 phosphorylation levels under serum stimulation were essentially indistinguishable between WT and *Dlk1*$^{+/p}$ pMEFs and also between *Grb10*$^{m/+}$ and *Grb10*$^{m/+}$/*Dlk1*$^{+/p}$ pMEFs (Figure 3.7).

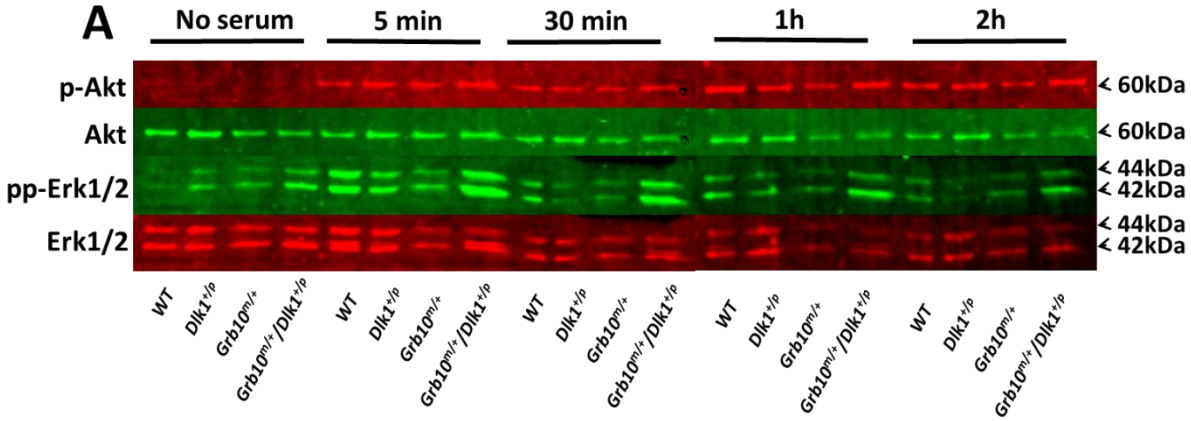

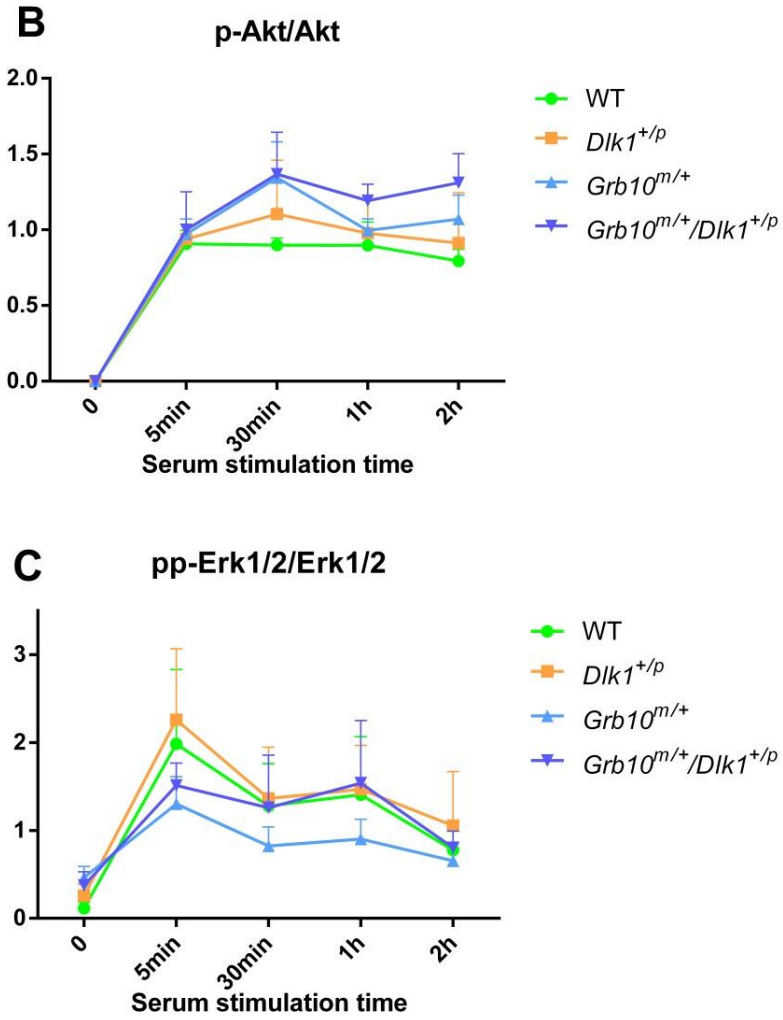

Figure 3.7 Levels of phosphorylated Akt and Erk1/2 following serum stimulation of WT, *Dlk1*$^{+/p}$, *Grb10*$^{m/+}$ and *Grb10*$^{m/+}$*/Dlk1*$^{+/p}$ pMEFs. Prolonged Akt phosphorylation was seen in pMEFs of all four genotype, as was rapid Erk1/2 phosphorylation, followed by a gradual decline. **A)** Western blots representative of three independent experiments. E14.5 pMEFs of the four genotypes (with no serum stimulation) were used as the negative controls. Total Akt and Erk1/2 levels were used as the loading controls for phosphorylated Akt and Erk1/2 levels, respectively. p-Akt and pp-Erk1/2 levels were normalised to the loading control and visualised in separated line charts for: **B)** p-Akt and **C)** pp-Erk1/2. WT, green line; *Dlk1*$^{+/p}$, orange line; *Grb10*$^{m/+}$, light blue line; *Grb10*$^{m/+}$*/Dlk1*$^{+/p}$, dark blue line. All values in graphs B and C represent means plus SEM and have been subject to Two-way ANOVA with Bonferroni post-tests.

3.2.8 Akt and Erk1/2 activities in E14.5 WT, *Dlk1*$^{+/p}$, *Grb10*$^{m/+}$ and *Grb10*$^{m/+}$/*Dlk1*$^{+/p}$ livers

Phosphorylated Akt and Erk1/2 levels were checked in E14.5 livers from mice of all four genotypes. In E14.5 WT, *Dlk1*$^{+/p}$, *Grb10*$^{m/+}$, and *Grb10*$^{m/+}$/*Dlk1*$^{+/p}$ livers, strong Akt phosphorylation levels were observed (Figure 3.8A). In contrast, p-Erk1/2 levels were relatively low, showing weak bands on Western blots (Figure 3.8A). Higher Akt phosphorylation level was observed in *Dlk1*$^{+/p}$ and *Grb10*$^{m/+}$/*Dlk1*$^{+/p}$ livers compared to both WT and *Grb10*$^{m/+}$, while p-Akt levels were similar between WT and *Grb10*$^{m/+}$ livers (Figure 3.8A, B). No statistically significant differences were found in Akt phosphorylation levels among the four genotypes (Figure 3.8B). Phosphorylation of Erk1/2 was upregulated in all three knockout livers compared to WT. *Grb10*$^{m/+}$ livers had a lower Erk1/2 phosphorylation level than *Dlk1*$^{+/p}$ and *Grb10*$^{m/+}$/*Dlk1*$^{+/p}$ (Figure 3.8A, C). Notably, Erk1/2 phosphorylation level was significantly increased in *Dlk1*$^{+/p}$ livers compared to WT with no other significant difference in level of phosphorylated Erk1/2 found among WT, *Dlk1*$^{+/p}$, *Grb10*$^{m/+}$, and *Grb10*$^{m/+}$/*Dlk1*$^{+/p}$ livers (Figure 3.8A, C).

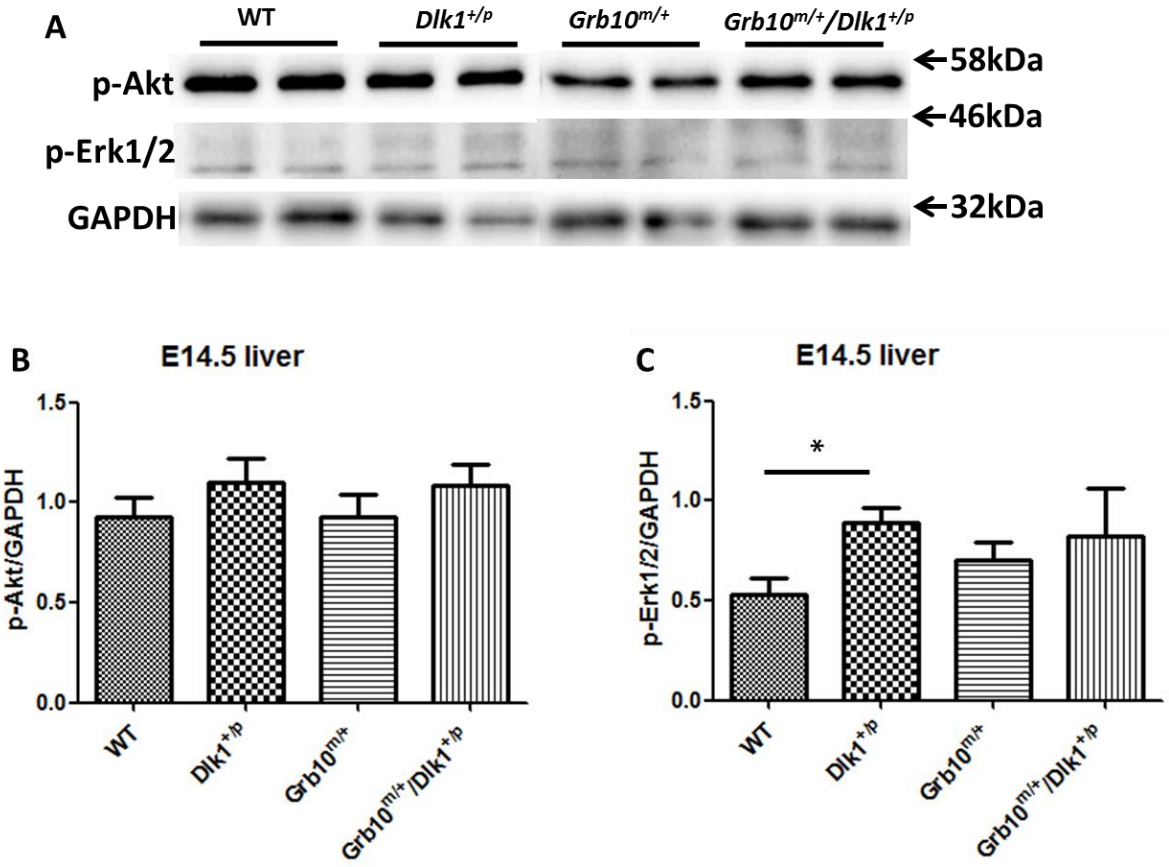

Figure 3.8 Patterns of phosphorylated Akt and Erk1/2 expression in E14.5 WT, *Dlk1*$^{+/p}$, *Grb10*$^{m/+}$ and *Grb10*$^{m/+}$*/Dlk1*$^{+/p}$ livers. A) Western blots representative of three independent experiments. GAPDH protein levels were used as the loading controls. Akt and Erk1/2 phosphorylation levels were normalised to the loading control and visualised in separated bar graphs for: **B)** p-Akt and **C)** p-Erk1/2. WT, dot filled bar; *Dlk1*$^{+/p}$, square filled bar; *Grb10*$^{m/+}$, transverse line filled bar; *Grb10*$^{m/+}$*/Dlk1*$^{+/p}$, string filled bar. All values represent means plus SEM and have been subject to One-way ANOVA with Tukey's *post hoc* analysis. WT n=9, *Dlk1*$^{+/p}$ n=8, *Grb10*$^{m/+}$ n=3, *Grb10*$^{m/+}$*/Dlk1*$^{+/p}$ n=3. * P<0.05**.**

3.2.9 Grb10 expression was reduced following mTORC1 inhibition in E14.5 WT and *Dlk1*$^{+/p}$ pMEFs

Grb10 was reported to be directly phosphorylated and stabilized by mTORC1 in pMEFs (Hsu *et al.*, 2011). To discover the impacts of mTORC1 in the biochemical link between Dlk1 and Grb10, pMEFs of all four genotypes were exposed to the mTORC1 inhibitors, rapamycin and Torin1 for 24 h. Grb10 expression levels were assessed, along with levels of phosphorylated S6K, by Western blotting (Figure 3.9A). No S6K phosphorylation was found in rapamycin or Torin1 treated pMEFs, indicating that mTORC1 downstream signals were blocked by the inhibitors after 24 h. Grb10 expression was reduced by either rapamycin or Torin1 treatment in WT and *Dlk1*$^{+/p}$ pMEFs (Figure 3.9). Furthermore, Grb10 expression levels were lower in pMEFs treated with Torin 1 than rapamycin, suggesting Torin1 was a more specific and stronger mTORC1 inhibitor (Figure 3.9). In *Dlk1*$^{+/p}$ pMEFs, Grb10 expression level was higher than WT without mTORC1 inhibition, as in previous experiments. Yet Grb10 protein expression levels were similar in rapamycin or Torin1 treated WT and *Dlk1*$^{+/p}$ pMEFs without statistical significance (Figure 3.9B).

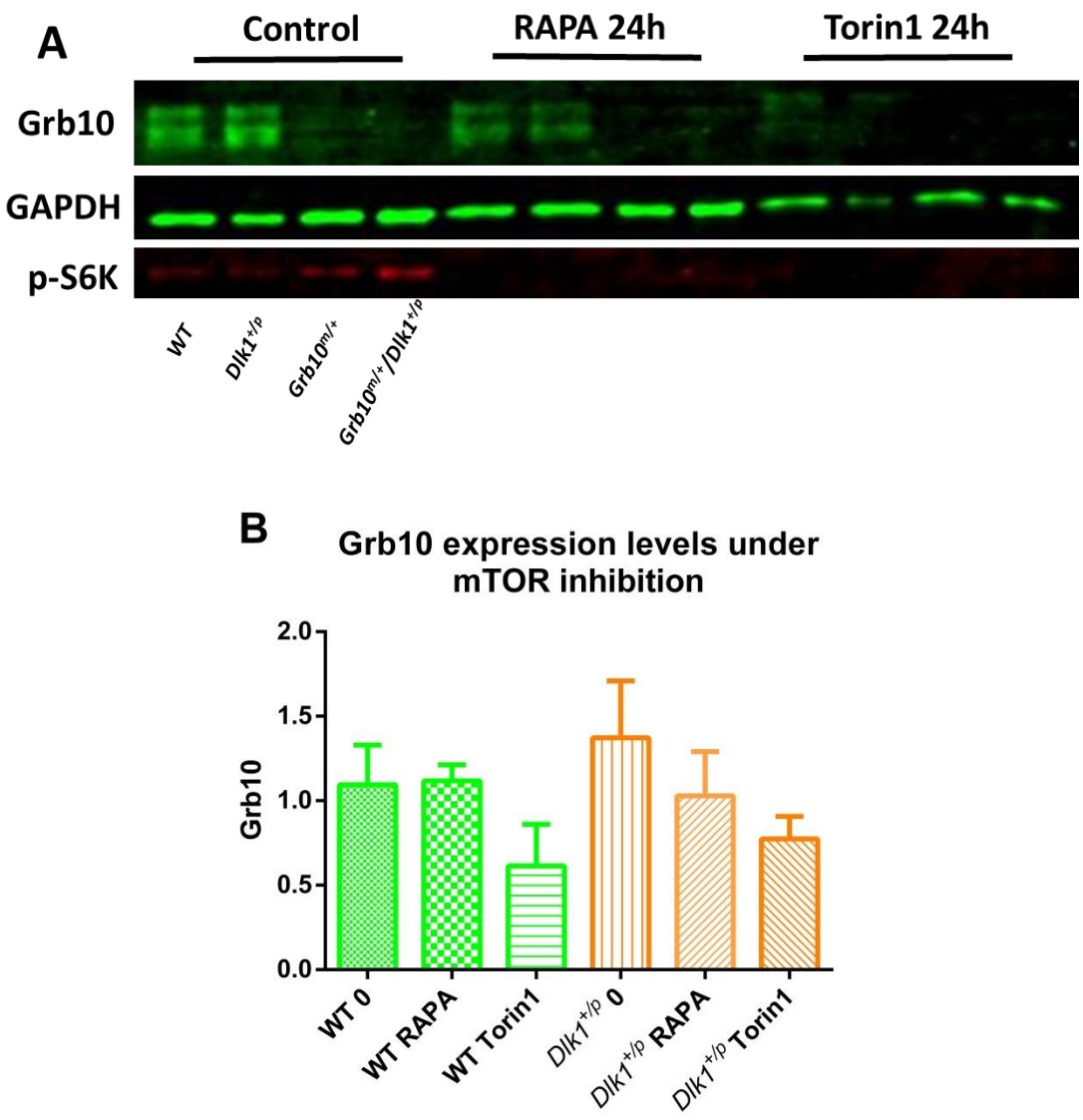

Figure 3.9 Changes of Grb10 expression in WT and *Dlk1*$^{+/p}$ pMEFs under mTORC1 inhibition. A) Western blots representative of three independent experiments. S6K phosphorylation levels were used as the positive controls. Cells from WT and *Dlk1*$^{+/p}$ (no inhibitor treatment) were used as the negative controls. GAPDH protein levels were used as the loading controls. **B)** Grb10 expression levels were normalised to the loading control. Quantification of Grb10 bands was visualised as a bar chart. WT, green bars; *Dlk1*$^{+/p}$, orange bars. All values represent means SEM and have been subject to Owo-way ANOVA with Tukey's *post hoc* analysis. WT n=3, *Dlk1*$^{+/p}$ n=3, *Grb10*$^{m/+}$ n=3, *Grb10*$^{m/+}$*/Dlk1*$^{+/p}$ n=3. Experiments were repeated three times.

3.3 Discussion

Paternally-expressed *Dlk1* promotes fetal growth while maternally-expressed *Grb10* inhibits fetal growth (Moon *et al*., 2002; Charalambous *et al*., 2003; Madon-Simon *et al*., 2014). The respective growth regulatory roles are consistent with the predominant theory for the evolution of imprinted gene expression, the parent-offspring conflict hypothesis over fetal growth (Haig, 2014). The global loss of *Dlk1* or *Grb10* gene also affects body size, including proportions of adipose and lean tissues of adult mice, *Dlk1* knockout mice are fatter, while *Grb10* knockouts are leaner (Moon *et al*., 2002; Smith *et al*., 2007; Madon-Simon *et al*., 2014). The opposite effects of Dlk1 and Grb10 on adult adipose: lean proportions may result from events started during prenatal development. Previous genetic studies of crosses between *Dlk1* and *Grb10* knockout mice indicate that $Grb10^{m/+}/Dlk1^{+/p}$ offspring have a phenotype that is very similar to that of $Grb10^{m/+}$ (Madon-Simon *et al*., 2014). This suggests that Dlk1 and Grb10 may act antagonistically through a common pathway to regulate the fetal growth. Additionally, Dlk1 acts upstream, as an inhibitor of Grb10, which in turn was an inhibitor of embryo growth (Madon-Simon *et al*., 2014). Yet, the biochemical interactions between Dlk1 and Grb10 leading to the antagonistic phenotypes in the $Dlk1^{+/p}$ and $Grb10^{m/+}$ pups are still unknown.

Here, I found that $Grb10^{m/+}$ and $Grb10^{m/+}/Dlk1^{+/p}$ embryos at E14.5 were significantly larger and heavier than WT and $Dlk1^{+/p}$ embryos, whereas the differences between WT and $Dlk1^{+/p}$ embryo weights were indistinguishable (Figure 3.1). Madon-Simon and colleagues (2014) reported that $Grb10^{m/+}$ and $Grb10^{m/+}/Dlk1^{+/p}$ pups were significantly larger while $Dlk1^{+/p}$ pups were significantly smaller than WT at birth (Madon-Simon *et al*., 2014). Yet no significant difference was found between WT and $Dlk1^{+/p}$ E14.5 embryos (Figure 3.1). These results suggest that Dlk1 may promote the fetal growth at

later gestation stage after E14.5 and before birth. In addition, the wet weights of *Grb10*$^{m/+}$/*Dlk1*$^{+/p}$ embryos were slightly lighter than *Grb10*$^{m/+}$ (Figure 3.1), however, *Grb10*$^{m/+}$ and *Grb10*$^{m/+}$/*Dlk1*$^{+/p}$ embryos were not statistically different. The failure to detect a statistical difference between these two groups may due to the small sample size (*Grb10*$^{m/+}$ n=25, *Grb10*$^{m/+}$/*Dlk1*$^{+/p}$ n=21) used in this study. A power calculation had been performed on the data of these two groups which suggested the required sample size to detect a statistical difference should be n=102 (*Grb10*$^{m/+}$ n=51, *Grb10*$^{m/+}$/*Dlk1*$^{+/p}$ n=51). More samples are need for a compelling conclusion.

At 6 months old, no significant differences in body weights were found in females and males among the genotypes studied: WT, *Dlk1*$^{+/p}$, *Grb10*$^{m/+}$ and *Grb10*$^{m/+}$/*Dlk1*$^{+/p}$ (Figure 3.2). Although *Grb10* knockout mice were heavier and *Dlk1* knockout were lighter than WT after birth until weaning at 3 weeks, the differences in body weight became smaller after weaning (Moon *et al*., 2002; Wang *et al*., 2007; Smith *et al*., 2007; Madon-Simon *et al*., 2014). The similar body weight among mice of all four genotypes at 6-month-old found in this study was consistent with previous studies (Figure 3.2). But WT and knockout adult mice tended to have different body composition. Adult *Dlk1*$^{+/p}$ females and males tended to have a larger proportion of fat mass and smaller lean mass compared to WT and *Grb10*$^{m/+}$ mice (Figure 3.2), again as shown previously (Moon *et al*., 2002; Madon-Simon *et al*., 2014). *Dlk1*$^{+/p}$ adults tended to development more fat mass might result because Dlk1 acts as an inhibitor of adipogenesis and an enhancer of myogenic development (Moon *et al*., 2002; Andersen *et al*., 2013). Notably, the obese phenotype was more obvious in *Dlk1*$^{+/p}$ females than males which might be due to the larger number of *Dlk1*$^{+/p}$ females used in this study or because Dlk1 may have a stronger effect on fat development in females. Previous mouse studies have also shown that *Grb10* knockout mice tend to develop a leaner phenotype (more lean mass and less fat mass) in adults using two different mouse lines (Wang

et al., 2007; Smith *et al*., 2007; Madon-Simon *et al*., 2014), providing genetic evidence that Grb10 promoted muscle development (Holt *et al*., 2012; Mokbel *et al*., 2014). Meanwhile, *Grb10*$^{m/+}$ and *Grb10*$^{m/+}$/*Dlk1*$^{+/p}$ adults were indistinguishable from each other in body composition (Madon-Simon *et al*., 2014). Here, *Grb10*$^{m/+}$ females at 6-month-old had a statistically significant lower fat mass/body weight ratio compared to WT (Figure 3.2C, I). No other statistical significance was found between WT and *Grb10*$^{m/+}$ mice. *Grb10*$^{m/+}$/*Dlk1*$^{+/p}$ mice were not significantly different from WT when compared the fat or lean mass contents (Figure 3.2I, J). But *Grb10*$^{m/+}$ and *Grb10*$^{m/+}$/*Dlk1*$^{+/p}$ females and males consistently tended to develop more lean mass and less fat mass (Figure 3.2C-H). This may be due to the small number of *Grb10*$^{m/+}$/*Dlk1*$^{+/p}$ mice used for this study.

The oppositely imprinted genes *Igf2r* and *Igf2* acted antagonistically through the same signalling pathway, and the interaction of IGF2R and IGF2 affected the expressions and functions of each other as IGF2R inhibits growth by targeting IGF2 for lysosomal degradation (Barlow *et al*., 1991; DeChiara *et al*., 1991; Nordin *et al*., 2014). Also, it has been reported that paternally expressed *Igf2* can influence expression of maternally expressed *CDKN1C* (Grandjean *et al*., 2000). Here, E14.5 pMEFs and livers from WT, *Dlk1*$^{+/p}$ and *Grb10*$^{m/+}$ mice were used as respective *in vitro* and *in vivo* models to investigate whether *Dlk1* deletion could alter the expression of *Grb10*, or whether *Grb10* deletion could alter the expression of *Dlk1*. Specifically, Grb10 protein expression levels in E14.5 *Dlk1*$^{+/p}$ pMEFs were found to be higher than WT cells under serum stimulation at all time intervals (Figure 3.3). In addition, when WT and *Dlk1*$^{+/p}$ pMEFs were cultured with CHX to block Grb10 synthesis, the Grb10 half-lives of WT and *Dlk1*$^{+/p}$ pMEFs were 2.757 h and 1.984 h, respectively, indicating a more rapid turnover of Grb10 in *Dlk1*$^{+/p}$ pMEFs than WT (Figure 3.4). Although no statistical significance was found between WT and *Dlk1*$^{+/p}$ pMEFs treated with serum or CHX at any time points, Grb10 expression was consistently

elevated in *Dlk1*$^{+/p}$ cells. Dlk1 expression could not be detected in pMEFs by Western blotting and instead was detected by ELISA, taking advantage of the fact that a proportion of Dlk1 was cleaved and released from the cell surface. The soluble form of Dlk1 has been associated with various biological processes (Wang and Sul, 2006; Andersen *et al*., 2013). ELISA may be more sensitive than Western blotting and in our experiment which measured soluble Dlk1 accumulated in the cell culture medium over 24 h and 48 h. Dlk1 expression was found to be lower in *Grb10*$^{m/+}$ compared to WT pMEFs (Figure 3.5). Collectively, Grb10 expression level was higher in *Dlk1*$^{+/p}$ pMEFs while soluble Dlk1 protein level was lower in *Grb10*$^{m/+}$ pMEFs, suggesting that Dlk1 and Grb10 affected the expression of each other in E14.5 pMEFs. The higher Grb10 expression in *Dlk1*$^{+/p}$ pMEFs was consistent with the genetic evidence that Dlk1 acts as an upstream inhibitor of Grb10 (Madon-Simon *et al*., 2014).

In E14.5 livers *Dlk1* or *Grb10* deletion again lead to each altering expression of the other signalling protein. However, in contrast to the observations in E14.5 pMEFs, Grb10 expression level was significantly reduced in *Dlk1*$^{+/p}$ livers, whereas Dlk1 was significantly increased in *Grb10*$^{m/+}$ livers (Figure 3.6). This is not obviously consistent with the genetic data. One possible reason is that different Dlk1 and Grb10 signalling pathways may be involved in pMEF and liver development, leading to the completely different effects of *Dlk1* and *Grb10* knockout in E14.5 pMEFs versus livers. Also, different tissues and cells might have immediate or delayed response to the global knockout of *Dlk1* or *Grb10*. E14.5 livers may respond to the global *Dlk1* or *Grb10* knockout at later stage. In general, Dlk1 and Grb10 displayed opposite expression effects to the other in E14.5 pMEF and liver. The dependent Dlk1 and Grb10 expression supported the hypothesis that these two genes were involved in the same pathway in control of the embryo growth, although the mechanism may be different in pMEFs and embryonic livers.

Two groups reported that Grb10 could be directly phosphorylated at S501/503 by mTORC1, and the phosphorylation enhanced the stability of Grb10 which in turn inhibited mTORC1 and IR/IGFR signalling in pMEFs (Hsu *et al*., 2011; Yu *et al*., 2011; Yea and Fruman, 2011). Therefore, *Dlk1* knockout may affect the mTORC1 regulated Grb10 phosphorylation in pMEFs. I attempted to address this using an anti-phospho-Grb10 antibody at S501/503 (Hsu *et al*., 2011; Yu *et al*., 2011), but this failed to detect specific phospho-Grb10 bands in E14.5 pMEF samples on Western blots (data not shown). Meanwhile, mTORC1 inhibition through rapamycin or Torin1 treatment of pMEFs reduced Grb10 expression in WT and $Dlk1^{+/p}$ pMEFs, indicating that Grb10 accumulation was affected by mTORC1 inhibition (Figure 3.9). However, Grb10 phosphorylation status in WT and $Dlk1^{+/p}$ pMEFs is currently still unclear.

Grb10 was reported to regulate IR, IGFR and other RTKs (Wick *et al*., 2003; Vecchione *et al*., 2003; Murdaca *et al*., 2004; Monami *et al*., 2008). Therefore I investigated whether the signalling downstream of these receptors were affected by the knockout of *Dlk1* and *Grb10*. Levels of phosphorylated Akt were found to be increased and phosphorylated Erk1/2 decreased in $Grb10^{m/+}$ and $Grb10^{m/+}/Dlk1^{+/p}$ E14.5 pMEFs, compared to $Dlk1^{+/p}$ and WT, when cells were starved and then stimulated with serum. Additionally, sustained Akt phosphorylation and rapid Erk1/2 phosphorylation responses were observed during the 2 h of serum stimulation (Figure 3.7). This was supported by the strong Akt and weak Erk1/2 phosphorylation signals detected in E14.5 livers among the four genotypes (Figure 3.8). Notably, the Akt and Erk1/2 activities in serum stimulated pMEFs were similar between $Grb10^{m/+}$ and $Grb10^{m/+}/Dlk1^{+/p}$ and also between $Dlk1^{+/p}$ and WT. These similarities at the biochemical level were consistent with the genetic findings that mice from these two groups had a similar phenotype, including growth and cell cycle characteristics of E14.5 pMEFs.

In addition, a higher Akt and Erk1/2 phosphorylation level was observed in E14.5 *Dlk1*$^{+/p}$ and *Grb10*$^{m/+}$/*Dlk1*$^{+/p}$ livers compared to WT, however, the differences between *Grb10*$^{m/+}$ and WT were not significant (Figure 3.8). This implied that Dlk1 may be more active during embryonic liver development than Grb10. Notably, Akt and Erk1/2 phosphorylation status was not similar between *Grb10*$^{m/+}$ and *Grb10*$^{m/+}$/*Dlk1*$^{+/p}$ and also between *Dlk1*$^{+/p}$ and WT which was different from the findings in E14.5 pMEFs. *Dlk1* and *Grb10* knockout led to different downstream signal phosphorylation responses among the four genotypes in E14.5 pMEFs versus livers. This suggests that different cell signalling pathways may be involved in pMEF and liver. To further uncover the signal pathways involved in Dlk1 and Grb10 on embryo growth, unbiased quantitative proteomics approaches will be performed on E14.5 WT, *Dlk1*$^{+/p}$, *Grb10*$^{m/+}$ and *Grb10*$^{m/+}$/*Dlk1*$^{+/p}$ pMEFs and livers. The findings will be discussed in next chapter.

In summary, 1) E14.5 embryo size was not affected by *Dlk1* deletion while *Grb10*$^{m/+}$ and *Grb10*$^{m/+}$/*Dlk1*$^{+/p}$ embryos were significantly enlarged at E14.5. At 6 months old, *Dlk1*$^{+/p}$ adults were fatter while *Grb10*$^{m/+}$ and *Grb10*$^{m/+}$/*Dlk1*$^{+/p}$ adults were leaner.

2) At the biochemical level, Dlk1 and Grb10 expression levels were oppositely affected by each other in E14.5 pMEFs and livers. Dlk1 acted as the upstream inhibitor of Grb10 in pMEFs as the Grb10 expression level was upregulated in *Dlk1*$^{+/p}$ pMEFs. However, the pattern of Dlk1 and Grb10 interactions in E14.5 livers was different from pMEFs.

3) RTK downstream Akt activity was slightly elevated and Erk1/2 reduced in *Grb10*$^{m/+}$ and *Grb10*$^{m/+}$/*Dlk1*$^{+/p}$ pMEFs stimulated by serum. Meanwhile, WT and *Dlk1*$^{+/p}$ pMEFs displayed similar Akt and Erk1/2 activities.

4) Downstream Akt and Erk1/2 signalling changes in knockout pMEFs supported the antagonistic functions of Dlk1 and Grb10 based on genetic evidence (Madon-Simon *et al*., 2014).

5) mTORC1 inhibition reduced Grb10 expression level in both WT and *Dlk1*$^{+/p}$ pMEFs which was in consistent with the evidence that Grb10 was stabilised by mTORC1 *in vitro* (Hsu *et al*., 2011; Yu *et al*., 2011).

Chapter 4

TMT quantitative proteomics of E14.5 *Dlk1* and *Grb10* knockout pMEFs and livers

4.1 Background

In this study, unbiased TMT quantitative proteomics analysis was adopted to identify potential signal partners and pathways involved in Dlk1 and Grb10 biochemical interactions. High throughput quantitative proteomics analysis can provide in-depth information for further Dlk1 and Grb10 function and potential mouse growth-regulatory pathway investigations, while only a few of genes or proteins can be studied using the normal targeted experiments. Unbiased method can provide more specific and even unknown targets for further Dlk1 and Grb10 experiments which may increase the targeted experiment efficiency. This work focused on proteomics and not transcriptomics study for the reason that cellular protein modifications, especially protein phosphorylation, manipulate the cell signal interactions during mouse growth regulation (Sharma *et al*., 2014). Transcriptomics analysis cannot provide the protein expression or phosphorylation information at the proteomics level. Proteomics analysis can better uncover the Dlk1 and Grb10 involved growth-regulatory pathways compare to transcriptomics. The new TMT reagents and improvements in quantitative proteomics currently allow the labelling of up to ten samples in a single analysis. This allowed comparison of two biological replicates each of E14.5 pMEF and liver samples of the four genotypes, WT, $Dlk1^{+/p}$, $Grb10^{m/+}$ and $Grb10^{m/+}/Dlk1^{+/p}$. The proteomes and phosphoproteomes from WT, $Dlk1^{+/p}$, $Grb10^{m/+}$ and $Grb10^{m/+}/Dlk1^{+/p}$ E14.5 pMEFs and livers were analysed and compared. Inevitably, the proteomics analysis used in this work has limitations. A small sample size (n=2) was adopted because one more TMT analysis will be required if we added more samples for each genotype. Another independent TMT analysis will increase the experimental errors and will be beyond our lab budget.

TMT is an isobaric chemical tag, containing a reporter, a balance and a reactive group (Figure 4.1). The reactive region can bind to the N-terminal end

of a peptide, labelling the peptide with a TMT tag (Thompson *et al*., 2003). Proteins are digested by trypsin prior to MS analyses, and each protein has a unique combination of peptides, or “fingerprint” (Thompson *et al*., 2003).

Figure 4.1 Basic structure of TMT tag. TMT tag contained a mass reporter, mass normalizer and NH_2 reactive group. Peptide will be labelled with the tag through reacting to the NH_2 reactive group.

TMT 10plex reagent was chose for this study which can label a maximum of ten samples for a single proteomics analysis. Each TMT tag has the same chemical structure (Figure 4.2A), while TMT reporter regions have varied molecular weights, through incorporation of heavy carbon or nitrogen isotopes, and the balance region normalizes the total molecular weight of each TMT tag to be identical (Figure 4.2B) (Thompson *et al*., 2003). After the first MS analysis, peptides from all different samples will generate a single MS peak in the spectrum as the TMT labelled peptides have an identical structure and molecular mass. TMT reporter ions are then released at higher energy collision dissociation (HCD) fragmentation sites prior to second MS analysis (Figure 4.2A). The intensities of peptide fragment ions based on mass to charge (m/z) ratios of the ions are then measured by MS/MS (McAlister *et al*., 2012). The quantification of protein abundance is measured from the peptide intensities, with software such as MaxQuant used to match peptide fingerprints against a protein database.

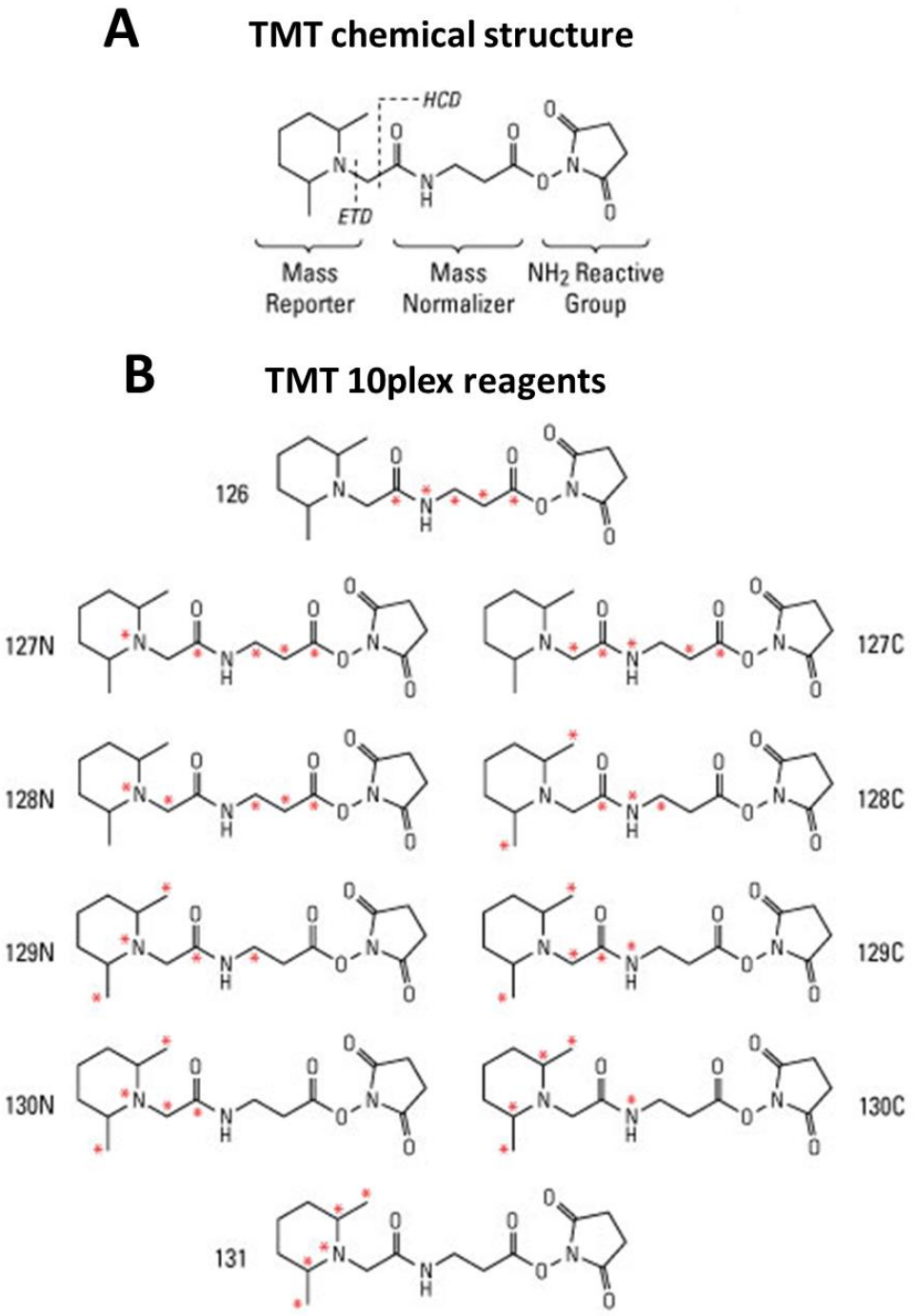

Figure 4.2 Chemical structure of TMT 10plex reagent. A) Each TMT tag has an identical chemical structure with three regions-a mass reporter, a mass normalizer and a NH_2 reactive group. HCD site-higher energy collision dissociation site. ETD site-electron transfer dissociation site. **B)** TMT 10plex reagent contains ten TMT tags with different molecular weight because of the incorporated 13C and 15N heavy isotopes. Red asterisks indicate the locations of 13C or 15N heavy isotopes in each structure. The figure was modified from https://www.thermofisher.com/order/catalog/product/90110

4.2 Methods

To compare the proteome and phosphoproteome among E14.5 WT, *Dlk1*$^{+/p}$, *Grb10*$^{m/+}$ and *Grb10*$^{m/+}$*/Dlk1*$^{+/p}$ embryos, fresh E14.5 pMEF cell lines and pure livers were derived from individual embryos. E14.5 pMEF and liver replicates of WT, *Dlk1*$^{+/p}$, *Grb10*$^{m/+}$ and *Grb10*$^{m/+}$*/Dlk1*$^{+/p}$ from different litters were selected to undertake two independent TMT analyses, one for pMEFs and one for livers (Figure 4.3A). Total proteins were extracted and digested to peptides from each pMEF and liver sample. Peptides of each sample were labelled with 8 different TMT isobaric tags from the TMT 10plex reagents prior to chromatography and mass spectrometry (MS) analyses (Figure 4.3A). MS spectra generated from the spectrometer were analysed by MaxQuant software to search against the Uniprot Mouse database downloaded on 170415 (73324 entries). The MS intensities from each sample acquired using MaxQuant were filtered for FDR below 1%. The MS intensity of each protein or phosphorylated site was considered as the protein expression or phosphorylation level, respectively (Figure 4.3B). Ratios of *Dlk1*$^{+/p}$, *Grb10*$^{m/+}$ and *Grb10*$^{m/+}$*/Dlk1*$^{+/p}$ values from each biological replicate versus WT were calculated and $\log_2$ transformed. The mean values of the $\log_2$ transformed ratios, representing the protein expression or phosphorylation fold changes of the knockout versus WT, were then used for bioinformatics analyses (Figure 4.3B).

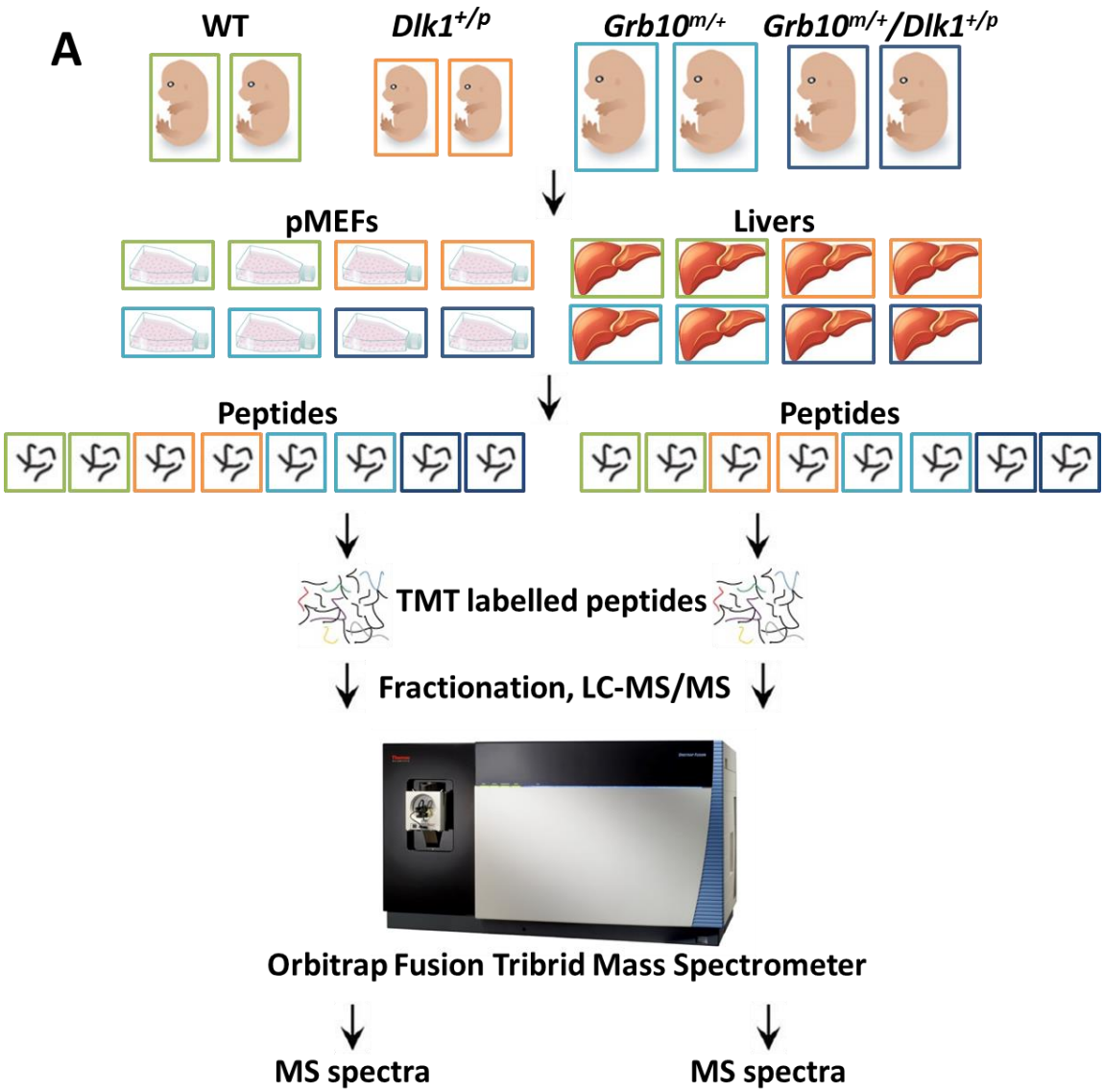
A
WT
Dlk1+/p
Grb10m/+
Grb10m/+/Dlk1+/p
pMEFs
Livers
Peptides
Peptides
TMT labelled peptides
Fractionation, LC-MS/MS
Orbitrap Fusion Tribrid Mass Spectrometer
MS spectra
MS spectra

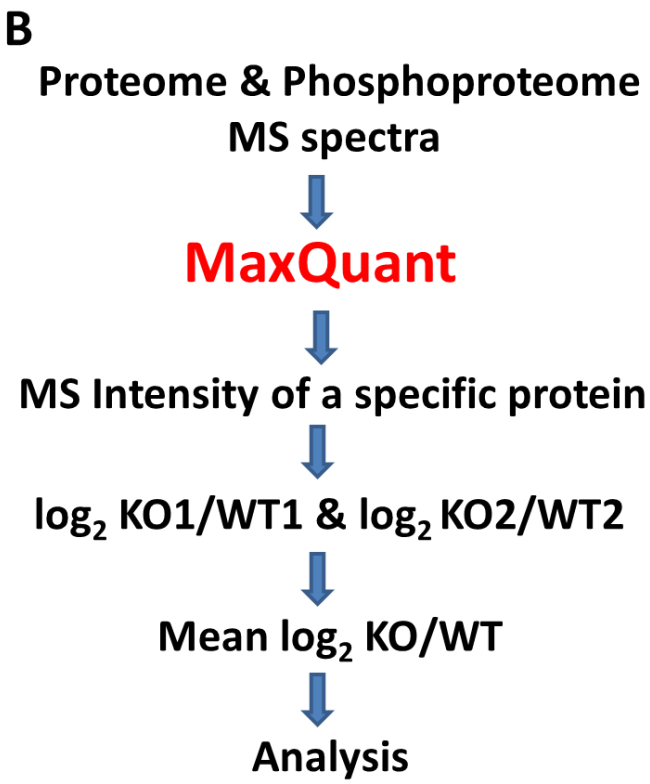

Figure 4.3 Workflow of TMT proteomics analysis. A) Samples from WT, *Dlk1*$^{+/p}$, *Grb10*$^{m/+}$ and *Grb10*$^{m/+}$/*Dlk1*$^{+/p}$ are labelled with green, orange, light blue and dark blue rectangles, respectively. E14.5 pMEF and liver TMT analyses were performed separately. **B)** Bioinformatics analysis strategy following MS analysis. Protein MS intensity from each TMT tag was extracted using MaxQuant v1.5.3.8 software. MS intensity ratio of knockout versus WT was calculated and then $\log_2$ transformed. Mean ratio of the two biological replicates was used for following bioinformatics analyses. Blue arrow indicated the order of data calculation steps. KO, knockout (*Dlk1*$^{+/p}$, *Grb10*$^{m/+}$ and *Grb10*$^{m/+}$/*Dlk1*$^{+/p}$).

4.3 Results

4.3.1 TMT quantitative proteomics data output

For E14.5 pMEF and liver total proteome, a list of 6174 proteins were identified, including 5499 proteins without missing values from any of the 8 samples in each dataset (Figure 4.4A). In parallel, 3208 phosphorylated sites were identified in the pMEF phosphoproteome of which 2061 were class I sites (localisation probability>0.75), and in the liver phosphoproteome, there were 4113 phosphorylated sites identified, with 2739 class I sites. However, a shorter list of 832 and 1269 "core" phosphorylation sites without missing values from all the samples were detected in pMEF and liver phosphoproteomes, respectively (Figure 4.4A). Within the 832 "core" pMEF phosphoproteins, 1457, 271 and 29 phosphorylated serine, threonine and tyrosine sites were identified, respectively (Figure 4.4B). Similarly, in the 1269 "core" liver phosphoproteins there were 2690, 383 and 53 phosphorylated serine, threonine and tyrosine sites, respectively (Figure 4.4B).

A **Summary of identified proteins**

	Proteome		Phosphoproteome	
	Response	Value	Response	Value
pMEFs	6174	5499	3208	832
Livers	6174	5499	4113	1269

B **Identified sites without missing values**

	pMEFs	Livers
pS	1457	2690
pT	271	383
pY	29	53
pSTY	1757	3126

Figure 4.4 Data output of TMT proteomics. A) Number of the identified proteins (Response) and proteins without missing value from any TMT tag

(Value) in pMEF and liver total proteomes and phosphoproteomes. **B)** Number of identified phosphorylated sites without missing value from any TMT tag in pMEF and liver phosphoproteomes. pS: phospho-Serine; pT: phospho-Threonine; pY: phosho-Tyrosine; pSTY: phospho-Serine, phospho-Threonine and phosho-Tyrosine.

4.3.2 PCA and HCL analyses for proteomics and phosphoproteomics profiles from the four genotypes of E14.5 pMEFs and livers

Dlk1$^{+/p}$ and *Grb10*$^{m/+}$ embryos and adults exhibited opposite growth and metabolic health phenotypes (Figure 3.1; 3.2) (Madon-Simon *et al*., 2014). Further, in crosses to generate mice of all four genotypes, *Grb10*$^{m/+}$ and *Grb10*$^{m/+}$*/Dlk1*$^{+/p}$ embryos were similar to each other and distinct from WT and *Dlk1*$^{+/p}$ embryos. To evaluate the similarity and divergence of *Dlk1*$^{+/p}$, *Grb10*$^{m/+}$ and *Grb10*$^{m/+}$*/Dlk1*$^{+/p}$ E14.5 embryos at a proteomics level, PCA analyses were carried out on pMEF and liver proteome and phosphoproteome data sets using JMP10 software (Ringnér, 2008), and HCL analyses based on Pearson correlation coefficient (*r*) were performed using GraphPad Prism 6 and MeV v4.9.0 software. PCA and HCL analyses were performed on the original MS intensities of replicates from all four genotypes and the mean $\log_2$ transformed ratios of knockout samples versus WT. PCA analyses of individual samples revealed that E14.5 pMEF proteomes and phosphoproteomes possessed 92.2% and 75.6% of data variability in component 1, respectively (Figure 4.5A, B). Meanwhile, 92.2% and 98.3% of data variability was retained in component 1 of the liver proteomes and phosphoproteomes, respectively (Figure 4.5C, D). However, PCA and HCL analyses of individual samples displayed low biological reproducibility as the replicates of each genotype did not share similarities in both their proteomes and phosphoproteomes (Figure 4.5A-H).

For the second set of PCA analyses, protein expression or phosphorylation changes in the knockout samples versus WT were considered as the variances. The protein expression or phosphorylation variations from each data set were reduced to a few principle components, and the first two components (component 1 and component 2) retained the largest variations among all the components. The data variations were expressed as a scatter plot projected to component 1 and component 2. The red arrows indicated the main direction of the data group projected to these two components (Figure

4.5I-L). In E14.5 pMEF and liver proteomes, component 1 possessed 80.7% and 61.3% of data variability, respectively. Notably, PCA revealed that *Grb10*$^{m/+}$ and *Grb10*$^{m/+}$*/Dlk1*$^{+/p}$ pMEFs and livers were closer at the total proteome level, while *Dlk1*$^{+/p}$ was divergent from *Grb10*$^{m/+}$ and *Grb10*$^{m/+}$*/Dlk1*$^{+/p}$ (Figure 4.5I, K). In parallel, 78% and 64.7% of data variability was retained in component 1 of the pMEF and liver phosphoproteomes, respectively.

HCL analyses showed that *Grb10*$^{m/+}$ and *Grb10*$^{m/+}$*/Dlk1*$^{+/p}$ samples, both pMEFs and livers, were consistently grouped in the same cluster, using protein expression or phosphorylation changes in the knockout samples versus WT (Figure 4.5E-H). For pMEF and liver proteomes and phosphoproteomes, Pearson correlation coefficient (***r***) between *Grb10*$^{m/+}$ and *Grb10*$^{m/+}$*/Dlk1*$^{+/p}$ samples were around 0.75, while Pearson correlation coefficient (***r***) between *Dlk1*$^{+/p}$ and *Grb10*$^{m/+}$, *Dlk1*$^{+/p}$ and *Grb10*$^{m/+}$*/Dlk1*$^{+/p}$ were lower than 0.5 (Figure 4.5E-H).

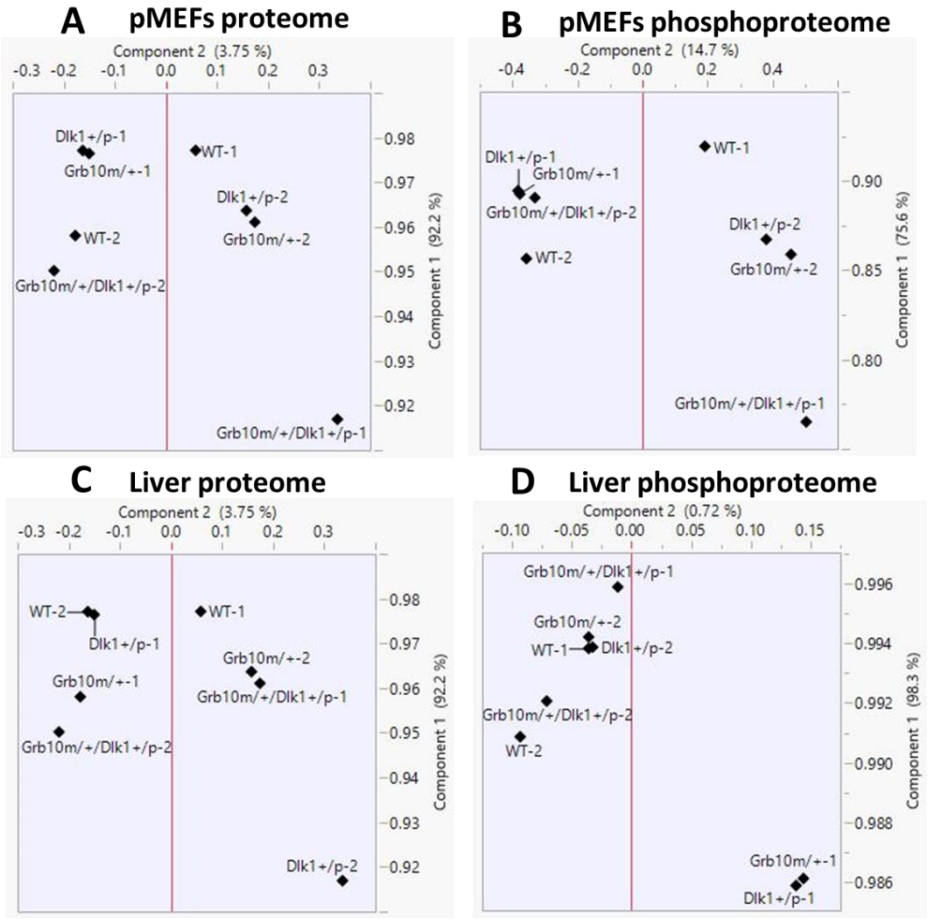
A
pMEFs proteome
Component 2 (3.75 %)
-0.3 -0.2 -0.1 0.0 0.1 0.2 0.3
Dlk1+/p-1
Grb10m/+-1
WT-1
Dlk1+/p-2
Grb10m/+-2
WT-2
Grb10m/+/Dlk1+/p-2
Grb10m/+/Dlk1+/p-1
0.98
0.97
0.96
0.95
0.94
0.93
0.92
Component 1 (92.2 %)
B
pMEFs phosphoproteome
Component 2 (14.7 %)
-0.4 -0.2 0.0 0.2 0.4
Dlk1+/p-1
Grb10m/+-1
Grb10m/+/Dlk1+/p-2
WT-1
Dlk1+/p-2
Grb10m/+-2
WT-2
Grb10m/+/Dlk1+/p-1
0.90
0.85
0.80
Component 1 (75.6 %)
C
Liver proteome
Component 2 (3.75 %)
-0.3 -0.2 -0.1 0.0 0.1 0.2 0.3
WT-2
Dlk1+/p-1
WT-1
Grb10m/+-2
Grb10m/+/Dlk1+/p-1
Grb10m/+-1
Grb10m/+/Dlk1+/p-2
Dlk1+/p-2
0.98
0.97
0.96
0.95
0.94
0.93
0.92
Component 1 (92.2 %)
D
Liver phosphoproteome
Component 2 (0.72 %)
-0.10 -0.05 0.00 0.05 0.10 0.15
Grb10m/+/Dlk1+/p-1
Grb10m/+-2
WT-1
Dlk1+/p-2
Grb10m/+/Dlk1+/p-2
WT-2
Grb10m/+-1
Dlk1+/p-1
0.996
0.994
0.992
0.990
0.988
0.986
Component 1 (98.3 %)
E
pMEFs proteome
0.0 0.92 1.0
DKO-1
Grb10KO-2
D1k1KO-2
WT-1
WT-2
D1k1KO-1
Grb10KO-1
DKO-2
r
-0.49859047
0.25070477
1.0
DKO-1
Grb10KO-2
D1k1KO-2
WT-1
WT-2
D1k1KO-1
Grb10KO-1
DKO-2
F
pMEFs phosphoproteome
0.0 0.75 1.0
DKO-1
Grb10KO-2
D1k1KO-2
WT-1
Grb10KO-1
D1k1KO-1
DKO-2
WT-2
r
-0.63847005
0.18076497
1.0
DKO-1
Grb10KO-2
D1k1KO-2
WT-1
Grb10KO-1
D1k1KO-1
DKO-2
WT-2
G
Liver proteome
0.0 0.92 1.0
D1k1KO-2
DKO-1
Grb10KO-2
WT-1
Grb10KO-1
WT-2
D1k1KO-1
DKO-2
r
-0.49859047
0.25070477
1.0
D1k1KO-2
DKO-1
Grb10KO-2
WT-1
Grb10KO-1
WT-2
D1k1KO-1
DKO-2
H
Liver phosphoproteome
0.0 0.98 1.0
D1k1KO-1
Grb10KO-1
WT-1
DKO-1
DKO-2
Grb10KO-2
WT-2
D1k1KO-2
r
-0.65402234
0.17298883
1.0
D1k1KO-1
Grb10KO-1
WT-1
DKO-1
DKO-2
Grb10KO-2
WT-2
D1k1KO-2

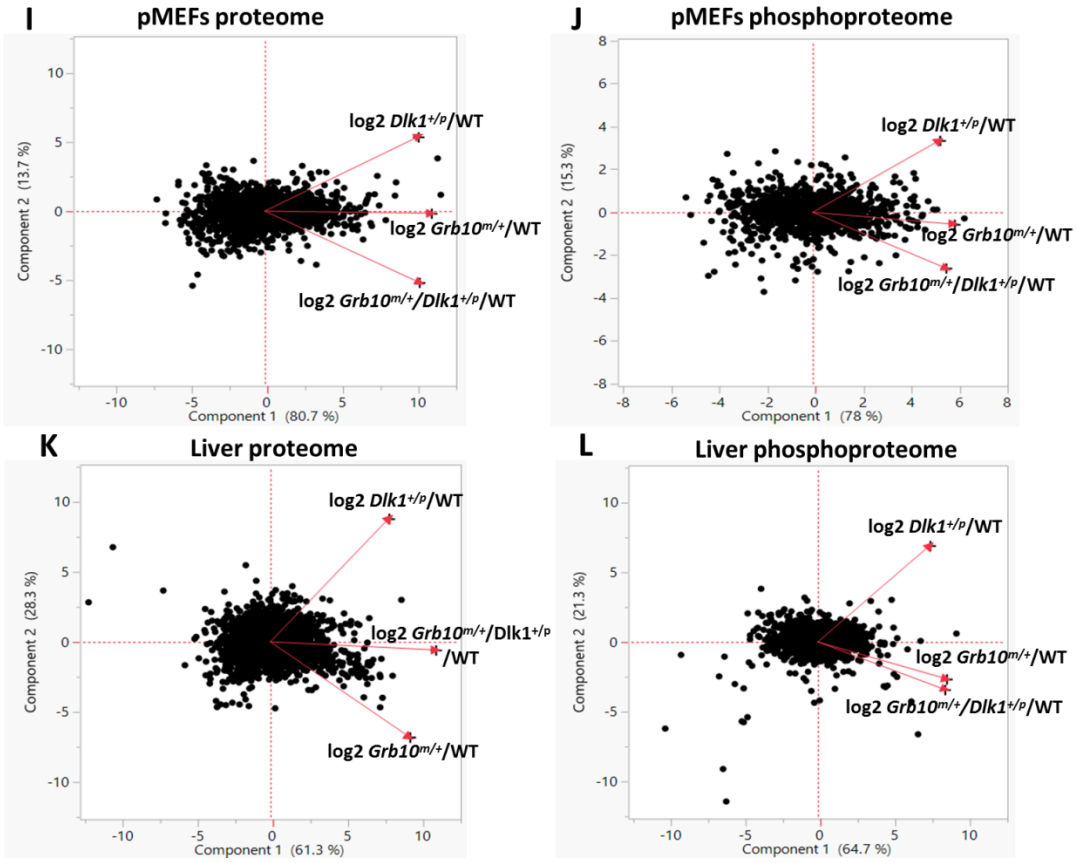
I
pMEFs proteome
log2 Dlk1+/p/WT
log2 Grb10m/+/WT
log2 Grb10m/+/Dlk1+/p/WT
Component 2 (13.7 %)
Component 1 (80.7 %)
J
pMEFs phosphoproteome
log2 Dlk1+/p/WT
log2 Grb10m/+/WT
log2 Grb10m/+/Dlk1+/p/WT
Component 2 (15.3 %)
Component 1 (78 %)
K
Liver proteome
log2 Dlk1+/p/WT
log2 Grb10m/+/Dlk1+/p/WT
log2 Grb10m/+/WT
Component 2 (28.3 %)
Component 1 (61.3 %)
L
Liver phosphoproteome
log2 Dlk1+/p/WT
log2 Grb10m/+/WT
log2 Grb10m/+/Dlk1+/p/WT
Component 2 (21.3 %)
Component 1 (64.7 %)

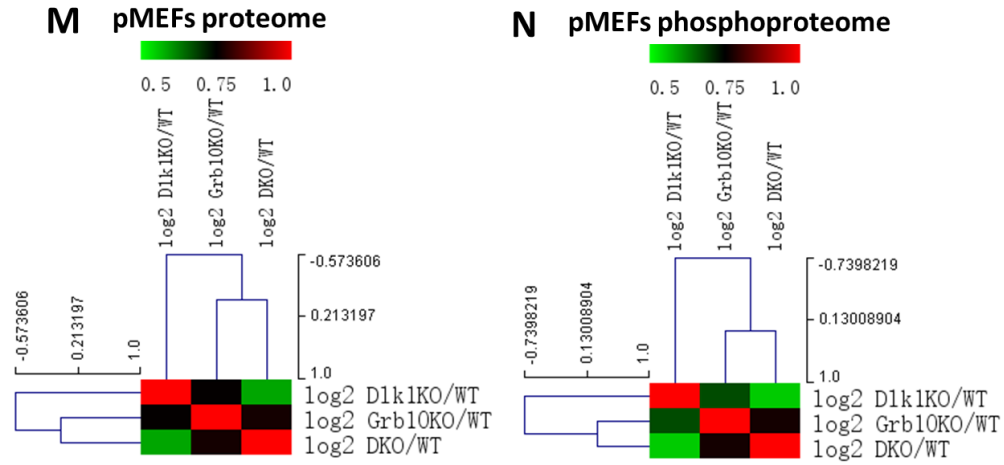
M
pMEFs proteome
0.5 0.75 1.0
log2 D1k1KO/WT
log2 Grb10KO/WT
log2 DKO/WT
-0.573606
0.213197
1.0
log2 D1k1KO/WT
log2 Grb10KO/WT
log2 DKO/WT
N
pMEFs phosphoproteome
0.5 0.75 1.0
log2 D1k1KO/WT
log2 Grb10KO/WT
log2 DKO/WT
-0.7398219
0.13008904
1.0
log2 D1k1KO/WT
log2 Grb10KO/WT
log2 DKO/WT

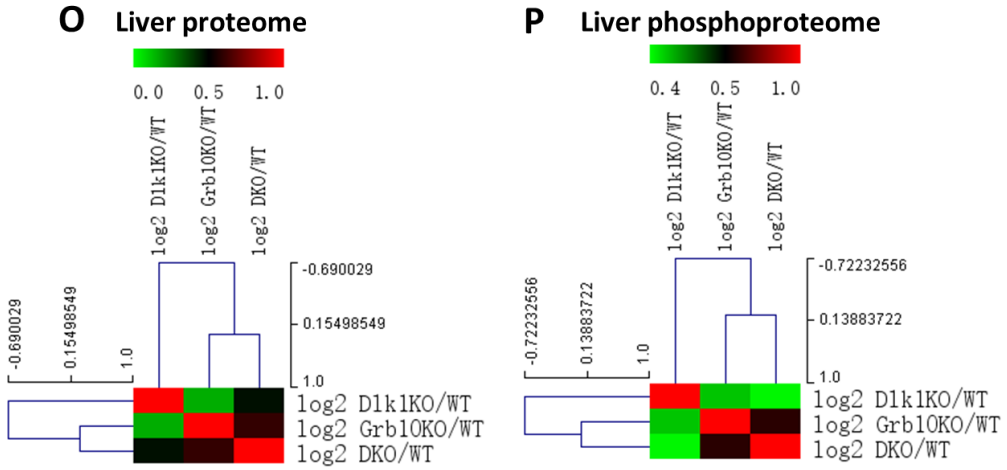
O
Liver proteome
0.0 0.5 1.0
log2 D1k1KO/WT
log2 Grb10KO/WT
log2 DKO/WT
-0.690029
0.15498549
1.0
log2 D1k1KO/WT
log2 Grb10KO/WT
log2 DKO/WT
P
Liver phosphoproteome
0.4 0.5 1.0
log2 D1k1KO/WT
log2 Grb10KO/WT
log2 DKO/WT
-0.72232556
0.13883722
1.0
log2 D1k1KO/WT
log2 Grb10KO/WT
log2 DKO/WT

Figure 4.5 PCA and HCL analyses of E14.5 pMEF and liver proteomes and phosphoproteomes. Protein expression or phosphorylation levels from all eight samples were projected to the first two components, and the variance projections on component 1 and component 2 were expressed as a two-dimensional scatter plot. **A)** pMEF proteome. **B)** pMEF phosphoproteome. **C)** Liver proteome. **D)** Liver phosphoproteome. HCL results of all eight samples were visualized as Heatmaps using Pearson correlation coefficient (***r***). Each square represented Pearson correlation coefficient (***r***) between any two samples. Green and red scale above the Heatmap indicated the Pearson correlation coefficient (***r***) values. **E)** pMEF proteome. **F)** pMEF phosphoproteome. **G)** Liver proteome. **H)** Liver phosphoproteome. Protein expression or phosphorylation ratios of knockout versus WT were projected to the first two components, and the variances were expressed as a two-dimensional scatter plot. Red arrow in each data set indicated the main direction of each knockout sample projected on component 1 and component 2. **I)** pMEF proteome. **J)** pMEF phosphoproteome. **K)** Liver proteome. **L)** Liver phosphoproteome. HCL analyses based on Pearson correlation coefficient (***r***) were visualized as Heatmaps among *Dlk1*$^{+/p}$, *Grb10*$^{m/+}$ and *Grb10*$^{m/+}$/*Dlk1*$^{+/p}$ samples using WT as the denominator. Each square represented Pearson correlation coefficient (***r***) between any two knockout samples. Green and red scale above the Heatmap indicated the Pearson correlation coefficient (***r***) values. **M)** pMEF proteome. **N)** pMEF phosphoproteome. **O)** Liver proteome. **P)** Liver phosphoproteome.

4.3.3 Distinct patterns of reduced expression were found in E14.5 pMEF and liver proteomes and phosphoproteomes

To look at the overall distribution of protein expression or phosphorylation detected by TMT proteomics analyses *in vitro* and *in vivo*, four scatter plots were presented for each individual pMEF and liver data set, using mean value of $\log_2$ *Grb10*$^{m/+}$/*Dlk1*$^{+/p}$/WT as the X-axis value and mean $\log_2$ *Dlk1*$^{+/p}$/WT or $\log_2$ *Grb10*$^{m/+}$/WT as the Y-axis values (Figure 4.6). A stringent 4-fold change was set as the threshold (faint dotted lines) for pMEF and liver proteomes because of the large data size, while a 1.5-fold change was set for pMEF and liver phosphoproteomes (Figure 4.6). As can be seen in the E14.5 pMEF proteome and phosphoproteome plots, a large amount of proteins displayed 4-fold down regulation in *Grb10*$^{m/+}$/*Dlk1*$^{+/p}$ compared to WT pMEFs. Most of those proteins had a reduction trend in *Dlk1*$^{+/p}$ and *Grb10*$^{m/+}$ pMEFs as well (Figure 4.6A, B). The liver proteome also showed a pattern of reduction in protein expression, similar to the pMEF proteome (Figure 4.6C), but it was less marked and there was a greater difference between expression profiles in response to single and double knockout of *Dlk1* and *Grb10* in E14.5 livers. In particular, a group of proteins were 4-fold down in *Dlk1*$^{+/p}$ compared to WT livers, and a relatively smaller amount of proteins were 4-fold downregulated in *Grb10*$^{m/+}$ and *Grb10*$^{m/+}$/*Dlk1*$^{+/p}$ livers (Figure 4.6C). In the E14.5 liver phosphoproteome plot, most of the scatter was located inside the 1.5-fold change threshold. A few phosphorylated proteins were more than 1.5-fold down in *Grb10*$^{m/+}$/*Dlk1*$^{+/p}$ livers (Figure 4.6D). Notably, E14.5 *Grb10*$^{m/+}$ and *Grb10*$^{m/+}$/*Dlk1*$^{+/p}$ pMEFs and livers behaved similarly at the proteomic level.

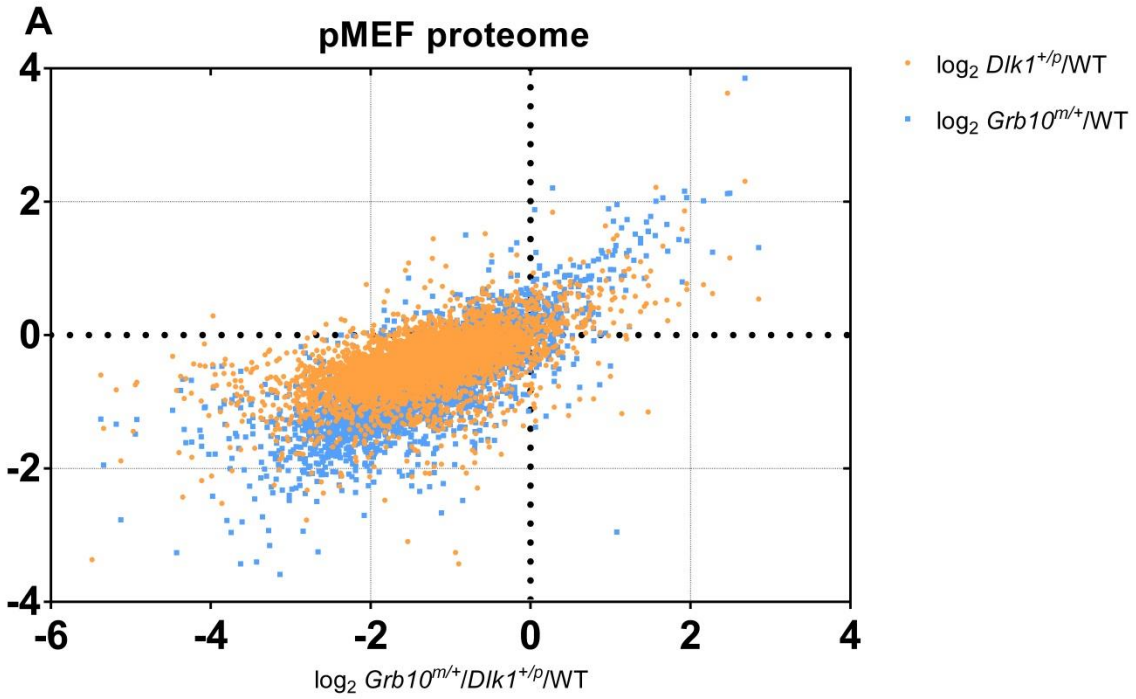
A
pMEF proteome
log2 Dlk1+/p/WT
log2 Grb10m/+/WT
log2 Grb10m/+/Dlk1+/p/WT

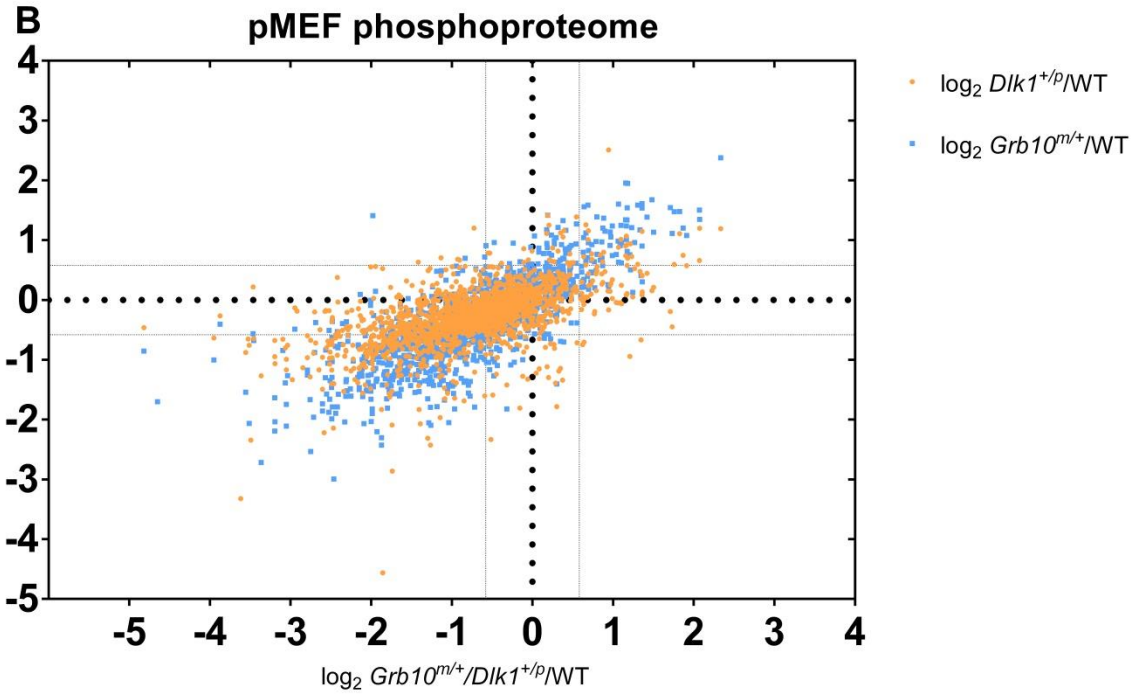
B
pMEF phosphoproteome
log2 Dlk1+/p/WT
log2 Grb10m/+/WT
log2 Grb10m/+/Dlk1+/p/WT

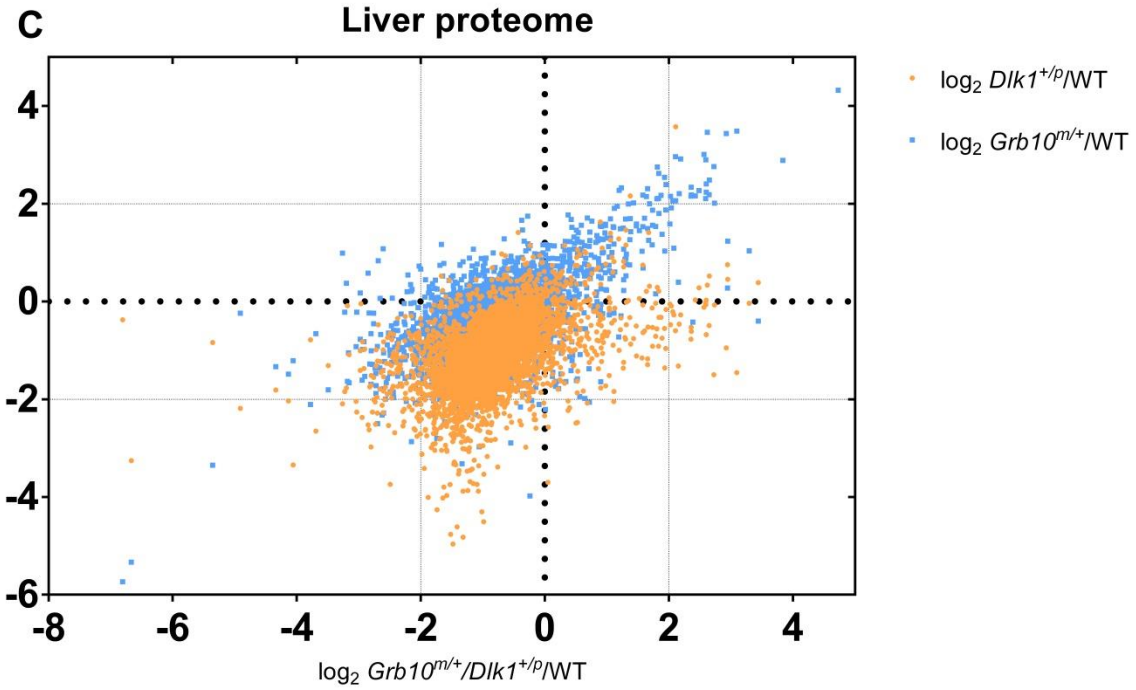
C
Liver proteome
4
2
0
-2
-4
-6
-8
-6
-4
-2
0
2
4
log2 Grb10m/+/Dlk1+/p/WT
log2 Dlk1+/p/WT
log2 Grb10m/+/WT

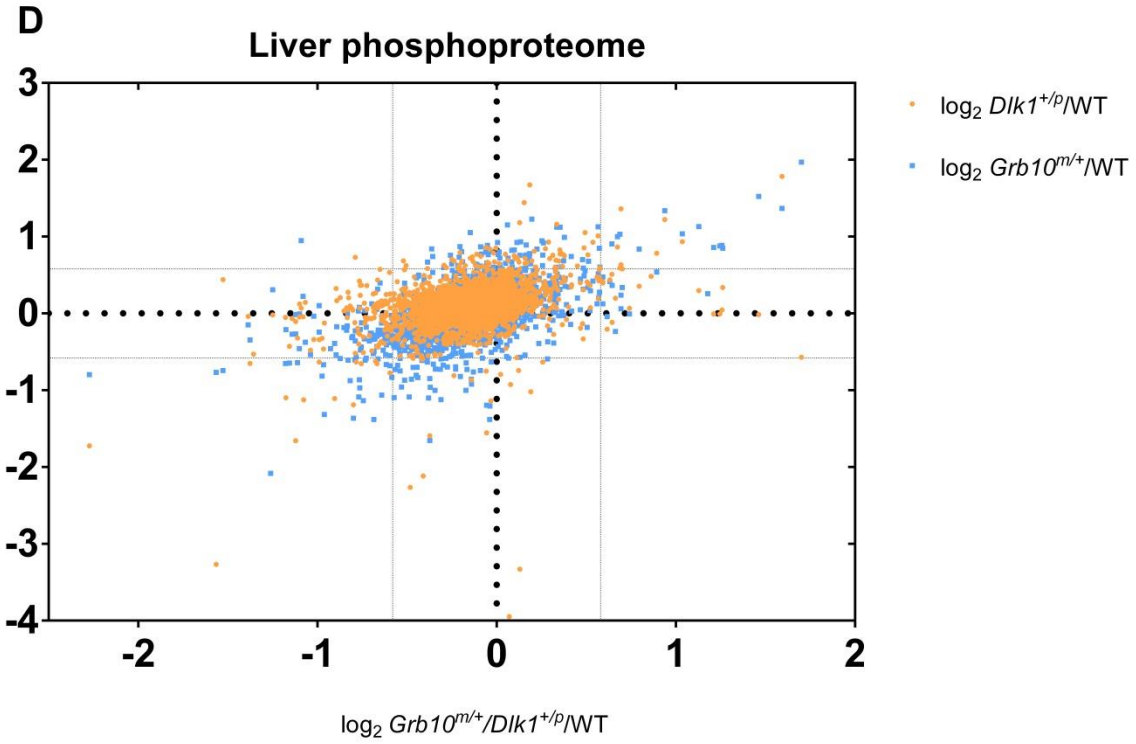
D
Liver phosphoproteome
3
2
1
0
-1
-2
-3
-4
-2
-1
0
1
2
log2 Grb10m/+/Dlk1+/p/WT
log2 Dlk1+/p/WT
log2 Grb10m/+/WT

Figure 4.6 Scatter plots of E14.5 pMEF and liver proteomes and phosphoproteomes. Each dot represented a logarithmically transformed protein or phosphorylated protein expression value, expressed as a ratio of knockout versus WT. Yellow dots were the proteins plotted for the expression or phosphorylation levels of *Dlk1*$^{+/p}$/WT against *Grb10*$^{m/+}$/*Dlk1*$^{+/p}$/WT. Blue dots were the proteins plotted for the expression or phosphorylation levels of *Grb10*$^{m/+}$/WT against *Grb10*$^{m/+}$/*Dlk1*$^{+/p}$/WT. Bold dotted lines were the X and Y axes. Faint dotted lines indicated 4-fold and 1.5-fold change thresholds for total proteomes and phosphoproteomes, respectively. **A)** pMEF proteome. **B)** pMEF phosphoproteome. **C)** Liver proteome. **D)** Liver phosphoproteome.

4.3.4 Transmembrane receptor signalling related GO-terms were enriched in *Dlk1*$^{+/p}$, *Grb10*$^{m/+}$, and *Grb10*$^{m/+}$/*Dlk1*$^{+/p}$ pMEF and liver proteome

To evaluate the biological functions of proteins and phosphorylated proteins with changes in levels outside of the respective 4- and 1.5-fold thresholds (Figure 4.6), GO-term enrichment analysis was carried out using these proteins as the target list and the complete data set as the background using online GO-term analysis tool “Gorilla” (http://cbl-gorilla.cs.technion.ac.il/). The enriched GO-terms from pMEF and liver proteomes and phosphoproteomes were combined and visualized as a Heatmap, in which green boxes indicated the significantly enriched terms (Figure 4.7). The detailed results of GO-term enrichment analysis were listed in tables in Appendix (Table 7.2). Notably, a number of GO-terms relating to membrane associated proteins were enriched in both pMEF and liver proteomes, indicating that a subset of proteins with differential expression in knockout pMEF and liver were involved in transmembrane receptor signaling at a total proteomics level. Relevant enriched GO-terms included: “membrane part”, “extracellular region”, “integral component of membrane”, “transmembrane receptor activity”, “transmembrane signaling receptor activity” and “transmembrane receptor protein kinase activity”. Additionally, the GO-terms “cytoplasmic part”, “vesicle”, “lysosome” and “lipid metabolic process” were enriched, but only in the pMEF proteome. The GO-terms “intrinsic/integral component of plasma membrane”, “elastic fiber”, “phagocytic vesicle”, “receptor activity”, “signaling receptor activity”, “signal transducer activity”, “molecular transducer activity”, “calcium ion binding” and “negative regulation of cell proliferation” were specifically enriched in the liver proteome. The GO-terms “hydrolase activity” and “ATPase activity” were enriched only in the pMEF phosphoproteome, while “negative regulation of immune system process”, “regulation of myeloid cell differentiation” and “negative regulation of hemopoiesis” GO-terms were specifically enriched in the liver phosphoproteome (Figure 4.7).

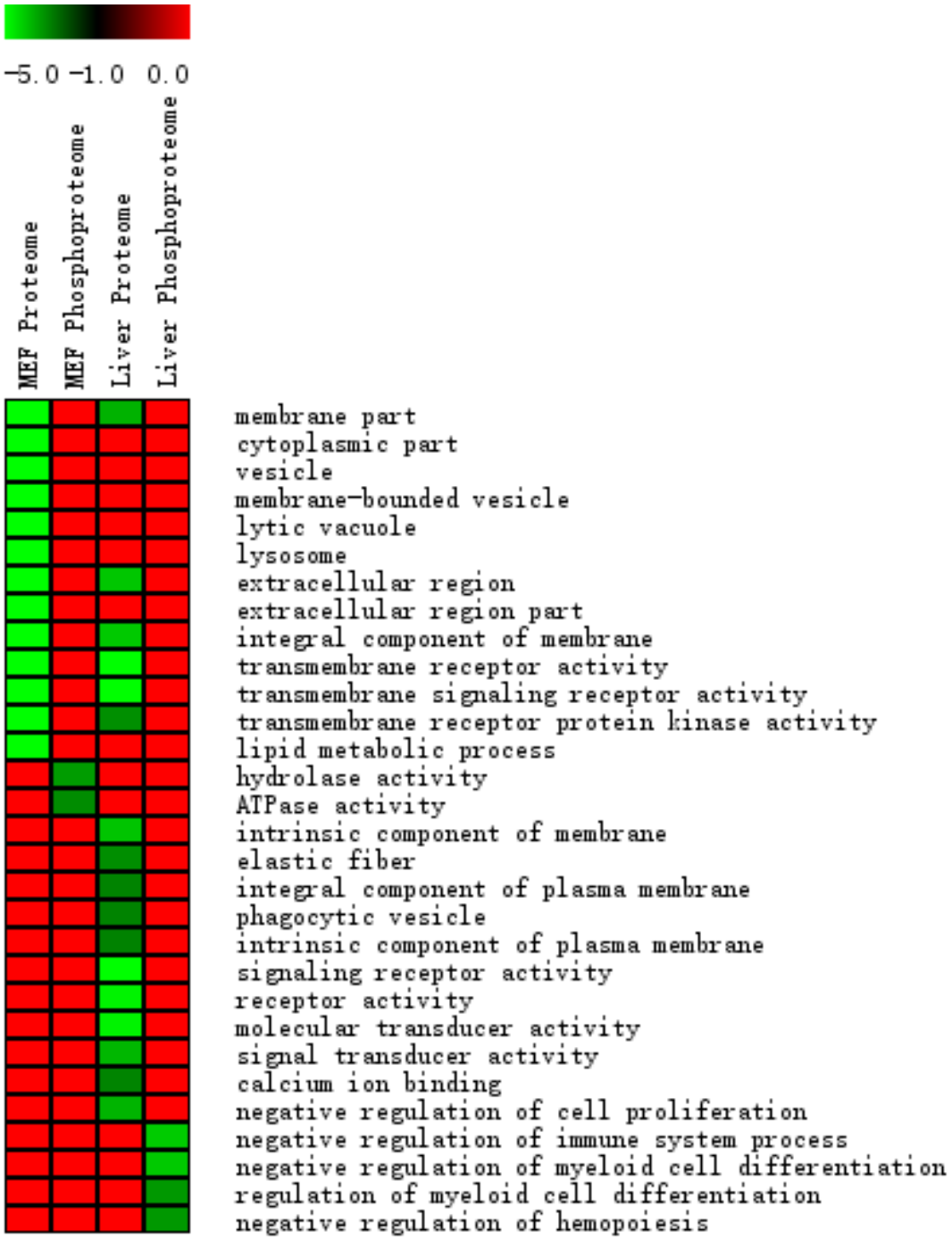

Figure 4.7 Heatmap summary of GO-term enrichment analyses of E14.5 pMEF and liver proteomes and phosphoproteomes. Four columns summarise GO-terms enriched in one or more of the E14.5 proteome data sets, from left to right: pMEF proteome, pMEF phosphoproteome, liver proteome and liver phosphoproteome. Enriched GO-terms discovered from the four data sets are listed to the right of the heat map. Enriched GO-terms are shown as green, while non-enriched GO-terms are red. Brightness of the green boxes indicates the significance of each enriched GO-term.

4.3.5 Proteomics analysis revealed expression of several RTKs was decreased in E14.5 *Dlk1*$^{+/p}$, *Grb10*$^{m/+}$ and *Grb10*$^{m/+}$/*Dlk1*$^{+/p}$ pMEFs and livers

A protein list was retrieved from the enriched molecular function GO-terms of “transmembrane receptor activity”, “transmembrane signaling receptor activity” and “transmembrane receptor protein kinase activity”, as these GO-terms were enriched in E14.5 pMEF and liver proteomes. The expression ratios of these proteins in knockout pMEF and liver versus WT were $\log_2$ transformed and expressed as a Heatmap with upregulated proteins in red and downregulated proteins in green boxes (Figure 4.8), and as two individual scatter plots using $\log_2$ *Grb10*$^{m/+}$/*Dlk1*$^{+/p}$ values as the X-axis (Figure 4.8). Interestingly, most of these proteins were downregulated in *Dlk1*$^{+/p}$, *Grb10*$^{m/+}$ and *Grb10*$^{m/+}$/*Dlk1*$^{+/p}$ compared to WT at the proteomic level. In particular, protein expression levels of several RTKs including PDGFRa, FGFR1, Tgfbr3, Ephb3, Lpar1, Npr3, Itpr1 and Ryr3 were reduced in *Dlk1*$^{+/p}$, *Grb10*$^{m/+}$ and *Grb10*$^{m/+}$/*Dlk1*$^{+/p}$ pMEF and liver compared to WT (Figure 4.8). In addition, Kcnk1 was the only protein with increase expression in *Dlk1*$^{+/p}$, *Grb10*$^{m/+}$ and *Grb10*$^{m/+}$/*Dlk1*$^{+/p}$ pMEF and liver. Ddr2, Erbb2 and Vmn1r30 expression were only increased in *Grb10*$^{m/+}$ pMEF and decreased in all the other knockout data sets. Ptpn6, Itgb2 and Abca1 expression levels were found to be specifically elevated in *Grb10*$^{m/+}$ and *Grb10*$^{m/+}$/*Dlk1*$^{+/p}$ livers. Sfrp1 and Fcgrt expression were slightly increased in *Grb10*$^{m/+}$ liver and decreased in other knockout data sets. Cd40 had a varied expression pattern in different data sets, showing an increase in *Dlk1*$^{+/p}$ pMEF, *Grb10*$^{m/+}$ and *Grb10*$^{m/+}$/*Dlk1*$^{+/p}$ livers and a decrease in *Dlk1*$^{+/p}$ liver and *Grb10*$^{m/+}$/*Dlk1*$^{+/p}$ pMEF (Figure 4.8).

A

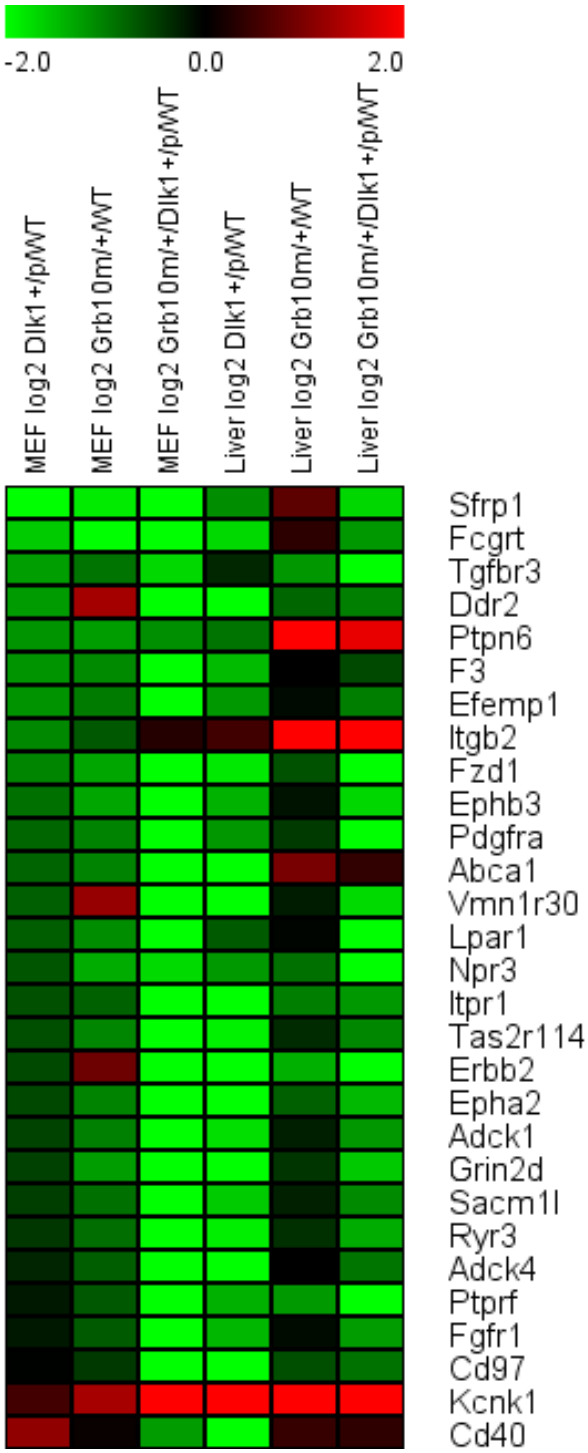
-2.0
0.0
2.0
MEF log2 Dlk1+/pWT
MEF log2 Grb10m/+WT
MEF log2 Grb10m/+/Dlk1+/pWT
Liver log2 Dlk1+/pWT
Liver log2 Grb10m/+WT
Liver log2 Grb10m/+/Dlk1+/pWT
Sfrp1
Fcgrt
Tgfbr3
Ddr2
Ptpn6
F3
Efemp1
Itgb2
Fzd1
Ephb3
Pdgfra
Abca1
Vmn1r30
Lpar1
Npr3
Itpr1
Tas2r114
Erbb2
Epha2
Adck1
Grin2d
Sacm1l
Ryr3
Adck4
Ptprf
Fgfr1
Cd97
Kcnk1
Cd40

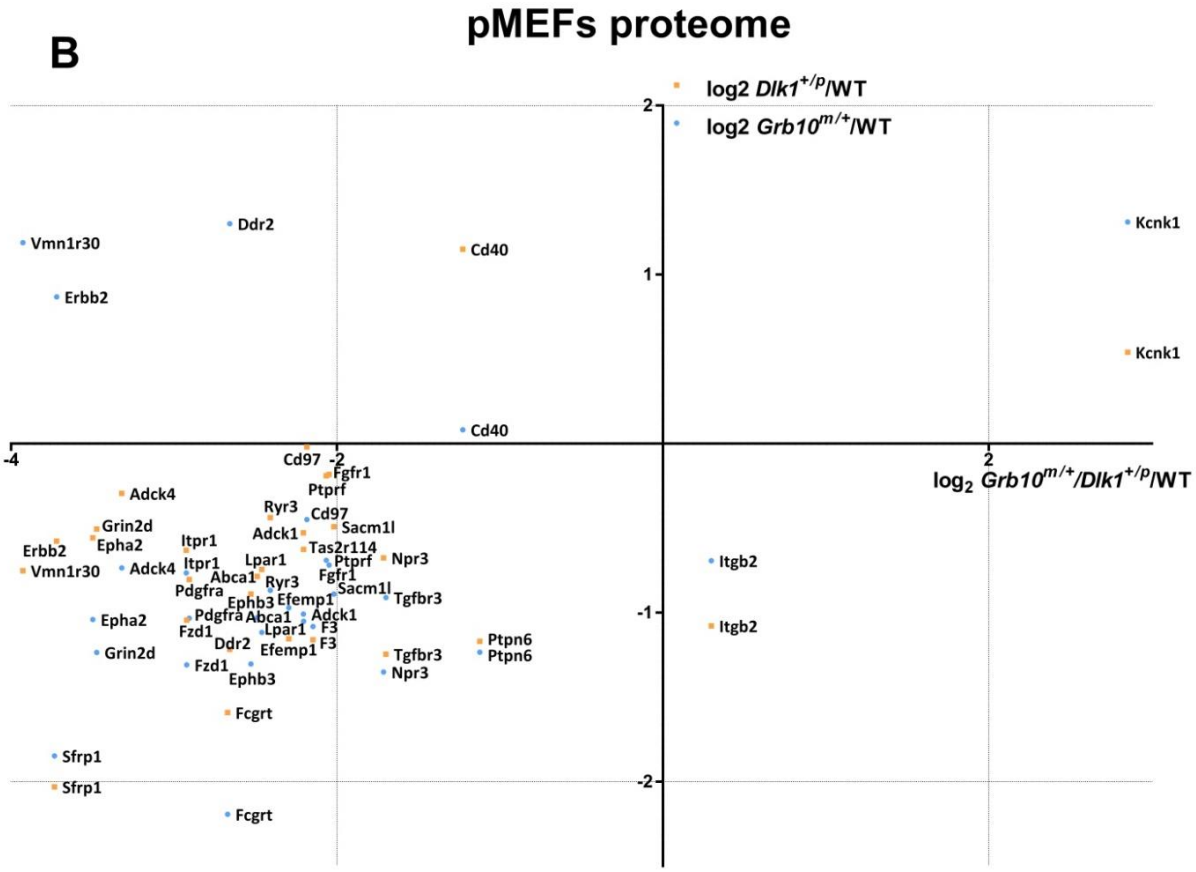
B
pMEFs proteome
log2 Dlk1+/p/WT
log2 Grb10m/+/WT
log2 Grb10m/+/Dlk1+/p/WT
Ddr2
Vmn1r30
Cd40
Kcnk1
Erbb2
Kcnk1
Cd40
Cd97
Fgfr1
Ptprf
Adck4
Ryr3
Cd97
Grin2d
Adck1
Sacm1l
Epha2
Itpr1
Tas2r114
Erbb2
Itpr1
Lpar1
Ptprf
Npr3
Vmn1r30
Adck4
Abca1
Fgfr1
Itgb2
Pdgfra
Ryr3
Sacm1l
Ephb3
Efemp1
Tgfbr3
Itgb2
Epha2
Pdgfra
Abca1
Adck1
Fzd1
Lpar1
F3
Ptpn6
Grin2d
Ddr2
Efemp1
F3
Tgfbr3
Ptpn6
Fzd1
Npr3
Ephb3
Fcgrt
Sfrp1
Sfrp1
Fcgrt

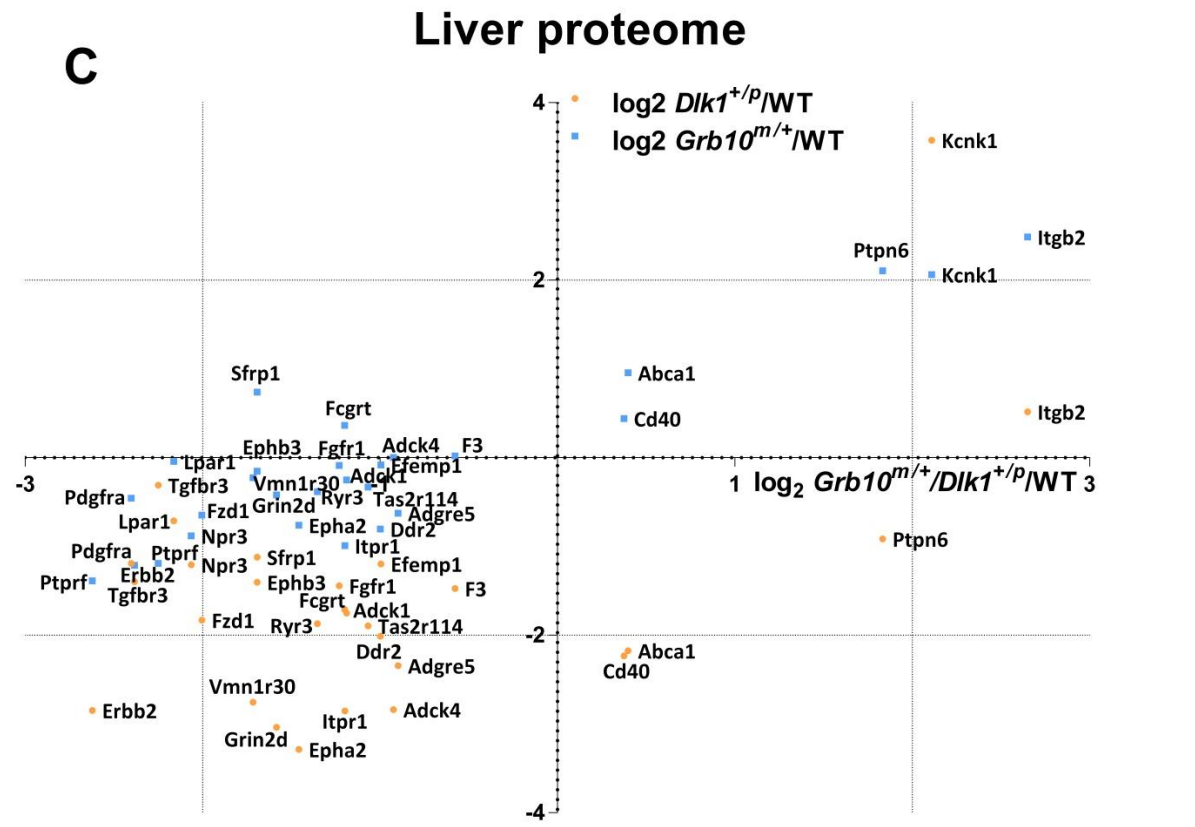
C
Liver proteome
log2 Dlk1+/p/WT
log2 Grb10m/+/WT
log2 Grb10m/+/Dlk1+/p/WT
Kcnk1
Itgb2
Ptpn6
Kcnk1
Sfrp1
Abca1
Fcgrt
Cd40
Itgb2
Ephb3
Fgfr1
Adck4
F3
Lpar1
Efemp1
Vmn1r30
Adck1
Pdgfra
Tgfbr3
Ryr3
Tas2r114
Grin2d
Fzd1
Adgre5
Lpar1
Epha2
Ddr2
Ptpn6
Npr3
Itpr1
Pdgfra
Ptprf
Npr3
Sfrp1
Efemp1
Ptprf
Erbb2
Ephb3
Fgfr1
F3
Tgfbr3
Fcgrt
Adck1
Fzd1
Ryr3
Tas2r114
Abca1
Ddr2
Cd40
Adgre5
Vmn1r30
Erbb2
Adck4
Itpr1
Grin2d
Epha2

Figure 4.8 Expression patterns of proteins from the enriched molecular function GO-terms found in pMEF and liver proteomes. A) Logarithmically transformed protein expression ratios of knockout against WT were expressed as a Heatmap. Columns represented E14.5 pMEF and liver proteome data sets. Proteins were listed on the right. Green, black and red boxes indicated upregulated, unchanged and downregulated proteins in knockout samples compared to WT, respectively. Scale above the Heatmap indicated protein fold change level. **B)** Scatter plot of protein expression in E14.5 pMEFs. **C)** Scatter plot of protein expression in E14.5 livers. Yellow dots indicated protein expression ratios of *Dlk1*$^{+/p}$/WT (Y-axis) against *Grb10*$^{m/+}$/*Dlk1*$^{+/p}$/WT (X-axis). Blue dots were the proteins plotted for the expression ratios of *Grb10*$^{m/+}$/WT (Y-axis) against *Grb10*$^{m/+}$/*Dlk1*$^{+/p}$/WT (X-axis).

4.3.6 Unsupervised clustering analysis identified distinct protein clusters with special expression or phosphorylation profiles in E14.5 pMEFs

To dissect out the protein or phosphorylated protein groups with similar expression or phosphorylation patterns in E14.5 pMEFs among the four genotypes, unsupervised clustering analysis utilizing a Fuzzy-c means algorithm was performed using GProX v1.1.16 software. 4- and 1.5-fold changes of knockout versus WT were set as the thresholds for pMEF proteome and phosphoproteome, respectively. Proteins or phosphorylated proteins outside of the fold change cut off were partitioned to different clusters. In each cluster, each protein or phosphorylated protein presented an individual curve with different colours. The colours represented the distance of each protein to the cluster centre calculated by the Fuzzy-c means algorithm.

In the pMEF proteome, four distinct protein expression patterns were identified (Figure 4.9A). Only 19 proteins were identified in cluster 1 which exhibited a special expression profile, with downregulation in *Dlk1*$^{+/p}$ and upregulation in *Grb10*$^{m/+}$ and *Grb10*$^{m/+}$*/Dlk1*$^{+/p}$ compared to WT. The 137 proteins in cluster 2 displayed upregulated expression levels in *Dlk1*$^{+/p}$ and downregulated in *Grb10*$^{m/+}$ and *Grb10*$^{m/+}$*/Dlk1*$^{+/p}$ compared to WT, while the 267 proteins in cluster 3 had increased expression levels in *Dlk1*$^{+/p}$ and decreased in *Grb10*$^{m/+}$ and *Grb10*$^{m/+}$*/Dlk1*$^{+/p}$ compared to WT (Figure 4.9A). In cluster 4, 449 protein expression levels were elevated in *Dlk1*$^{+/p}$, slightly elevated in *Grb10*$^{m/+}$ and reduced in *Grb10*$^{m/+}$*/Dlk1*$^{+/p}$ compared to WT (Figure 4.9A).

Next, the protein list from each cluster was extracted and GO-term enrichment analysis carried out against the whole data set of the pMEF proteome. The enriched GO-terms were expressed as a Heatmap with enriched GO-terms in green (Figure 4.9B). The detailed results of GO-term enrichment analysis were listed in tables (Table 7.3). In cluster 1, “brown fat cell differentiation” was the

only enriched GO-term (Figure 4.9B). “Extracellular region”, “extracellular space”, “extracellular region part” and “calcium ion binding” were the enriched GO-terms associated with proteins in cluster 2 (Figure 4.9B). GO-terms “transmembrane signalling receptor activity”, “transmembrane receptor activity”, “signalling receptor activity” and “signal transducer activity” were enriched in cluster 3 (Figure 4.9B). In cluster 4, mitochondrion function associated GO-terms of “mitochondrion”, “cytoplasmic part”, “mitochondrial part”, “membrane part” and small molecule catabolic and metabolic associated GO-terms of “organic acid catabolic process”, “carboxylic acid catabolic process”, “organic acid metabolic process”, “alpha-amino acid catabolic process”, “small molecule catabolic process”, “oxoacid metabolic process”, “cellular amino acid catabolic process”, “carboxylic acid metabolic process”, “cellular amino acid metabolic process” were enriched (Figure 4.9B).

In parallel, 6 clusters of phosphorylated proteins were identified according to expression profiles between the different genotypes. Numbered 1-6, these clusters comprised 453, 301, 99, 152, 87 and 91 phosphorylated proteins, respectively (Figure 4.9C). Expression relative to WT of phosphorylated proteins in cluster 1 decreased in *Grb10*$^{m/+}$*/Dlk1*$^{+/p}$ and increased in *Dlk1*$^{+/p}$ and *Grb10*$^{m/+}$, while in contrast those in cluster 5 increased in *Grb10*$^{m/+}$*/Dlk1*$^{+/p}$ and decreased in *Dlk1*$^{+/p}$ and *Grb10*$^{m/+}$ (Figure 4.9C). The phosphorylated proteins in cluster 2 showed relatively high levels of phosphorylation in *Dlk1*$^{+/p}$ and a dramatic reduction in *Grb10*$^{m/+}$ and *Grb10*$^{m/+}$*/Dlk1*$^{+/p}$ compared to WT (Figure 4.9C). Cluster 3 had a pattern of downregulation in *Dlk1*$^{+/p}$, upregulation in *Grb10*$^{m/+}$ and a lower upregulation level in *Grb10*$^{m/+}$*/Dlk1*$^{+/p}$ (Figure 4.9C). Expression of phosphoproteins versus WT in clusters 4 was upregulated in *Grb10*$^{m/+}$ and downregulated in *Dlk1*$^{+/p}$ and *Grb10*$^{m/+}$*/Dlk1*$^{+/p}$, while in contrast those in cluster 6 downregulated in *Grb10*$^{m/+}$ and upregulated in *Dlk1*$^{+/p}$ and *Grb10*$^{m/+}$*/Dlk1*$^{+/p}$ (Figure 4.9C).

GO-term enrichment analysis revealed that GO-term of “response to radiation” was enriched in Cluster 1 (Figure 4.9D). In cluster 4, associated GO-terms were “regulation of secretion”, “regulation of peptide transport”, “regulation of secretion by cell”, “regulation of sequence-specific DNA binding transcription factor activity” and “positive regulation of sequence-specific DNA binding transcription factor activity”. No enriched GO-terms were identified in the other clusters in E14.5 pMEF phosphoproteome (Figure 4.9D).

A

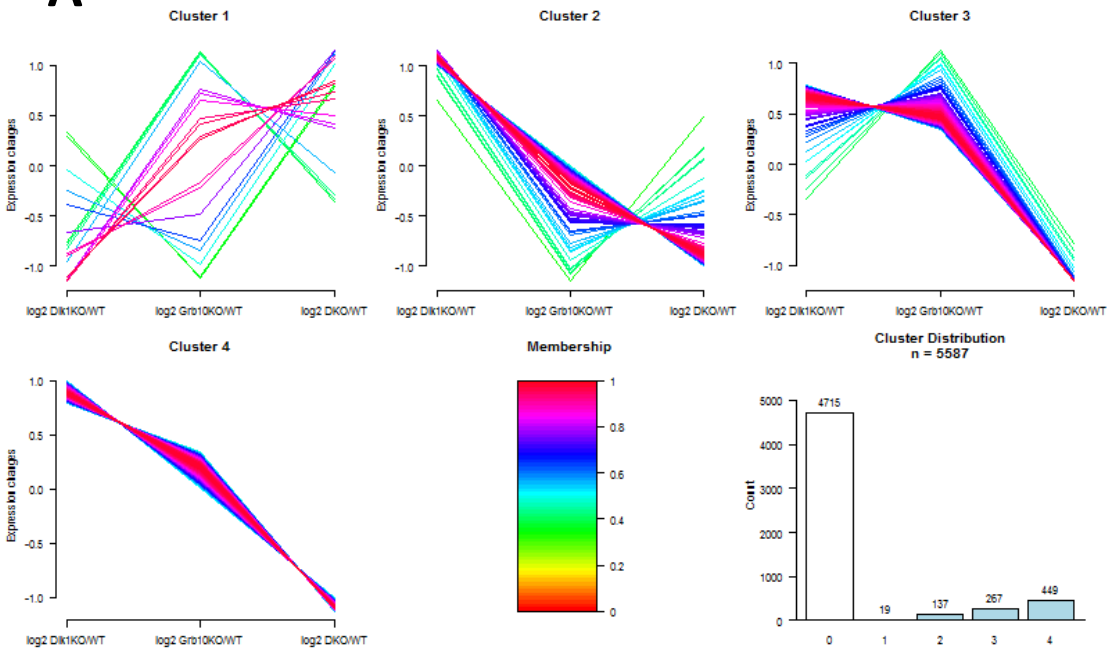

B

brown fat cell differentiation
extracellular region
extracellular space
extracellular region part
calcium ion binding
biological adhesion
transmembrane signaling receptor activity
transmembrane receptor activity
signaling receptor activity
signal transducer activity
mitochondrion
cytoplasmic part
mitochondrial part
membrane part
organic acid catabolic process
carboxylic acid catabolic process
organic acid metabolic process
alpha-amino acid catabolic process
small molecule catabolic process
oxoacid metabolic process
cellular amino acid catabolic process
carboxylic acid metabolic process
cellular amino acid metabolic process

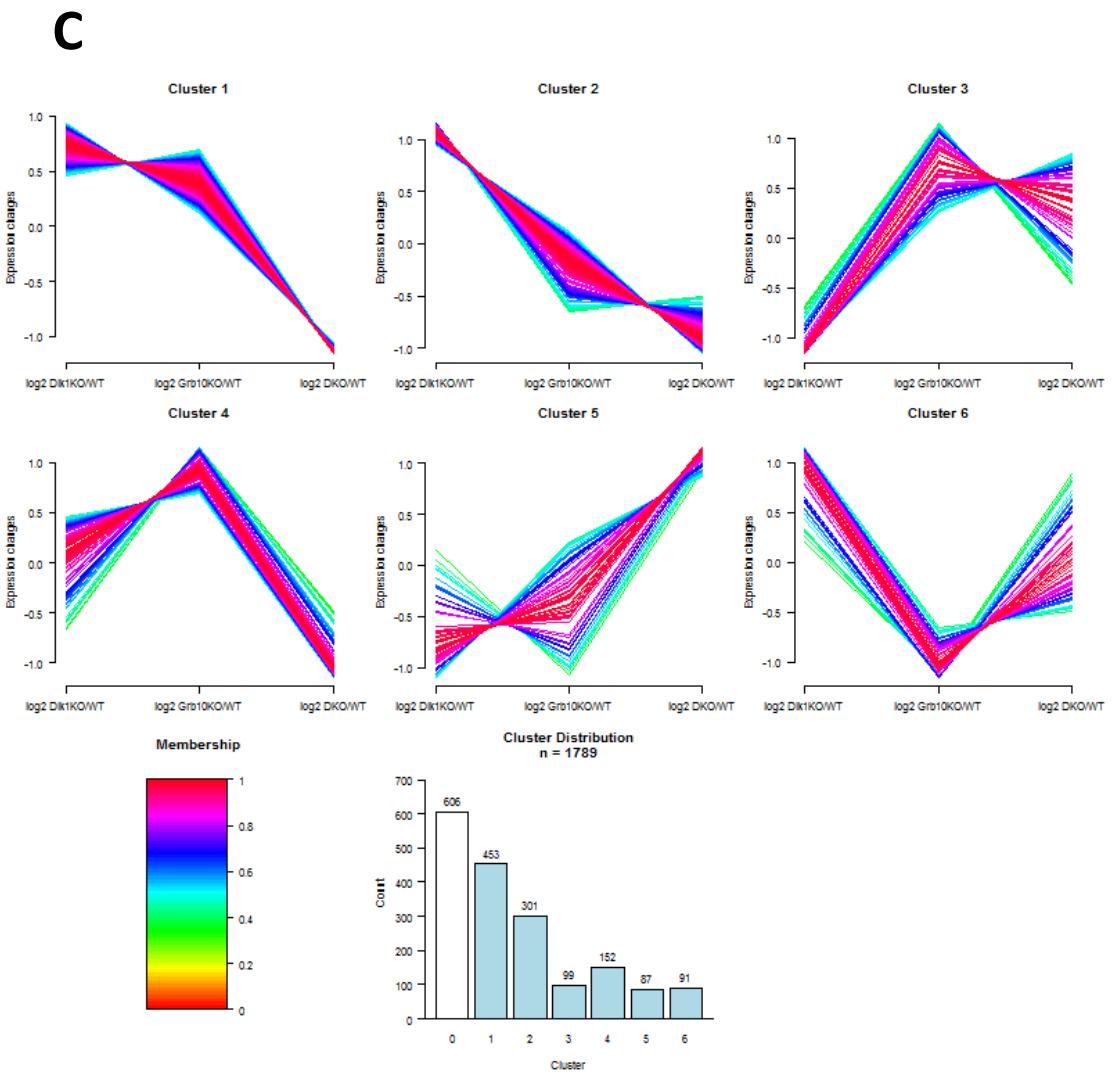

Figure 4.9 Hierarchy clustering and GO-term enrichment analyses of E14.5 pMEF total proteome and phosphoproteome. A) Four protein clusters were identified with distinct expression patterns among the *Dlk1*$^{+/p}$, *Grb10*$^{m/+}$, and *Grb10*$^{m/+}$*/Dlk1*$^{+/p}$ pMEF proteomes, each expressed relative to their expression in WT. Curve colour indicates the distance of the protein from the cluster centre according to the indicated scale (membership). A bar graph shows the number of proteins in each cluster and the background (cluster 0). *Dlk1KO*, *Dlk1*$^{+/p}$; *Grb10KO, Grb10*$^{m/+}$; *DKO*, *Grb10*$^{m/+}$*/Dlk1*$^{+/p}$. **B)** GO-terms enriched (based on p-Value) within each cluster (1, 2, 3 and 4) were extracted

and expressed as a Heatmap. Columns labelled with numbers represent the corresponding cluster in A, with enriched GO-terms from all clusters listed on the right. Green and red boxes indicate the enriched and non-enriched GO-terms for each protein cluster. **C)** Six clusters of phosphorylated proteins were identified with special phosphorylation profiles among the *Dlk1*$^{+/p}$, *Grb10*$^{m/+}$, and *Grb10*$^{m/+}$*/Dlk1*$^{+/p}$ versus WT. **D)** Enriched GO-terms from each cluster were expressed as a Heatmap. Columns labelled with numbers represent the corresponding cluster in C, with enriched GO-terms listed on the right.

4.3.7 Proteins were clustered according to expression patterns in E14.5 liver *Dlk1*$^{+/p}$, *Grb10*$^{m/+}$ and *Grb10*$^{m/+}$/*Dlk1*$^{+/p}$ livers

Unsupervised clustering analysis was carried out on E14.5 liver proteome and phosphoproteome using the same strategy as pMEF as described for pMEF samples (see section 4.3.6). Among proteins expressed at levels beyond the 4-fold change thresholds, 6 subsets of proteins with special expression profiles were acquired by clustering analysis. The 92 proteins in cluster 1 had an expression pattern of decrease in *Dlk1*$^{+/p}$ and elevation in *Grb10*$^{m/+}$ and *Grb10*$^{m/+}$/*Dlk1*$^{+/p}$ compared to WT proteome. Meanwhile the 176 and 108 proteins in cluster 2 and 3 showed decreased expression level in *Dlk1*$^{+/p}$ and increased in *Grb10*$^{m/+}$ compared to WT, while *Grb10*$^{m/+}$/*Dlk1*$^{+/p}$ levels intermediate between those of *Dlk1*$^{+/p}$ and *Grb10*$^{m/+}$ (Figure 4.10A). The 85 proteins in cluster 4 had similar expression levels between WT and *Dlk1*$^{+/p}$, while they were increased in *Grb10*$^{m/+}$ and reduced in *Grb10*$^{m/+}$/*Dlk1*$^{+/p}$ compared to WT. In cluster 5, the 45 proteins had an expression profile of elevation in *Dlk1*$^{+/p}$ and reduction in *Grb10*$^{m/+}$ and *Grb10*$^{m/+}$/*Dlk1*$^{+/p}$ compared to WT. A small group of 21 proteins in cluster 6 had increased expression levels in *Dlk1*$^{+/p}$ and *Grb10*$^{m/+}$/*Dlk1*$^{+/p}$ and decreased in *Grb10*$^{m/+}$ compared to WT (Figure 4.10A).

The subsequent GO-term enrichment analysis uncovered that B cell and immune system associated GO-terms of “regulation of B cell activation”, “immune response-regulating signalling pathway”, “immune effector process”, “regulation of B cell proliferation”, “regulation of mononuclear cell proliferation”, “regulation of lymphocyte proliferation”, “immune system process”, “regulation of leukocyte proliferation”, “immune response-regulating cell surface receptor signaling pathway”, “positive regulation of B cell activation”, “positive regulation of interleukin-12 production” were enriched in cluster 1 (Figure 4.10B). Additionally, GO-terms of “transmembrane signaling receptor activity”, “transmembrane receptor activity”, “receptor activity”, “molecular transducer

activity” and “signalling receptor activity” were enriched in both cluster 1 and 4 (Figure 4.10B). Besides, “extracellular region”, “extracellular space”, “G-protein coupled receptor activity”, “secretion”, “cell migration” and “cell motility” GO-terms were also found to be enriched in cluster 4 (Figure 4.10B). GO-terms of “negative regulation of cell proliferation”, “multicellular organismal process”, “negative regulation of epithelial cell proliferation” and “osteoblast differentiation” were enriched in cluster 5 and “cell differentiation” and “identical protein binding” in cluster 6 (Figure 4.10B). No enriched GO-terms were found in cluster 2 and 3 (Figure 4.10B).

In liver phosphoproteome, 5 clusters with distinct phosphorylation patterns were discovered. Protein phosphorylation levels in were lower in *Dlk1*$^{+/p}$ and the lowest in *Grb10*$^{m/+}$*/Dlk1*$^{+/p}$ cluster 1 and higher in *Dlk1*$^{+/p}$ and the highest in *Grb10*$^{m/+}$*/Dlk1*$^{+/p}$ in cluster 3, while the changes in *Grb10*$^{m/+}$ were opposite to *Dlk1*$^{+/p}$ and *Grb10*$^{m/+}$*/Dlk1*$^{+/p}$ in these two clusters (Figure 4.10C). Notably, phosphorylated proteins in cluster 4 and 5 illustrated opposite phosphorylation levels in *Dlk1*$^{+/p}$ and *Grb10*$^{m/+}$ proteomes, either increase or decrease, and the changes in *Grb10*$^{m/+}$*/Dlk1*$^{+/p}$ proteome was similar as WT (Figure 4.10C). Phosphorylation level of proteins in cluster 2 had a gradual down regulation pattern in *Grb10*$^{m/+}$ and *Grb10*$^{m/+}$*/Dlk1*$^{+/p}$ and were upregulated in *Dlk1*$^{+/p}$ compare to WT (Figure 4.10C).

The following GO-term enrichment analysis indicated that “positive regulation of cellular metabolic process”, “regulation of cellular metabolic process”, “positive regulation of metabolic process”, “positive regulation of nucleobase-containing compound metabolic process” and “positive regulation of macromolecule metabolic process” GO-terms were enriched in cluster 2 containing 112 phosphoproteins, while “translational elongation”, “large ribosomal subunit”, “ribosomal subunit” and “ribonucleoprotein complex” were enriched in 43 phosphoproteins from cluster 3 (Figure 4.10D). And 84

phosphoproteins in cluster 5 possessed biological function annotations of “integral component of plasma membrane” and “intrinsic component of plasma membrane” (Figure 4.10D). No enriched GO-terms were found in cluster 1 and 4 which contained 93 and 55 phosphorylated proteins, respectively (Figure 4.10D).

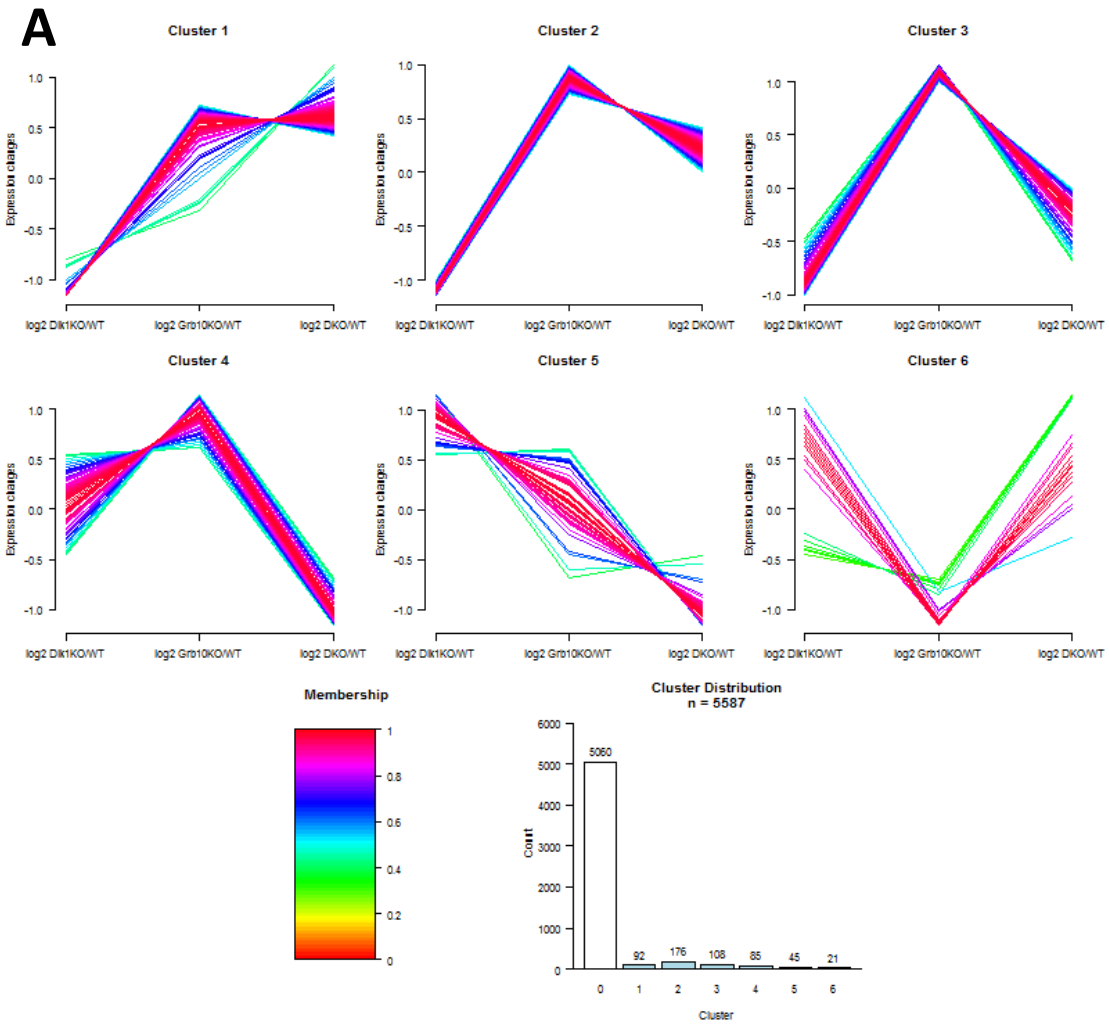

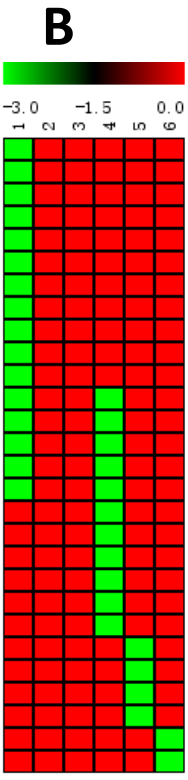

regulation of B cell activation
immune response-regulating signaling pathway
immune effector process
regulation of B cell proliferation
regulation of mononuclear cell proliferation
regulation of lymphocyte proliferation
immune system process
regulation of leukocyte proliferation
immune response-regulating cell surface receptor signaling pathway
positive regulation of B cell activation
positive regulation of interleukin-12 production
transmembrane signaling receptor activity
transmembrane receptor activity
receptor activity
molecular transducer activity
signaling receptor activity
extracellular region
extracellular space
G-protein coupled receptor activity
secretion
cell migration
cell motility
negative regulation of cell proliferation
multicellular organismal process
negative regulation of epithelial cell proliferation
osteoblast differentiation
cell differentiation
identical protein binding

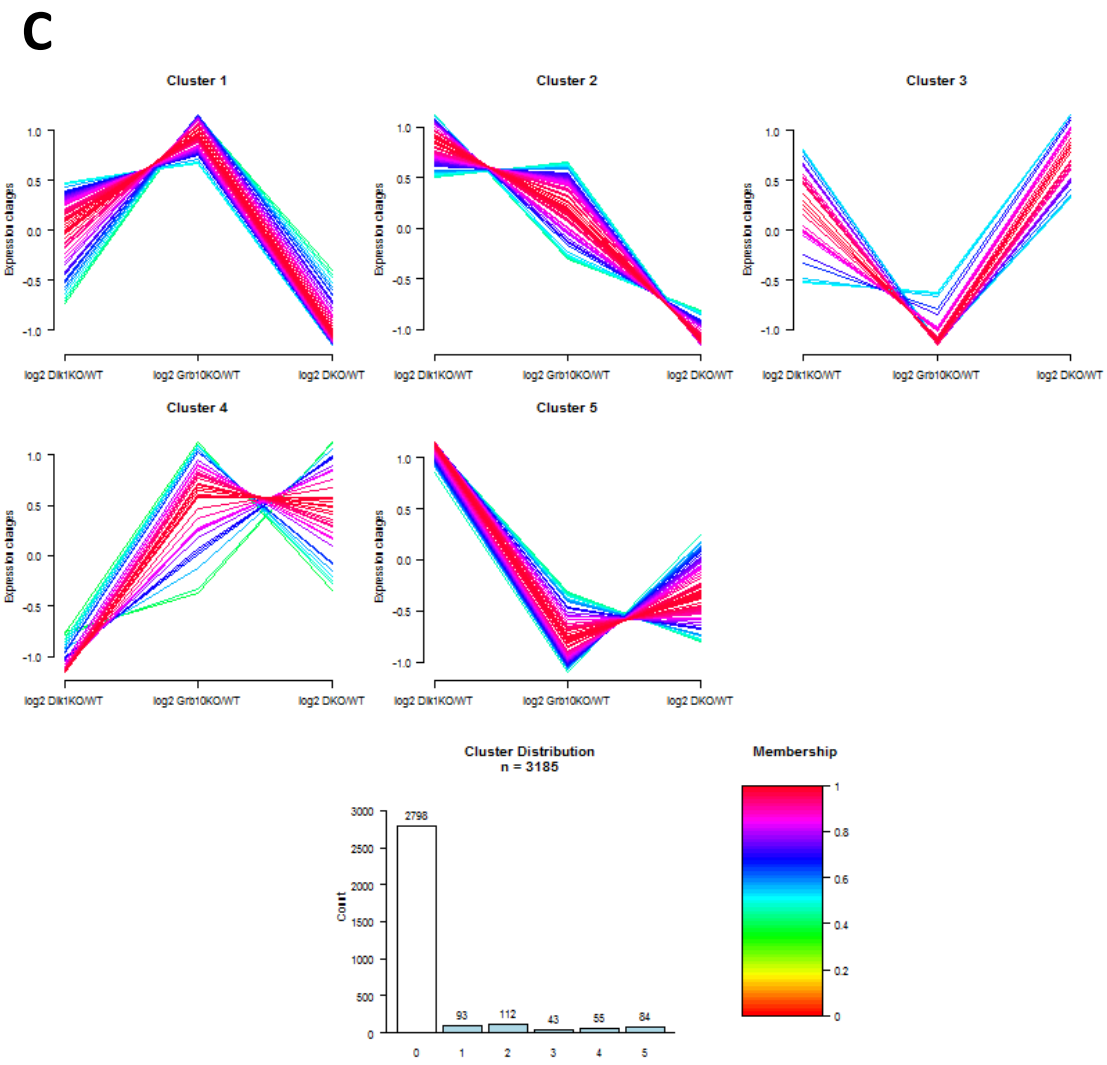

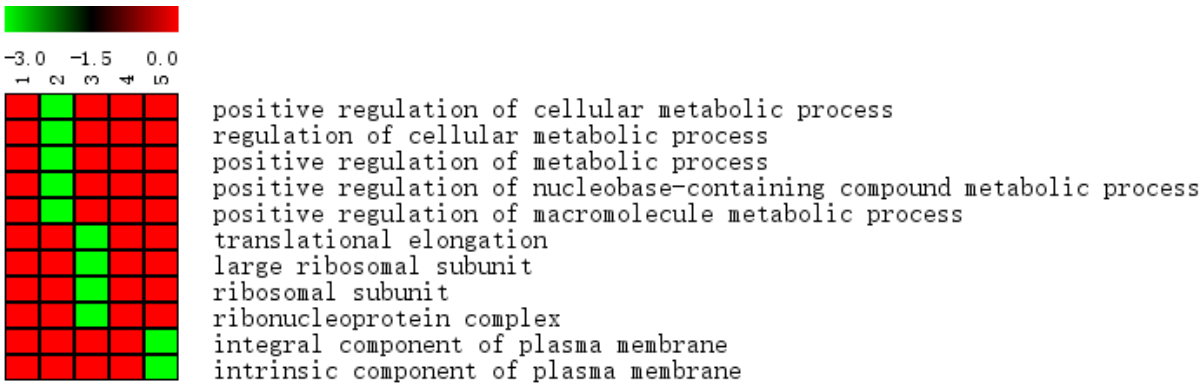

Figure 4.10 Hierarchy clustering and GO-term enrichment analyses of E14.5 liver total proteome and phosphoproteome. A) Six protein clusters were grouped with different expression patterns among the *Dlk1*$^{+/p}$, *Grb10*$^{m/+}$ and *Grb10*$^{m/+}$/*Dlk1*$^{+/p}$ liver proteomes. Each curve indicated a protein

expression ratio of knockout versus WT. Curve colour indicates the distance of the protein from the cluster centre according to the indicated scale (membership). A bar graph shows the number of proteins numbers in each cluster and the background (cluster 0). *Dlk1KO*, *Dlk1*$^{+/p}$; *Grb10KO, Grb10*$^{m/+}$; *DKO*, *Grb10*$^{m/+}$/*Dlk1*$^{+/p}$. **B)** GO-terms enriched (based on p-Values) within each cluster (1, 2, 3, 4, 5 and 6) were extracted and visualized as a Heatmap. Columns labelled with numbers represent the corresponding cluster in A, with enriched GO-terms from all clusters listed on the right. Green and red boxes indicate the enriched and non-enriched GO-terms for each protein cluster. **C)** Five clusters of phosphorylated proteins were identified with distinct expression patterns among the *Dlk1*$^{+/p}$, *Grb10*$^{m/+}$ and *Grb10*$^{m/+}$/*Dlk1*$^{+/p}$ liver phosphoproteomes. Each curve represents levels of a phosphorylated protein, relative to WT expression. **D)** Enriched GO-terms from cluster were expressed as a Heatmap. Columns labelled with numbers represented the corresponding cluster in C, with enriched GO-terms listed on the right.

4.4 Discussion

Two independent TMT quantitative proteomics analyses generated four data sets for the proteomes and phosphoproteomes of E14.5 pMEFs and livers from four genotypes, WT, *Dlk1*$^{+/p}$, *Grb10*$^{m/+}$ and *Grb10*$^{m/+}$/*Dlk1*$^{+/p}$. The analyses provided a wealth of information, including expression levels of thousands of proteins and phosphorylated proteins, for Dlk1 and Grb10 function and signalling studies (Figure 4.4). PCA and HCL analyses on the mean ratios of knockout versus WT revealed that *Grb10*$^{m/+}$ and *Grb10*$^{m/+}$/*Dlk1*$^{+/p}$ had higher Pearson correlation coefficient value and was grouped in the same cluster at the proteomics level, while *Dlk1*$^{+/p}$ was divergent in both pMEFs and livers. Interestingly, *Grb10*$^{m/+}$ and *Grb10*$^{m/+}$/*Dlk1*$^{+/p}$ had even higher Pearson correlation coefficient value in E14.5 pMEF and liver phosphoproteomes, suggesting the overall signal transduction through phosphorylation was similar in these two samples (Figure 4.5I-P). The PCA and HCL analyses of proteomic and phosphoproteomic data supported the published genetic evidence that while *Dlk1*$^{+/p}$ and *Grb10*$^{m/+}$ single mutants had opposite phenotypes, including growth and metabolic health characteristics, *Grb10*$^{m/+}$/*Dlk1*$^{+/p}$ double mutants were indistinguishable from *Grb10*$^{m/+}$ (Moon *et al*., 2002; Smith *et al*., 2007; Wang *et al*., 2007; Madon-Simon *et al*., 2014). However, PCA and HCL analyses for the individual samples failed to group the replicates of each genotype in the same cluster, and these results were relatively noisy which were difficult to tell the similarities and divergence among the four genotypes (Figure 4.5A-H). All samples from E14.5 pMEFs or livers were pulled and analysed in the same TMT proteomics process. The low correlation between the biological replicates of each genotype suggested that the experimental noise and error were relatively high. This study only chose two biological repeats for each genotype. For a more reliable result, more biological repeats are required.

Strikingly, the scatter plots of the four data sets presented a consistent pattern of reduced expression in *Dlk1*$^{+/p}$, *Grb10*$^{m/+}$ and *Grb10*$^{m/+}$*/Dlk1*$^{+/p}$ proteomes and phosphoproteomes compared to WT, indicating that Dlk1 and Grb10 may promote wide-scale protein stabilisation or phosphorylation at E14.5 *in vitro* and *in vivo* (Figure 4.6). This could be a product of immediate and downstream effects of signalling defects in the knockouts. It is known that *Dlk1* and *Grb10* are widely expressed in the embryo, and both have a significant impact on fetal growth (Moon *et al*., 2002; Charalambous *et al*., 2003; Charalambous *et al*., 2010; Charalambous *et al*., 2014; Madon-Simon *et al*., 2014). This may explain the emergence of the large scale of protein expression or phosphorylation reduction in E14.5 embryos caused by *Dlk1* and *Grb10* single and double knockout. Notably, more proteins were 4-fold down regulated in the *Dlk1*$^{+/p}$ liver proteome, whereas larger numbers of proteins were down regulated in *Grb10*$^{m/+}$ and *Grb10*$^{m/+}$*/Dlk1*$^{+/p}$ pMEF proteomes (Figure 4.6). This suggests that Dlk1 and Grb10 may have different effects in E14.5 pMEF and liver development and function, respectively.

GO-term enrichment analysis was performed to uncover the biological functional properties of the proteins with greatest fold changes in *Dlk1*$^{+/p}$, *Grb10*$^{m/+}$ and *Grb10*$^{m/+}$*/Dlk1*$^{+/p}$ proteomes and phosphoproteomes. Proteins or phosphorylated proteins were not separated based on upregulation or downregulation levels in the three knockout for GO-term enrichment analyses, as protein expression or phosphorylation levels were largely decreased according to the scatter plot for each data set (Figure 4.6). Notably, a few different GO-terms were associated with RTK signalling activity, “transmembrane receptor activity”, “transmembrane signaling receptor activity” and “transmembrane receptor protein kinase activity”, were enriched in both E14.5 pMEF and liver proteomes (Figure 4.7), suggesting that Dlk1 and Grb10 may be involved in RTK signal transduction in E14.5 embryo. It is well established that Grb10 can interact with and regulate several RTKs *in vitro* and

in vivo (Wick *et al*., 2003; Vecchione *et al*., 2003; Murdaca *et al*., 2004; Monami *et al*., 2008; Wang *et al*., 2007; Smith *et al*., 2007; Plasschaert and Bartolomei, 2015). The role of Dlk1 in RTK signalling is not well demonstrated so far. The GO-term enrichment results were consistent with the previous studies demonstrating roles for Grb10 in RTK signalling and also indicated a role for Dlk1 in regulating RTK signalling pathways. Similarities in proteomic changes in both single and double mutants for *Dlk1* and *Grb10* are consistent with the genetic evidence that both factors may influence one or more common signalling pathways during fetal development (Madon-Simon *et al*., 2014).

In $Dlk1^{+/p}$, $Grb10^{m/+}$ and $Grb10^{m/+}/Dlk1^{+/p}$ liver proteomes, enriched GO-term of "negative regulation of cell proliferation" indicated that Dlk1 and Grb10 may affect proliferation of one or more cell types in liver. In addition, GO-terms of "intrinsic/integral component of plasma membrane", "elastic fiber", "receptor activity", "signaling receptor activity", "signal transducer activity", "molecular transducer activity" and "calcium ion binding" were specifically enriched in liver proteome (Figure 4.7), suggesting that Dlk1 and Grb10 may be active factors involved in these biological processes in E14.5 livers.

The GO-terms "lytic vacuole" and "lysosome" were specifically enriched in pMEF knockout proteomes (Figure 4.7), suggesting that Dlk1 and Grb10 may participate in membrane receptor-mediated endocytosis in E14.5 pMEFs. It has been reported that Grb10 regulates the IGF1R lysosomal degradation process in collaboration with Nedd4 in pMEFs which overexpressed IGF1R or Grb10 (Monami *et al*., 2008). A role for Dlk1 in lysosomal function in pMEFs is not yet known, however, the GO-term enrichment analysis suggested that Dlk1 may also play a role in receptor-mediated endocytosis of E14.5 pMEFs. Further, GO-term related to phagocytosis ("phagocyte vesicle") was specifically enriched in the E14.5 liver proteome (Figure 4.7), suggesting that Dlk1 and Grb10 may regulate different aspects of endocytosis in E14.5 pMEFs

and liver.

Dlk1 and *Grb10* knockout mice as adults displayed increased and reduced adiposity, respectively, as demonstrated in Chapter 3 (Figure 3.2) and several previous studies (Moon *et al*., 2002; Lee *et al*., 2003; Charalambous *et al*., 2003; Smith *et al*., 2007; Wang *et al*., 2007; Charalambous *et al*., 2010; Charalambous *et al*., 2014; Madon-Simon *et al*., 2014). Here, the GO-term "lipid metabolic process" was enriched in $Dlk1^{+/p}$, $Grb10^{m/+}$ and $Grb10^{m/+}/Dlk1^{+/p}$ pMEF proteomes (Figure 4.7), further supporting roles for Dlk1 and Grb10 in lipid development or metabolism at the proteomic level. The adult adipose development and lipid metabolism affected by Dlk1 and Grb10 may be consequences of earlier altered development happened at the embryonic stage. Meanwhile, "hydrolase activity" and "ATPase activity" GO-terms were enriched in the pMEF knockout phosphoproteomes while "negative regulation of hemopoiesis" was enriched in the liver knockout phosphoproteome (Figure 4.7). This demonstrated that Dlk1 and Grb10 may affect the signal transductions of these biological processes in E14.5 pMEFs and livers.

Interestingly, the only overlap in enriched GO-terms between samples was in several membrane protein GO-terms, as discussed above. No overlap in GO-terms was found between pMEF proteome and phosphoproteme, liver proteome and phosphoproteome. This suggests that Dlk1 and Grb10 knockout may have different long-term (protein expression) and short-term (phosphorylation) effects on cells or tissues in E14.5 embryo. Similarly, there was no overlap in enriched GO-terms from the pMEF and liver phosphoproteome (Figure 4.7), suggesting that the direct downstream signalling effects are tissue specifically different in the embryo.

Since molecular function GO-terms of "transmembrane receptor activity",

“transmembrane signalling receptor activity”, “transmembrane receptor protein kinase activity” were enriched in E14.5 pMEF and liver proteomes, the 29 proteins belonging to these GO-terms were evaluated by generating a Heatmap and scatter plots to compare their expression levels (Figure 4.8). Strikingly, most of these proteins displayed 4-fold down regulation in the knockout pMEF and liver proteomes versus WT on the Heatmap (Figure 4.8A). However, the corresponding phosphorylation levels of these proteins were not significantly changed in the phosphoproteomes. This could mean that the phosphorylation levels of these proteins were actually upregulated in the knockout pMEFs and livers as the corresponding total protein expression levels were reduced. Phosphoproteomics analysis can detect only a few phosphorylated tyrosine sites (Figure 4.2B), consisting of less than 2% of all the pSTY sites because of the technique limitation (Sharma *et al*., 2014). Therefore, it is possible that the RTK tyrosine phosphorylation information was missing or inaccurate, for some reason, in the phosphoproteomics analysis. For these reasons, changes in phosphorylation status of multiple RTKs in cells of all four genotypes were later evaluated using a mouse phospho-RTK array among (Chapter 5).

GO-term enrichment analysis showed that a broad range of biological functions were significantly enriched in pMEF and liver knockout proteomes and phosphoproteomes. This suggested that Dlk1 and Grb10 were involved in a variety of developmental processes in the E14.5 embryo. Clustering analysis was performed to further separate the proteins falling out of the expression or phosphorylation change thresholds which grouped several protein clusters with differential expression or phosphorylation responses to $Dlk1^{+/p}$, $Grb10^{m/+}$ and $Grb10^{m/+}/Dlk1^{+/p}$ knockout in cells and tissues from E14.5 embryos. Notably, several clusters in the four data sets exhibited a special pattern that $Dlk1^{+/p}$ and $Grb10^{m/+}$ displayed opposite protein expression or phosphorylation changes compared to WT, while $Grb10^{m/+}/Dlk1^{+/p}$ was consistently similar to

Grb10$^{m/+}$ but with slightly smaller changes (Figure 4.9A, C; Figure 4.10A, C). This was in agreement with the *Grb10*$^{m/+}$*/Dlk1*$^{+/p}$ phenotype discovered in the mice in Chapter 3 and a previous genetic study (Madon-Simon *et al*., 2014) and also added evidence to the hypothesis that Dlk1 and Grb10 play antagonistic functions potentially on the common pathway.

The clustering analysis provided valuable information for future Dlk1 and Grb10 studies on specific areas. For instance, proteins in cluster 1 from the pMEF proteome were enriched in the GO-term “brown fat differentiation” in E14.5 *Dlk1*$^{+/p}$, *Grb10*$^{m/+}$ and *Grb10*$^{m/+}$*/Dlk1*$^{+/p}$ pMEFs (Figure 4.9B). Evidence exists from previous studies demonstrated the involvement of both Dlk1 and Grb10 in BAT development and thermogenesis (Charalambous *et al*., 2014; Liu *et al*., 2014). Proteins in this cluster might interact with Dlk1 and Grb10 in regulating brown fat differentiation. Transmembrane receptor activity associated GO-terms were enriched in cluster 3 of pMEF proteome (Figure 4.9B) while RTK activity correlated GO-terms were specifically enriched in cluster 1 and 4 of liver proteome (Figure 4.10B) which was consistent with the GO-enrichment analysis for the whole pMEF or liver proteome (Figure 4.7). This further suggests that Dlk1 and Grb10 can be important cell signalling regulators in RTK signalling. It is known that Dlk1 and Grb10 are correlated with adipogenesis and myogenesis at the transcriptional level (Mortensen *et al*., 2012; Holt *et al*., 2012; Traustadóttir *et al*., 2013; Charalambous *et al*., 2014; Andersen *et al*., 2013; Mokbel *et al*., 2014), while biological function of sequence-specific DNA binding transcription factor activity was overrepresented in pMEF phosphoproteome (Figure 4.9D). Proteins in this cluster can be candidates for further Dlk1 and Grb10 involved transcription process studies. In liver proteome, proteins in cluster 1 were found to be related to B cell development and immune system response (Figure 4.10B). Dlk1 was reported to be associated with B cell development derived from adult bone marrow and spleen using *Dlk1* knockout mice (Raghunandan *et al*.,

2008). The role of Grb10 in B cell development is currently not well studied. Here, GO-term enrichment analysis showed that Dlk1 and Grb10 associated B cell or immune system development events may also exist in the embryonic livers. A relatively small number of enriched GO-terms were identified in pMEF and liver phosphoproteome, while more information was found in the total proteomes. This may because protein expression was broadly affected by the global deletion of *Dlk1* or *Grb10*, while dynamic signal response was more sensitive to short-term stimulation. Clustering and the following GO-term enrichment analysis also indicate some GO-terms that relate to functions where there is no evidence for Dlk1/Grb10 involvement. The information needs some initial validation similar as the signalling studies I did following with the proteomics analysis in next chapter.

Chapter 5

Evidence that Dlk1 and Grb10 interact through a common receptor tyrosine kinase

5.1 Introduction

In the previous chapter, RTK signal activity related GO-terms were found to be significantly enriched in E14.5 pMEF and liver proteomes by GO-term enrichment analysis (Figure 4.7). Most of the proteins belonging to the identified enriched GO-terms, for instance PDGFRa, were found to have reduced expression levels in *Dlk1*$^{+/p}$, *Grb10*$^{m/+}$ and *Grb10*$^{m/+}$*/Dlk1*$^{+/p}$ pMEFs and livers compared to WT (Figure 4.8). One of a few proteins, for instance Erb-B2 receptor tyrosine kinase 2 (Erbb2), had different expression levels among the four genotypes (Figure 4.8). Initial experiments focused on PDGFRa and Erbb2 as two targets to evaluate the accuracy of the TMT proteomics analysis utilizing Western blotting. It is known that PDGFRa and PDGFRb can form functional heterodimers in the cell membrane (Borkham-Kamphorst and Weiskirchen, 2016). However, PDGFRb did not show significant expression changes among the four genotypes in the pMEF and liver proteomes. Therefore, PDGFRb was selected as a negative control for TMT validation experiments.

Further, several RTKs and their signalling partners in those enriched RTK activity related GO-terms exhibited changed protein expression levels among the four genotypes in the pMEF and liver proteomes (Figure 4.7; Figure 4.8). However, the corresponding phosphorylation changes of these RTKs and downstream signal partners were not detected in the pMEF and liver phosphoproteomes. Hence, a mouse phospho-RTK array was used to evaluate RTK phosphorylation levels comparing E14.5 pMEFs of all four genotypes. This indicated altered phosphorylation in a small number of RTKs in E14.5 pMEFs, notably PDGFRa, but also EGFR.

For the RTK signalling studies in E14.5 pMEFs, candidate pathways through PDGFRa and FGF1R were of interest as they both exhibited decreased

expression levels in *Dlk1*$^{+/p}$, *Grb10*$^{m/+}$ and *Grb10*$^{m/+}$/*Dlk1*$^{+/p}$ pMEF and liver proteomes (Figure 4.8). EGFR signalling was selected based on the phospho-RTK array results. Furthermore, previous mouse genetic studies in our laboratory have indicated that Grb10 may control growth independently of either IGF or IR signalling (Charalambous *et al*., 2003 and unpublished data). However, published biochemical data provides compelling evidence for a functional interaction between Grb10 and IGF1R or IR. Hence, involvement of Dlk1 and Grb10 in IGF/insulin signalling was also considered in parallel with PDGFR, FGF1R and EGFR. The corresponding ligands: PDGF-AA/BB, FGF1, EGF, IGF1 and insulin were used to stimulate pMEFs of all four genotypes prior to analyses of downstream signalling events.

The experiments in this chapter were aimed at validating the proteomics data and identifying signalling mechanisms influenced by either or both, Dlk1 and Grb10. Western blotting of several RTKs and mouse phospho-RTK array were used to validating the proteomic data. Candidate RTK signalling studies were selected based on the proteomics data (Chapter 4), mouse phospho-RTK array results and previous Dlk1 and Grb10 studies (literature).

5.2 Results

5.2.1 PDGFRa, Erbb2 and PDGFRb expression patterns found by Western blotting were similar those from TMT analysis

To evaluate the expression patterns of several RTKs, independently of the TMT analysis (Chapter 4), the same portion of E14.5 pMEF cell lysates which were prepared for TMT analysis were used as the technical replications for Western blotting validation. Three other biological replications of E14.5 pMEFs from the four genotypes were also prepared for Western blotting validation. PDGFRa expression was reduced in *Dlk1*$^{+/p}$ and significantly reduced in *Grb10*$^{m/+}$ and *Grb10*$^{m/+}$*/Dlk1*$^{+/p}$ pMEFs compared to WT, with the lowest levels being in *Grb10*$^{m/+}$*/Dlk1*$^{+/p}$ pMEFs (Figure 5.1A, B). Erbb2 expression was decreased in *Dlk1*$^{+/p}$ and *Grb10*$^{m/+}$*/Dlk1*$^{+/p}$ pMEFs and increased in *Grb10*$^{m/+}$ pMEFs compared to WT. However, no statistical significance was found by One-way ANOVA analysis for Erbb2 expression among the four genotypes (Figure 5.1 A, C). No significant PDGFRb expression differences were found among WT, *Dlk1*$^{+/p}$, *Grb10*$^{m/+}$ and *Grb10*$^{m/+}$*/Dlk1*$^{+/p}$ pMEFs (Figure 5.1 A, D). These results were similar as the TMT data from E14.5 pMEF total proteome (Figure 4.8).

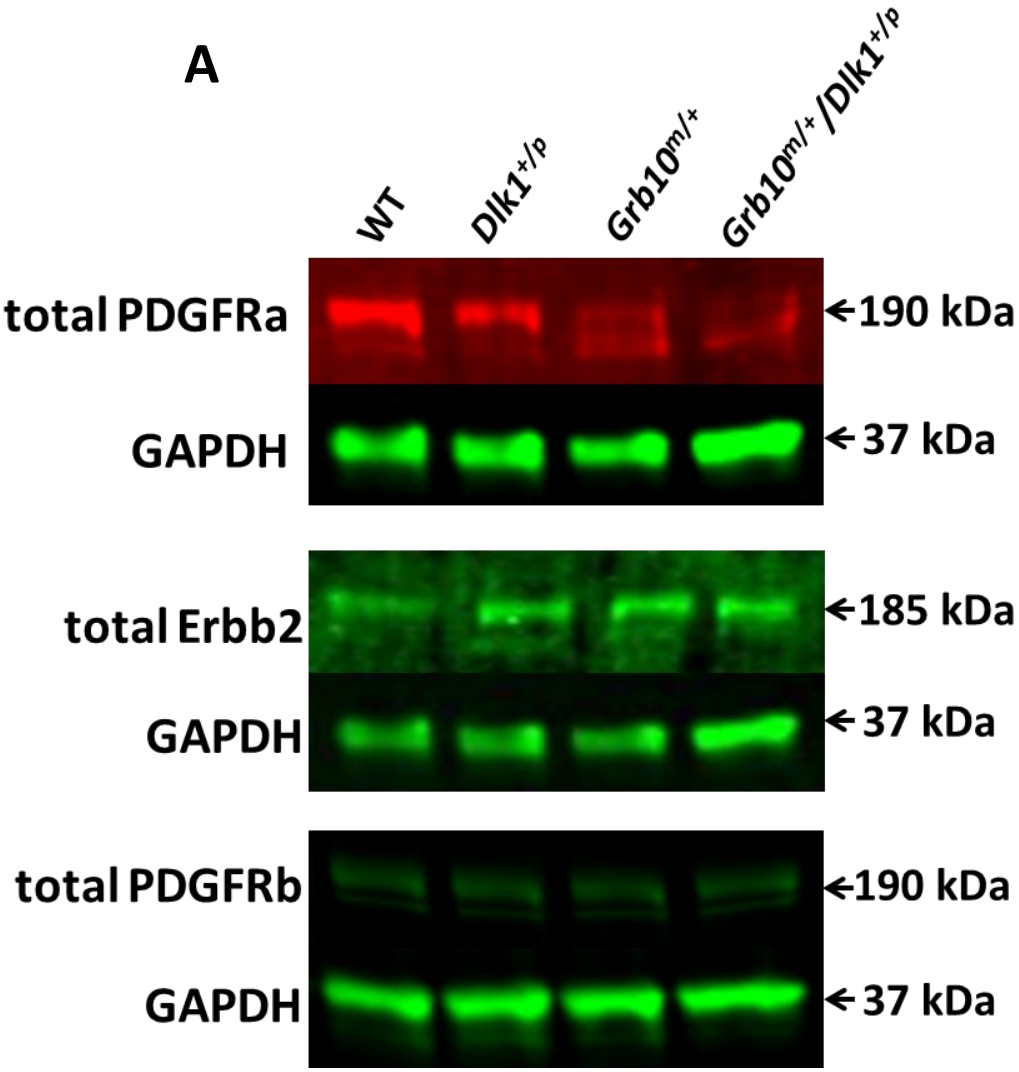
A
WT
Dlk1+/p
Grb10m/+
Grb10m/+/Dlk1+/p
total PDGFRa
←190 kDa
GAPDH
←37 kDa
total Erbb2
←185 kDa
GAPDH
←37 kDa
total PDGFRb
←190 kDa
GAPDH
←37 kDa

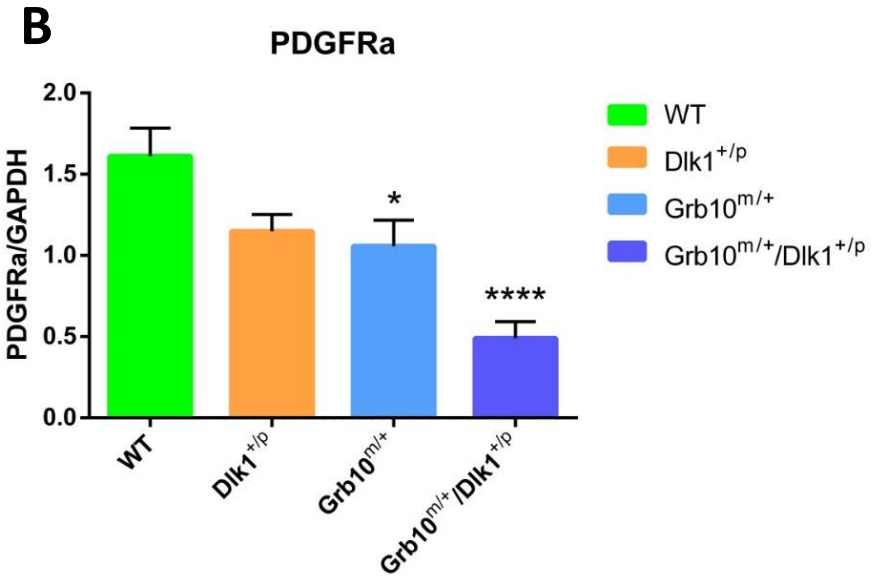
B
PDGFRa
PDGFRa/GAPDH
2.0
1.5
1.0
0.5
0.0
*
****
WT
Dlk1+/p
Grb10m/+
Grb10m/+/Dlk1+/p
WT
Dlk1+/p
Grb10m/+
Grb10m/+/Dlk1+/p

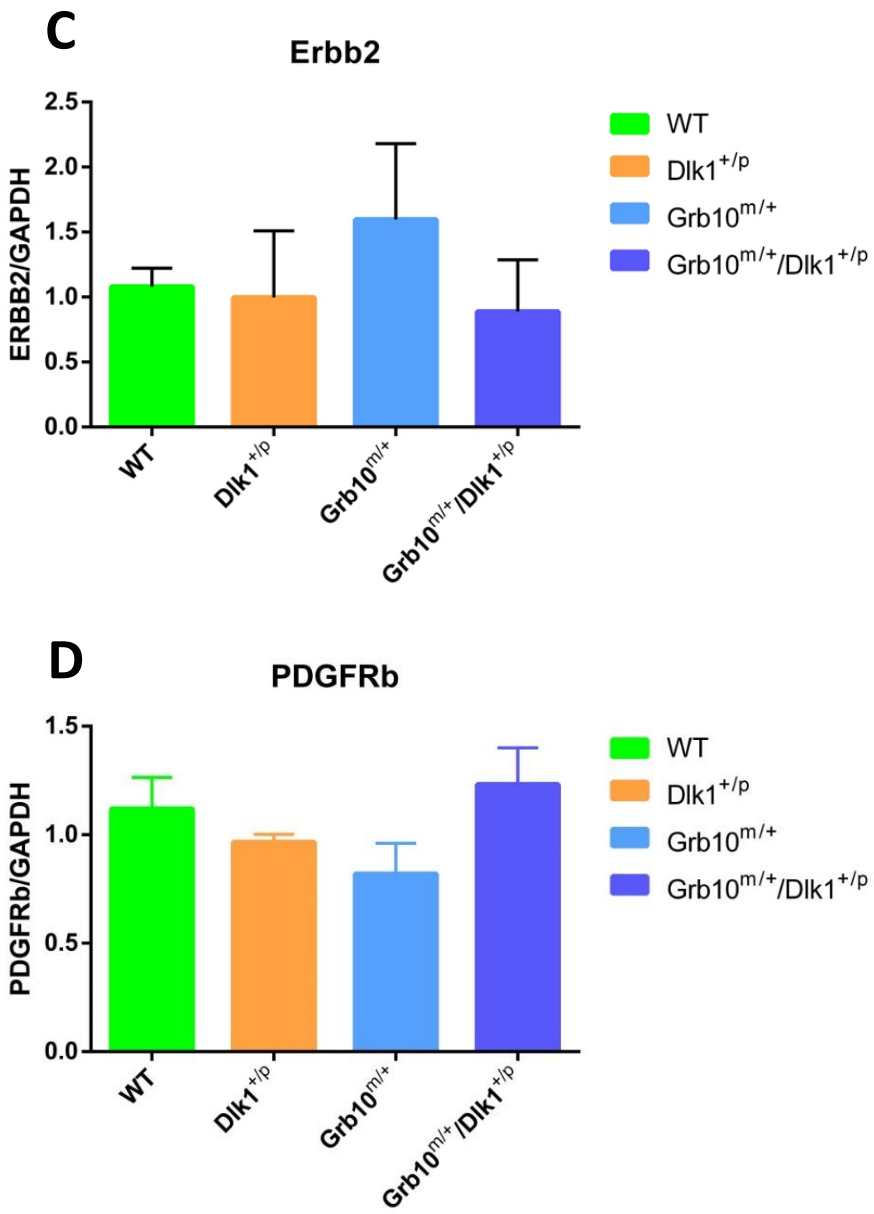

Figure 5.1 PDGFRa, Erbb2 and PDGFRb expression levels in E14.5 pMEFs of four different genotypes, evaluated by Western blotting. A) Representative Western blots probed with antibodies specific for PDGFRa, Erbb2 and PDGFRb proteins in E14.5 pMEFs of the four indicated genotypes. An anti-GAPDH antibody was used to provide the loading control. PDGFRa, Erbb2 or PDGFRb expression levels were normalised to the GAPDH loading control and expressed as bar charts (B-D). **B)** PDGFRa (number of biological replicates n= 5) **C)** Erbb2 (n = 3) **D)** PDGFRb (n = 2). WT, green bars; *Dlk1*$^{+/p}$, orange bars; *Grb10*$^{m/+}$, light blue bars; *Grb10*$^{m/+}$*/Dlk1*$^{+/p}$, dark blue bars. All values represent means plus SEM and have been subject to One-way ANOVA with Tukey's *post hoc* analysis. *P<0.05, **** P<0.0001**.**

5.2.2 Mouse phospho-RTK array analysis indicated similar RTK phosphorylation levels in WT, *Dlk1*$^{+/p}$, *Grb10*$^{m/+}$ and *Grb10*$^{m/+}$/*Dlk1*$^{+/p}$ pMEFs

To compare the RTK phosphorylation profiles in WT, *Dlk1*$^{+/p}$, *Grb10*$^{m/+}$ and *Grb10*$^{m/+}$/*Dlk1*$^{+/p}$ pMEFs, mouse phospho-RTK array was carried out. Cell lysates of the four genotypes were collected from confluence pMEFs cultured in complete medium and then incubated with the phopho-RTK array. Each array contained 39 phosphorylated RTK capture antibodies with duplicated dots (Figure 5.2A; Table 7.1). In E14.5 pMEFs, only a few of these RTKs displayed strong phosphorylation levels including PDGFRa, EGFR, HGFR and VEGFR3 (labelled with 1-4 numbers) (Figure 5.2A). Several RTKs had moderate phosphorylation levels, such as MuSK (labelled with 5) (Figure 5.2A). And some RTKs exhibited low phosphorylation levels, for instance EphR B6 (labelled with 6) (Figure 5.2A). PDGFRa phosphorylation level was the highest among 39 mouse RTKs (Figure 5.2). Interestingly, PDGFRb phosphorylation level was very low in E14.5 pMEFs (indicated by red arrow). The mean pixel densities of phosphorylated PDGFRa, EGFR, HGFR, VEGFR3, MuSK and EphR B6 dots on each array were measured and presented as a bar chart (Figure 5.2B). In all cases, RTK phosphorylation levels were essentially indistinguishable when arrays were compared following exposure to protein extracts from WT, *Dlk1*$^{+/p}$, *Grb10*$^{m/+}$ and *Grb10*$^{m/+}$/*Dlk1*$^{+/p}$ pMEFs (Figure 5.2A, B).

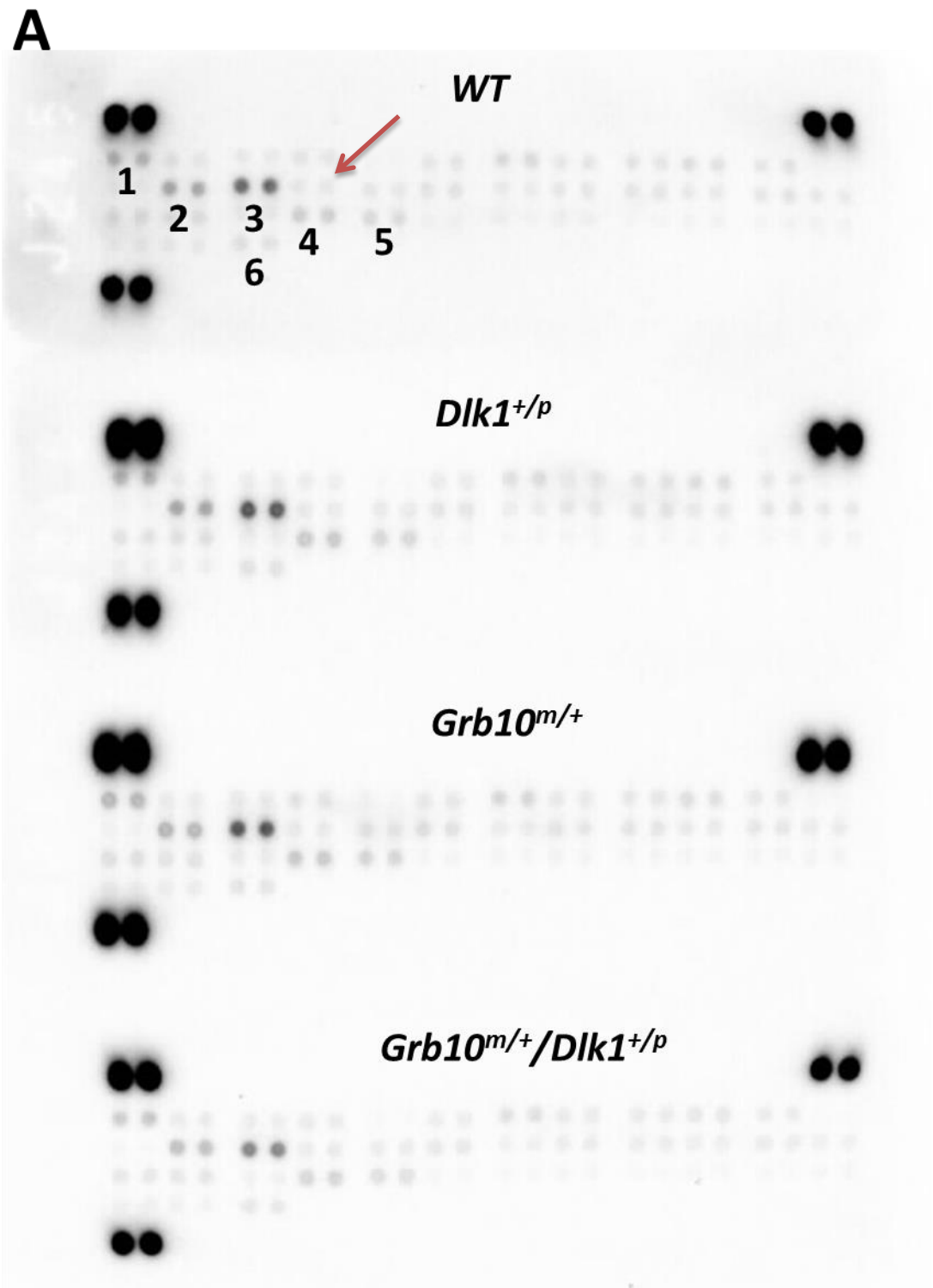

1 p-EGFR, 2 p-HGFR, 3 p-PDGFRa,

4 p-VEGFR3, 5 p-MuSK, 6 p-EphR B6,

Red arrow p-PDGFRb

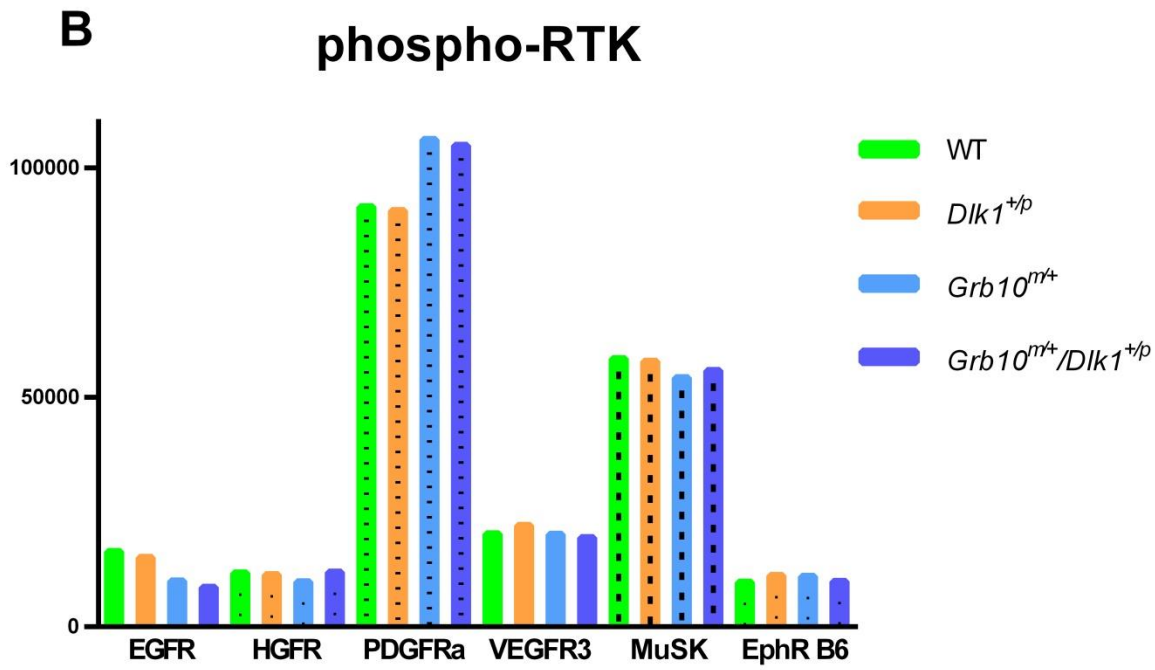

Figure 5.2 Mouse phospho-RTK array analysis of E14.5 pMEFs of four different genotypes. Each array had duplicated dots for 39 phosphorylated RTK antibodies. Three pairs of reference spots, containing phospho-Tyrosine antibodies, were located at three corners of each array. Reference spots, used for aligning the target spots, were not considered as the loading control. **A)** EGFR, HGFR, PDGFRa, VEGFR3, MuSK and EphR B6 displayed relatively strong phosphorylation levels in E14.5 pMEFs among all four genotypes which were labelled with numbers (1-6) on the graph. The position of phosphorylated PDGFRb antibody was indicated with a red arrow. **B)** Mean pixel intensities for each RTK duplicated dots were measured, and mean intensities of EGFR, HGFR, PDGFRa, VEGFR3, MuSK and EphR B6 were expressed as a bar graph (WT, green bar; *Dlk1*$^{+/p}$, orange bar; *Grb10*$^{m/+}$, light blue bar; *Grb10*$^{m/+}$*/Dlk1*$^{+/p}$, dark blue bar). All values are from a single experiment using a commercially available phospho-RTK array.

5.2.3 PDGF-AA triggered rapid downstream Akt and Erk1/2 signal responses in WT, *Dlk1*$^{+/p}$, *Grb10*$^{m/+}$ and *Grb10*$^{m/+}$/*Dlk1*$^{+/p}$ pMEFs

PDGF-AA is a specific ligand of PDGFRa which does not cross react with other PDGF receptors, notably PDGFRb (Borkham-Kamphorst and Weiskirchen, 2016). Hence PDGF-AA was used to specifically activate PDGFRa in E14.5 pMEFs. Cells were starved for overnight (12-14 h) in DMEM medium containing 1% BSA and no FBS. The next day, cells were stimulated with 30 ng/ml murine PDGF-AA for 5 min, 30 min and 60 min. PDGFRa and PDGFRb expression and downstream Akt and Erk1/2 phosphorylation levels were measured.

PDGFRa expression in *Dlk1*$^{+/p}$ and *Grb10*$^{m/+}$ pMEFs was both slightly downregulated when cells were stimulated with PDGF-AA, while PDGFRa expression in WT and *Grb10*$^{m/+}$/*Dlk1*$^{+/p}$ pMEFs remained essentially unchanged during the 1 h stimulation time. PDGFRa expression was elevated in *Dlk1*$^{+/p}$, *Grb10*$^{m/+}$ and *Grb10*$^{m/+}$/*Dlk1*$^{+/p}$ compared to WT when cells were starved overnight (“0” time point) (Figure 5.3A, B). Particularly, PDGFRa expression was significantly increased in *Grb10*$^{m/+}$ pMEFs compared to WT at “0” time point (Figure 5.3A, B). Meanwhile PDGFRb expression was relatively stable in WT, *Dlk1*$^{+/p}$, *Grb10*$^{m/+}$ and *Grb10*$^{m/+}$/*Dlk1*$^{+/p}$ pMEFs under PDGF-AA treatment (Figure 5.3A, C). This indicated that exposure to 30 ng/ml PDGF-AA did not cause degradation of either PDGFRa or PDGFRb in E14.5 pMEFs. These compared to a reduction of PDGFRa expression and no changes in PDGFRb expression in *Dlk1*$^{+/p}$, *Grb10*$^{m/+}$ and *Grb10*$^{m/+}$/*Dlk1*$^{+/p}$ pMEFs compared to WT, when cells were cultured with complete medium containing 10% FBS (Figure 5.1).

Downstream Akt and Erk1/2 phosphorylation levels were relatively low after overnight starvation. However, both were activated by PDGF-AA and showed the highest phosphorylation level at 5 min. At later time points, 30 and 60 mins,

phosphorylation of Akt and Erk1/2 was reduced, but not fully in comparison with levels following overnight serum starvation (Figure 5.3A, D, E). No significant differences of Akt phosphorylation levels were found in pMEFs when compared among four genotypes, although Akt phosphorylation was consistently slightly higher in *Dlk1*$^{+/p}$, *Grb10*$^{m/+}$ and *Grb10*$^{m/+}$/*Dlk1*$^{+/p}$ pMEFs compared to WT (Figure 5.3A, D). Erk1/2 phosphorylation displayed a similar response pattern to PDGF-AA stimulation among cells of the four genotypes (Figure 5.3A, E).

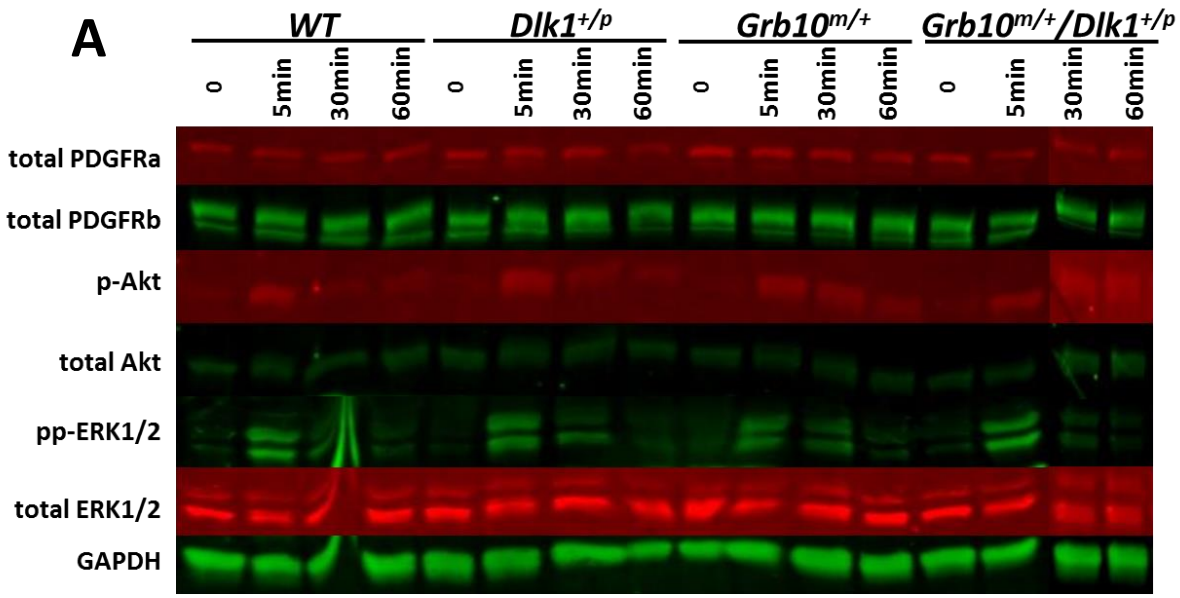
A
WT
Dlk1+/p
Grb10m/+
Grb10m/+/Dlk1+/p
0
5min
30min
60min
total PDGFRa
total PDGFRb
p-Akt
total Akt
pp-ERK1/2
total ERK1/2
GAPDH

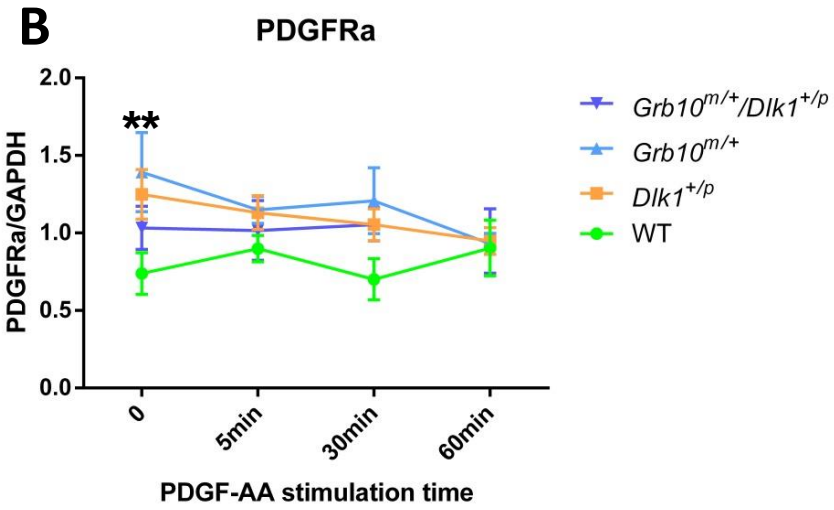
B
PDGFRa
**
PDGFRa/GAPDH
2.0
1.5
1.0
0.5
0.0
0
5min
30min
60min
PDGF-AA stimulation time
Grb10m/+/Dlk1+/p
Grb10m/+
Dlk1+/p
WT

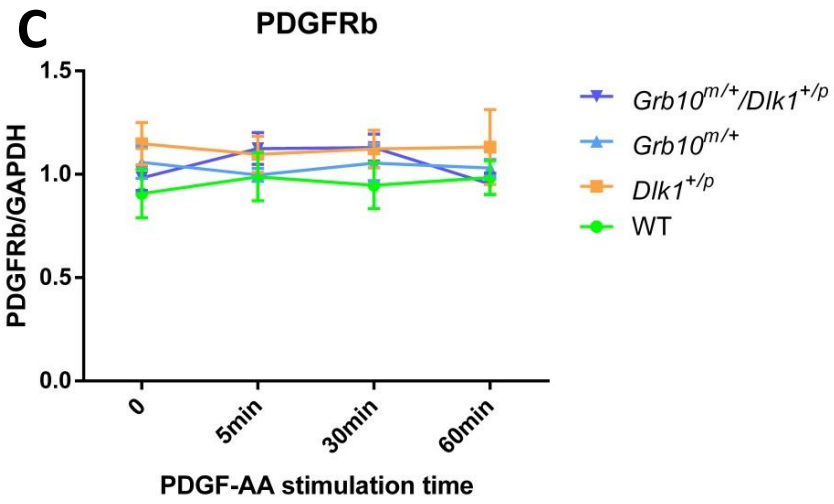
C
PDGFRb
PDGFRb/GAPDH
1.5
1.0
0.5
0.0
0
5min
30min
60min
PDGF-AA stimulation time
Grb10m/+/Dlk1+/p
Grb10m/+
Dlk1+/p
WT

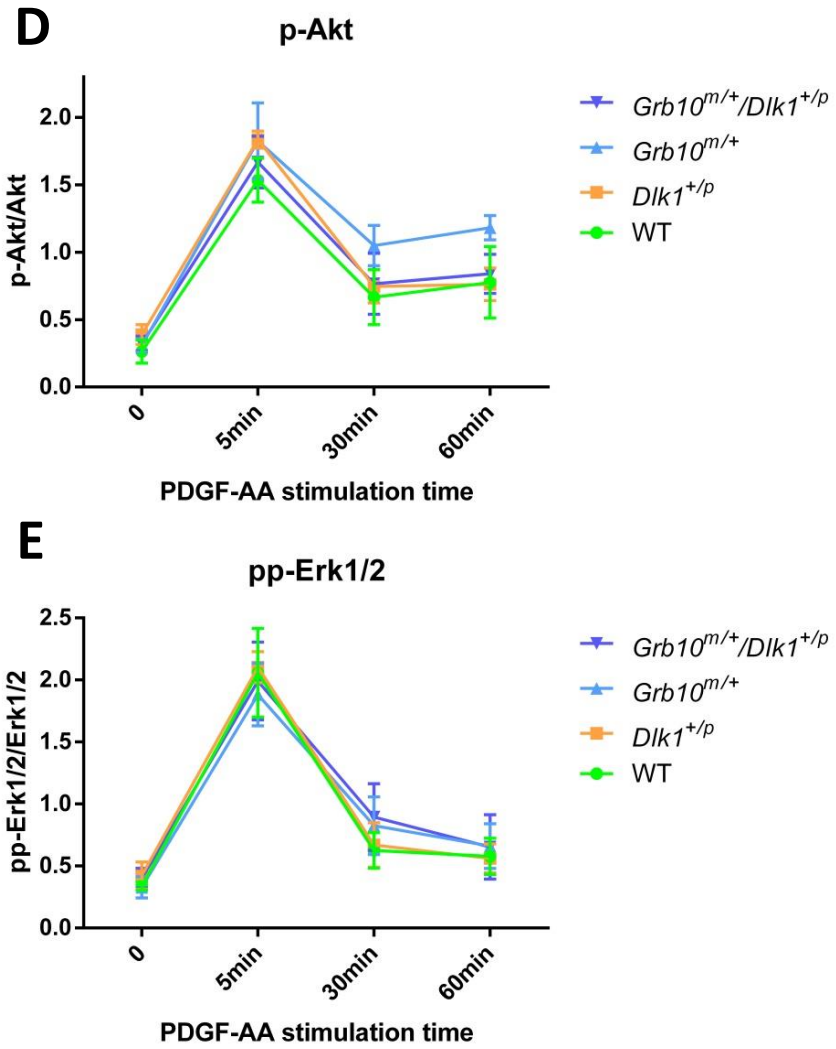

Figure 5.3 PDGF receptor expression levels and downstream signal protein phosphorylation status in PDGF-AA stimulated E14.5 pMEFs of the four genotypes. A) Western blots representative of six independent experiments. Overnight serum starved E14.5 pMEFs of each genotype (no PDGF-AA stimulation) were used as negative controls. GAPDH protein level was used as the loading control for PDGFRa and PDGFRb, while total Akt and Erk1/2 were controls for phosphorylated Akt and Erk1/2 levels, respectively. Western blots were scanned and values normalised to loading controls were plotted in separated line charts for: **B)** PDGFRa, **C)** PDGFRb, **D)** p-Akt and **E)** pp-Erk1/2. WT, green line; *Dlk1*$^{+/p}$, orange line; *Grb10*$^{m/+}$, light blue line; *Grb10*$^{m/+}$*/Dlk1*$^{+/p}$, dark blue line. All values represent means plus SEM and have been subject to Two-way ANOVA with Bonferroni post-tests. WT n=4, *Dlk1*$^{+/p}$ n=4, *Grb10*$^{m/+}$ n=4, *Grb10*$^{m/+}$*/Dlk1*$^{+/p}$ n=4. ** P<0.01**.**

5.2.4 PDGF-BB induced sustained Akt phosphorylation in pMEFs of all genotypes and a stronger Erk1/2 response in *Dlk1*$^{+/p}$, *Grb10*$^{m/+}$ and *Grb10*$^{m/+}$/*Dlk1*$^{+/p}$ pMEFs

PDGF-BB is the only ligand that can activate all three PDGF receptor dimers, PDGFRaa, bb and ab (Borkham-Kamphorst and Weiskirchen, 2016). To investigate the responses of PDGF receptors and downstream Akt and Erk1/2 signals to PDGF-BB stimulation, cells were treated with 30 ng/ml murine PDGF-BB after overnight starvation.

PDGF-BB caused modest but significant reductions in PDGFRa and PDGFRb expression levels during the PDGF-BB stimulation period in WT, *Dlk1*$^{+/p}$, *Grb10*$^{m/+}$ and *Grb10*$^{m/+}$/*Dlk1*$^{+/p}$ pMEFs (Figure 5.4A-C). PDGFRa expression was elevated in *Dlk1*$^{+/p}$, *Grb10*$^{m/+}$ and *Grb10*$^{m/+}$/*Dlk1*$^{+/p}$ pMEFs when cells were cultured without 10% FBS, and a significant elevation of PDGFRa was observed in *Dlk1*$^{+/p}$ pMEF compared to WT at “0” time point (Figure 5.3A, B). In general, PDGFRa expression was higher in *Dlk1*$^{+/p}$, *Grb10*$^{m/+}$ and *Grb10*$^{m/+}$/*Dlk1*$^{+/p}$ pMEFs compared to WT during the PDGF-BB stimulation period (Figure 5.4A, B). No distinct or significant PDGFRb expression differences were found among WT, *Dlk1*$^{+/p}$, *Grb10*$^{m/+}$ and *Grb10*$^{m/+}$/*Dlk1*$^{+/p}$ pMEFs treated with PDGF-BB (Figure 5.4 A, C).

PDGF-BB stimulation led to prolonged Akt signalling as the Akt phosphorylation level went up rapidly after 5 min and was sustained for the full 60 min duration of the experiment in pMEFs of all four genotypes (Figure 5.4A, D). Akt phosphorylation level was consistently lower in *Dlk1*$^{+/p}$, *Grb10*$^{m/+}$ and *Grb10*$^{m/+}$/*Dlk1*$^{+/p}$ pMEFs compared to WT, but no significant difference was found among pMEFs of the four genotypes (Figure 5.4 A, D).

In parallel, the highest Erk1/2 phosphorylation level was found at 5 min in WT, *Dlk1*$^{+/p}$, *Grb10*$^{m/+}$ and *Grb10*$^{m/+}$/*Dlk1*$^{+/p}$ pMEFs under PDGF-BB treatment, and

then Erk1/2 activities quickly dropped to lower level at 30 min and to the lowest level at 60 min (Figure 5.4A, E). Notably, Erk1/2 phosphorylation level was increased in *Dlk1*$^{+/p}$ and *Grb10*$^{m/+}$*/Dlk1*$^{+/p}$ pMEFs and significantly increased in *Grb10*$^{m/+}$ pMEFs compared to WT, showing Erk1/2 signal activity was more sensitive to PDGF-BB stimulation in *Dlk1*$^{+/p}$, *Grb10*$^{m/+}$ and *Grb10*$^{m/+}$*/Dlk1*$^{+/p}$ pMEFs, but especially in *Grb10*$^{m/+}$ pMEFs (Figure 5.4A, E).

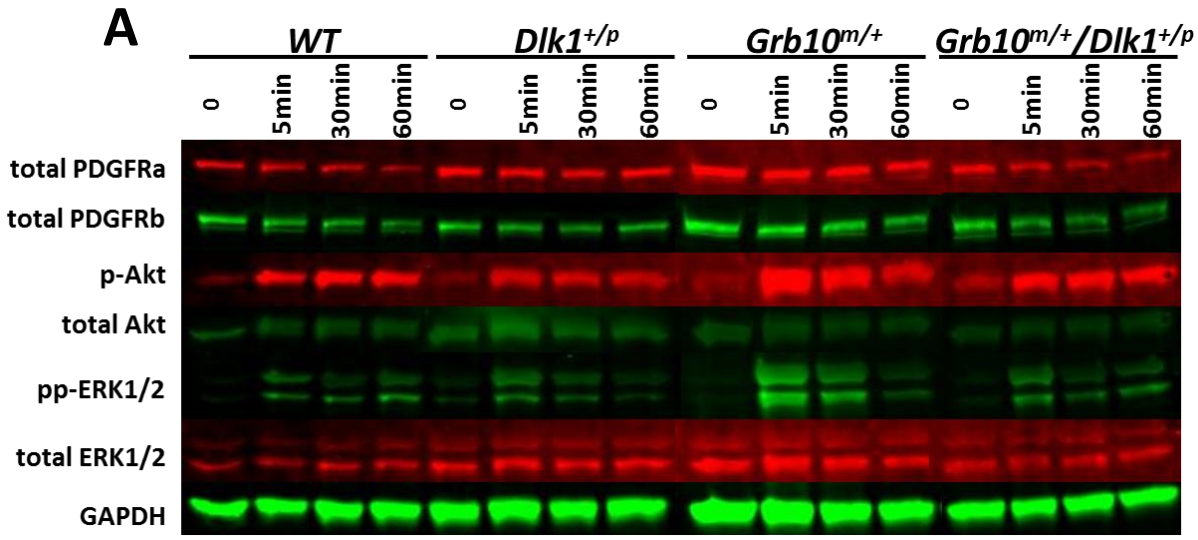
A
WT
Dlk1+/p
Grb10m/+
Grb10m/+/Dlk1+/p
0
5min
30min
60min
total PDGFRa
total PDGFRb
p-Akt
total Akt
pp-ERK1/2
total ERK1/2
GAPDH

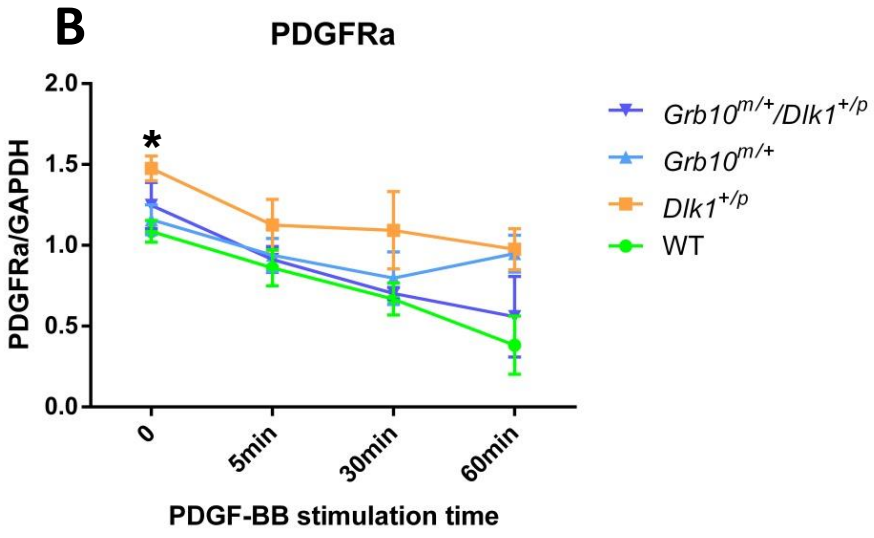
B
PDGFRa
PDGFRa/GAPDH
2.0
1.5
1.0
0.5
0.0
*
0
5min
30min
60min
PDGF-BB stimulation time
Grb10m/+/Dlk1+/p
Grb10m/+
Dlk1+/p
WT

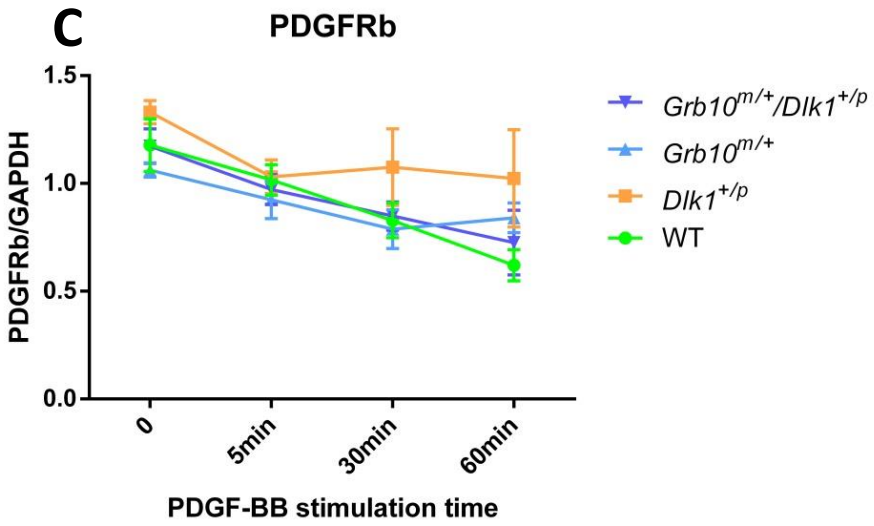
C
PDGFRb
PDGFRb/GAPDH
1.5
1.0
0.5
0.0
0
5min
30min
60min
PDGF-BB stimulation time
Grb10m/+/Dlk1+/p
Grb10m/+
Dlk1+/p
WT

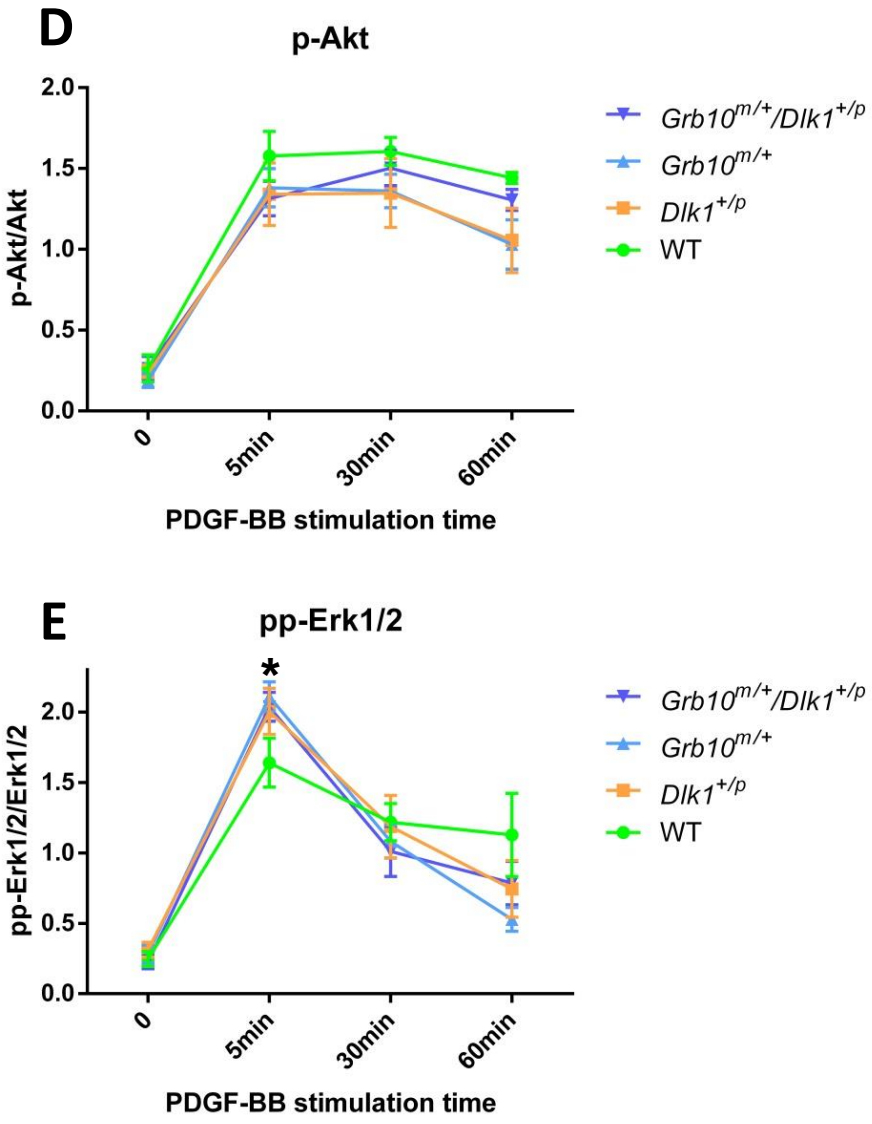

Figure 5.4 PDGF receptor expression and downstream signal phosphorylation levels measured in PDGF-BB stimulated E14.5 pMEFs of the four different genotypes. A) Western blots representative of seven independent experiments. Overnight serum starved E14.5 pMEFs of the indicated genotypes, without PDGF-BB stimulation, were used as the negative controls. GAPDH protein level was used as the loading control for PDGFRa and PDGFRb while total Akt and Erk1/2 were the controls for phosphorylated Akt and Erk1/2 levels, respectively. PDGFRa, PDGFRb, p-Akt and pp-Erk1/2 levels were normalised to the loading control and visualised in separated line charts for: **B)** PDGFRa, **C)** PDGFRb, **D)** p-Akt and **E)** pp-Erk1/2. WT, green line; *Dlk1*$^{+/p}$, orange line; *Grb10*$^{m/+}$, light blue line; *Grb10*$^{m/+}$*/Dlk1*$^{+/p}$, dark blue line. All values represent means plus SEM and have been subject to Two-way ANOVA with Bonferroni post-tests. WT n=4, *Dlk1*$^{+/p}$ n=4, *Grb10*$^{m/+}$ n=4, *Grb10*$^{m/+}$*/Dlk1*$^{+/p}$ n=4. * P<0.05.

5.2.5 Higher phosphorylation levels of PI3K and Grb2 were stimulated by PDGF-AA and PDGF-BB, respectively, in *Grb10*$^{m/+}$ and *Grb10*$^{m/+}$/*Dlk1*$^{+/p}$ pMEFs

Autophosphorylation and dimerization of PDGFRa and PDGFRb result in autophosphorylation of tyrosine residues, followed by activation of downstream signals including PI3K and growth factor receptor bound protein 2 (Grb2) (Ostman and Heldin, 2001). To determine the phosphorylation levels of PDGFRa and PDGFRb under PDGF-AA and PDGF-BB stimulation, pMEF lysates were extracted from PDGF-AA or PDGF-BB stimulated cells. The lysates were immunoprecipitated (IP) using a mouse anti-p-Tyr antibody, and then specific phosphorylated proteins were identified on IP Western blots using antibodies specific to total PDGFRa, PDGFRb, PI3K p85 subunit and Grb2 (Figure 5.5A). Aliquot of cell lysates were used to run a standard WB along with the IP as a control (Figure 5.5A).

Very low level of p-PDGFRa and p-PDGFRb were detected in WT, *Dlk1*$^{+/p}$, and *Grb10*$^{m/+}$/*Dlk1*$^{+/p}$ pMEFs during 30 min of PDGF-AA stimulation (Figure 5.5A, B). Interestingly, PDGFRa phosphorylation level at 5 min and PDGFRb phosphorylation levels at 0 and 5 min were significantly higher in *Grb10*$^{m/+}$ pMEFs in comparison with WT (Figure 5.5A, B). PDGFRa and PDGFRb phosphorylation dropped to low levels at 30 min (Figure 5.5A, B). Meanwhile, total PDGFRa and PDGFRb expression levels were stable and similar among WT, *Dlk1*$^{+/p}$, *Grb10*$^{m/+}$ and *Grb10*$^{m/+}$/*Dlk1*$^{+/p}$ pMEFs during PDGF-AA stimulation, suggesting PDGFRa signalling in *Grb10*$^{m/+}$ pMEFs was more sensitive to PDGF-AA stimulation (Figure 5.3A-C; Figure 5.5A).

PI3K activation levels were upregulated in *Grb10*$^{m/+}$ and *Grb10*$^{m/+}$/*Dlk1*$^{+/p}$ compared to WT and *Dlk1*$^{+/p}$ pMEFs treated with PDGF-AA, and WT and *Dlk1*$^{+/p}$ pMEFs exhibited a comparatively low level of PI3K activation (Figure 5.5A, B). Particularly, PI3K activation was significantly higher at 5 min and 30

min in *Grb10*$^{m/+}$ compared to WT pMEFs, which was consistent with the higher PDGFRa phosphorylation level found in *Grb10*$^{m/+}$ pMEFs (Figure 5.5B). As described before (Figure 5.3A, D), Akt phosphorylation levels peaked at 5 min and went down afterwards when pMEFs were stimulated by PDGF-AA, while PI3K activation responded to PDGF-AA stimulation in a similar pattern (Figure 5.5A, B). Grb2 phosphorylation levels were slightly higher in *Grb10*$^{m/+}$ and *Grb10*$^{m/+}$*/Dlk1*$^{+/p}$ compared to WT and *Dlk1*$^{+/p}$ pMEFs. However, a low phosphorylation level of Grb2 was discovered in PDGF-AA sitmulated pMEFs of all four genotyopes (Figure 5.5A).

In parallel, PDGFRa and PDGFRb signalling were activated by PDGF-BB, as pMEFs of all four genotypes displayed high PDGFRa and PDGFRb phosphorylation levels which peaked at 5 min and then went down to a low level at 30 min (Figure 5.5 A, B). PDGFRa phosphorylation levels were similar among the four genotypes during the 30 min of PDGF-BB stimulation (Figure 5.5A, C). PDGFRb phosphorylation level was slightly higher in *Grb10*$^{m/+}$ pMEF at 5 min in comparison with the other three genotypes (Figure 5.5A, C). Total PDGFRb levels were reduced by PDGF-BB stimulation and no distinguishable differences were found among all four genotypes (Figure 5.3A-C; Figure 5.5A). Collectively, these results suggested that PDGFRb signalling was more sensitive to PDGF-BB stimulation in *Grb10*$^{m/+}$ pMEFs.

PI3K phosphorylation was stimulated by PDGF-BB in pMEFs to activate both PDGFRa and PDGFRb (Figure 5.5A). PI3K phosphorylation level was similar among WT, *Dlk1*$^{+/p}$ and *Grb10*$^{m/+}$*/Dlk1*$^{+/p}$ pMEFs but higher in *Grb10*$^{m/+}$ pMEFs (Figure 5.5A, C). PDGFRa and PDGFRb phosphorylation levels dropped rapidly after 5 min, while p-PI3K levels reduced gradually from 5 min to 30 min (Figure 5.5A, C). PI3K displayed prolonged signalling under PDGF-BB stimulation, supporting the sustained p-Akt activity observed in PDGF-BB treated pMEFs as mentioned before (Figure 5.4A, D; Figure 5.5A, C).

Additionally, Grb2 phosphorylation level was lowest in WT. *Grb10*$^{m/+}$ and *Grb10*$^{m/+}$*/Dlk1*$^{+/p}$ pMEFs showed higher p-Grb2 level than WT and *Dlk1*$^{+/p}$ (Figure 5.5A, C). Erk1/2 phosphorylation levels were higher in *Dlk1*$^{+/p}$, *Grb10*$^{m/+}$ and *Grb10*$^{m/+}$*/Dlk1*$^{+/p}$ pMEFs stimulated by PDGF-BB as mentioned before (Figure 5.4A, E; Figure 5.5A). These results indicated a more active MAPK/ERK signal pathway stimulated by PDGF-BB in *Dlk1*$^{+/p}$, *Grb10*$^{m/+}$ and *Grb10*$^{m/+}$*/Dlk1*$^{+/p}$ pMEFs.

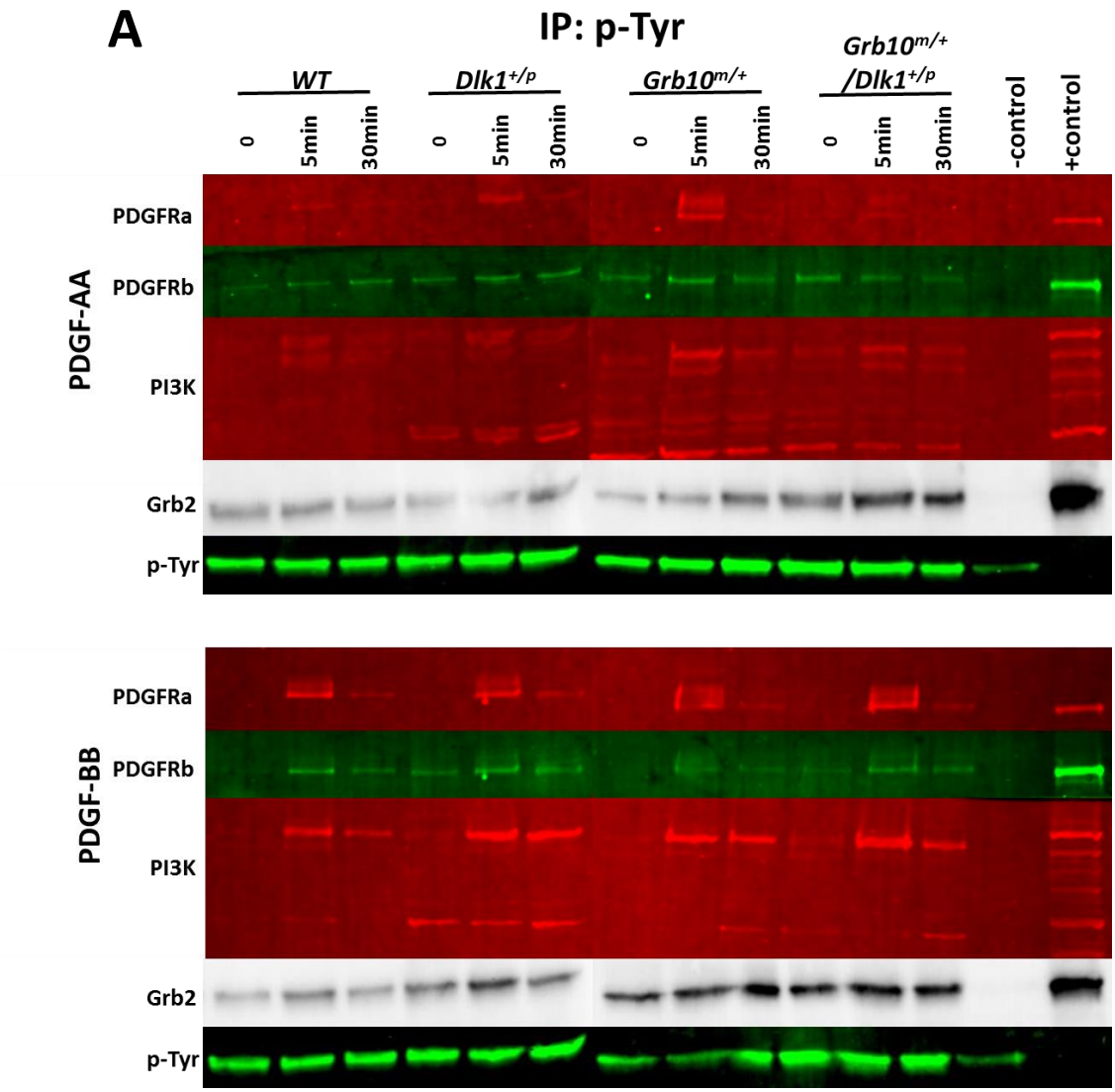
A
IP: p-Tyr
WT
Dlk1+/p
Grb10m/+
Grb10m/+ /Dlk1+/p
0
5min
30min
-control
+control
PDGF-AA
PDGF-BB
PDGFRa
PDGFRb
PI3K
Grb2
p-Tyr

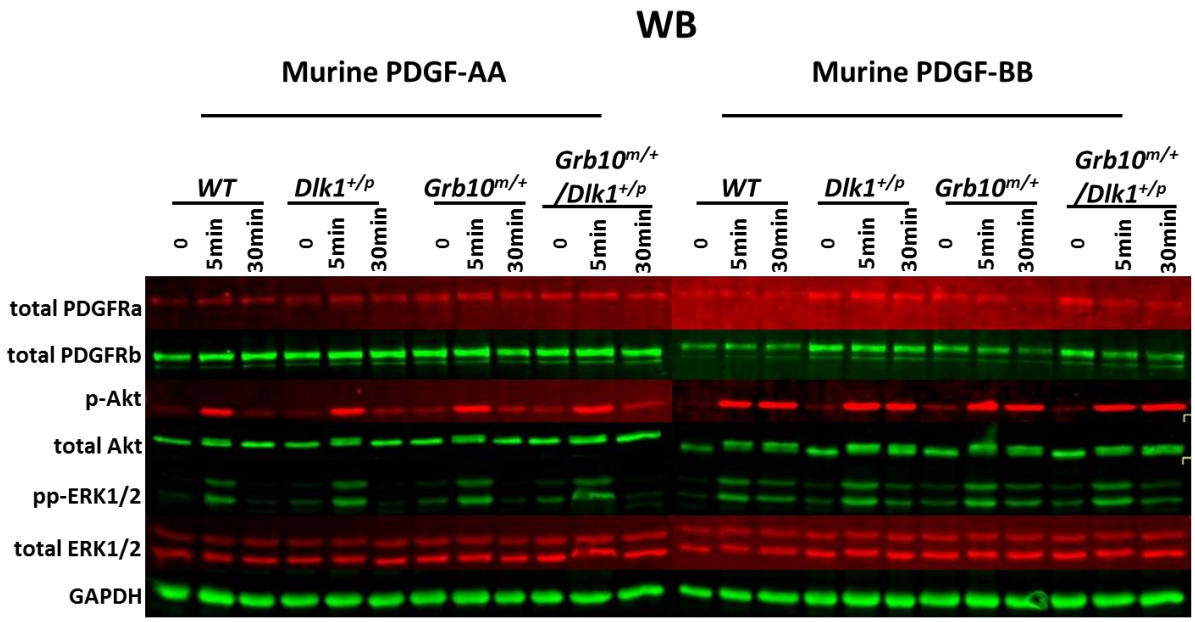
WB
Murine PDGF-AA
Murine PDGF-BB
WT
Dlk1+/p
Grb10m/+
Grb10m/+ /Dlk1+/p
0
5min
30min
total PDGFRa
total PDGFRb
p-Akt
total Akt
pp-ERK1/2
total ERK1/2
GAPDH

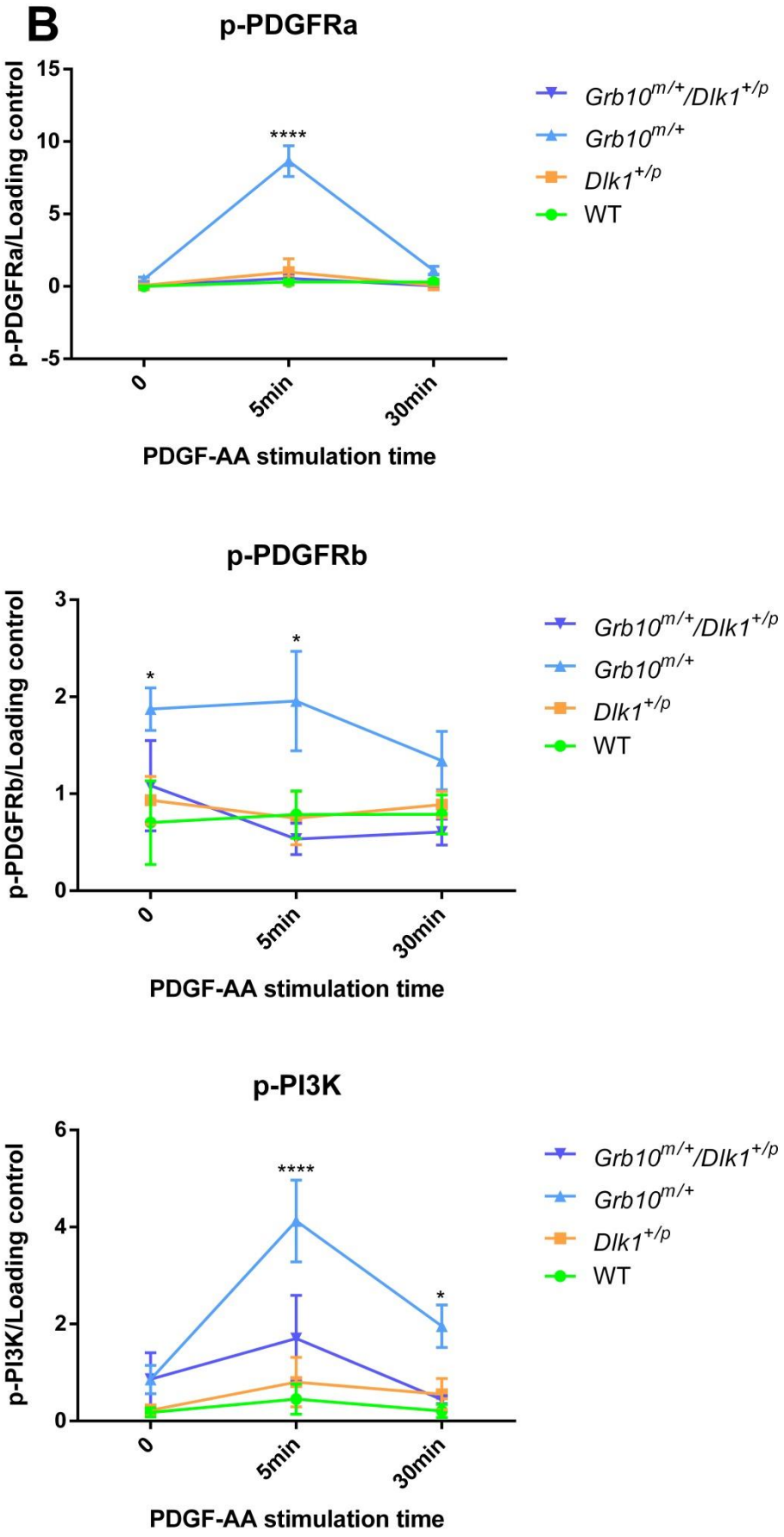
B
p-PDGFRa
p-PDGFRa/Loading control
15
10
5
0
-5
****
0
5min
30min
PDGF-AA stimulation time
Grb10m/+/Dlk1+/p
Grb10m/+
Dlk1+/p
WT
p-PDGFRb
p-PDGFRb/Loading control
3
2
1
0
*
*
0
5min
30min
PDGF-AA stimulation time
Grb10m/+/Dlk1+/p
Grb10m/+
Dlk1+/p
WT
p-PI3K
p-PI3K/Loading control
6
4
2
0
****
*
0
5min
30min
PDGF-AA stimulation time
Grb10m/+/Dlk1+/p
Grb10m/+
Dlk1+/p
WT

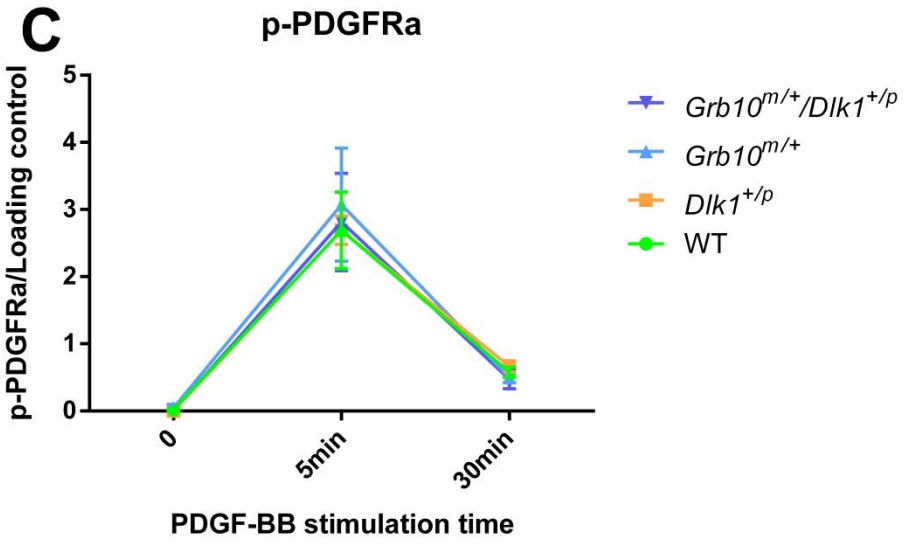
C
p-PDGFRa
p-PDGFRa/Loading control
5
4
3
2
1
0
0
5min
30min
PDGF-BB stimulation time
Grb10m/+/Dlk1+/p
Grb10m/+
Dlk1+/p
WT

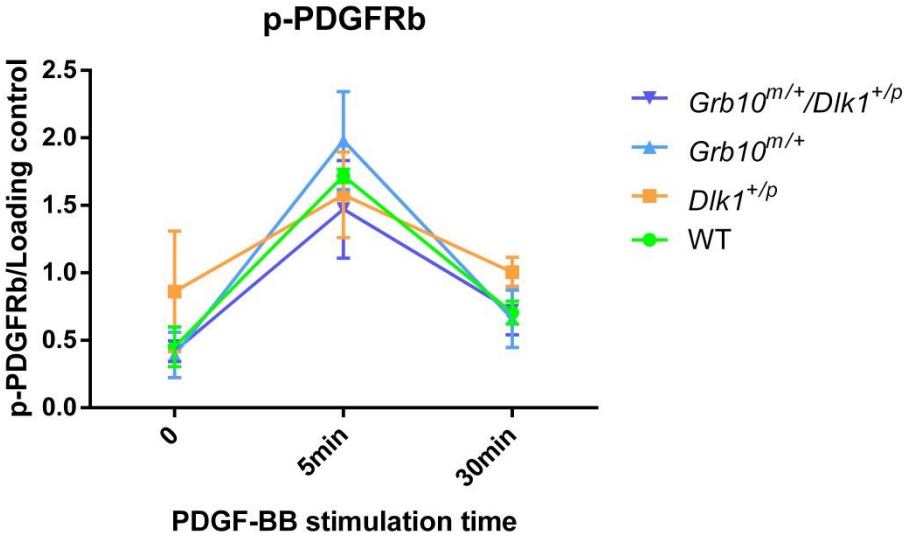
p-PDGFRb
p-PDGFRb/Loading control
2.5
2.0
1.5
1.0
0.5
0.0
0
5min
30min
PDGF-BB stimulation time
Grb10m/+/Dlk1+/p
Grb10m/+
Dlk1+/p
WT

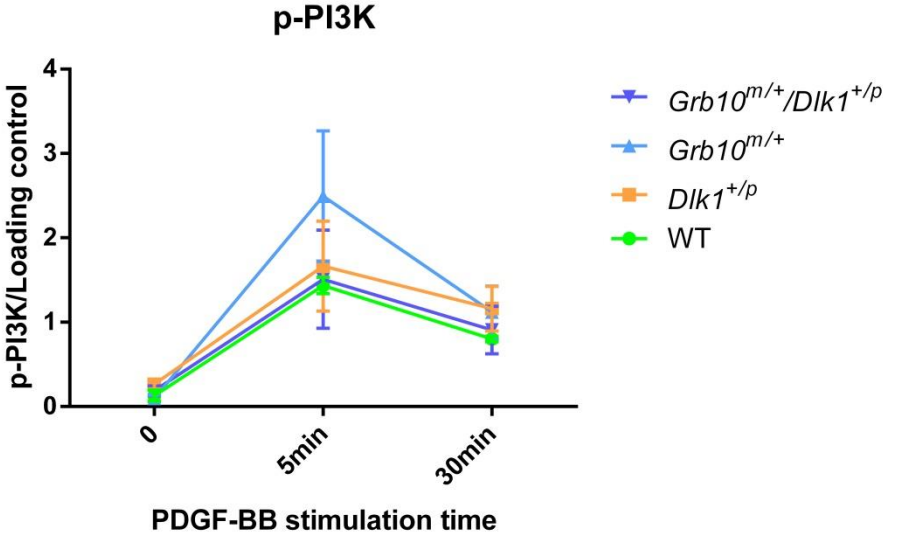
p-PI3K
p-PI3K/Loading control
4
3
2
1
0
0
5min
30min
PDGF-BB stimulation time
Grb10m/+/Dlk1+/p
Grb10m/+
Dlk1+/p
WT

Figure 5.5 PDGFRa and PDGFRb IP from E14.5 pMEFs under PDGF-AA and BB stimulation. A) Representative immunoprecipitation (IP p-Tyr; top) and Western blots (WB; bottom) of three independent experiments in each case except Grb2 immunoprecipitation which was repeated once. Overnight serum starved E14.5 pMEFs of the indicated genotypes, without PDGF-AA/BB stimulation, were used as the negative controls. Light chain of p-Tyr antibody level was used as the loading control. PDGFRa, PDGFRb and PI3K activation levels, under PDGF-AA/BB stimulation, were normalised to the loading control and visualised in separated line charts for: **B)** PDGF-AA stimulation and **C)** PDGF-BB stimulation. WT, green line; *Dlk1*$^{+/p}$, orange line; *Grb10*$^{m/+}$, light blue line; *Grb10*$^{m/+}$*/Dlk1*$^{+/p}$, dark blue line. All values represent means plus SEM and have been subject to Two-way ANOVA with Bonferroni post-tests. * P<0.05, **** P<0.0001.

5.2.6 Lower Erk1/2 activity was discovered in *Dlk1*$^{+/p}$, *Grb10*$^{m/+}$ and *Grb10*$^{m/+}$/*Dlk1*$^{+/p}$ pMEFs during EGF stimulation

To determine the EGFR signalling activities in pMEFs among four genotypes, cells were stimulated with 100 ng/ml EGF for 5 min, 30 min and 60 min. In response to EGF stimulation, Akt phosphorylation level peaked at 5 min and then dropped down rapidly in WT, *Dlk1*$^{+/p}$, *Grb10*$^{m/+}$ and *Grb10*$^{m/+}$/*Dlk1*$^{+/p}$ pMEFs. No significant difference in Akt phosphorylation levels were found among the four genotypes (Figure 5.6A, B). Meanwhile, Erk1/2 activities were downregulated in *Dlk1*$^{+/p}$, *Grb10*$^{m/+}$ and *Grb10*$^{m/+}$/*Dlk1*$^{+/p}$ pMEFs compared to WT (Figure 5.6A, C). In particular, pp-Erk1/2 level was reduced in *Dlk1*$^{+/p}$ pMEFs at 5 min and in *Grb10*$^{m/+}$ and *Grb10*$^{m/+}$/*Dlk1*$^{+/p}$ pMEFs at 30 min, when compared to WT (Figure 5.6A, C).

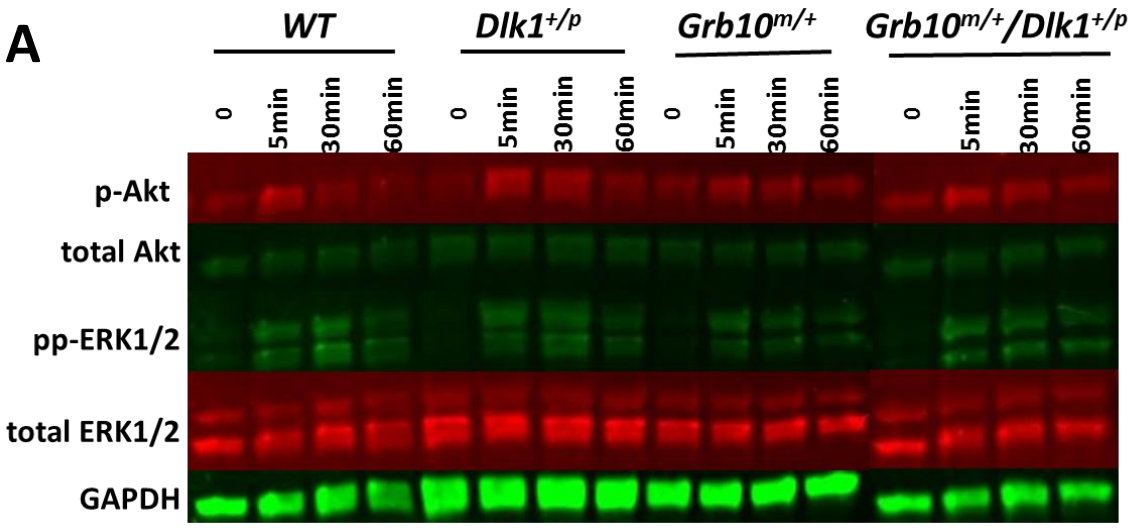

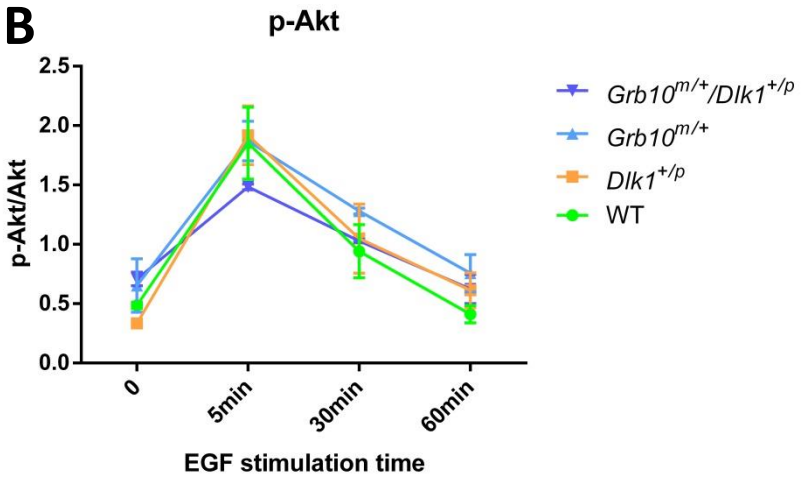

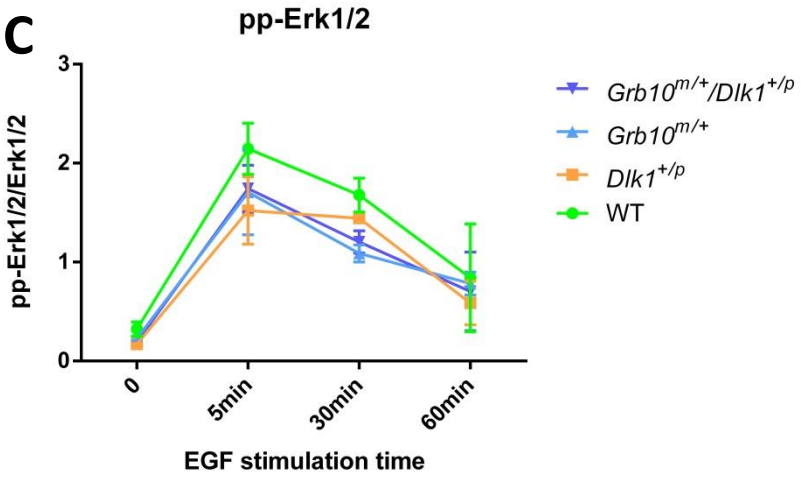

Figure 5.6 Akt and Erk1/2 phosphorylation activities in response to EGF stimulation of E14.5 pMEFs of different genotypes. A) Western blots representative of two independent experiments. Overnight serum starved pMEFs of each genotype (no EGF stimulation) were used as the negative controls. GAPDH protein level was used as the loading control for EGFR, while total Akt and Erk1/2 were controls for phosphorylated Akt and Erk1/2 levels, respectively. Western blots were scanned and values normalised to loading controls were plotted in separated line graphs for: **B)** EGFR and **C)** pp-Erk1/2. WT, green line; *Dlk1*$^{+/p}$, orange line; *Grb10*$^{m/+}$, light blue line; *Grb10*$^{m/+}$*/Dlk1*$^{+/p}$, dark blue line.

5.2.7 FGFR1 signalling was indistinguishable in E14.5 pMEFs of the four genotypes

FGFR1 was one of the downregulated RTKs discovered by the GO-term enrichment analysis in E14.5 pMEF total proteome (see section 4.5). To evaluate the FGFR1 signalling response, pMEFs of the four genotypes were treated with 10 ng/ml FGF1 for different time intervals within 1 h (Figure 5.7A). Total FGFR1 expression did not change much in WT and *Dlk1*$^{+/p}$ pMEFs, while it was found to be slightly reduced in *Grb10*$^{m/+}$ and *Grb10*$^{m/+}$/*Dlk1*$^{+/p}$ pMEFs during the 60 min stimulation time (Figure 5.7A, B). Moreover, FGFR1 expression was found to be lower in *Grb10*$^{m/+}$ and lowest in *Grb10*$^{m/+}$/*Dlk1*$^{+/p}$ pMEFs by proteomics analysis (Figure 4.5A). In parallel, a higher and transient Erk1/2 phosphorylation was found in *Grb10*$^{m/+}$/*Dlk1*$^{+/p}$ pMEFs which peaked at 5 min (Figure 5.7A, C). Erk1/2 signal activity was similar and weak among WT, *Dlk1*$^{+/p}$ and *Grb10*$^{m/+}$ pMEFs (Figure 5.7A, C). No statistically significant difference of Erk1/2 phosphorylation level was found among the four genotypes. Downstream Akt signalling was not active during the 1 hour of FGF1 stimulation time (Figure 5.7).

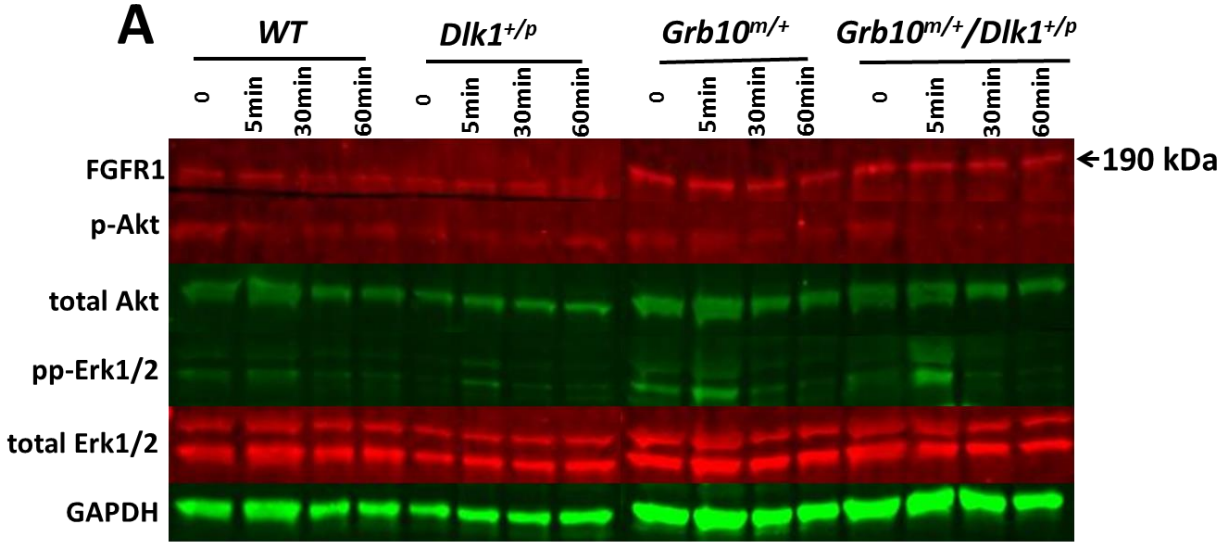

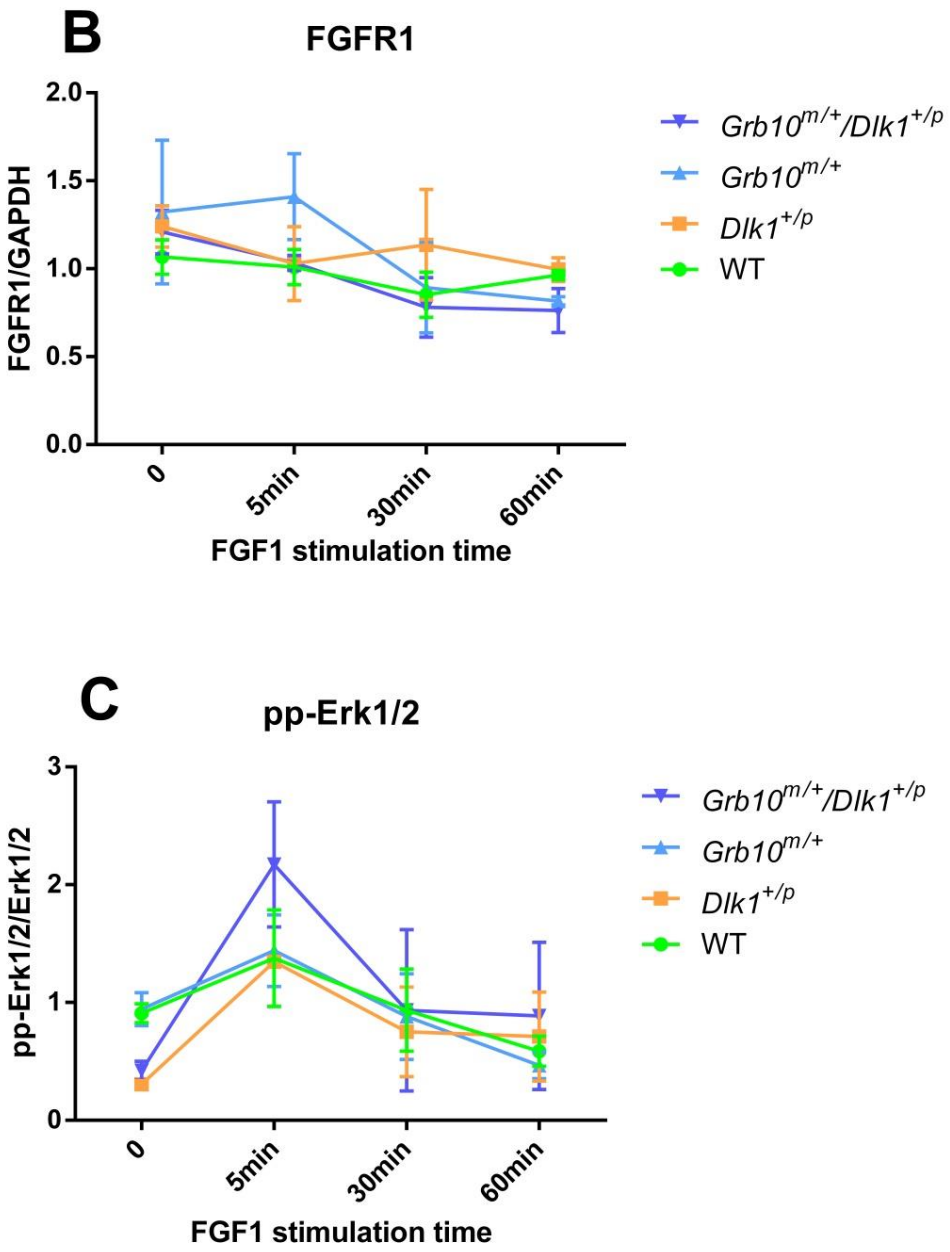

Figure 5.7 FGFR1 expression and downstream signal phosphorylation levels were measured in FGF1 stimulated E14.5 pMEFs of all four genotypes. A) Western blots representative of two independent experiments. Overnight serum starved E14.5 pMEFs of each genotype (no FGF1 stimulation) were used as the negative controls. GAPDH protein level was used as the loading control for FGFR1, while total Akt and Erk1/2 were controls for phosphorylated Akt and Erk1/2 levels, respectively. Western blots were scanned and values normalised to loading controls were plotted in separated line charts for: **B)** FGFR1 and **C)** pp-Erk1/2. WT, green line; *Dlk1*$^{+/p}$, orange line; *Grb10*$^{m/+}$, light blue line; *Grb10*$^{m/+}$/*Dlk1*$^{+/p}$, dark blue line. All values represent means plus SEM and have been subject to Two-way ANOVA with Bonferroni post-tests.

5.2.8 *Grb10*$^{m/+}$ and *Grb10*$^{m/+}$/*Dlk1*$^{+/p}$ pMEFs displayed strong insulin stimulated Akt signalling

Grb10 was reported to negatively regulate insulin receptor signalling in pMEFs (Yu *et al*., 2011). To investigate if Dlk1 and Grb10 were involved in embryonic growth through insulin signalling, pMEFs were stimulated with 20 nM insulin. Insulin receptor beta (IRb) expression was not affected by insulin treatment in WT, *Dlk1*$^{+/p}$, *Grb10*$^{m/+}$ and *Grb10*$^{m/+}$/*Dlk1*$^{+/p}$ pMEFs as the IRb expression stayed stable thoughout the stimulation time-course (Figure 5.8A, B). No significant differences in IRb expression were found among WT, *Dlk1*$^{+/p}$ and *Grb10*$^{m/+}$/*Dlk1*$^{+/p}$ pMEFs, while *Grb10*$^{m/+}$ pMEFs showed a slightly higher IRb expression among all four genotypes (Figure 5.8A, B). Interestingly, an elevation of Akt phosphorylation was found in *Grb10*$^{m/+}$ and *Grb10*$^{m/+}$/*Dlk1*$^{+/p}$ pMEFs compared to WT and *Dlk1*$^{+/p}$ under all the time points, and the Akt phosphorylation sustained in *Grb10*$^{m/+}$ and *Grb10*$^{m/+}$/*Dlk1*$^{+/p}$ pMEFs during the stimulation period (Figure 5.8A, C). A rapid Erk1/2 phosphorylation response pattern was found that was similar in pMEFs of all four genotypes (Figure 5.8A, D).

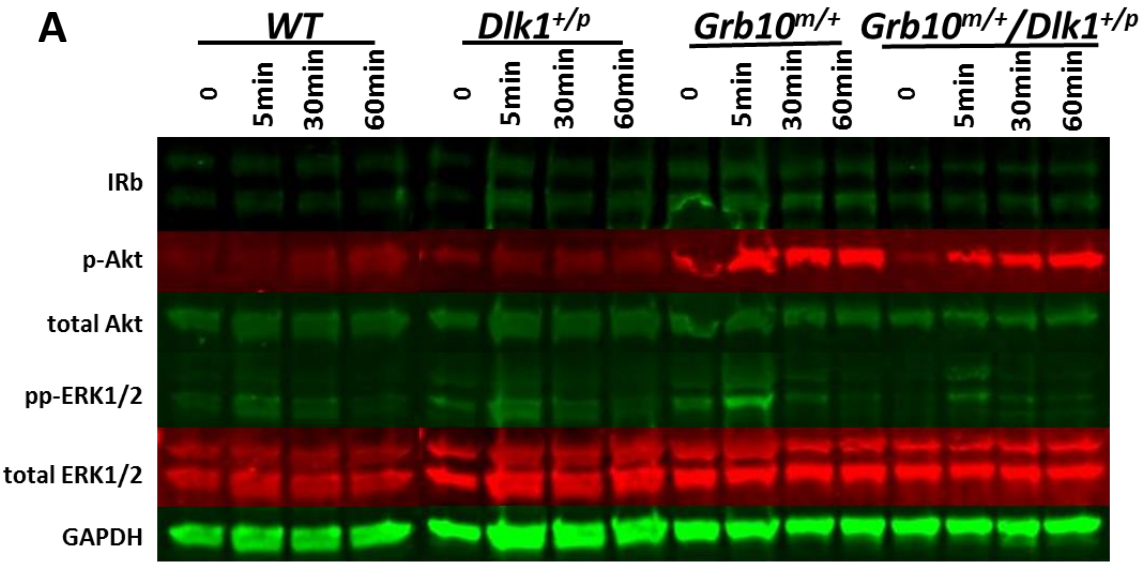

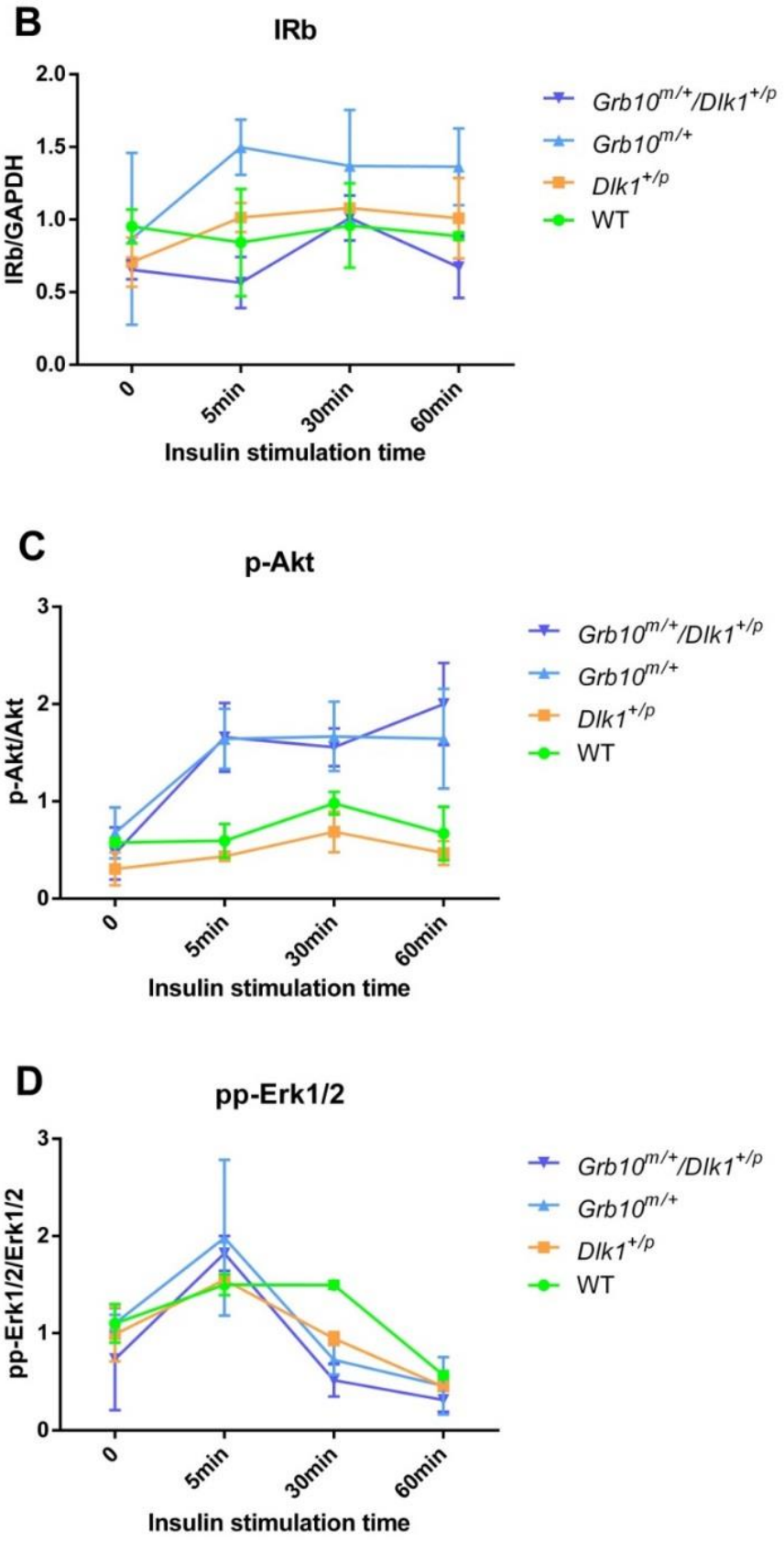
B
IRb
IRb/GAPDH
2.0
1.5
1.0
0.5
0.0
0
5min
30min
60min
Insulin stimulation time
Grb10m/+/Dlk1+/p
Grb10m/+
Dlk1+/p
WT
C
p-Akt
p-Akt/Akt
3
2
1
0
0
5min
30min
60min
Insulin stimulation time
Grb10m/+/Dlk1+/p
Grb10m/+
Dlk1+/p
WT
D
pp-Erk1/2
pp-Erk1/2/Erk1/2
3
2
1
0
0
5min
30min
60min
Insulin stimulation time
Grb10m/+/Dlk1+/p
Grb10m/+
Dlk1+/p
WT

Figure 5.8 IRb expression and downstream Akt and Erk1/2 phosphorylation levels were measured in insulin stimulated E14.5 pMEFs of the four different genotypes. A) Western blots representative of two independent experiments. Overnight serum starved E14.5 pMEFs of each genotype (no insulin stimulation) were used as the negative controls. GAPDH protein level was used as the loading control for IRb, while total Akt and Erk1/2 were controls for phosphorylated Akt and Erk1/2 levels, respectively. Western blots were scanned and values normalised to loading controls were plotted in separated line charts for: **B)** IRb, **C)** p-Akt and **D)** pp-Erk1/2. WT, green line; *Dlk1*$^{+/p}$, orange line; *Grb10*$^{m/+}$, light blue line; *Grb10*$^{m/+}$*/Dlk1*$^{+/p}$, dark blue line.

5.2.9 IGF1R signalling was independent from Dlk1 and Grb10 in E14.5 pMEFs

IGF signalling is a major fetal growth regulatory pathway (Barlow *et al*., 1991; DeChiara *et al*., 1991; Nordin *et al*., 2014). Yet genetic evidence derived from *Grb10*$^{m/+}$ and *IGF1R*$^{+/p}$ crossed mice suggested that *Grb10* acted primarily on growth independently of Insulin/IGF signalling (Charalambous *et al*., 2003; unpublished data). To evaluate if IGF1 signalling was modified by *Dlk1* or *Grb10* knockout at a biochemical level, pMEFs of the four different genotypes were treated with 50 ng/ml IGF1 for 5 min, 30 min and 60 min (Figure 5.9). A very weak signal response was detected from IRb and downstream Akt and Erk1/2 during the stimulation time-course, indicating that IGF1 signalling was not involved in Dlk1 and Grb10 on early embryo development (Figure 5.9).

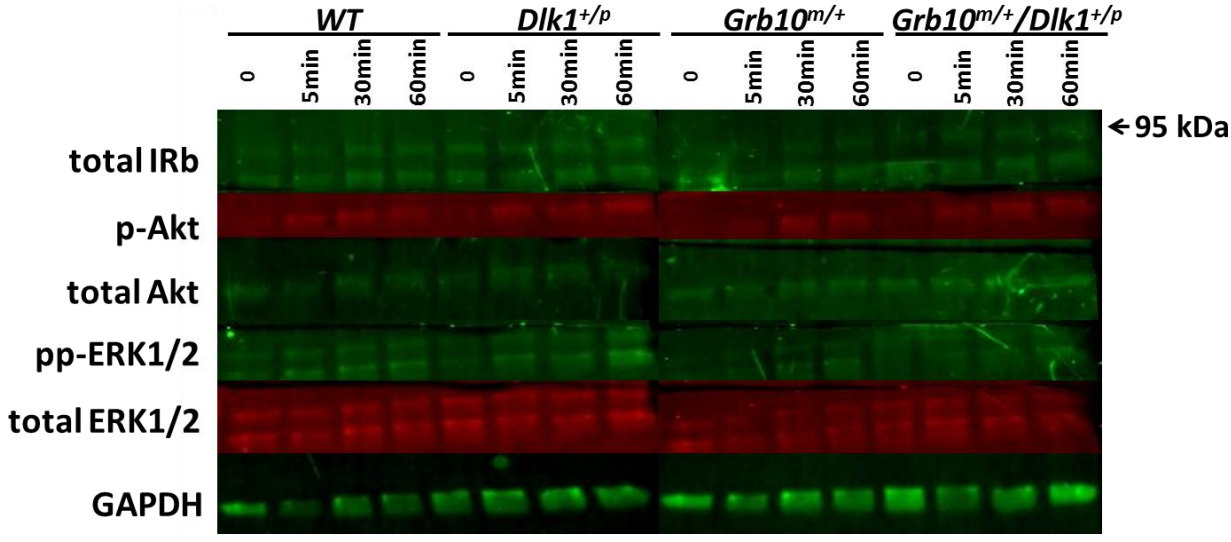

Figure 5.9 IRb expression, downstream Akt and Erk1/2 phosphorylation levels in IGF1 stimulated E14.5 pMEFs among the four genotypes. Western blots representative of one experiment. Overnight serum starved E14.5 pMEFs of each genotype (no IGF1 stimulation) were used as the negative controls. GAPDH protein level was used as the loading control for IRb, while total Akt and Erk1/2 were controls for phosphorylated Akt and Erk1/2 levels, respectively.

5.3 Discussion

This chapter focused on evaluating dynamic RTK downstream signalling in E14.5 WT, *Dlk1*$^{+/p}$, *Grb10*$^{m/+}$ and *Grb10*$^{m/+}$/*Dlk1*$^{+/p}$ pMEFs and was guided by the previous described TMT proteomics results (Chapter 4). Firstly, I chose three RTK targets to check the accuracy of the proteomics analysis. The PDGFRa, PDGFRb and Erbb2 Western blottings in E14.5 pMEFs showed results consistent with the proteomics data (Figure 4.8; Figure 5.1). PDGFRa expression was down-regulated in the three knockout pMEFs. Erbb2 expression was reduced in *Dlk1*$^{+/p}$ and *Grb10*$^{m/+}$/*Dlk1*$^{+/p}$ pMEFs and elevated in *Grb10*$^{m/+}$ pMEFs. PDGFRb expression was similar among the four genotypes (Figure 5.1). Unfortunately, none of the PDGFRa, PDGFRb and Erbb2 antibodies worked well on WB of E14.5 liver lysates, so their expression status in liver using this technique remains unknown (data not shown).

Secondly, a mouse phospho-RTK array displayed an equivalent tyrosine phosphorylation level among four genotypes, whereas most of the total RTK expression levels were reduced in *Dlk1*$^{+/p}$, *Grb10*$^{m/+}$ and *Grb10*$^{m/+}$/*Dlk1*$^{+/p}$ pMEFs according to the TMT proteomics data (Figure 4.8). In particular, PDGFRa showed the highest phosphorylation level among the 39 RTKs on the array, suggesting a relatively strong PDGFRa signalling activity in E14.5 pMEFs (Figure 5.2). Since total PDGFRa expression levels were reduced in *Dlk1*$^{+/p}$, *Grb10*$^{m/+}$ and *Grb10*$^{m/+}$/*Dlk1*$^{+/p}$ pMEFs compared to WT, according to both proteomics and Western blot analyses, this means that PDGFRa may have higher phosphorylation activity in the knockout pMEFs.

A third set of experiments aimed to evaluate signalling responses through some of the identified receptors by stimulating pMEFs of different genotypes with the cognate ligands, PDGF-AA/BB, EGF, FGF1, IGF1 and insulin. PDGF-AA and PDGF-BB were used to stimulate the PDGF receptors to evaluate the phosphorylation levels of the receptors and downstream signals

in E14.5 pMEFs.

PDGF-AA induced a significantly higher PDGFRa phosphorylation level in *Grb10*$^{m/+}$ pMEFs compared to WT. Meanwhile the PDGFRa phosphorylation level stimulated by PDGF-AA was relatively low in WT, *Dlk1*$^{+/p}$ and *Grb10*$^{m/+}$*/Dlk1*$^{+/p}$ pMEFs. In addition, two direct downstream signal partners of PDGF receptors, PI3K and Grb2, had higher phosphorylation levels in *Grb10*$^{m/+}$ and *Grb10*$^{m/+}$*/Dlk1*$^{+/p}$ compared to WT and *Dlk1*$^{+/p}$ pMEFs under PDGF-AA treatment (Figure 5.5A, B). However, the downstream Akt and Erk1/2 phosphorylation activities stimulated by PDGF-AA were similar and transient in pMEFs of the four genotypes (Figure 5.3; Figure 5.5). Collectively, these results indicated that the downstream PDGFRa signalling was more sensitive in *Grb10*$^{m/+}$ and *Grb10*$^{m/+}$*/Dlk1*$^{+/p}$ than WT and *Dlk1*$^{+/p}$ pMEFs, especially in *Grb10*$^{m/+}$, and the downstream Akt and Erk1/2 responses activated by PDGF-AA were rapid and similar among pMEFs of the four genotypes. These results indicated that Grb10 normally negatively regulated the downstream PDGFRa signalling (as judged by PDGFRa phosphorylation and downstream PI3K and Grb2 activation) in E14.5 pMEFs treated with PDGF-AA.

By contrast, PDGF-BB promoted sustained PI3K and Akt phosphorylation in WT, *Dlk1*$^{+/p}$, *Grb10*$^{m/+}$ and *Grb10*$^{m/+}$*/Dlk1*$^{+/p}$ pMEFs, suggesting a more active downstream PI3K/Akt signalling under PDGF-BB treatment than PDGF-AA. Furthermore, PDGF-BB treatment led to higher Grb2 and Erk1/2 phosphorylation levels in *Dlk1*$^{+/p}$, *Grb10*$^{m/+}$ and *Grb10*$^{m/+}$*/Dlk1*$^{+/p}$ pMEFs than WT. PDGFRa and PDGFRb phosphorylation levels induced by PDGF-BB were stronger than PDGF-AA. However, no distinct difference of p-PDGFRa or p-PDGFRb was found in pMEFs among the four genotypes. In addition, PDGF-BB induced the reduced PDGFRa and PDGFRb expression in pMEFs (Figure 5.4; Figure 5.5). Overall, PDGF-BB simultaneously activated the

PDGFRa and PDGFRb and caused the PDGF receptor degradation. Activation of the PDGF receptors was associated with higher levels of phosphorylated PI3K and Grb2, as well as their respective downstream targets Akt and Erk1/2. Both Dlk1 and Grb10 appeared to act as inhibitors of the PDGF-BB/PDGF receptors/Grb2/Erk1/2 pathway, as the Erk1/2 phosphorylation level was elevated in *Dlk1*$^{+/p}$, *Grb10*$^{m/+}$ and *Grb10*$^{m/+}$*/Dlk1*$^{+/p}$ pMEFs in comparison with WT. This is consistent with studies showing that Grb10 acts as an inhibitor of several RTKs (Wick *et al*., 2003; Vecchione *et al*., 2003; Dufresne and Smith, 2005; Monami *et al*., 2008; Hsu *et al*., 2011; Yu *et al*., 2011; Liu *et al*., 2014).

Strikingly, PDGF-AA and PDGF-BB raised differential signal responses in E14.5 pMEFs. This was presumably due to the different targets of these two ligands. PDGF-AA specifically activates PDGFRa homodimers, while PDGF-BB can simultaneously stimulate heterodimers and homodimers of PDGFRa and PDGFRb (Borkham-Kamphorst and Weiskirchen, 2016). Hence, a sustained activation of PI3K-Akt pathway and more active Grb2-Erk1/2 signalling were detected in E14.5 pMEFs induced by PDGF-BB (Figure 5.3; Figure 5.4; Figure 5.5). Notably, mouse phospho-RTK array and PDGF-BB stimulation both showed strong PDGFRa phosphorylation levels in E14.5 pMEFs among the four genotypes. Yet the PDGFRa phosphorylation was relatively low in pMEFs incubated with PDGF-AA. The phospho-RTK array was performed using protein lysates from pMEFs cultured with 10% FBS. The numerous growth factors in the serum, possibly including PDGF-BB, induced and maintained the high PDGFRa phosphorylation level in pMEFs. Also, the serum may cause the PDGFRa degradation in *Dlk1*$^{+/p}$, *Grb10*$^{m/+}$ and *Grb10*$^{m/+}$*/Dlk1*$^{+/p}$ pMEFs, as PDGFRa expression levels were lower in the three knockout pMEFs compared to WT, when cells were cultured with medium containing serum. And PDGFRa expression levels were higher in knockout pMEFs compared to WT when cells were serum starved overnight (Figure

5.3A-C). This suggests that Dlk1 and Grb10 might play an important role in regulating the PDGFRa turnover and activity in pMEFs. Besides, the very low phosphorylation level of PDGFRb appeared in the PDGF-AA treated pMEFs was unexpected. This might be the cross talks between the PDGFRa and PDGFRb, or the PDGFRb antibody was not completely specific. Altogether, PDGF-AA and PDGF-BB stimulation studies uncovered that Dlk1 and Grb10 may interact with each other via PDGFR signalling in E14.5 pMEFs.

In similar experiments, EGF induced transient Akt phosphorylation and FGF1 essentially no p-Akt activation, with similar responses seen in E14.5 WT, *Dlk1*$^{+/p}$, *Grb10*$^{m/+}$ and *Grb10*$^{m/+}$*/Dlk1*$^{+/p}$ pMEFs. Furthermore, Erk1/2 phosphorylation levels stimulated by FGF1 were similar in pMEFs among the four genotypes, while reduced Erk1/2 phosphorylation was found in *Dlk1*$^{+/p}$, *Grb10*$^{m/+}$ and *Grb10*$^{m/+}$*/Dlk1*$^{+/p}$ pMEFs treated with EGF (Figure 5.6; Figure 5.7). The unaltered response to EGF and FGF1 stimulation in pMEFs of all four genotypes demonstrates the specificity of the effect of Dlk1 and Grb10 through PDGF receptors.

The downstream Akt and Erk1/2 activities were very low in E14.5 WT, *Dlk1*$^{+/p}$, *Grb10*$^{m/+}$ and *Grb10*$^{m/+}$*/Dlk1*$^{+/p}$ pMEFs stimulated with 50 ng/ml IGF1 (Figure 5.9). This suggests that Dlk1 and Grb10 may not be involved in IGF1R signalling, supporting the genetic evidence that Grb10 acted independently from IGF1R signalling to promote fetal growth (Charalambous *et al*., 2003). However, the low Akt and Erk1/2 activities could due to the relatively low concentration of IGF1 used in this study.IGF1 concentration was chose based on previous studies (Belletti *et al*., 2002; You *et al*., 2002; Wu *et al*., 2005), but some groups used 100 ng/ml IGF1 to stimulate MEF cells (Rui *et al*., 2001; Akundi *et al*., 2012). Different IGF1 concentrations (possibly 50 ng/ml, 100 ng/ml and 150 ng/ml) should be tested in the future.

Meanwhile, under insulin treatment, a significantly higher Akt phosphorylation level was detected in *Grb10*$^{m/+}$ and *Grb10*$^{m/+}$/*Dlk1*$^{+/p}$ pMEFs than WT and *Dlk1*$^{+/p}$ (Figure 5.8). *Grb10*$^{m/+}$ mice were large and lean (greater muscle mass) as adults (Figure 3.2) and could clear a glucose load more efficiently and exhibit enhanced insulin signalling in peripheral tissues (Smith *et al*., 2007; Wang *et al*., 2007). Collectively, *Grb10*$^{m/+}$ and *Grb10*$^{m/+}$/*Dlk1*$^{+/p}$ pMEFs illustrated a more sensitive insulin and Akt signalling. It is known that insulin signalling plays essential roles in metabolism and has a modest effect on fetal growth (Guo 2014). *Insr* knockout mice were born about 10% smaller than WT (Accilli *et al*., 1996; Joshi *et al*., 1996; Kitamura *et al*., 2003). Numerous biochemical studies have demonstrated that Grb10 negatively regulates insulin signalling through IR *in vitro* and *in vivo* (Wick *et al*., 2003; Wang *et al*., 2007; Smith *et al*., 2007; Zhang *et al*., 2012; Andrew, 2012). Indistinguishable changes of Akt and Erk1/2 phosphorylation levels were found between WT and *Dlk1*$^{+/p}$ pMEFs treated with insulin. Ruiz-Hidalgo and co-workers reported that Dlk1 inhibited adipogenesis in insulin stimulated 3T3-L1 cells through ERK/MAPK pathway, and the mRNA levels of IGF1R and IRS1 were not affected by Dlk1 (Ruiz-Hidalgo *et al*., 2002). In this work, Erk1/2 phosphorylation level was similar in undifferentiated WT and *Dlk1*$^{+/p}$ pMEFs when stimulated with insulin, demonstrating that Dlk1 may be specifically involved in adipogenic differentiation of pMEFs. The role of Dlk1 in other insulin signalling, such as glucose metabolism, is less well studied. The higher insulin signalling found in *Grb10*$^{m/+}$ and *Grb10*$^{m/+}$/*Dlk1*$^{+/p}$ pMEFs could contribute to the higher proliferation rate of these cells (Madon-Simon *et al*., 2014). Genetic evidence from our laboratory from crosses between *Insr* knockout and *Grb10* knockout mice indicate that Grb10 influences growth largely independently of insulin receptor (unpublished data). Nevertheless, this could be investigated further using pMEF cell cultures. The involvement of Grb10 in insulin signalling could be a unique Grb10 function independent of Dlk1.

In conclusion, PDGFRa and PDGFRb signalling was identified as the potential cell signal pathways involved in Dlk1 and Grb10 interactions in E14.5 pMEFs. The candidate RTK signal pathways were selected based on TMT proteomics and phopho-RTK array results as well as the literatures (Figure 5.10). Downstream signal activities of PDGFRa and PDGFRb were found to be more sensitive in *Dlk1*$^{+/p}$, *Grb10*$^{m/+}$ and *Grb10*$^{m/+}$/*Dlk1*$^{+/p}$ pMEFs compared to WT However, the downstream signal activities of other candidate RTKs, including FGFR1, EGFR, IGF1R and InsR, were not significantly changed in the knockout pMEFs.

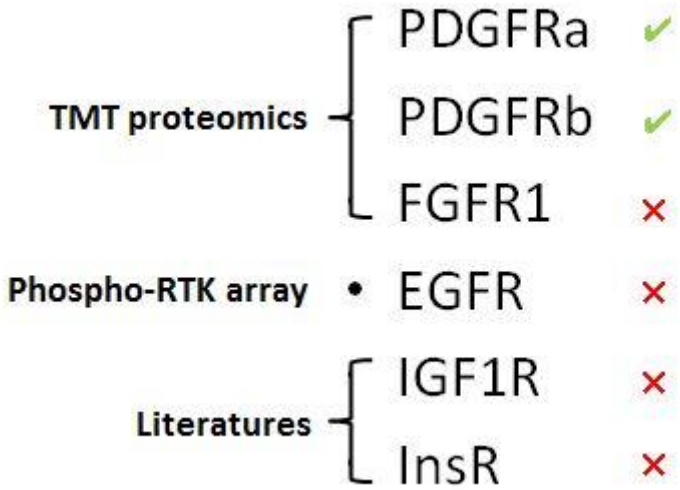

Figure 5.10 Summary of candidate RTK signal pathways studied in this work. PDGFRa and PDGFRb were found to be the best candidate RTKs involved in the crosstalk of Dlk1 and Grb10 proteins in E14.5 pMEFs.

Chapter 6

Final discussion

6.1 Conclusions of major findings

How imprinted genes regulate embryonic growth which subsequently affects adult physiology is not well studied. This is hampered by the lack of knowledge of the imprinted gene interactions and cellular signal pathways involved in growth control. Oppositely imprinted genes, *Dlk1* and *Grb10*, form a mammalian growth-regulatory axis, potentially independent from the IGF signalling pathway (Moon *et al*., 2002; Charalambous *et al*., 2003; Madon-Simon *et al*., 2014). In this study, I looked for evidence of signalling between Dlk1 and Grb10 in pMEFs and livers derived from E14.5 WT, $Dlk1^{+/p}$, $Grb10^{m/+}$ and $Grb10^{m/+}/Dlk1^{+/p}$ embryos that might explain their opposing phenotypic roles in fetal growth and energy homeostasis. My focus was on biochemical methods, including unbiased TMT quantitative proteomics analyses.

In chapter 3, I found that $Dlk1^{+/p}$ embryos had a body size indistinguishable from WT at E14.5, while $Grb10^{m/+}$ and $Grb10^{m/+}/Dlk1^{+/p}$ embryos were significantly enlarged compared to WT and $Dlk1^{+/p}$. In parallel, $Dlk1^{+/p}$ adults were fatter whereas $Grb10^{m/+}$ and $Grb10^{m/+}/Dlk1^{+/p}$ were leaner than WT at 6-month-old. This was in keeping with previously published studies on *Dlk1* and *Grb10* knockout mice (Moon *et al*., 2002; Charalambous *et al*., 2003; Smith *et al*., 2007; Wang *et al*., 2007; Charalambous *et al*., 2014; Madon-Simon *et al*., 2014). At a biochemical level, Dlk1 and Grb10 proteins each affected expression of the other in E14.5 pMEFs and livers. However, the Dlk1 and Grb10 expression patterns were opposite between E14.5 pMEFs and livers. The Grb10 expression level was higher in $Dlk1^{+/p}$ pMEFs and significantly lower in $Dlk1^{+/p}$ livers compared to WT, while soluble Dlk1 protein level was lower in $Grb10^{m/+}$ pMEFs and significantly higher in $Grb10^{m/+}$ livers. Genetic evidence supports the hypothesis that Dlk1 acts as an upstream inhibitor of Grb10 in regulating mouse fetal growth (Madon-Simon *et al*., 2014). Only the Dlk1/Grb10 expression profiles in E14.5 pMEFs fit this hypothesis.

This may due to the possibility of a more prominent role in cell proliferation in pMEFs versus insulin-regulated lipid metabolism in liver. Furthermore, WT and *Dlk1*$^{+/p}$, *Grb10*$^{m/+}$ and *Grb10*$^{m/+}$/*Dlk1*$^{+/p}$ exhibited similar Akt and Erk1/2 phosphorylation levels in serum-induced E14.5 pMEFs, suggesting a similar downstream signal activation responses between these two groups. This further supports the genetic evidence that *Grb10*$^{m/+}$ and *Grb10*$^{m/+}$/*Dlk1*$^{+/p}$ are similar while *Dlk1*$^{+/p}$ is divergent at the biochemical level (Madon-Simon *et al*., 2014). Lastly, mTOR inhibition reduced Grb10 expression level in WT and *Dlk1*$^{+/p}$ pMEFs which is consistent with previous phosphoproteome and biochemical studies of mTOR, showing that Grb10 was stabilized and directly phosphorylated by mTORC1 (Hsu *et al*., 2011; Yu *et al*., 2011; Liu *et al*., 2014).

In chapter 4, I compared the proteomes and phosphoproteomes from E14.5 pMEFs and livers among the four genotypes using TMT proteomics analyses. I found that *Grb10*$^{m/+}$ and *Grb10*$^{m/+}$/*Dlk1*$^{+/p}$ were similar while *Dlk1*$^{+/p}$ was divergent in E14.5 pMEFs and livers at a proteomics level using PCA and HCL analyses in consideration of the biological replicates from each genotype. This is consistent with the genetic evidence derived from *Dlk1*$^{+/p}$ and *Grb10*$^{m/+}$ crossed mice (Madon-Simon *et al*., 2014). Global knockout of *Dlk1* or *Grb10* broadly affected the protein expression and phosphorylation in E14.5 pMEFs and livers at a proteomics level. Dlk1 and Grb10 act as a cell ligand and cytoplasmic adaptor, respectively (Smas and Sul, 1993; Wang and Sul, 2006; Hudak and Sul, 2013; Holt and Siddle, 2005; Ceccarelli and Sicheri, 2009), and both are important cell signalling proteins which regulate mouse fetal growth and many cellular processes, such as adipogenesis and myogenesis (Moon *et al*., 2003; Charalambous *et al*., 2003; Charalambous *et al*., 2014; Andersen *et al*., 2013; Holt *et al*., 2012; Mokbel *et al*., 2014; Liu *et al*., 2014). This can explain why either *Dlk1* or *Grb10* deletion causes largely a reduction of protein expression or phosphorylation in proteomes and phosphoproteomes of pMEF and liver. RTK activity associated GO-terms were significantly

enriched in pMEF and liver total proteomes of *Dlk1*$^{+/p}$, *Grb10*$^{m/+}$ and *Grb10*$^{m/+}$*/Dlk1*$^{+/p}$ when compared to WT. Particularly striking, given the signalling roles predicted for Dlk1 and Grb10, the expression levels of several RTKs and signal partners, such as PDGFRa, FGF1R and protein tyrosine phosphatase receptor type F (PTPRF), were reduced in *Dlk1*$^{+/p}$, *Grb10*$^{m/+}$, *Grb10*$^{m/+}$*/Dlk1*$^{+/p}$ pMEF and liver proteomes. This suggests that Dlk1 and Grb10 may interact with one or more RTK signalling pathways in E14.5 pMEFs and livers. Clustering followed by GO-term enrichment analyses uncovered groups of proteins linked with known Dlk1 and Grb10 functions according to the literature, and further supported the notion that Dlk1 and Grb10 both are involved in RTK signal networks. The identification, in parallel, of proteins not previously associated with Dlk1 or Grb10 suggests potential novel functions for both signalling molecules. RTKs are key developmental regulators involved in a wide range of cellular processes in mammals, and aberrant RTK signalling can result in cancer and other developmental disorders (Casaletto and McClatchey, 2012). Furthermore, Grb10 is known as a binding partner of a variety of RTKs through its multiple domains (Wang *et al*., 1999; Jahn *et al*., 2002; Vecchione *et al*., 2003; Murdaca *et al*., 2004; Holt and Siddle, 2005; Ceccarelli and Sicheri, 2009). Dlk1 is a putative ligand for which the physiological receptor is still unknown. It is possible that Dlk1 can also bind and activate some RTKs (Falix *et al*., 2012).

In chapter 5, I examined several candidate RTKs and activated these with their specific ligands in E14.5 WT, *Dlk1*$^{+/p}$, *Grb10*$^{m/+}$ and *Grb10*$^{m/+}$*/Dlk1*$^{+/p}$ pMEFs to verify the major findings of proteomics analyses. In knockout cells, changes in signalling through PDGFRa and PDGFRb were consistent with a role for these receptors as targets for Dlk1 and Grb10 action. In the case of Grb10 these RTKs could be direct targets as Grb10 has been shown to interact with PDGFR *in vitro* (Wang *et al*., 1999), while the interaction of Dlk1 might be direct or indirect as no published data has provided evidence for direct

interaction between Dlk1 and PDGFR. Firstly, total PDGFRa expression was reduced in E14.5 *Dlk1*$^{+/p}$, *Grb10*$^{m/+}$ and *Grb10*$^{m/+}$/*Dlk1*$^{+/p}$ pMEFs compared to WT by Western blotting which confirmed the proteomics data. PDGFRa displayed strong phosphorylation level in E14.5 pMEFs using mouse phospho-RTK array analysis, and PDGFRa phosphorylation level was similar among the four genotypes. Furthermore, the specific activation of PDGFRa signalling by PDGF-AA induced significantly higher PDGFRa, Grb2 and PI3K phosphorylation levels in *Grb10*$^{m/+}$ pMEFs. In parallel, simultaneous stimulation of PDGFRa and PDGFRb by PDGF-BB caused a prolonged Akt phosphorylation among all four genotypes and a stronger Erk1/2 phosphorylation in the three knockout pMEFs compared to WT. These results suggest that Grb10 inhibits PDGFRa signalling activity, while Dlk1 and Grb10 both reduce the PDGFR downstream Erk1/2 activation in pMEFs. Meanwhile, EGF stimulation caused phosphorylation of Erk1/2 to a lower level in knockout pMEFs. A previous study reported that Grb10 interacts with EGFR through its SH2 domain (Ooi *et al*., 1995). However, the role of Grb10 in EGFR signalling is not well demonstrated. FGF1 stimulated low level of Akt and similar Erk1/2 phosphorylation levels among the four genotypes, suggesting that Dlk1 and Grb10 might be independent from FGF1R signalling in E14.5 pMEFs. Additionally, there was little response to IGF through Akt or Erk1/2, consistent with growth regulation by Dlk1 and Grb10 being independent of IGF signalling on pMEFs. This is consistent with the genetic evidence that Grb10 regulates mouse fetal growth independently from IGF pathway (Charalambous *et al*., 2003). Insulin stimulated pMEFs displayed strong Akt phosphorylation level specifically in *Grb10*$^{m/+}$ and *Grb10*$^{m/+}$/*Dlk1*$^{+/p}$ cells and indistinguishable Erk1/2 activation among the four genotypes, suggesting an inhibition role of Grb10 insulin signalling through Akt-mTOR pathway, consistent with the role for Grb10 in insulin signalling widely reported in the literature (e.g. Smith *et al*., 2007; Yu *et al*., 2011).

6.2 Is PDGFR the major growth receptor in the Dlk1/Grb10 growth regulatory pathway?

Among all the RTKs investigated in this study, PDGFR signalling was identified as the best candidate pathway for *Dlk1/Grb10*-mediated growth regulation based on the proteomics, mouse phospho-RTK array and cell signalling analyses on E14.5 WT, $Dlk1^{+/p}$, $Grb10^{m/+}$ and $Grb10^{m/+}/Dlk1^{+/p}$ pMEFs. PDGFRa and PDGFRb both are essential factors in mouse embryonic development as either *PDGFRa* or *PDGFRb* null embryos usually die before birth (Soriano 1994; Soriano 1997; French *et al*., 2008). *PDGFRa* knockout embryos were slightly smaller than WT with abnormal neural crest and somite development (Soriano 1997). *PDGFRb* null embryos had similar body size as WT, but the *PDGFRb* knockout significantly affected the embryonic kidney development (Soriano 1994). The signalling studies in Chapter 5 showed that Dlk1 and Grb10 were involved in the PDGF receptor signalling in E14.5 pMEFs, and that signal transduction through PDGFRa and PDGFRb was not identical (Figure 6.1). It has been reported that E14.5 $Grb10^{m/+}$ and $Grb10^{m/+}/Dlk1^{+/p}$ pMEFs had a higher proliferation rate and $Dlk1^{+/p}$ lower than WT, and no difference was found in the cell size of E14.5 pMEFs among the four genotypes (Madon-Simon *et al*., 2014). Madon-Simon and colleagues hypothesised that a higher cell proliferation rate may lead to the enlarged embryo size of $Grb10^{m/+}$ and $Grb10^{m/+}/Dlk1^{+/p}$ at E14.5 (Madon-Simon *et al*., 2014). PI3K-Akt and MAPK-Erk1/2 are known as the PDGF receptor downstream signalling pathways which mediate cell differentiation and proliferation, respectively (reviewed in Andrae *et al*., 2008; Borkham-Kamphorst and Weiskirchen, 2016). According to the biochemical results found in this study, Dlk1 and Grb10 may regulate the differentiation and proliferation of E14.5 pMEFs via PDGF receptors through PI3K-Akt and MAPK-Erk1/2 pathways (Figure 6.1).

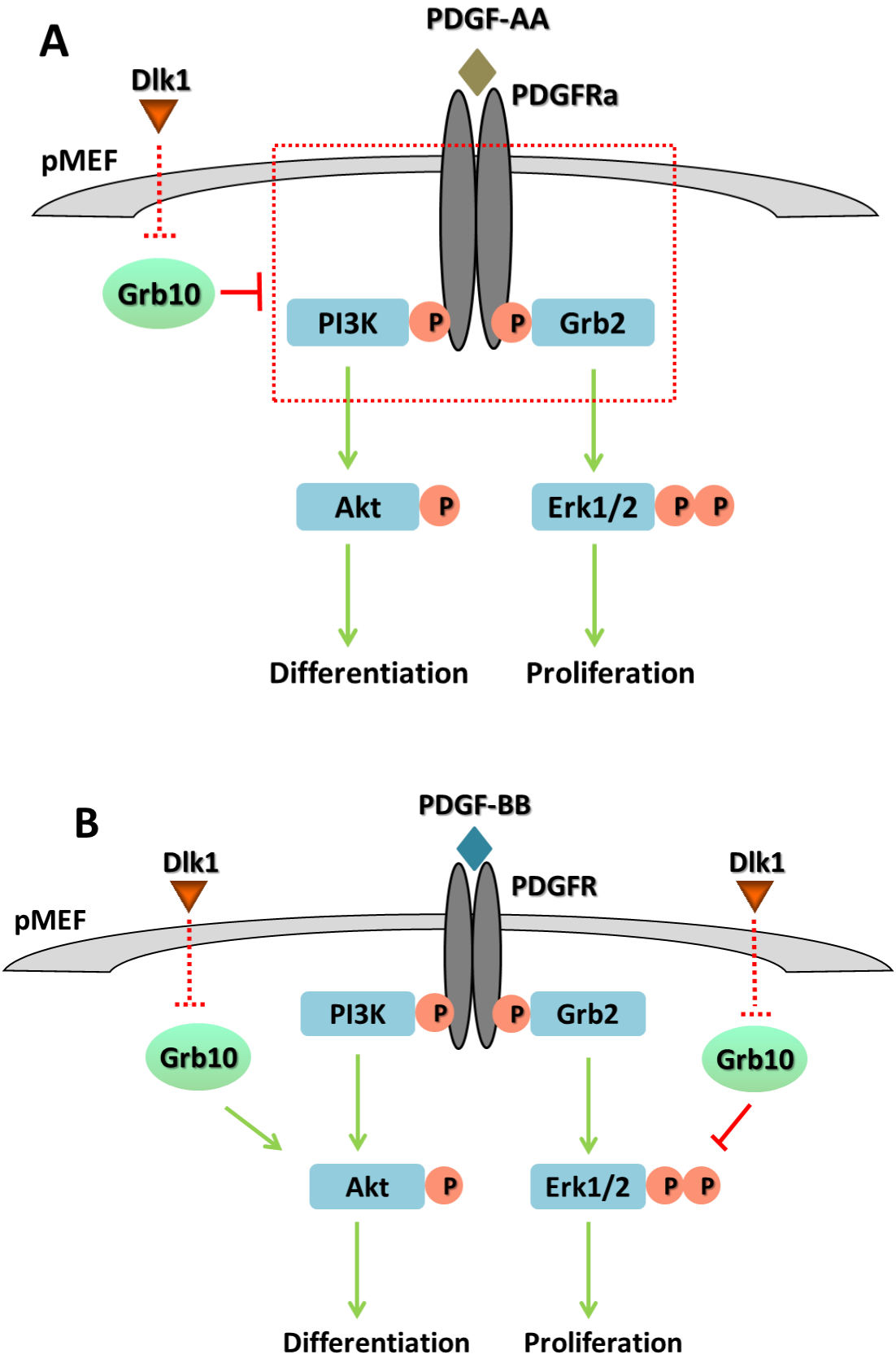
A
PDGF-AA
Dlk1
PDGFRa
pMEF
Grb10
PI3K
P
P
Grb2
Akt
P
Erk1/2
P
P
Differentiation
Proliferation
B
PDGF-BB
Dlk1
PDGFR
Dlk1
pMEF
PI3K
P
P
Grb2
Grb10
Grb10
Akt
P
Erk1/2
P
P
Differentiation
Proliferation

Figure 6.1 Proposed Dlk1 and Grb10 signal interactions through PDGFRa and PDGFRb in E14.5 pMEFs. A) PDGF-AA stimulated significantly higher PDGFRa and PI3K phosphorylation levels in *Grb10*$^{m/+}$ pMEFs. Grb10 inhibits the phosphorylation of PDGFRa and PI3K in PDGF-AA treated E14.5 pMEFs. **B)** PDGF-BB induced significantly higher Erk1/2 and slightly lower Akt phosphorylation levels in E14.5 *Dlk1*$^{+/p}$, *Grb10*$^{m/+}$ and *Grb10*$^{m/+}$/*Dlk1*$^{+/p}$ pMEFs than WT. Dlk1 inhibits Grb10 which consequently facilitates downstream Akt phosphorylation and suppresses Erk1/2 phosphorylation in PDGF-BB treated E14.5 pMEFs.

6.3 Future works

This study left the following questions: Is the stronger Erk1/2 phosphorylation induced by PDGF-BB in E14.5 *Dlk1*$^{+/p}$, *Grb10*$^{m/+}$ and *Grb10*$^{m/+}$/*Dlk1*$^{+/p}$ pMEFs related to cell proliferation rate? How do the downstream signals change the cell behaviours of knockout E14.5 pMEFs?

This can be addressed by checking the cell cycle characteristics, measurements of the expression levels of proliferation markers and correlated downstream transcription factors (*e.g. Cyclin dependent kinase 1* (*Cdk1*) and cAMP response element binding protein (CREB)) among WT, *Dlk1*$^{+/p}$, *Grb10*$^{m/+}$ and *Grb10*$^{m/+}$/*Dlk1*$^{+/p}$ pMEFs (Santamaria *et al*., 2007; Mayr and Montminy, 2001). The complete signal transduction through Dlk1, Grb10 and PDGFRs to the downstream signalling and cellular output (cell proliferation or cell cycle) will need to be fully demonstrated in the future.

Can the phenotype and PDGFR signalling alterations be mimicked by short-term deletion of *Dlk1* and *Grb10* in E14.5 pMEFs? Also, can the changes be rescued?

E14.5 *Dlk1* and *Grb10* single and double knockdown pMEF cell lines can be generated using *Dlk1* and *Grb10* siRNAs cloned into Lentivirus. Immortal pMEF (*p53*$^{-/-}$) cell lines need to be generated before introducing the *Dlk1* and *Grb10* siRNAs (Carnero *et al*., 2000). The rescue experiments can be

performed by introducing Dlk1 or Grb10 proteins to *Dlk1*$^{+/p}$, *Grb10*$^{m/+}$ and *Grb10*$^{m/+}$*/Dlk1*$^{+/p}$ pMEFs. The cellular output and signal changes from the knockdown and transgenic cell lines may be measured and compared with the knockout cells.

Which domains of Grb10 are required for its correct sub-cellular localisation, phosphorylation and activity when interacting with RTKs, mTOR or other cellular functional kinases?

This can be addressed by making GFP-fusions to both full-length and mutant Grb10 proteins, including those lacking the five recognised signalling motifs (Proline-rich domain, SH2, PH, BPS and RAS), as well as specific phosphorylation sites. These Grb10-GFP fusion proteins will be introduced into WT and *Grb10*$^{m/+}$ pMEFs in order to evaluate the effects on sub-cellular localisation, cell behaviour (cell proliferation and cell cycle characteristics) and downstream signalling events. Again immortal pMEF cell lines will be used for these experiments (Carnero *et al*., 2000).

Can the expression and phosphorylation variations of RTKs, especially PDGFRs, uncovered by quantitative proteomics be verified in E14.5 livers?

The Dlk1, Grb10 and RTK signalling studies carried out in E14.5 pMEF cultures could in principle be carried out in E14.5 hepatocytes derived from E14.5 livers (Gouon-Evans *et al*., 2006). Specific antibodies are required for the WB and immunostaining experiments for hepatocytes and embryonic liver tissue sections.

How might the expression and phosphorylation status of PDGFRs change in other embryonic tissues or cells?

The PDGFRa and PDGFRb expression and phosphorylation patterns in embryonic tissues of WT, *Dlk1*$^{+/p}$, *Grb10*$^{m/+}$ and *Grb10*$^{m/+}$/*Dlk1*$^{+/p}$ are still unknown. This can be measured by staining whole embryos or separate tissue sections from the four genotypes. These two receptors may be widely expressed in the embryo as both are important embryonic growth factors (Soriano 1994; Soriano 1997; French *et al*., 2008). PDGF receptors may have overlap expression with Dlk1 and Grb10 which are both reported to be broadly expressed in the embryo (Moon *et al*., 2002; Wang *et al*., 2006; Garfield *et al*., 2011; Charalambous *et al*., 2014). Whole E14.5 embryo sections from WT were stained with PDGFRa and Grb10 antibodies (Figure 6.2). PDGFRa and Grb10 were both widely expressed in E14.5 mouse embryos. Specifically, PDGFRa showed relatively strong expression levels in the embryonic nose, maxilla, lips, tongue, teeth, lung, stomach and limb, while Grb10 was relatively highly expressed in the embryonic liver and inner surface of stomach lumen. Additionally, PDGFRa and Grb10 were both expressed in muscle and dermis.

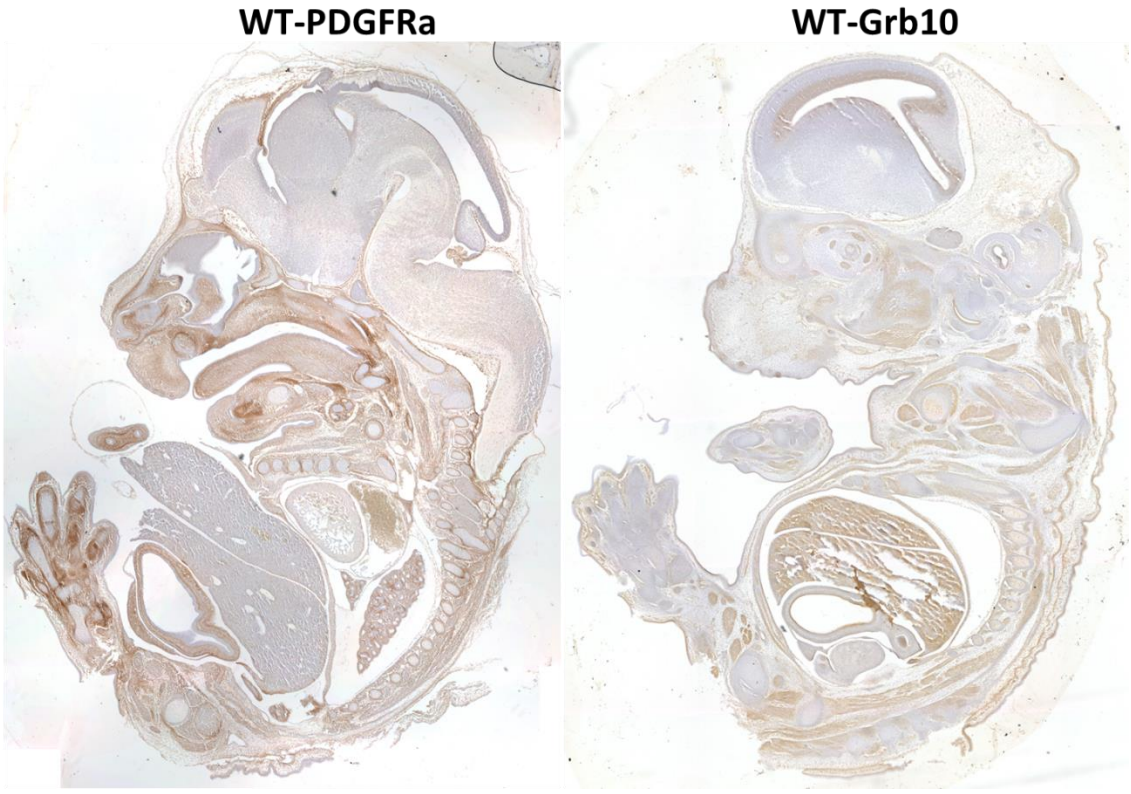

Figure 6.2 PDGFRa and Grb10 expression in WT E14.5 embryos.

Representative WT E14.5 embryo section stained with PDGFRa or Grb10 antibody.

How will the early developmental signalling affect the postnatal physiology, especially the regulation of adult body composition? Can the Dlk1, Grb10 and PDGFR signalling variations be traced from early embryonic stages to adults?

Dlk1 and Grb10 are both essential programming factors during embryogenesis (Moon *et al*., 2002; Charalambous *et al*., 2003; Charalambous *et al*., 2010; Madon-Simon *et al*., 2014). They also regulate the adult fat and muscle formation through early embryonic development (Moon *et al*., 2002; Andersen *et al*., 2009; Andersen *et al*., 2013; Charalambous *et al*., 2014; Madon-Simon *et al*., 2014). PDGFRa was expressed in adipocyte precursor cells based on the cell lineage study (Berry and Rodeheffer, 2013), and PDGFRa activation reduced the ratio of adipocyte/fibroblast in Day 1 mouse embryos (Sun *et al*., 2017). Transgenic mice with higher PDGFRa activity developed smaller WAT mass at 18 days old (Sun *et al*., 2017). PDGFRa was also a marker of adipogenic cell populations in skeletal muscle progenitors (Pannérec *et al*., 2013) and was highly activated in those cells during adult skeletal muscle regeneration (Mueller *et al*., 2016). It can be predicted that PDGFR signalling may be the key signal pathway between Dlk1 and Grb10 in regulation of adult body composition and physiology. However, this needs to be verified by checking the expression and phosphorylation levels of PDGFRs and the downstream signals in developing and adult fat and muscle tissues from the four genotypes. Also, Dlk1, Grb10 and PDGFR signals may affect the development or functions of other adult tissues such as liver, pancreas and lung as Dlk1 and Grb10 both have been shown to be involved in the development or metabolism of these tissues (Raghunandan *et al*., 2008; Zhang *et al*., 2012; Charalambous *et al*., 2014; Madon-Simon *et al*., 2014).

Appendix

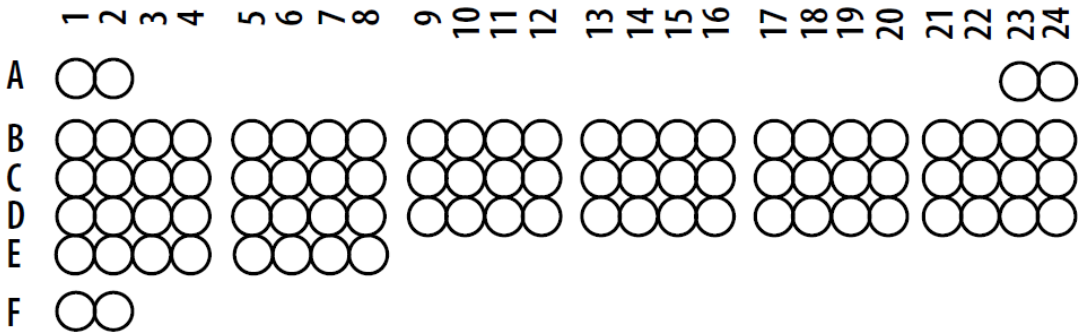

Coordinate	RTK/Control	Coordinate	RTK/Control
A1, A2	___	C17, C18	Tie-1
A23, A24	___	C19, C20	Tie-2
B1, B2	EGF R	C21, C22	TrkA
B3, B4	ErbB2	C23, C24	TrkB
B5, B6	ErbB3	D1, D2	TrkC
B7, B8	ErbB4	D3, D4	VEGF R1
B9, B10	FGF R2 (IIIc)	D5, D6	VEGF R2
B11, B12	FGF R3	D7, D8	VEGF R3
B13, B14	FGF R4	D9, D10	MuSK
B15, B16	Insulin R	D11, D12	EphA1
B17, B18	IGF-I R	D13, D14	EphA2
B19, B20	Axl	D15, D16	EphA3
B21, B22	Dtk	D17, D18	EphA6
B23, B24	Mer	D19, D20	EphA7
C1, C2	HGF R	D21, D22	EphA8
C3, C4	MSP R	D23, D24	EphB1
C5, C6	PDGF Rα	E1, E2	EphB2
C7, C8	PDGF Rβ	E3, E4	EphB4
C9, C10	SCF R	E5, E6	EphB6
C11, C12	Flt-3	E7, E8	PBS
C13, C14	M-CSF R	F1, F2	___
C15, C16	c-Ret		

Table 7.1 Full list of RTK targets on mouse phospho-RTK array. Table is modified from https://resources.rndsystems.com/pdfs/datasheets/ary014.pdf

A

GO Term	P-value	FDR q-value	Enrichment	N	B	n	b
membrane part	2.29E-08	2.87E-05	1.4	3445	881	503	180
cytoplasmic part	4.95E-08	3.10E-05	1.21	3445	1813	503	320
vesicle	2.61E-07	1.09E-04	1.34	3445	989	503	193
membrane-bounded vesicle	7.37E-07	2.31E-04	1.34	3445	926	503	181
lytic vacuole	3.05E-06	7.63E-04	2.36	3445	84	503	29
lysosome	3.05E-06	6.36E-04	2.36	3445	84	503	29
extracellular region	3.06E-06	5.48E-04	1.9	3445	173	503	48
extracellular region part	3.65E-06	5.72E-04	1.31	3445	946	503	181
integral component of membrane	7.78E-06	1.08E-03	1.44	3445	533	503	112
transmembrane receptor activity	1.10E-06	3.20E-03	2.68	3445	64	503	25
transmembrane signaling receptor activity	2.20E-06	3.20E-03	2.65	3445	62	503	24
transmembrane receptor protein kinase activity	2.34E-06	2.26E-03	4.89	3445	14	503	10
lipid metabolic process	1.52E-06	1.37E-02	1.9	3445	184	503	51

B

GO Term	P-value	FDR q-value	Enrichment	N	B	n	b
hydrolase activity	3.49E-04	3.68E-01	1.32	478	60	295	49
ATPase activity	6.24E-04	3.29E-01	1.62	478	15	295	15

C

GO Term	P-value	FDR q-value	Enrichment	N	B	n	b
integral component of membrane	6.87E-05	8.61E-02	1.54	3445	533	290	69
extracellular region	7.59E-05	4.75E-02	2.06	3445	173	290	30
intrinsic component of membrane	8.27E-05	3.45E-02	1.52	3445	546	290	70
membrane part	1.57E-04	4.92E-02	1.36	3445	881	290	101
elastic fiber	5.91E-04	1.48E-01	11.88	3445	3	290	3
integral component of plasma membrane	8.56E-04	1.79E-01	2.44	3445	73	290	15
phagocytic vesicle	8.80E-04	1.58E-01	4.75	3445	15	290	6
intrinsic component of plasma membrane	9.12E-04	1.43E-01	2.35	3445	81	290	16
transmembrane receptor activity	5.64E-07	1.64E-03	3.53	3445	64	290	19
transmembrane signaling receptor activity	1.63E-06	2.37E-03	3.45	3445	62	290	18
signaling receptor activity	5.58E-06	5.40E-03	3.19	3445	67	290	18
receptor activity	1.51E-05	1.10E-02	2.71	3445	92	290	21
molecular transducer activity	1.51E-05	8.80E-03	2.71	3445	92	290	21
signal transducer activity	1.34E-04	6.47E-02	2.17	3445	137	290	25
transmembrane receptor protein kinase activity	5.68E-04	2.36E-01	5.09	3445	14	290	6
calcium ion binding	8.46E-04	3.07E-01	2.12	3445	112	290	20
negative regulation of cell proliferation	1.50E-04	1.00E+00	2.24	3445	122	290	23

D

GO Term	P-value	FDR q-value	Enrichment	N	B	n	b
negative regulation of immune system process	6.43E-05	2.71E-01	3.65	598	12	123	9
negative regulation of myeloid cell differentiation	6.86E-05	1.45E-01	4.86	598	6	123	6
regulation of myeloid cell differentiation	3.99E-04	5.61E-01	4.17	598	7	123	6
negative regulation of hemopoiesis	3.99E-04	4.21E-01	4.17	598	7	123	6

Table 7.2 GO-term enrichment analysis results of E14.5 pMEF and liver proteomes and phosphoproteomes. A) E14.5 pMEF proteome. **B)** E14.5 pMEF phosphoproteome. **C)** E14.5 liver proteome. **D)** E14.5 liver phosphoproteome. N: total number of genes; B: total number of genes in the corresponding GO term; n: total gene numbers outside of the fold change threshold; b: obtained gene numbers outside of the fold change threshold in the corresponding GO term. Enrichment: (b/n)/(B/N).

A

GO Term	P-value	FDR q-value	Enrichment	N	B	n	b
Cluster 1							
brown fat cell differentiation	0.000158	1	98.31	3441	7	10	2
Cluster 2							
extracellular region	1.76E-10	2.36E-07	5.4	3441	177	72	20
extracellular space	4.30E-09	2.88E-06	4.29	3441	234	72	21
extracellular region part	5.27E-05	2.35E-02	1.79	3441	963	72	36
calcium ion binding	1.95E-05	4.90E-02	4.57	3441	115	72	11
biological adhesion	5.89E-05	5.66E-01	3.75	3441	153	72	12
Cluster 3							
transmembrane signaling receptor activity	3.11E-06	7.84E-03	5.45	3441	53	131	11
transmembrane receptor activity	4.58E-06	5.77E-03	5.25	3441	55	131	11
signaling receptor activity	1.11E-05	9.35E-03	4.82	3441	60	131	11
signal transducer activity	2.35E-05	1.48E-02	3.23	3441	130	131	16
Cluster 4							
mitochondrion	1.69E-11	2.26E-08	1.96	3441	577	265	87
cytoplasmic part	7.35E-11	4.91E-08	1.29	3441	2111	265	210
mitochondrial part	0.00000289	0.00129	2	3441	285	265	44
membrane part	0.00000404	0.00135	1.46	3441	905	265	102
organic acid catabolic process	2.84E-08	0.000273	4.41	3441	53	265	18
carboxylic acid catabolic process	2.84E-08	0.000137	4.41	3441	53	265	18
organic acid metabolic process	0.000000152	0.000485	2.27	3441	240	265	42
alpha-amino acid catabolic process	0.000000157	0.000376	7.21	3441	18	265	10
small molecule catabolic process	0.000000275	0.000528	3.56	3441	73	265	20

oxoacid metabolic process	0.000000385	0.000616	2.23	3441	239	265	41
cellular amino acid catabolic process	0.000000466	0.00064	5.95	3441	24	265	11
carboxylic acid metabolic process	0.000000741	0.00089	2.23	3441	227	265	39
cellular amino acid metabolic process	0.00000164	0.00175	3.01	3441	95	265	22

B

GO Term	P-value	FDR q-value	Enrichment	N	B	n	b
Cluster 1							
response to radiation	0.000911	1	2.64	344	9	116	8
Cluster 4							
regulation of secretion	0.000592	1	4.58	344	11	41	6
regulation of peptide transport	0.000648	1	3.92	344	15	41	7
regulation of secretion by cell	0.000815	0.977	5.24	344	8	41	5
regulation of sequence-specific DNA binding transcription factor activity	0.000815	0.733	5.24	344	8	41	5

C

GO Term	P-value	FDR q-value	Enrichment	N	B	n	b
Cluster 1							
regulation of B cell activation	1.55E-04	1.00E+00	14.04	3441	28	35	4
immune response-regulating signaling pathway	2.04E-04	9.79E-01	13.11	3441	30	35	4
immune effector process	3.46E-04	5.53E-01	7.93	3441	62	35	5
regulation of B cell proliferation	4.04E-04	5.54E-01	19.66	3441	15	35	3

regulation of mononuclear cell proliferation	4.67E-04	5.61E-01	10.63	3441	37	35	4
regulation of lymphocyte proliferation	4.67E-04	4.98E-01	10.63	3441	37	35	4
immune system process	5.01E-04	4.81E-01	4.12	3441	191	35	8
regulation of leukocyte proliferation	5.73E-04	5.01E-01	10.08	3441	39	35	4
immune response-regulating cell surface receptor signaling pathway	7.09E-04	5.24E-01	16.39	3441	18	35	3
positive regulation of B cell activation	7.09E-04	4.86E-01	16.39	3441	18	35	3
positive regulation of interleukin-12 production	9.86E-04	6.31E-01	39.33	3441	5	35	2
transmembrane signaling receptor activity	1.64E-04	4.12E-01	9.27	3441	53	35	5
transmembrane receptor activity	1.95E-04	2.46E-01	8.94	3441	55	35	5
receptor activity	1.98E-04	1.66E-01	6.78	3441	87	35	6
molecular transducer activity	1.98E-04	1.25E-01	6.78	3441	87	35	6
signaling receptor activity	2.96E-04	1.49E-01	8.19	3441	60	35	5
		Cluster 4					
transmembrane signaling receptor activity	5.48E-04	6.90E-01	7.21	3441	53	45	5
transmembrane receptor activity	6.52E-04	5.47E-01	6.95	3441	55	45	5
receptor activity	8.11E-04	5.10E-01	5.27	3441	87	45	6
molecular transducer activity	8.11E-04	4.08E-01	5.27	3441	87	45	6
signaling receptor activity	9.74E-04	4.09E-01	6.37	3441	60	45	5
extracellular region	1.96E-07	2.62E-04	5.62	3441	177	45	13
extracellular space	2.83E-05	1.89E-02	3.92	3441	234	45	12
G-protein coupled receptor activity	4.24E-04	1.00E+00	19.12	3441	12	45	3
secretion	2.33E-05	2.24E-01	6.44	3441	95	45	8
cell migration	5.35E-05	2.57E-01	4.99	3441	138	45	9

cell motility	9.28E-05	2.97E-01	4.65	3441	148	45	9
Cluster 5							
negative regulation of cell proliferation	2.84E-04	1.00E+00	7.91	3441	128	17	5
multicellular organismal process	2.91E-04	1.00E+00	3.52	3441	518	17	9
negative regulation of epithelial cell proliferation	3.75E-04	1.00E+00	20.24	3441	30	17	3
osteoblast differentiation	5.95E-04	1.00E+00	17.35	3441	35	17	3
Cluster 6							
cell differentiation	1.85E-04	1.00E+00	7.04	3441	349	7	5
identical protein binding	3.27E-04	8.25E-01	6.25	3441	393	7	5

D

GO Term	P-value	FDR q-value	Enrichment	N	B	n	b
Cluster 2							
positive regulation of cellular metabolic process	5.91E-04	1.00E+00	2.01	597	131	43	19
regulation of cellular metabolic process	6.16E-04	1.00E+00	1.58	597	255	43	29
positive regulation of metabolic process	7.17E-04	1.00E+00	1.93	597	144	43	20
positive regulation of nucleobase-containing compound metabolic process	9.38E-04	1.00E+00	2.24	597	93	43	15
positive regulation of macromolecule metabolic process	9.96E-04	9.03E-01	1.94	597	136	43	19
Cluster 3							
large ribosomal subunit	3.02E-04	2.04E-01	18.66	597	6	16	3

ribosomal subunit	3.02E-04	1.02E-01	18.66	597	6	16	3
ribonucleoprotein complex	6.20E-04	1.40E-01	4.08	597	64	16	7
translational elongation	6.75E-04	1.00E+00	37.31	597	2	16	2
			Cluster 5				
integral component of plasma membrane	5.53E-04	3.74E-01	9.05	597	11	24	4
intrinsic component of plasma membrane	5.53E-04	1.87E-01	9.05	597	11	24	4

Table 7.3 GO-term enrichment analysis results of protein clusters identified from E14.5 pMEF and liver proteomes and phosphoproteomes. A) E14.5 pMEF proteome. **B)** E14.5 pMEF phosphoproteome. **C)** E14.5 liver proteome. **D)** E14.5 liver phosphoproteome. N: total number of genes; B: total number of genes in the corresponding GO term; n: total gene numbers outside of the fold change threshold; b: obtained gene numbers outside of the fold change threshold in the corresponding GO term. Enrichment: (b/n)/(B/N).

Reference

Abdallah, B. M., Jensen, C. H., Gutierrez, G., Leslie, R. G., Jensen, T. G. and Moustapha, K. (2004) 'Regulation of human skeletal stem cells differentiation by dlk1/pref-1', *Journal of Bone & Mineral Research the Official Journal of the American Society for Bone & Mineral Research, 19*(5), pp. 841-852.

Accili, D., Drago, Lee, J., E. J., Johnson, M. D., Cool, M. H., Salvatore, P., Asico, L. D., José, P. A., Taylor, S. I. and Westphal, H. (1996) 'Early neonatal death in mice homozygous for a null allele of the insulin receptor gene', *Nature genetics*, 12(1), pp.106-109.

Akundi, R. S., Zhi, L. and Büeler, H. (2012) 'PINK1 enhances insulin-like growth factor-1-dependent Akt signaling and protection against apoptosis', *Neurobiology of disease*, *45*(1), pp. 469-478.

Andersen, D. C., Jensen, L., Schrøder, H. D. and Jensen, C. H. (2009) '"The preadipocyte factor" DLK1 marks adult mouse adipose tissue residing vascular cells that lack in vitro adipogenic differentiation potential', *FEBS Letters*, 583(17), pp. 2947–2953.

Andersen, D. C., Laborda, J., Baladron, V., Kassem, M., Sheikh, S. P. and Jensen, C. H. (2013) 'Dual role of delta-like 1 homolog (DLK1) in skeletal muscle development and adult muscle regeneration', *Development*, 140(18), pp. 3743–3753.

Andrae, J., Gallini, R. and Betsholtz, C. (2008) 'Role of platelet-derived growth factors in physiology and medicine', *Genes & development,* 22(10), pp. 1276–1312.

Appelbe, O. K., Yevtodiyenko, A., Muniz-Talavera, H. and Schmidt, J. V. (2013) 'Conditional deletions refine the embryonic requirement for Dlk1', *Mechanisms of Development*, 130(2–3), pp. 143–159.

Ásta, G., Jensen, C. H., Thomassen, M., Christian, H., Mortensen, S. B., Laborda, J., Baladrón, V., Sheikh, S. P. and Andersen, D. C. (2016)

‘Evidence of non-canonical NOTCH signaling : Delta-like 1 homolog (DLK1) directly interacts with the NOTCH1 receptor in mammals’, *Cellular Signalling*. Elsevier Inc., 28(4), pp. 246–254.

Baker, J., Liu, J. P., Robertson, E. J. and Efstratiadis, A. (1993) 'Role of insulin-like growth factors in embryonic and postnatal growth', *Cell*. *75*(1), pp.73-82.

Baladrón, V., Ruiz-Hidalgo, M. J., Nueda, M. L., Díaz-Guerra, M. J. M., García-Ramírez, J. J., Bonvini, E., Gubina, E. and Laborda, J. (2005). 'dlk acts as a negative regulator of Notch1 activation through interactions with specific EGF-like repeats', *Experimental cell research*, *303*(2), pp.343-359.

Barlow, D. P. and Bartolomei, M. S. (2014). 'Genomic imprinting in mammals', *Cold Spring Harbor perspectives in biology*, *6*(2), p.a018382.

Barlow, D. P., Stoger, R, Herrmann, B. G., Saito, K. and Schweifer, N. (1991) 'The mouse insulin-like growth factor type-2 receptor is imprinted and closely linked to the Tme locus', *Nature,* 349 (6304), pp. 84–87.

Bartolomei, M. S. and Ferguson-Smith, A. C. (2011). 'Mammalian genomic imprinting', *Cold Spring Harbor perspectives in biology*, *3*(7), p.a002592.

Belletti, B., Drakas, R., Morrione, A., Tu, X., Prisco, M., Yuan, T., Casaburi, I. and Baserga, R. (2002). 'Regulation of Id1 protein expression in mouse embryo fibroblasts by the type 1 insulin-like growth factor receptor', *Experimental cell research*, *277*(1), pp.107-118.

Berry, R. and Rodeheffer, M. S. (2013). 'Characterization of the adipocyte cellular lineage in vivo', *Nature cell biology*, *15*(3), pp. 302-308.

Borkham-Kamphorst, E. and Weiskirchen, R. (2016) 'The PDGF system and its antagonists in liver fibrosis', *Cytokine & growth factor reviews*, 28, pp. 53-61.

Carnero, A., Hudson, J. D., Hannon, G. J. and Beach, D. H. (2000) 'Loss-of-function genetics in mammalian cells: the p53 tumor suppressor model', *Nucleic acids research*, 28(11), p. 2234-2241

Casaletto, J. B. and McClatchey, A. I. (2012). 'Spatial regulation of receptor tyrosine kinases in development and cancer', *Nature reviews. Cancer*, 12(6), p. 387.

Ceccarelli, D. F. and Sicheri, F. (2009) 'Grb-ing hold of insulin signaling', *Nature Structural & Molecular Biology,* 16(8), pp. 803-804.

Chacón, M. R., Miranda, M., Jensen, C. H., Fernández-Real, J. M., Vilarrasa, N., Gutiérrez, C., Näf, S., Gomez, J. M. and Vendrell, J. (2008) 'Human serum levels of fetal antigen 1 (FA1/Dlk1) increase with obesity, are negatively associated with insulin sensitivity and modulate inflammation in vitro', *International Journal of Obesity*, 32(7), pp. 1122–1129.

Charalambous, M., Cowley, M., Geoghegan, F., Smith, F. M., Radford, E. J., Marlow, B. P., Graham, C. F., Hurst, L. D. and Ward, A. (2010) 'Maternally-inherited Grb10 reduces placental size and efficiency', *Developmental Biology*. Elsevier Inc., 337(1), pp. 1–8.

Charalambous, M., Ferron, S. R., Da Rocha, S. T., Murray, A. J., Rowland, T., Ito, M., Schuster-Gossler, K., Hernandez, A. and Ferguson-Smith, A. C. (2012) 'Imprinted gene dosage is critical for the transition to independent life', *Cell Metabolism*. Elsevier Inc., 15(2), pp. 209–221.

Charalambous, M., Smith, F. M., Bennett, W. R., Crew, T. E., Mackenzie, F., Ward, A. and Mackenziet, F. (2003) 'Disruption of the Imprinted Grb10 Gene Leads to Disproportionate Overgrowth by an Igf2-Independent Mechanism Disruption of the imprinted Grb10 gene leads to disproportionate overgrowth by an Igf2-independent mechanism', *Proceedings of the National Academy of Sciences of the United States of America*, 100(14), pp. 8292–8297.

Charalambous, M., Da Rocha, S.T., Radford, E.J., Medina-Gomez, G., Curran, S., Pinnock, S.B., Ferrón, S.R., Vidal-Puig, A. and Ferguson-Smith, A.C.,

(2014). 'DLK1/PREF1 regulates nutrient metabolism and protects from steatosis', *Proceedings of the National Academy of Sciences*, *111*(45), pp.16088-16093.

Chen, L., Qanie, D., Jafari, A., Taipaleenmaki, H., Jensen, C. H., Saamanen, A. M., Sanz, M. L. N., Laborda, J., Abdallah, B. M. and Kassem, M. (2011) 'Delta-like 1/fetal antigen-1 (Dlk1/FA1) is a novel regulator of chondrogenic cell differentiation via inhibition of the Akt kinase-dependent pathway', *Journal of Biological Chemistry*, 286(37), pp. 32140–32149.

Cleaton, M. A. M., Dent, C. L., Howard, M., Corish, J. A., Gutteridge, I., Sovio, U., Gaccioli, F., Takahashi, N., Bauer, S. R., Charnock-Jones, D. S., Powell, T. L., Smith, G. C. S., Ferguson-Smith, A. C. and Charalambous, M. (2016) 'Fetus-derived DLK1 is required for maternal metabolic adaptations to pregnancy and is associated with fetal growth restriction', *Nature Genetics*, 48(12), pp. 1473–1480.

Cowley, M., Garfield, A. S., Madon-Simon, M., Charalambous, M., Clarkson, R. W., Smalley, M. J., Kendrick, H., Isles, A. R., Parry, A. J., Carney, S., Oakey, R. J., Heisler, L. K., Moorwood, K., Wolf, J. B. and Ward, A. (2014) 'Developmental Programming Mediated by Complementary Roles of Imprinted Grb10 in Mother and Pup', *PLoS Biology*, 12(2), p.e1001799.

DeChiara, T. M., Robertson, E. J. and Efstratiadis, A. (1991) 'Parental imprinting of the mouse insulin-like growth factor II gene', *Cell* 64 (4), pp. 849–859.

Deng, Y., Zhang, M. and Riedel, H. (2008) 'Mitogenic roles of Gab1 and Grb10 as direct cellular partners in the regulation of MAP kinase signaling', *Journal of Cellular Biochemistry*, 105(5), pp. 1172–1182..

Dent, C. L. and Isles, A. R. (2014) 'Brain-expressed imprinted genes and adult behaviour: The example of Nesp and Grb10', *Mammalian Genome*, 25(1–2), pp. 87–93.

Depetris, R. S., Wu, J. and Hubbard, S. R. (2009) 'Structural and functional studies of the Ras-associating and pleckstrin-homology domains of Grb10

and Grb14.', *Nature structural & molecular biology*, 16(8), pp. 833–9.

Desbuquois, B., Carré, N. and Burnol, A. F. (2013) 'Regulation of insulin and type 1 insulin-like growth factor signaling and action by the Grb10/14 and SH2B1/B2 adaptor proteins', *FEBS Journal*, 280(3), pp. 794–816.

Doiron, B., Hu, W., Norton, L. and Defronzo, R. A. (2012) 'Lentivirus shRNA Grb10 targeting the pancreas induces apoptosis and improved glucose tolerance due to decreased plasma glucagon levels', *Diabetologia*, 55(3), pp. 719–728.

Driskell, R. R., Lichtenberger, B. M., Hoste, E., Kretzschmar, K., Simons, B. D., Charalambous, M., Ferron, S. R., Herault, Y., Pavlovic, G., Ferguson-Smith, A. C. and Watt, F. M. (2013) 'Distinct fibroblast lineages determine dermal architecture in skin development and repair', *Nature*. Nature Publishing Group, 504(7479), pp. 277–281.

Dufresne, A. M. and Smith, R. J. (2005) 'The adapter protein Grb10 is an endogenous negative regulator of insulin-like growth factor signaling', *Endocrinology*, 146(10), pp. 4399–4409.

Eden, E., Navon, R., Steinfeld, I., Lipson, D. and Yakhini, Z. (2009) 'GOrilla: A Tool For Discovery And Visualization of Enriched GO Terms in Ranked Gene Lists', *BMC Bioinformatics*, 10:48.

Eden, E., Lipson, D., Yogev, S. and Yakhini, Z. (2007) 'Discovering Motifs in Ranked Lists of DNA sequences', *PLoS Computational Biology*, 3(3):e39.

Falix, F. A., Aronson, D. C., Lamers, W. H. and Gaemers, I. C. (2012) 'Possible roles of DLK1 in the Notch pathway during development and disease', *Biochimica et Biophysica Acta - Molecular Basis of Disease*. Elsevier B.V., 1822(6), pp. 988–995.

Fowden, A. L., Coan, P. M., Angiolini, E., Burton, G. J. and Constancia, M. (2011) 'Imprinted genes and the epigenetic regulation of placental phenotype', *Progress in Biophysics and Molecular Biology*. Elsevier Ltd,

106(1), pp. 281–288.

French, W. J., Creemers, E. E. and Tallquist, M. D. (2008) ‘Platelet-Derived Growth Factor Receptors Direct Vascular Development Independent of Vascular Smooth Muscle Cell Function’, *Molecular and Cellular Biology*, 28(18), pp. 5646–5657.

Garfield, A. S., Cowley, M., Smith, F. M., Moorwood, K., Stewart-Cox, J. E., Gilroy, K., Baker, S., Xia, J., Dalley, J. W., Hurst, L. D., Wilkinson, L. S., Isles, A. R. and Ward, A. (2011) ‘Distinct physiological and behavioural functions for parental alleles of imprinted Grb10’, *Nature*. Nature Publishing Group, 469(7331), pp. 534–538.

Gouon-Evans, V., Boussemart, L., Gadue, P., Nierhoff, D., Koehler, C. I., Kubo, A., Shafritz, D. A. and Keller, G. (2006) ' BMP-4 is required for hepatic specification of mouse embryonic stem cell-derived definitive endoderm', *Nature biotechnology*, 24(11), pp. 1402-1411.

Grandjean, V., Smith, J., Schofield, P. N. and Ferguson-Smith, A. C. (2000) 'Increased igf-ii protein affects p57kip2expression in vivo and in vitro: implications for beckwith-wiedemann syndrome', *Proceedings of the National Academy of Sciences of the United States of America, 97*(10), pp. 5279-5284.

Guo, S. (2014) 'Insulin Signaling, Resistance, and the Metabolic Syndrome: Insights from Mouse Models to Disease Mechanisms', *J Endocrinol*, 220(2), T1–T23.

Haig, D. (2014) ‘Coadaptation and conflict, misconception and muddle, in the evolution of genomic imprinting’, *Heredity*. Nature Publishing Group, 113(2), pp. 96–103.

Haig, D. (2014) 'Frugal fat or munificent muscle: genomic imprinting and metabolism', *BMC biology*, 12(1), p. 104.

Holman, L. and Kokko, H. (2014) ‘The evolution of genomic imprinting: Costs,

benefits and long-term consequences', *Biological Reviews*, 89(3), pp. 568–587.

Holt, L. J. and Siddle, K. (2005) 'Grb10 and Grb14: enigmatic regulators of insulin action – and more?', *Biochemical Journal*, 388(2), p. 393.

Holt, L. J., Turner, N., Mokbel, N., Trefely, S., Kanzleiter, T., Kaplan, W., Ormandy, C. J., Daly, R. J. and Cooney, G. J. (2012) 'Grb10 regulates the development of fiber number in skeletal muscle', *The FASEB Journal*, *26*(9), pp. 3658-3669.

Hsu, P. P., Kang, S. A., Rameseder, J., Zhang, Y., Ottina, K. A., Lim, D., Peterson, T. R., Choi, Y., Gray, N. S., Yaffe, M. B. and Marto, J. A. (2011) 'The mTOR-regulated phosphoproteome reveals a mechanism of mTORC1-mediated inhibition of growth factor signaling', *Science*, 332(6035), pp. 1317-1322.

Huang, Q. and Szebenyi, D. M. E. (2010) 'Structural basis for the interaction between the growth factor-binding protein GRB10 and the E3 ubiquitin ligase NEDD4', *Journal of Biological Chemistry*, 285(53), pp. 42130–42139.

Hudak, C. S. and Sul, H. S. (2013) 'Pref-1, a gatekeeper of adipogenesis', *Frontiers in Endocrinology*, 4(JUL), pp. 1–6.

Inbar-Feigenberg, M., Choufani, S., Butcher, D. T., Roifman, M. and Weksberg, R. (2013) 'Basic concepts of epigenetics', *Fertility and Sterility*. Elsevier Inc., 99(3), pp. 607–615.

Jahn, T., Seipel, P., Urschel, S., Peschel, C. and Duyster, J. (2002) 'Role for the adaptor protein Grb10 in the activation of Akt.', *Molecular and cellular biology*, 22(4), pp. 979–91.

Joshi, R. L., Lamothe, B., Cordonnier, N., Mesbah, K., Monthioux, E., Jami, J., Bucchini, D. (1996) 'Targeted disruption of the insulin receptor gene in the mouse results in neonatal lethality', *EMBO J*, 15, pp. 1542–1547.

Kabir, N. N. and Kazi, J. U. (2014) ‘Grb10 is a dual regulator of receptor tyrosine kinase signaling’, *Molecular Biology Reports*, 41(4), pp. 1985–1992.

Kelsey, G. and Bartolomei, M.S. (2012) 'Imprinted genes… and the number is?', *PLoS genetics*, *8*(3), p.e1002601.

Kitamura, T., Kahn C. R. and Accili, E. (2003) 'Insulin receptor knockout mice', *Annual review of physiology*, 65, pp.313-332.

Lee, K., Villena, J. A., Moon, Y. S., Kim, K. H., Lee, S., Kang, C. and Sul, H. S. (2003) ‘Inhibition of adipogenesis and development of glucose intolerance by soluble preadipocyte factor-1 (Pref-1)’, *Journal of Clinical Investigation*, 111(4), pp. 453–461.

Lau, M. M., Stewart, C. E., Liu, Z., Bhatt, H., Rotwein, P. and Stewart, C. L. (1994) 'Loss of the imprinted IGF2/cation-independent mannose 6-phosphate receptor results in fetal overgrowth and perinatal lethality', *Genes & Development*, 8(24), pp. 2953-2963.

Liu, B. and Liu, F. (2014) ‘Feedback regulation of mTORC1 by Grb10 in metabolism and beyond’, *Cell Cycle*, 13(17), pp. 2643–2644.

Liu, M., Bai, J., He, S., Villarreal, R., Hu, D., Zhang, C., Yang, X., Liang, H., Slaga, T. J., Yu, Y., Zhou, Z., Blenis, J., Scherer, P. E., Dong, L. Q. and Liu, F. (2014) ‘Grb10 promotes lipolysis and thermogenesis by phosphorylation-dependent feedback inhibition of mTORC1’, *Cell Metabolism*, 19(6), pp. 967–980.

McAlister, G. C., Huttlin, E. L., Haas, W., Ting, L., Jedrychowski, M. P., Rogers, J. C., Kuhn, K., Pike, I., Grothe, R. A., Blethrow, J. D. and Gygi, S. P. (2012) 'Increasing the multiplexing capacity of tmt using reporter ion isotopologues with isobaric masses', *Analytical Chemistry,* 84(17), pp. 7469-7478.

Madon-Simon, M., Cowley, M., Garfield, A. S., Moorwood, K., Bauer, S. R. and Ward, A. (2014) ‘Antagonistic roles in fetal development and adult physiology for the oppositely imprinted Grb10 and Dlk1 genes’, *BMC Biology*, 12(1), pp. 771.

Mayr, B. and Montminy, M. (2001) 'Transcriptional regulation by the phosphorylation-dependent factor CREB', *Nature Review Molecular Cell Biology*, 2(8), pp. 559-609.

Mokbel, N., Hoffman, N. J., Girgis, C. M., Small, L., Turner, N., Daly, R. J., Cooney, G. J. and Holt, L. J. (2014) ‘Grb10 Deletion Enhances Muscle Cell Proliferation, Differentiation and GLUT4 Plasma Membrane Translocation’, *Journal of Cellular Physiology*, 229(11), pp. 1753–1764.

Monami, G., Emiliozzi, V. and Morrione, A. (2008) ‘Grb10/Nedd4-mediated multiubiquitination of the insulin-like growth factor receptor regulates receptor internalization’, *Journal of Cellular Physiology*, 216(2), pp. 426–437.

Moon, Y. S., Smas, C. M., Lee, K., Villena, J. A., Kim, K., Yun, E. J. and Sul, H. S. (2002) ‘Mice Lacking Paternally Expressed Pref-1/Dlk1 Display Growth Retardation and Accelerated Adiposity’, *Molecular and cellular biology*, *22*(15), pp. 5585-5592.

Mortensen, S. B., Jensen, C. H., Schneider, M., Thomassen, M., Kruse, T. A., Laborda, J., Sheikh, S. P. and Anderson, D. C. (2012). 'Membrane-tethered delta-like 1 homolog (dlk1) restricts adipose tissue size by inhibiting preadipocyte proliferation', *Diabetes, 61*(11), pp. 2814-2822.

Mueller, A. A., Van Velthoven, C. T., Fukumoto, K. D., Cheung, T. H., & Rando, T. A. (2016) 'Intronic polyadenylation of PDGFRα in resident stem cells attenuates muscle fibrosis', *Nature*, *540*(7632), pp. 276-279.

Murdaca, J., Treins, C., Monthouël-Kartmann, M. N., Pontier-Bres, R., Kumar, S., Van Obberghen, E. and Giorgetti-Peraldi, S. (2004) ‘Grb10 prevents Nedd4-mediated vascular endothelial growth factor receptor-2

degradation', *Journal of Biological Chemistry*, 279(25), pp. 26754–26761.

Nordin, M., Bergman, D., Halje, M., Engström, W., and Ward, A. (2014) 'Epigenetic regulation of the igf2/h19 gene cluster', *Cell Proliferation, 47*(3), pp. 189-199.

Nueda, M. L., Baladrón, V., Sánchez-Solana, B., Ballesteros, M. Á. and Laborda, J. (2007) 'The EGF-like Protein dlk1 Inhibits Notch Signaling and Potentiates Adipogenesis of Mesenchymal Cells', *Journal of Molecular Biology*, 367(5), pp. 1281–1293.

Ooi, J., Yajnik, V., Immanuel, D., Gordon, M., Moskow, J. J., Buchberg, A. M. and Margolis, B. (1995) 'The cloning of Grb10 reveals a new family of SH2 domain proteins', *Oncogene*, 10(8), pp. 1621–1630.

Ostman, A. and Heldin, C. H. (2001) 'Involvement of platelet-derived growth factor in disease: development of specific antagonists', *Adv Cancer Res*, 80, pp. 1-38.

Pannérec, A., Formicola, L., Besson, V., Marazzi, G. and Sassoon, D. A. (2013) 'Defining skeletal muscle resident progenitors and their cell fate potentials', *Development,* 140(14), pp. 2879-2891.

Patten, M. M., Ross, L., Curley, J. P., Queller, D. C., Bonduriansky, R. and Wolf, J. B. (2014) 'The evolution of genomic imprinting: theories, predictions and empirical tests', *Heredity,* 113(2), pp. 119-128.

Peters, J. (2014) 'The role of genomic imprinting in biology and disease: an expanding view', *Nature Reviews Genetics*. Nature Publishing Group, 15(8), pp. 517–530.

Plasschaert, R. N. and Bartolomei, M. S. (2015) 'Tissue-specific regulation and function of Grb10 during growth and neuronal commitment', *Proceedings of the National Academy of Sciences of the United States of America*, 112(22), pp. 6841–6847.

Qian, P., He, X. C., Paulson, A., Li, Z., Tao, F., Perry, J. M., Guo, F., Zhao, M., Zhi, L., Venkatraman, A., Haug, J. S., Parmely, T., Li, H., Dobrowsky, R. T., Ding, W. X., Kono, T., Ferguson-Smith, A. C. and Li, L. (2016) 'The Dlk1-Gtl2 Locus Preserves LT-HSC Function by Inhibiting the PI3K-mTOR Pathway to Restrict Mitochondrial Metabolism', *Cell Stem Cell*, 18(2), pp. 214–228.

Raghunandan, R., Ruiz-Hidalgo, M., Jia, Y., Ettinger, R., Rudikoff, E., Riggins, P., Farnsworth, R., Tesfaye, A., Laborda, J. and Bauer, S. R. (2008) 'Dlk1 Influences Differentiation and Function of B Lymphocytes', *Stem Cells and Development*, 17, pp. 495–507.

Ramos, F. J., Langlais, P. R., Hu, D., Dong, L. Q. and Liu, F. (2006) 'Grb10 mediates insulin-stimulated degradation of the insulin receptor: a mechanism of negative regulation', *American journal of physiology. Endocrinology and metabolism*, 290(6), pp. E1262-6.

Ringnér, M. and Ringner, M. (2008) 'What is principal component analysis?', *Nat Biotech*, 26(3), pp. 303–304.

Rigbolt, K. T. G., Vanselow, J. T. & Blagoev, B. (2011) 'GProX, a user-friendly platform for bioinformatics analysis and visualization of quantitative proteomics data', *Mol. Cell. Proteomics*, 10, O110.007450.

Rui, L., Fisher, T. L., Thomas, J. and White, M. F. (2001) 'Regulation of insulin/insulin-like growth factor-1 signaling by proteasome-mediated degradation of insulin receptor substrate-2', *Journal of Biological Chemistry*, *276*(43), pp. 40362-40367.

Ruiz-Hidalgo, M. J., Gubina, E., Tull, L., Baladrón, V. and Laborda, J., (2002) 'Dlk modulates mitogen-activated protein kinase signaling to allow or prevent differentiation', *Experimental cell research*, *274*(2), pp.178-188.

Saeed, A. I., Bhagabati, N. K., Braisted, J. C., Liang, W., Sharov, V., Howe, E. A., Li, J., Thiagarajan, M., White, J. A. and Quackenbush, J. (2006) 'TM4 microarray software suite', *Methods in Enzymology*, 411, pp. 134-193.

Sánchez-Solana, B., Nueda, M.L., Ruvira, M.D., Ruiz-Hidalgo, M.J., Monsalve, E.M., Rivero, S., García-Ramírez, J.J., Díaz-Guerra, M.J.M., Baladrón, V. and Laborda, J. (2011). 'The EGF-like proteins DLK1 and DLK2 function as inhibitory non-canonical ligands of NOTCH1 receptor that modulate each other's activities', *Biochimica et Biophysica Acta (BBA)-Molecular Cell Research*, *1813*(6), pp.1153-1164.

Santamaria, D., Barrière, C., Cerqueira, A., Hunt, S., Tardy, T., Newton, K., Cáceres, J. f., Dubus, P. and Barbacid, M. (2007) ' Cdk1 is sufficient to drive the mammalian cell cycle', *Nature*, 448(7155), p. 811-815.

Schneider, G., Sellers, Z. P. and Ratajczak, M. Z. (2016) 'Parentally imprinted genes regulate hematopoiesis—new evidence from the Dlk1–Gtl2 locus', *Stem Cell Investigation*, 3, pp. 29–29.

Serrano-Lopez, J. and Cancelas, J. A. (2016) 'Mom Knows Best: Imprinted Control of Hematopoietic Stem Cell Quiescence', *Cell Stem Cell*. Elsevier Inc., 18(2), pp. 158–160.

Sharma, K., C J D'Souza, R., Tyanova, S., Schaab, C., Wiśniewski, J. R., Cox, J. and Mann, M. (2014) ' Ultradeep human phosphoproteome reveals a distinct regulatory nature of Tyr and Ser/Thr-based signaling', *Cell reports*, 8(5), pp. 1583-1594.

Shin, S., Suh, Y., Zerby, H. N. and Lee, K. (2014) 'Membrane-bound delta-like 1 homolog (Dlk1) promotes while soluble Dlk1 inhibits myogenesis in C2C12 cells', *FEBS Letters*. Federation of European Biochemical Societies, 588(7), pp. 1100–1108.

Shiura, H., Miyoshi, N., Konishi, A., Wakisaka-Saito, N., Suzuki, R., Muguruma, K., Kohda, T., Wakana, S., Yokoyama, M., Ishino, F. and Kaneko-Ishino, T. (2005) 'Meg1/Grb10 overexpression causes postnatal growth retardation and insulin resistance via negative modulation of the IGF1R and IR cascades', *Biochemical and Biophysical Research Communications*, 329(3), pp. 909–916.

Smas, C.M., Chen, L. and Sul, H.S. (1997) 'Cleavage of

Membrane-Associated pref-1 Generates a Soluble Inhibitor of Adipocyte Differentiation', *Molecular and Cellular Biology*, 17(2), pp. 977–988.

Smas, C. M. and Sul, H. S. (1993) 'Pref-1, a protein containing EGF-like repeats, inhibits adipocyte differentiation', *Cell*, 73(4), pp. 725–734.

Smith, F. M., Holt, L. J., Garfield, A. S., Charalambous, M., Koumanov, F., Perry, M., Bazzani, R., Sheardown, S. A., Hegarty, B. D., Lyons, R. J., Cooney, G. J., Daly, R. J. and Ward, A. (2007) 'Mice with a Disruption of the Imprinted Grb10 Gene Exhibit Altered Body Composition, Glucose Homeostasis, and Insulin Signaling during Postnatal Life', *Molecular and Cellular Biology*, 27(16), pp. 5871–5886.

Soriano, P. (1994) 'Abnormal kidney development and hematological disorders in PDGF beta-receptor mutant mice.', *Genes & Development*, 8(16), pp. 1888–1896.

Soriano, P. (1997) 'The PDGFα receptor is required for neural crest cell development and for normal patterning of the somites', *Development*, 124(14), pp. 2691–2700.

Spencer, H. G. and Clark, A. G. (2014) 'Non-conflict theories for the evolution of genomic imprinting', *Heredity*. Nature Publishing Group, 113(2), pp. 112–118.

Sun, C., Berry, W. L. and Olson, L. E. (2017) 'PDGFRα controls the balance of stromal and adipogenic cells during adipose tissue organogenesis', *Development*, 144(1), pp. 83–94.

Takahashi, K. and Yamanaka, S. (2006) 'Induction of Pluripotent Stem Cells from Mouse Embryonic and Adult Fibroblast Cultures by Defined Factors', *Cell*, 126(4), pp. 663–676.

Thompson, A., Schäfer, J. J., Kuhn, K., Kienle, S., Schwarz, J., Schmidt, G. G., Neumann, T. and Hamon, C. (2003) 'Tandem mass tags: a novel quantificaiton strategy for comparative analysis of complex protein

mixtures by MS/MS', *Analytical chemistry*, 75(8), pp. 1895–1904.

Thoreen, C. C., Kang, S. A., Chang, J. W., Liu, Q., Zhang, J., Gao, Y., Reichling, L. J., Sim, T., Sabatini, D. M. and Grey, N. S. (2009) 'An atp-competitive mammalian target of rapamycin inhibitor reveals rapamycin-resistant functions of mtorc1', *Journal of Biological Chemistry,* 284(12), pp. 8023-8032.

Traustadóttir, G. A., Jensen, C. H., Garcia Ramirez, J. J., Beck, H. C., Sheikh, S. P. and Andersen, D. C. (2017) 'The non-canonical NOTCH1 ligand Delta-like 1 homolog (DLK1) self interacts in mammals', *International Journal of Biological Macromolecules*, 97, pp. 460–467.

Traustadóttir, G. A., Kosmina, R., Sheikh, S. P., Charlotte, H. and Andersen, D. C. (2013) 'Preadipocytes proliferate and differentiate under the guidance of Delta-like 1 homolog (DLK1)', *Adipocyte*, *2*(4), pp. 272-275.

Traustadóttir, G.Á., Jensen, C.H., Thomassen, M., Beck, H.C., Mortensen, S.B., Laborda, J., Baladrón, V., Sheikh, S.P. and Andersen, D.C. (2016) 'Evidence of non-canonical NOTCH signaling: Delta-like 1 homolog (DLK1) directly interacts with the NOTCH1 receptor in mammals', *Cellular signalling*,*28*(4), pp. 246-254.

Tseng Y.H., Butte, A.J., Kokkotou, E., Yechoor, V.K., Taniguchi, C.M., Kriauciunas, K.M., Cypess, A.M., Niinobe, M., Yoshikawa, K., Patti, M.E. and Kahn, C.R. (2005) 'Prediction of preadipocyte differentiation by gene expression reveals role of insulin receptor substrates and necdin'. *Nature cell biology*, *7*(6), p. 601.

Vecchione, A., Marchese, A., Henry, P., Rotin, D. and Morrione, A. (2003) 'The Grb10/Nedd4 complex regulates ligand-induced ubiquitination and stability of the insulin-like growth factor I receptor.', *Molecular and cellular biology*, 23(9), pp. 3363–72.

Wang, J., Dai, H., Yousaf, N., Moussaif, M., Deng, Y., Boufelliga, A., Swamy, O. R., Leone, M. E. and Riedel, H. (1999) 'Grb10, a Positive, Stimulatory Signaling Adapter in Platelet-Derived Growth Factor BB-, Insulin-Like

Growth Factor I-, and Insulin-Mediated Mitogenesis', *Molecular and Cellular Biology*, 19(9), pp. 6217–6228.

Wang, L., Balas, B., Christ-roberts, C. Y., Kim, R. Y., Ramos, F. J., Kikani, C. K., Li, C., Deng, C., Reyna, S., Musi, N., Lily, Q., Defronzo, R. A., Liu, F., Wang, L., Balas, B., Christ-roberts, C. Y., Kim, R. Y., Ramos, F. J., Kikani, C. K., Li, C., Deng, C., Reyna, S., Musi, N., Dong, L. Q., Defronzo, R. A. and Liu, F. (2007) 'Peripheral Disruption of the Grb10 Gene Enhances Insulin Signaling and Sensitivity In Vivo Peripheral Disruption of the Grb10 Gene Enhances Insulin Signaling and Sensitivity In Vivo', *Molecular and cellular biology*, *27*(18), pp. 6497-6505.

Wang, Y. and Sul, H. S. (2006) 'Ectodomain Shedding of Preadipocyte Factor 1 (Pref-1) by Tumor Necrosis Factor Alpha Converting Enzyme (TACE) and Inhibition of Adipocyte Differentiation', *Molecular and cellular biology*, 26(14), pp. 5421–5435.

Wang, Y., Zhao, L., Smas, C. and Sul, H. S. (2010) 'Pref-1 Interacts with Fibronectin To Inhibit Adipocyte Differentiation', *Molecular and cellular biology*, 30(14), pp. 3480–3492.

Wang, Z. Q., Fung, M. R., Barlow, D. P. and Wagner, E. F. (1994) 'Regulation of embryonic growth and lysosomal targeting by the imprinted Igf2/Mpr gene', *Nature*, 372(6505), pp. 464-467.

Ward, A. (2012) 'New role for grb10 signaling in the pancreas', *Diabetes,* 61(12), pp. 3066-3067.

Warren, K. J., Fang, X., Gowda, N. M., Thompson, J. J. and Heller, N. M. (2016) 'The TORC1-activated Proteins , p70S6K and GRB10 , Regulate IL-4 Signaling and M2 Macrophage Polarization by Modulating Phosphorylation of Insulin Receptor Substrate-2', *Journal of Biological Chemistry*, 291(48), pp. 24922–24930.

Wick, K. L. R., Werner, E. D., Langlais, P., Ramos, F. J., Dong, L. Q., Shoelson, S. E. and Liu, F. (2003) 'Grb10 inhibits insulin-stimulated insulin receptor substrate (IRS)-phosphatidylinositol 3-kinase/Akt signaling

pathway by disrupting the association of IRS-1/IRS-2 with the insulin receptor', *Journal of Biological Chemistry*, 278(10), pp. 8460–8467.

Wilkins, J.F., (2014) 'Genomic imprinting of Grb10: coadaptation or conflict?', *PLoS biology*, *12*(2), p.e1001800.

Wolf, J. B. (2013). 'Evolution of genomic imprinting as a coordinator of coadapted gene expression', *Proceedings of the National Academy of Sciences of the United States of America*, 110(13), pp. 5085–5090.

Wolf, J. B., Cowley, M. and Ward, A. (2015) 'Coadaptation between Mother and Offspring : Why Not ?', *PLoS biology*, 13(3), pp. 3–5.

Wu, A., Tu, X., Prisco, M. and Baserga, R. (2005) 'Regulation of upstream binding factor 1 activity by insulin-like growth factor I receptor signaling', *Journal of Biological Chemistry*, *280*(4), pp. 2863-2872.

Yan, X., Himburg, H. A., Pohl, K., Quarmyne, M., Tran, E., Zhang, Y., Fang, T., Kan, J., Chao, N. J., Zhao, L., Doan, P. L. and Chute, J. P. (2016) 'Deletion of the Imprinted Gene Grb10 Promotes Hematopoietic Stem Cell Self-Renewal and Regeneration', *Cell Reports*. 17(6), pp. 1584–1594.

Yao, J., Huang, Y., Huang, R., Shi, R., Chen, P., Zhu, B., Li, M., Jiang, X., Zheng, M., Jiang, Y. and Yang, X. (2012) 'Epigenetic modifications and mRNA levels of the imprinted gene Grb10 in serially passaged fibroblast cells', *Biochimie*, 94(12), pp. 2699–2705.

Yea, S. S. and Fruman, D. A. (2011) 'New mTOR targets Grb attention', *Science*, 332(6035), pp. 1270-1271.

You, H., Zheng, H., Murray, S. A., Yu, Q., Uchida, T., Fan, D. and Xiao, Z. X. J. (2002) 'IGF‐1 induces Pin1 expression in promoting cell cycle S‐phase entry', *Journal of cellular biochemistry*, *84*(2), pp. 211-216.

Yu, Y., Yoon, S. O., Poulogiannis, G., Yang, Q., Ma, X. M., Villén, J., Kubica,

N., Hoffman, G. R., Cantley, L. C., Gygi, S. P. and Blenis, J. (2011) 'Phosphoproteomic analysis identifies Grb10 as an mTORC1 substrate that negatively regulates insulin signaling', *Science*, 332(6035), pp. 1322-1326.

Zhang, H., Nøhr, J., Jensen, C. H., Petersen, R. K., Bachmann, E., Teisner, B., Larsen, L. K., Mandrup, S. and Kristiansen, K. (2003) 'Insulin-like growth factor-1/insulin bypasses Pref-1/FA1-mediated inhibition of adipocyte differentiation', *Journal of Biological Chemistry*, 278(23), pp. 20906–20914.

Zhang, J., Zhang, N., Liu, M., Li, X., Zhou, L., Huang, W., Xu, Z., Liu, J., Musi, N., DeFronzo, R. A., Cunningham, J. M., Zhou, Z., Lu, X. Y. and Liu, F. (2012) 'Disruption of growth factor receptor-binding protein 10 in the pancreas enhances β-cell proliferation and protects mice from streptozotocin-induced β-cell apoptosis', *Diabetes*, 61(12), pp. 3189–3198.